Risk assessment of bridge decks prone to vortex induced vibrations

Dissertation

submitted to and approved by the

Department of Architecture, Civil Engineering and Environmental Sciences
University of Braunschweig – Institute of Technology

and the

Faculty of Engineering
University of Florence

in candidacy for the degree of a
Doktor-Ingenieur (Dr.-Ing.) /
Dottore di Ricerca in "Riduzione del Rischio da Catastrofi Naturali su Strutture ed Infrastrutture" *)

by
Antonino Maria Marra
Born 26.06.1982
from Melito di Porto Salvo (RC), Italy

Submitted on	15 September 2011
Oral examination on	04 November 2011
Professorial advisors	Prof. G. Bartoli
	Prof. U. Peil

2011

*) Either the German or the Italian form of the title may be used.

To my parents
Gaetana and Bruno,
my aunt Isabella and
my sister Domenica

Abstract

The present dissertation deals with the risk assessment of bridge decks prone to vortex induced vibrations, which is presently recognized as a key issue in the design of flexible bridges.

A procedure is proposed to quantify the risk associated with vortex-shedding of bridge decks. The framework adopted is in line with the general risk management framework developed by the International Graduate College 802. Performance-based-design approach is followed and the risk is quantified by using a modified version of the PEER equation.

First, the hazard analysis is developed. It consists in evaluating the probability of the hazard (wind speed and direction) by means of the Weibull distribution. The wind data are also analyzed by using a hybrid model, which consists of estimating the model parameters without considering wind calms. The results are compared with those obtained through the classical approach.

In the second part of the dissertation the structural vulnerability analysis is conducted. It evaluates the probability of the structural response during vortex-induced vibrations. A careful revision of the state of the art knowledge is firstly reported on both the phenomenological aspects and mathematical modeling of vortex-induced vibration of bluff bodies. It led to the conclusion that no model is able to provide reliable predictions of the structural response at values of the Scruton number different from that at which the aeroelastic parameters are estimated. In this work, the Ehsan-Scanlan model was studied in depth because it is considered suitable for practical applications to bridge decks. Wind tunnel tests were performed to apply Ehsan-Scanlan's model to a idealized case study. They have also shown an interaction between the three degree of freedom (heaving, pitching and rolling mode) of the sectional model in the lock-in conditions. Static and aeroelastic tests on a rectangular cylinder were conducted in smooth flow. In particular, static tests were used to estimate the aerodynamic coefficients and the Strouhal number. Ambient vibration tests were carried out to measure the response during lock-in for different reduced velocities. Finally, decay-to-resonance tests were performed to estimate the aeroelastic parameters of the empirical model. Highlighted in this analysis is the physical coherence of the van der Pol-type equation used to model vortex-induced vibrations of structures prone to wind excitation (bridges, towers, chimneys, cables, etc.). Even though the validity of the identification procedure employed in Ehsan-Scanlan's model to determine the aeroelastic parameters of the model is demonstrated, a limit of the procedure is observed when the limit-cycle oscillation amplitude is estimated from experimental signals. The precise value of the limit-cycle oscillation amplitude, on which the model parameters strongly depend, is uncertain and in practice the choice is left to the analyst. In addition, an alternative identification procedure is

proposed based on the direct numerical solution of the nonlinear differential equation. This method is not based on any approximate solution and so it can be useful for the identification of the aeroelastic parameters in cases where Ehsan-Scanlan's model is modified and no approximate solution is available.

In the third part of the dissertation the application of the developed procedure to a case study is reported. The effects in terms of risk due to the different assumptions standing behind the procedure are highlighted.

Finally, the perspectives of future developments of this research work are discussed.

Sommario

Valutazione del rischio di impalcati da ponte suscettibili alle vibrazioni indotte dai vortici

La presente dissertazione riguarda la valutazione del rischio di impalcati da ponte suscettibili alle vibrazioni indotte dai vortici. Al momento, tale fenomeno rappresenta un problema di rilievo nella progettazione di ponti flessibili.

E' proposta una procedura per quantificare il rischio associato al distacco di vortici di impalcati da ponte. La procedura é strutturata seguendo lo schema generale di gestione del rischio proposto dal International Graduate College 802. seguito un approccio alla progettazione basato sulle prestazioni (Performance-based-design approach) e il rischio stato quantificato usando una versione modificata dellequazione proposta dal centro PEER.

In primo luogo stata sviluppata lanalisi di pericolosit (hazard analysis) che consiste nella valutazione della probabilit dell'hazard (velocit e direzione del vento) usando la distribuzione di Weibull. I dati di vento sono stati analizzati usando un modello ibrido, in cui la stima dei parametri del modello fatta trascurando le calme di vento. I risultati cos ottenuti sono stati confrontati con quelli derivanti dallapplicazione dellapproccio classico.

Nella seconda parte della tesi stata condotta lanalisi di vulnerabilit strutturale (structural vulnerabiliy analysis), in cui determinata la risposta strutturale durante le vibrazioni indotte dai vortici. Il primo passo consistito in uno studio accurato dei lavori presenti in letteratura riguardanti sia gli aspetti fenomenologici che di modellazione delle vibrazioni indotte dai vortici dei corpi tozzi. La conclusione fondamentale della revisione di letteratura che nessun modello esistente in grado di predire con la dovuta accuratezza la risposta strutturale a valori del numero di Scruton diversi da quello a cui i parametri aeroelastici sono determinati sperimentalmente. In questo lavoro, modello di Ehsan e Scanlan stato studiato in dettaglio perch potrebbe essere usato per applicazioni pratiche agli impalcati da ponte. Prove in galleria del vento sono state condotte sia per applicare il modello ad un caso di studio ideale che per mostrare leffetto dellinterazione tra i tre gradi di libert (verticale, torsionale e rollio) del modello sezione sulla risposta in lock-in. Le prove sperimentali sono state di tipo statico e dinamico su un cilindro rettangolare in flusso laminare. In particolare, le prove statiche hanno fornito i coefficienti aerodinamici ed il numero di Strouhal. Vibrazioni ambientali sono state condotte per misurare la risposta in lock-in a diverse velocit ridotte. Infine, prove di decadimento a risonanza sono state svolte per stimare i parametri aeroelastici del modello empirico. stata dimostrata la coerenza fisica dellequazione di van der Pol usata per modellare le vibrazioni indotte dai vortici di strutture suscettibili allazione del vento (ponti, torri, ciminiere, cavi, ecc.).

Inoltre, stato evidenziato un limite nella procedura di identificazione dei parametri aeroelastici usata nel modello di Ehsan e Scanlan riguardante la stima dell'ampiezza del ciclo limite dal segnale sperimentale. In particolare, il valore dell'ampiezza di oscillazione del ciclo limite, da cui i parametri aeroelastici dipendono significativamente, incerta e la cui scelta lasciata praticamente all'analista. Alternativamente, stata proposta una procedura di identificazione basata soluzione numerica diretta dell'equazione differenziale non lineare. Questo metodo non essendo basato su una soluzione approssimata pu essere utile per l'identificazione dei parametri aeroelastici nel caso in cui il modello di Ehsan-Scanlan fosse modificato e non fosse disponibile alcuna soluzione approssimata.

Nella terza parte della dissertazione riportata l'applicazione della procedura sviluppata ad un caso di studio. Sono evidenziati gli effetti in termini di rischio dovuti alle diverse assunzioni che stanno dietro la procedura.

Infine, sono discusse le prospettive ed i sviluppi futuri di questo lavoro di ricerca.

Zusammenfassung

Risikobewertung von Brcken, die zu wirbelerregten Schwingungen neigen

Die vorliegende Arbeit beschftigt sich mit der Risikobewertung von Brcken, bei denen unter Windanstrmung wirbelerregte Schwingungen auftreten. Eine Untersuchung der Tragwerksantwort unter der speziellen Windbelastung wird gegenwrtig als unerlsslich beim Entwurf von schlanken Brcken angesehen. Zur Quantifizierung des Risikos im Zusammenhang mit wirbelerregten Schwingungen wird ein Ansatz vorgestellt, der sich an die bekannte PEER-Gleichung anlehnt. Im ersten Schritt wird die Gefhrdung des Standorts der Brcke ermittelt. Dabei werden die Auftretenswahrscheinlichkeiten der Windereignisse fr den Standort analysiert. Sowohl fr die Windgeschwindigkeit als auch fr die Windrichtung wird eine Weibull-Verteilung angenommen. Die Winddaten werden auch mit einem Hybridmodell untersucht, wobei die Modellparameter ohne die Bercksichtigung von windstillen Zeitrumen bestimmt werden. Die Ergebnisse beider Verfahren werden verglichen. Im nchsten Schritt wird die Schwingungsreaktion des Bauwerks auf die Anregung durch den Wind bewertet. Wie eine Literaturrecherche zeigt, ist keines der aus dem Fachschrifttum bekannten Modelle in der Lage, zuverlssig das Schwingungsverhalten der Brcke fr Scruton-Zahlen vorherzusagen, fr die nicht die aeroelastischen Parameter identifiziert wurden. Das Ehsan-Scanlan-Modell liefert jedoch brauchbare Ergebnisse fr praktische Anwendungen im Brckenbau und wird deshalb hier verwendet. Die numerische Lsung der auftretenden Van-der-Pol-Gleichung wird mit speziell dazu durchgefhrten Windkanalmessungen verglichen. Auftretende Probleme bei der Ermittlung der Amplituden der Grenzzyklen werden ausfhrlich diskutiert. Zustzlich wird eine alternative Vorgehensweise zur Bestimmung der aeroelastischen Parameter des Ehsan-Scanlan-Modells vorgestellt. In einer Fallstudie werden die Mglichkeiten des entwickelten Verfahrens zur Risikobewertung verdeutlicht. Abschlieend wird ein Ausblick fr weitere Entwicklungen in diesem Forschungsgebiet vorgestellt.

Acknowledgements

First of all, I would like to thank the advisor of my Master Thesis at the University of Reggio Calabria, Prof. Francesco Ricciardelli, who introduced me in the world of Wind Engineering through his lectures and transmitted his passion for the scientific research.

The significant experience of the International Doctoral Couse I have just finished was mainly possible for the work of its coordinators Prof. Claudio Borri and Prof. Udo Peil to whom I express my sincere gratitude. My German tutor, Prof. Udo Peil, deserves a further thank for his supervision.

A thank go also to Mrs Serena Cartei for the help she gave me during the three years I spent in Florence.

My acknowledgement also goes to Mrs Yvonne Wissmann for her kindness and support during the period spent in Germany.

I would like to thank all the people I known during these three years. Among them a sincere thank to Engg. Laura Nardi, Giuseppe Rossi, Andrea Corridori, Laura Baro whereby I have shared all the steps of this wonderful experience.

A thank go also to the people I known in Germany. Among them, Eng. Arno Kirch deserves a special thanks for his availability and support during my period in Braunschweig. I also thank Dr. Tobias Wagner for his contribution in translating the abstract in German.

The last year of the Course I known Eng. Tommasso Massai, who became very fast one of the best friends I have in Florence. A big thank for his friendship, moral support and scientific discussions we had during these years.

I would like to express a special thank to Dr. Claudio Mannini for his friendship, moral support and scientific supervision. His invaluable help of constructive comments and suggestions throughout the thesis works have contributed to the success of this research. He represents for me a reference point for the research but not only.

Finally, I express a sincere thank to my Italian tutor, Prof. Gianni Bartoli, for his moral support and constant supervision. He represents for me a model to follow in the research and in the life.

List of Figures

List of Tables

Contents

Chapter 1

Introduction

1.1 Research topic motivations

Since several years now, the sensitivity to wind actions of cable-stayed and suspended-span bridges as well as that of modern footbridges is more than evident. The increasing of their flexibility due to the use of new materials, more advanced computational techniques, longer spans and, for footbridges, the necessity to be transparent for obtaining an architectural appealing has lead wind to become the principal issue for the design of such structures.

The interaction of the bridge elements (deck, towers, cables, suspenders) with the wind flow can give rise to static deformations, forcing responses and aeroelastic instabilities. In particular, referring to the deck, static horizontal deformations are provided by the mean wind velocity. Forcing response in the along and across-wind directions are due to the fluctuating part of the wind velocity caused by the turbulence of the atmospheric boundary layer. Finally, aeroelastic instabilities which could be observed on a bridge deck are torsional divergence, flutter and vortex-induced oscillation.

Vortex-induced vibration (VIV), known as lock-in, is a phenomenon in which the vibration of a body immersed in a fluid flow is governed by the shedding of vortices from its surface. Such condition is realized for a bridge deck when the frequency of vortex shedding is very close to the bending or pitching natural frequency, so that large-amplitude vibrations can occur.

The importance of vortex-induced vibrations in the design of bridge decks has nowadays been clarified. If it is not properly studied its effects can produce fatigue damage accumulation on structural elements and the reduction of travel safety and/or comfort levels for both road and railway users.

The first recorded event of bridge deck vortex-induced vibrations was observed during the construction of the Menai Straits Bridge (1826). This would seem to be an early suggestion that transverse horizontal wind may excite longitudinal vertical oscillations in suspension bridges (Buonopane and Billington, 1993). Conversely, a recent example is represented by the vortex-shedding excitation of the Storebaelt suspension bridge. During the final phases of deck erection low-frequency vertical oscillations of the girder were observed by both workers and supervision staff. Wind analysis and structural monitoring program allowed to individuate the cause of the oscillations. In ten vibration events occurring for wind direction almost perpendicular to the bridge axis and wind speeds in the range 4-12 m/s, the structure showed

relatively large-amplitude harmonic oscillations which could be associated with a single vertical mode (Larsen *et al.*, 2000). These results allow to consider it as a vortex-induced vibration. The structural impact of the oscillations (Fig. 1.1) was not relevant but the visual impact could distract motorists and maybe reduce the road safety. Thus it was decided to mitigate the oscillations by guide vanes. Vortex-

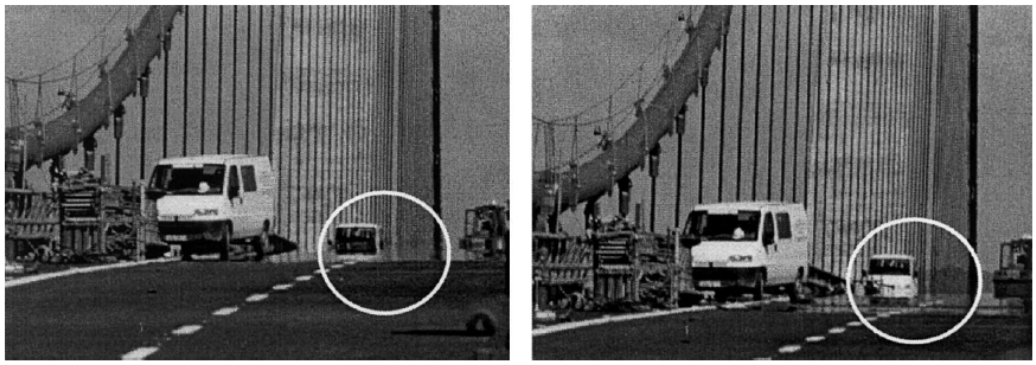

Fig. 1.1 View along the deck of the East Bridge at crest (left) and trough (right) of a large amplitude vertical oscillation (Larsen *et al.*, 2000).

induced vibrations have also been observed on many other bridges (Smith, 1980; Kumarasena and Ehsan, 1991; Owen *et al.*, 1996; Battista and Pfeil, 2000; Larsen *et al.*, 2000; Fujino, 2002).

For modern bridge deck shapes, e.g. twin and multi-box girders, vortex-induced vibrations seem to be the most important problem. These new deck sections show a strong interaction between the section and the vortices. In fact, the vortices shed from the upwind girder drift across the air gap and impinge on the downwind girder (Larose *et al.*, 2003). To avoid large vortex-induced oscillations, guide vanes are often installed on the section, as shown in Fig. 1.2 (referring to Stonecutters Bridge). This choice, taken during the design phase, can suggest the use of aerodynamic appendices as the unique strategy to reduce the vortex-shedding response of that particular section.

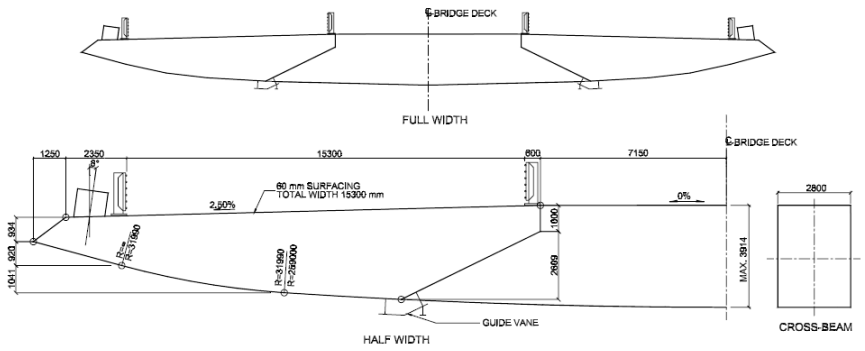

Fig. 1.2 Section of the proposed Stonecutters Bridge (Larose *et al.*, 2003).

The above examples of vortex-induced vibrations underline the importance of

risk assessment of large oscillations in the early stage of bridge deck design.

1.2 Outline of the work

The present dissertation is composed by ten chapters: three of them (Chapter 2, 4 and 5) represents literature reviews, in the remaining chapters the original work is reported. They are briefly described below.

In Chapter 2 the general risk management framework developed into the IGC 802 is carefully described because it is used to frame the problem of vortex-induced vibrations of bridge decks treated in the present dissertation. In addition, the Performance-Based Design approach is described because is followed in this work. PEER's equation is also treated because it represents a tool for quantitative evaluations of risk and some of its applications to wind engineering are reported.

In Chapter 3 the hazard analysis for vortex-induced vibrations of bridge decks is treated. In particular, the modeling of moderate wind in the atmospheric bourdary layer is discussed. Then, a statistical analysis of anemometric data is performed by using the Weibull model. It consists in omnidirectional and directional analyses in which the results obtained by the classical approach are compared with those of the hybrid one.

In Chapter 4 a short review on the phenomenon of vortex-induced vibrations of bluff bodies is reported to provide a useful background for the comprehension of Chapter 5.

In Chapter 5 a review on vortex-induced vibration modeling of bluff bodies is conducted trying to describe carefully the works present in the literature. In particular, the existing models are classified and compared.

In Chapter 6 the experimental part carried out in this work is treated. It consists in static and aeroelastic wind tunnel tests on a rectangular cylinder in smooth flow. Static tests are performed to verify the quality of the model by comparing the results (Strouhal number and aerodynamic coefficients) with those present in the literature. Ambient vibration tests are needed to study in detail the lock-in oscillations and a particular kind of aeroelastic tests, called decay-to-resonance tests, are used to estimate the aeroelastic parameters of an existing model.

In Chapter 7 the use of the van der Pol-type modeling is discussed in detail. The coherence of the van der Pol-type equation for modeling vortex-induced vibrations of wind-sensitive structures is demonstrated. In addition, a model based on such equation is selected for a careful study. In particular, the validity of the assumptions standing behind its identification procedure are demonstrated and a limit of the procedure itself is highlighted. Finally, in contrast to that reported in the literature, the use of the equivalent mass obtained by considering the mass of all structural elements of the bridge, other than that of the deck (i.e. cables, towers etc.), is suggested in the calculation of the lock-in response of the entire bridge.

In Chapter 8 a direct numerical identification method is proposed to estimate the aeroelastic parameters of a van der Pol-type equation. The direct numerical identification resulted as reliable as that present in the literature based on an approximate solution of the equation. The method proposed could be useful for nonlinear differential equations for which no approximate solutions are available.

In Chapter 9 a procedure to conduct the VIV-risk assessment of bridge decks is proposed and applied to an idealized case study. The effects of the assumptions

standing behind the procedure are shown.

In Chapter 10 the final conclusions of the disseratation and future developments of the present work are reported.

1.3 Contributions of the present research work

The research activity developed into the present dissertation represents a contribute in the risk management research as well as in the wind engineering one. In particular, an effort is made to frame the problem of vortex-induced vibration of bridge decks into the risk management. Moreover, for the wind engineering field, an attempt to improve the present capabilities of modeling such a phenomenon is done.

In detail the contributions of the present research work can be listed as follow:

- Development of a procedure to conduct the VIV-risk assessment of bridge decks;
- Application of the procedure to an idealized case study;
- Experimental tests in wind tunnel have shown an the interaction between the two degree of freedom (heaving and pitching) of the sectional model during lock-in both on ambient vibrations and decay-to-resonance tests;
- The coherence of the van der Pol-type equation in modeling vortex-induced vibrations of wind-sensitive structures is demonstrated;
- The validity of the assumptions of an identification procedure present in the literature is demonstrated and a limit in the choice of the limit-cycle oscillation amplitude from the experimental signal is highlighted;
- The use of an equivalent mass given by considering not only the deck mass but also all the elements of the bridge (i.e. deck, cables, towers, etc.) in calculating the lock-in response of the entire bridge;
- A direct numerical identification method is proposed to estimate the aeroelastic parameters of an eventual modified version of the van der Pol-type equation of the model present in the literature.

Chapter 2

Risk management

2.1 Introduction

The word *risk* can be a very equivocal term for the several meanings it may assume (Augusti *et al.*, 2001). Generally, risk is sensed for the presence of a danger. Conversely, safety is its counterpart and is sensed when danger is absent. For an engineering point of view such definition of risk is not useful. In fact, the possibility of an unwanted event can never been excluded altogether. Therefore, risk has to be formulated in probabilistic terms. In the last decades more and more attention was spent to manage the risk in many different fields. In particular, the range of application of risk management is very large; in fact, applications to finance, engineering, medical science, insurance industry and disaster management can be found. Therefore, the several disciplines involved into the risk management have given rise to a great diversity of definitions and methods.

Next section describes a risk management framework proposed with the aim to give a standard procedure in managing disaster risk. In section 2.3 Performance-Based Design is introduced as a possible methodology to follow for risk assessment. The chapter ends with some conclusions.

2.2 Risk management framework

An attempt to remove the ambiguities in risk management was conducted by Pliefke *et al.* (2006) and Pliefke *et al.* (2007) proposing a standard methodology for managing disaster risk in compliance with AS/NZS 4360 (AS/NZS-Standard, 1999).

According to AS/NZS 4360 the risk management process can be defined as the

> *"Systematic application of policies, procedures and practices to the task of identifying, analyzing, evaluating, treating and monitoring risk"*

In Fig. 2.1 the general risk management framework proposed by Pliefke *et al.* (2007) is reported. The risk management process can be divided into three main parts:

- *risk identification*
- *risk assessment*
- *risk treatment*

which are accompanied by a *risk review* step and continuous *risk monitoring*. Risk review constantly introduces new information, knowledge and experience about the risk. In contrast, risk monitoring captures the exchange of information of all people involved in the risk management process.

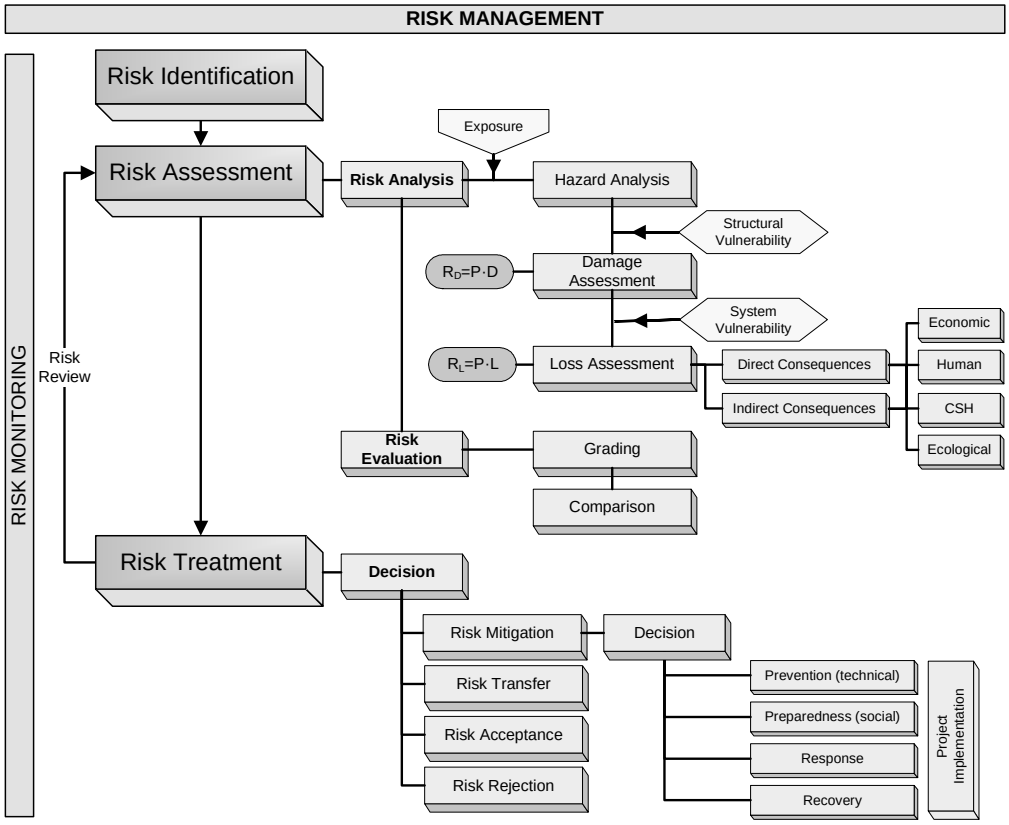

Fig. 2.1 Risk management process (Pliefke *et al.*, 2006, 2007).

2.2.1 Risk identification

Risk identification starts with the definition of the system, which can be a building, a city, etc.. Next, all sources of events that can compromise the functionality of the system must be identified (hazard identification).

2.2.2 Risk assessment

Risk assessment is subdivided into *risk analysis* and *risk evaluation* (Fig. 2.1). The former quantifies the risk whereas the latter is devoted to the comparison with other competing risks.

Risk analysis starts with *hazard analysis* that defines the probability of occurrence of all the hazards identified. Next, the structural behavior of the system has to be determined depending on the hazard load. Once the system structural response is known, the damage of the system can be determined. The relation between the hazard intensity and the resulting damage is called *structural vulnerability*. Finally,

loss assessment is conducted evaluating the consequences due to the damage levels of the system (*system vulnerability*). The consequences can be divided into *direct* and *indirect consequences*. The former occur when the disaster takes place, the latter occur with a certain time delay. Moreover, the consequences can be divided into *tangible* and *intangible consequences*. Tangible consequences are directly measurable in monetary terms, whereas for intangible consequences it is not possible to provide a monetary value (fatalities, pollution of the environment, loss of cultural, social and historical values, etc.).

Risk analysis terminates with the quantification of risk, which can be distinguished in *structural risk* and *total risk*. Structural risk is the product of the annual probability of occurrence of the hazard multiplied by the expected damage:

$$\text{Structural risk} = \text{Probability} \times \text{Damage [Damage measure/year]}$$

Such risk definition is clearly important for engineers involved in the prediction of the behavior of structures under the action of hazards. Total risk is the product of the annual probability of occurrence of the hazard and the expected loss:

$$\text{Total risk} = \text{Probability} \times \text{Loss [Loss unit/year]}$$

The risk evaluation phase stars after that risk analysis phase is concluded. Its scope is to make the considered risk comparable with other competing risks for the system by the use of adequate risk measures.

2.2.3 Risk treatment

Risk treatment is the last main part of the risk management framework (Fig. 2.1). In this phase a decision whether to accept, to transfer, to reject and to reduce a given risk has to be taken.

When the risk has to be mitigated, pre-disaster (*prevention*, *preparedness*) and post-disaster interventions (*response*, *recovery*) can be applied depending on the time the risk reduction project is implemented. All the possible risk reduction strategies have in common the effect of reducing the vulnerability of the system.

Prevention refers to technical measures like structural strenthening, that are to be applied before the disaster take place.

Preparedness regards social activities (evacuation plans, emergency training) that are used to limit harm shortly before the occurrence of the disaster.

Response involves all activities that are applied immediately after the disaster takes place, such as the organization of help and shelter for injured and harmed people as well as the coordination of emergency forces.

Finally, recovery is constituted of all activities that have to be applied to return to the pre-disaster status of the system.

2.3 Performance-Based Design

A methodology to conduct the risk assessment is represented by the *Performance-Based Design* (PBD). It is based on the satisfaction of salient performance requirements with a sufficiently high probability throughout the life of the structure (Augusti and Ciampoli, 2008). In the design of engineering facilities, the PBD does not require to ensure the needing of ensuring their resistance at the minimum cost in a

deterministic way. In fact, PBD approach is aimed to minimize the total probabilistically calculated losses throughout the facility lifetime.

The PBD was developed in the USA with reference to seismic risk and design. The first attempt to extend the PBD approach to Wind Engineering was made by Paulotto *et al.* (2004) and was based on the PEER[1] equation (Cornell and Krawinkler, 2000):

$$p(DV) = \int\int\int p(DV|DM)|dp(DM|EDP)||dp(EDP|IM)||dp(IM)| \qquad (2.1)$$

where

- IM is the *Intensity Measure* which represents a measure of the magnitude of the action;
- EDP is the *Engineering Demand Parameter* which describes the structural response;
- DM is the *Damage Measure*;
- DV is the *Decision Variable*, a parameter which governs the design decision.

The term $p(IM)$ represents the probability of exceedance of the intensity measure, it is evaluated through *hazard analysis*. $p(EDP|IM)$ is a term obtained by *structural analysis*, which concerns the probability of exceedance of a certain level of the structural response, given a particular value of the intensity measure. The term $p(DM|EDP)$, provided by *damage analysis*, is the probability of exceedance of a particular level of damage given a certain value of the structural response. The product of the last two terms are called *structural vulnerability*. Finally, $p(DV|DM)$ is a probability measure of the cost of damage, it can be obtained through the *loss analysis*.

Because of its multidisciplinarity, PBD requires the contribute of scientists (meteorologists, geophysicists, etc.), engineers and economists. In particular, engineers are involved in the development of the structural vulnerability term (structural and damage analysis).

In developing the PBD approach, the explicit form of the term which relates the measure of the damage DM to the structural response EDP is very difficult to be found. In fact, both for the limited availability of experimental data and for the difficulties in numerically simulating the actual damage of a structures, in wind engineering an attempt was done to express the damage in terms of the structural response (Paulotto *et al.*, 2004). Therefore, the Eq. (2.1) can be simplified as follow:

$$p(DV) = \int\int\int p(DV|DM)|dp(DM|IM)||dp(IM)| \qquad (2.2)$$

In wind engineering, the term $p(DM|IM)$ is expressed by *fragility curves*. They give the probability of exceeding a specific damage given a particular value of the intensity measure, which generally is represented by the mean wind velocity.

To apply the PBD, the definition of the performances must be conducted. They are formulated in terms of ultimate limit states (low performance levels) and serviceability limit states (high performance levels).

[1]It is a framework formula for performance-based earthquake engineering, advocated and used by researchers at the Pacific Earthquake Engineering Research (PEER) Center.

So far very few applications of the PBD to wind engineering have been performed. Paulotto *et al.* (2004) conducted the first steps for its application to tall buildings, Mannini (2006) proposed a model of probabilistic flutter assessment to define the term $p(EDP|IM)$. Augusti and Ciampoli (2008), in the framework of PBD, compaired the results obtained by the Subset Simulation method with those of Monte Carlo simulations for the evaluation of the probability to exceed an appropriate discomfort threshold for a pedestrian suspended footbridge.

2.4 Conclusions

Any procedure useful for practical applications has to be composed by the succession of different steps (framework) and by different methodologies (input-output relations) which connect each step. Therefore, in this chapter, a broad risk management framework present in the literature was carefully described, as it will be used for VIV-risk assessment of bridge decks. In addition, the PBD approach was also presented because it will be the methodology used. PEER's equation was also treated since a modified version will be applied for the quantitative evaluation of the risk. Applications of PBD to wind engineering (PBWE: Performance Based Wind Engineering) are very limited and to the author's knowledge it has never been applied to VIV-risk quantification of bridge decks.

Chapter 3

Directional wind statistics

3.1 Introduction

In this chapter, the hazard analysis will be conducted and the last term of the PEER equation $p(IM)$ will be defined.
Vortex-induced vibrations of flexible bridges is here analysed in the framework of the serviceability limit state, therefore the corresponding wind range concerns moderate wind speeds. In Section 3.2, the main assumptions for modeling wind speed are explained and justified.

Moreover, since the lock-in response can occur under a specific range of yaw angles (see Section 4.4), the directional wind statistics have to be taken into account to conduct a risk analysis. Therefore, in Section 3.3, a statistical distribution which enables to model the directional characteristics of the wind speeds is presented and the procedure to estimate its parameters is reported.

In Section 3.4, the analysis is conducted by using real data. First of all, the omnidirectional probability analysis is performed by comparing the results obtained with the classical approach (wind calms are included to estimate the parameters of the probability distribution) and those given by the hybrid model, where wind calms are neglected. After, the directional analysis is developed by using only the hybrid model. Finally, the chapter ends with some conclusions.

3.2 Wind modeling for serviceability limit state

At moderate wind speeds, at which vortex-induced vibrations occur, the wind flow may be less turbulent than that of strong wind and the profile could be flatter as well (Simiu and Miyata, 2006; Cook, 1985; Peil and Nolle, 1994; Peil, 1998; Peil and Telljohann, 1999; Clobes *et al.*, 2011). Because of the horizontal configuration of a bridge deck, with respect to the wind actions, the second issue does not matter, in fact, wind profile is considered constant for strong wind also. Conversely, wind profile should be taken into account to predict the response of a chimney. The characterization of the turbulence could be a problem because at moderate wind speeds, near 10 m/s, atmospheric boundary layer cannot be considered neutrally stable, which is the case of strong wind in which turbulence is induced mechanically, but thermal effects must be considered and standard models for strong winds cannot be used (Simiu and Miyata, 2006; Cook, 1985; Peil and Nolle, 1994; Peil, 1998; Peil and Telljohann, 1999; Clobes *et al.*, 2011). Fortunately, as shown by extensive

experimental results, vortex-shedding forces are more correlated in the spanwise direction as turbulence is reduced and then to assume their strong effect a smooth flow is conservative. So, in modeling moderate wind speeds, smooth flow assumption is conservative.

As the bridge response depends on the yaw angle between the horizontal wind velocity vector and the deck axis (see Section 4.4), the directional probability of wind must be taken into account as well.

3.3 Directional probability distribution for moderate winds

With the exception of particular wind regimes (high frequencies of null winds, unimodal, bimodal, bitangential regimes, etc.), for which mixture distributions are more appropriate (Carta *et al.*, 2008a,b, 2009), *Weibull distribution* (Weibull, 1951) is commonly accepted as the mean wind speed distribution at any velocity (i.e., low, moderate and high wind speed) (Deaves and Lines, 1997). Consequently, it can be used not only for ultimate limit states but also for serviceability, energetic and fatigue calculations (Kasperski, 2009; Repetto and Solari, 2004). Therefore, the probability that the mean wind speed U exceeds an assigned threshold u when the wind direction is within the sector $(\theta_{inf}, \theta_{sup})$, can be evaluated by the following Weibull exceedance probability function:

$$P(U > u|\theta_{inf} < \theta < \theta_{sup}) = exp\left[-\left(\frac{u}{b}\right)^a\right] \tag{3.1}$$

where the two parameters a and b generally vary from sector to sector, i.e., depend on the sector defined by θ_{inf} and θ_{sup}. The corresponding probability density function is given by

$$p(u < U < u + du|\theta_{inf} < \theta < \theta_{sup}) = \frac{a}{b}\left(\frac{u}{b}\right)^{(a-1)} exp\left[-\left(\frac{u}{b}\right)^a\right] \tag{3.2}$$

It allows to evaluate the probability that the mean wind speed is within u and $u+du$ when θ is within the sector $(\theta_{inf}, \theta_{sup})$.

3.3.1 Parameter estimation procedure

To estimate all the parameters it is useful to define the following auxiliary variables[1]:

$$X = 100\ln(2.5u) \qquad Y = 100\ln\ln\left(\frac{1}{P}\right) \tag{3.3}$$

Using the previous variables, the distribution of Eq. (3.1) is correct if the data are distributed along the following straight line:

$$Y = mX + c \tag{3.4}$$

Therefore, it is easy to show that the two parameters a and b can be obtained by

$$a = m \tag{3.5}$$

$$b = \frac{1}{2.5} exp\left(-\frac{c}{100a}\right) \tag{3.6}$$

[1]Here, the definition of the auxiliary variables follows that proposed by Boccotti (2000) and Boccotti (2004). Obviously, the coefficients "100"and "2.5"can be chosen arbitrarily.

3.4 Application

3.4.1 Data

The available data[2] refer to the period from 1st January 1961 to 31st December 2010 (50 years). They are composed by 8 daily measures (one each 3 hours) of the mean wind speed over 10 minutes for 36 directional sectors. The total number of data is 143672 but only 143102 (including wind calms) are useful due to the errors occuring in some registrations.

3.4.2 Omnidirectional probability

The analysis of the omnidirectional probability is performed before the directional one. Eq. (3.1) may be rewritten as follow:

$$P(U > u) = exp\left[-\left(\frac{u}{b}\right)^{a}\right] \tag{3.7}$$

As previously said, the present study refers to the statistical description of moderate wind speeds and then wind calms have to be included in the analysis.

A way to take into account wind calms was proposed by Takle and Brown (1978). They reduced the problem of properly including calm periods into the distribution by defining a hybrid density function

$$p_H(u < U < u + du) = P_0\delta(u) + (1 - P_0)p^*(u < U < u + du) \tag{3.8}$$

where P_0 is the probability of observing wind calms, $\delta(u)$ the Dirac delta function and

$$p^*(u < U < u + du) = \frac{a^*}{b^*}\left(\frac{u}{b^*}\right)^{a^*-1} exp\left[-\left(\frac{u}{b^*}\right)^{a^*}\right] \tag{3.9}$$

is the classical Weibull probability density function in which the symbol * is used to underline that its parameters are estimated without taking into account the wind calms. When $u = 0$ for the definition of the Dirac delta function $\delta(u) = 1$ and then $p_H = P_0$. Conversely, when $u \neq 0$ we have $\delta(u) = 0$ and consequently $p_H = (1 - P_0)p^*(u < U < u + du)$.

The occurrence probability function applying the hybrid model is given by:

$$P_H(U > u) = (1 - P_0)P^*(U > u) \tag{3.10}$$

where $P^*(U > u)$ is given by Eq. (3.7) in which the parameters are estimated in the same way as those of Eq. (3.9).

This method removes those measurements considered as wind calms and fits the Weibull distribution to the remaining wind data. Then, the zero wind speeds are reintroduced to have the proper mean and variance and to renormalize the distribution.

In Fig. 3.1, the comparison between the hybrid probability of occurrence $P^*(U > u)$ and the classical one $P(U > u)$ is reported. The calculation of both was conducted

[2]The data are those of Monte Argentario station, located in Tuscany, Italy, and were kindly provided by Col. G. P. Cesolari from Centro Nazionale di Meteorologia e Climatologia Aeronautica Servizio Climatologia e Documentazione, Pomezia (RM), Italy.

by using the method proposed by Deaves and Lines (1997). It can be seen that function $P^*(U > u)$, obtained by the hybrid model, starts from a value of probability of 1 at $u = 0$ since the wind calms are neglected. Conversely, function $P(U > u)$ shows a probability less than 1 at $u = 0$ since wind calms ($P_0 = 0.0985$) are taken into account in the classical approach.

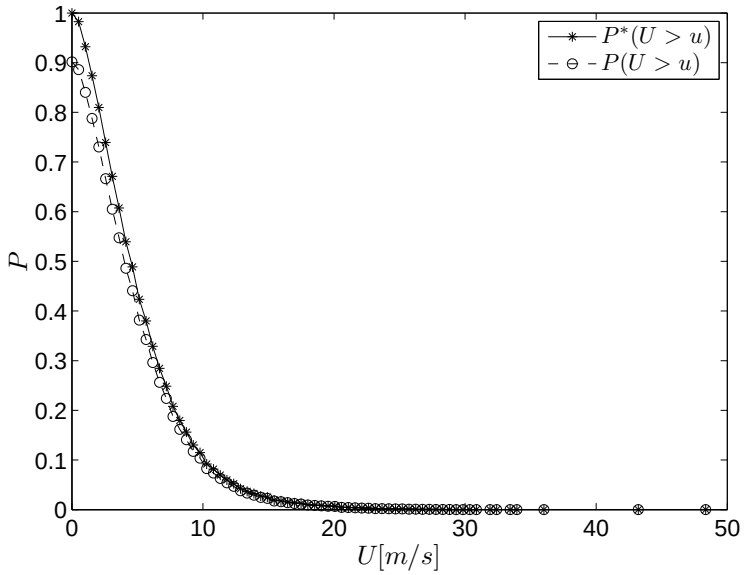

Fig. 3.1 Comparison between the hybrid probability of occurrence $P^*(U > u)$ (star points) and the classical one $P(U > u)$ (circle points) obtained by the wind data.

By using the auxiliary variables defined in Eqs. (3.3), the two omnidirectional parameters can be estimated by means of the least-square method (Fig. 3.2).

The results obtained are the following:

$$\text{without wind calms} \qquad a^* = 1.3816 \qquad b^* = 6.1477 \tag{3.11}$$

$$\text{with wind calms} \qquad a = 1.1633 \qquad b = 4.8848 \tag{3.12}$$

Obviously, the parameters a and b, determined by using the classical approach, are obtained excluding the point corresponding to $u = 0$ where the auxiliary variable X cannot be defined.

As shown in Fig. 3.2 and Fig. 3.3, the results obtained by using the hybrid model fit better the data than the classical approach.

3.4.3 Directional probability

A directional probability analysis is conducted by considering separately the data which fall within each sector. Given the good performance shown by the hybrid model in the omnidirectional analysis, the directional analysis is conducted by applying only this approach. Here, Eqs. (3.1, 3.10, 3.9, 3.8) may be rewritten respectively as

$$P_i^*(U > u|\theta_{inf,i} < \theta < \theta_{sup,i}) = exp\left[-\left(\frac{u}{b_i^*}\right)^{a_i^*}\right] \tag{3.13}$$

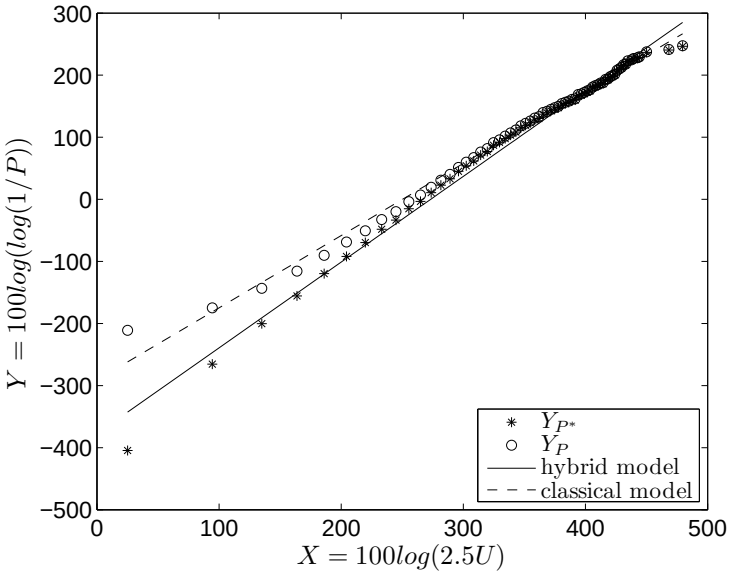

Fig. 3.2 Auxiliary variable plane for the hybrid probability of occurrence $P^*(U > u)$ (star points) and the classical one $P(U > u)$ (circle points).

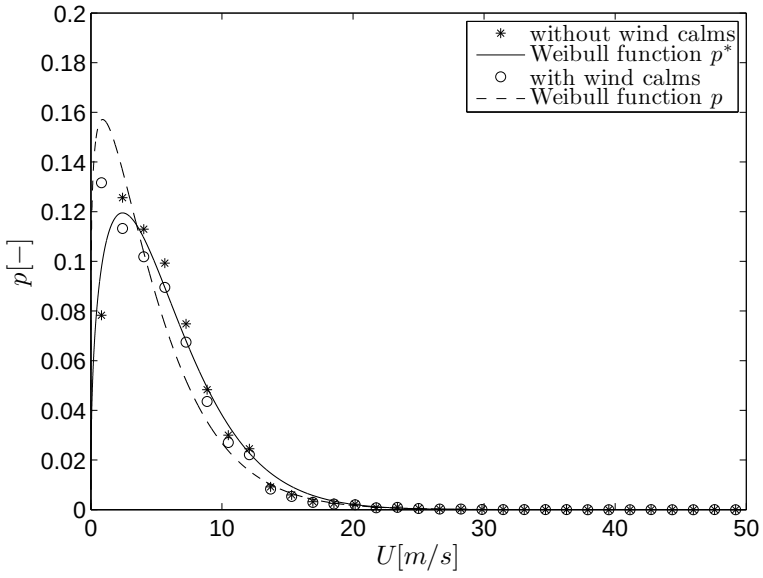

Fig. 3.3 Comparison of the hybrid probability density function $p^*(u < U < u + du)$ (solid line) and the classical one $p(u < U < u + du)$ (dashed line) with the corresponding data.

$$P_{H,i}(U > u|\theta_{inf,i} < \theta < \theta_{sup,i}) = (1 - P_0)P_i^*(U > u|\theta_{inf,i} < \theta < \theta_{sup,i}) \tag{3.14}$$

$$p_i^*(u < U < u + du|\theta_{inf,i} < \theta < \theta_{sup,i}) = \frac{a_i^*}{b_i^*}\left(\frac{u}{b_i^*}\right)^{a_i^*-1} exp\left[-\left(\frac{u}{b_i^*}\right)^{a_i^*}\right] \tag{3.15}$$

$$\begin{aligned} p_{H,i}(u < U < u + du|\theta_{inf,i} < \theta < \theta_{sup,i}) = \\ = P_0\delta(u) + (1 - P_0)p_i^*(u < U < u + du|\theta_{inf,i} < \theta < \theta_{sup,i}) \end{aligned} \tag{3.16}$$

where a_i^* and b_i^* represent the coefficients of the i-th sector.

Fig. 3.4 reports the probability of occurrence for each sector. The approximation provided by the Weibull distribution is shown in Fig. 3.5, where it is apparent that for some sectors the straight lines well approximate the data reported in terms of auxiliary variables. In some sectors, a slight deviation from the straight line is observed at high wind speeds. Same considerations can be done by comparing the probability density function of the data for each sector with the corresponding function obtained by using the Weibull distribution (Fig. 3.6), the parameters of which one reported in Table 3.1. Finally, in Fig. 3.7 and 3.8 the model parameters and the probability of each sector are shown in polar form.

Eq. (3.15) represents a conditional probability, but a joint probability function is needed in the PBD approach [Eq. (2.2)], which may be obtained by:

$$\begin{aligned} p_i^*(u < U < u + du, \theta_{inf,i} < \theta < \theta_{sup,i}) = \\ = P_i^*(\theta_{inf,i} < \theta < \theta_{sup,i})p_i^*(u < U < u + du|\theta_{inf,i} < \theta < \theta_{sup,i}) \end{aligned} \tag{3.17}$$

where

$$P_i^*(\theta_{inf,i} < \theta < \theta_{sup,i}) = \frac{\text{number of data which fall within the i-th sector}}{\text{number of total data}} \tag{3.18}$$

3.5 Conclusions

In this chapter the hazard part of the risk analysis regarding vortex-induced vibrations of bridge decks has been reported. In particular, the last term in Eq. (2.2) of the PBD approach has been dealt with.

As the omnidirectional analysis has shown, the hybrid model seems to fit better the data especially at low/moderate wind speeds than the classical approach. The Weibull distribution seems to be adequate also for modeling the directional wind characteristics.

Table 3.1 Directional parameters and probability for each sector.

Sector	Angle range	a^*	b^*	$P^*(\theta_{inf,i} < \theta < \theta_{sup,i})$
1	$0 - 10^o$	1.3893	6.1246	0.0240
2	$10^o - 20^o$	1.4024	6.5330	0.0304
3	$20^o - 30^o$	1.4355	6.6059	0.0343
4	$30^o - 40^o$	1.4022	7.0869	0.0316
5	$40^o - 50^o$	1.4279	7.1062	0.0323
6	$50^o - 60^o$	1.4133	6.7609	0.0395
7	$60^o - 70^o$	1.4400	6.3428	0.0337
8	$70^o - 80^o$	1.4962	6.1114	0.0324
9	$80^o - 90^o$	1.4399	6.1930	0.0337
10	$90^o - 100^o$	1.3362	5.9034	0.0221
11	$100^o - 110^o$	1.3310	5.7253	0.0198
12	$110^o - 120^o$	1.3506	5.7099	0.0207
13	$120^o - 130^o$	1.3510	5.6358	0.0144
14	$130^o - 140^o$	1.3011	6.0086	0.0129
15	$140^o - 150^o$	1.3560	5.9471	0.0184
16	$150^o - 160^o$	1.5074	6.2874	0.0223
17	$160^o - 170^o$	1.5715	6.3885	0.0286
18	$170^o - 180^o$	1.5673	6.9805	0.0487
19	$180^o - 190^o$	1.5118	6.3177	0.0303
20	$190^o - 200^o$	1.4495	6.0443	0.0314
21	$200^o - 210^o$	1.4274	5.8642	0.0439
22	$210^o - 220^o$	1.4468	5.5745	0.0506
23	$220^o - 230^o$	1.5327	5.7806	0.0514
24	$230^o - 240^o$	1.4806	6.0133	0.0522
25	$240^o - 250^o$	1.3757	5.7182	0.0276
26	$250^o - 260^o$	1.3619	5.7480	0.0184
27	$260^o - 270^o$	1.2997	5.5349	0.0196
28	$270^o - 280^o$	1.3465	4.9549	0.0130
29	$280^o - 290^o$	1.3770	4.9706	0.0126
30	$290^o - 300^o$	1.3903	5.3031	0.0171
31	$300^o - 310^o$	1.4458	5.7484	0.0152
32	$310^o - 320^o$	1.4943	5.7919	0.0181
33	$320^o - 330^o$	1.4531	5.8531	0.0216
34	$330^o - 340^o$	1.4742	5.8428	0.0222
35	$340^o - 350^o$	1.4663	5.9339	0.0247
36	$350^o - 360^o$	1.5042	6.5513	0.0302

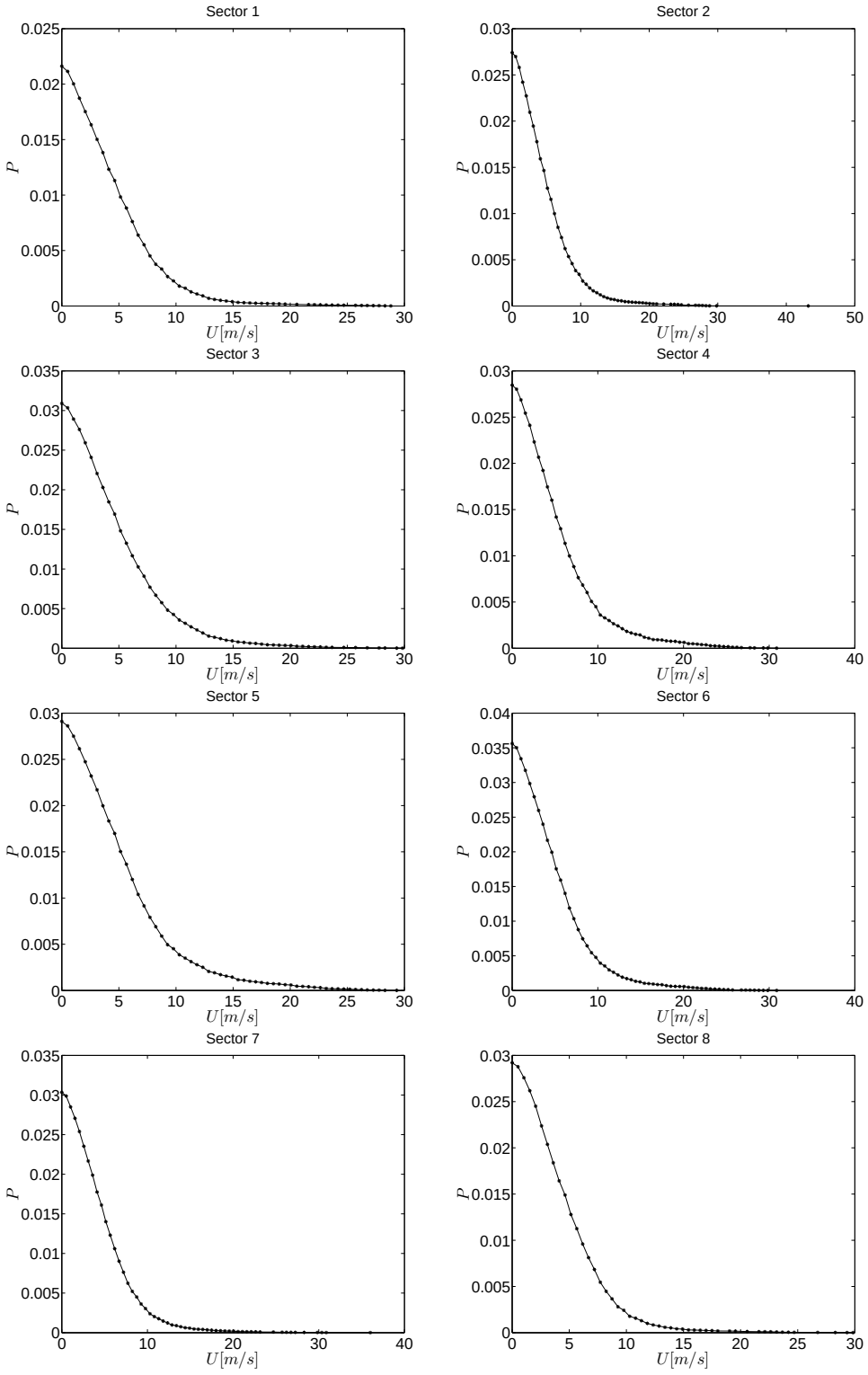

Fig. 3.4 Probability of occurrence $P_{H,i}(U > u, \theta_{inf,i} < \theta < \theta_{sup,i}) = (1 - P_0)P_i^*(\theta_{inf,i} < \theta < \theta_{sup,i})P_i^*(U > u|\theta_{inf,i} < \theta < \theta_{sup,i})$ for each sector.

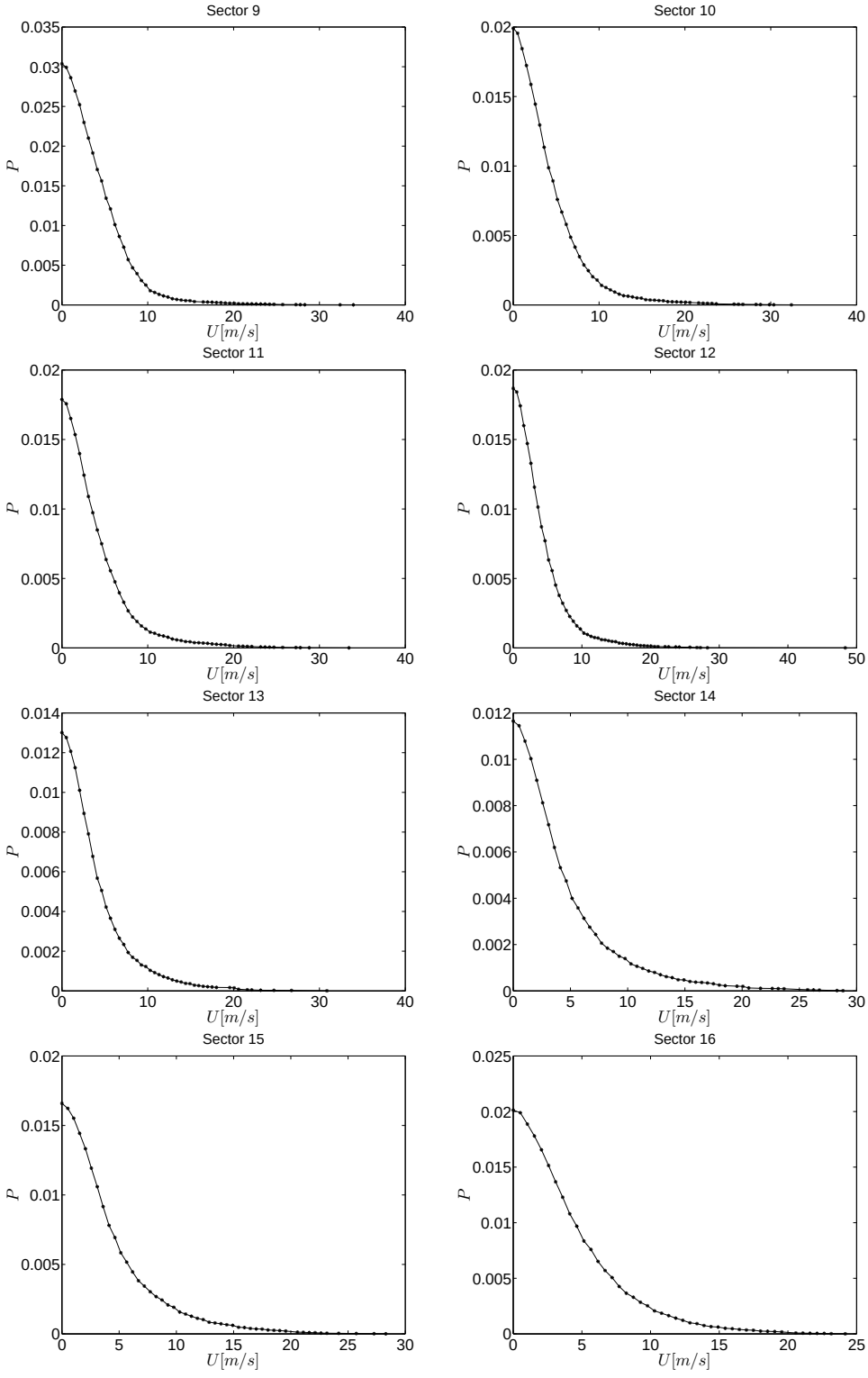

Fig. 3.4 (continued).

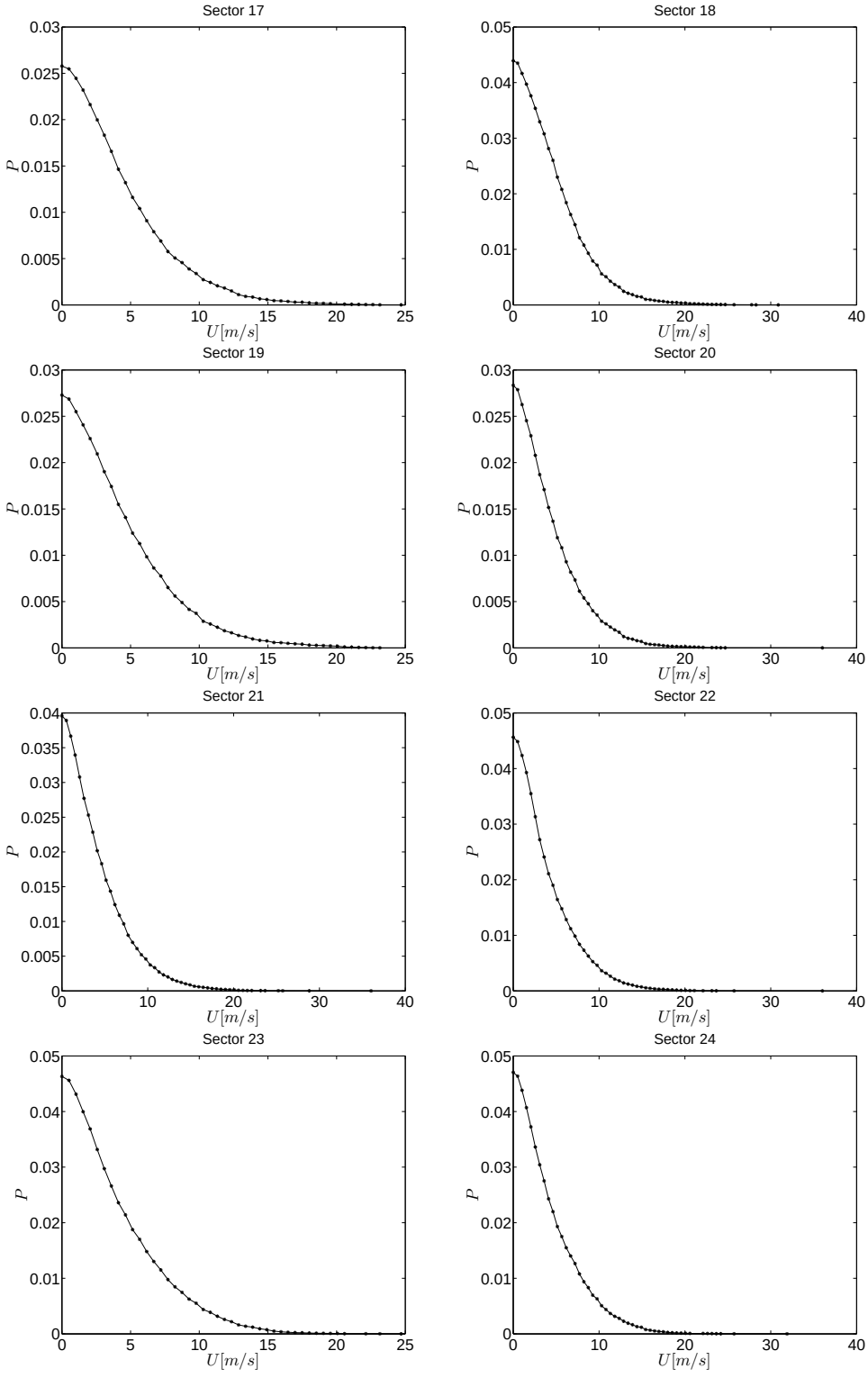

Fig. 3.4 (continued).

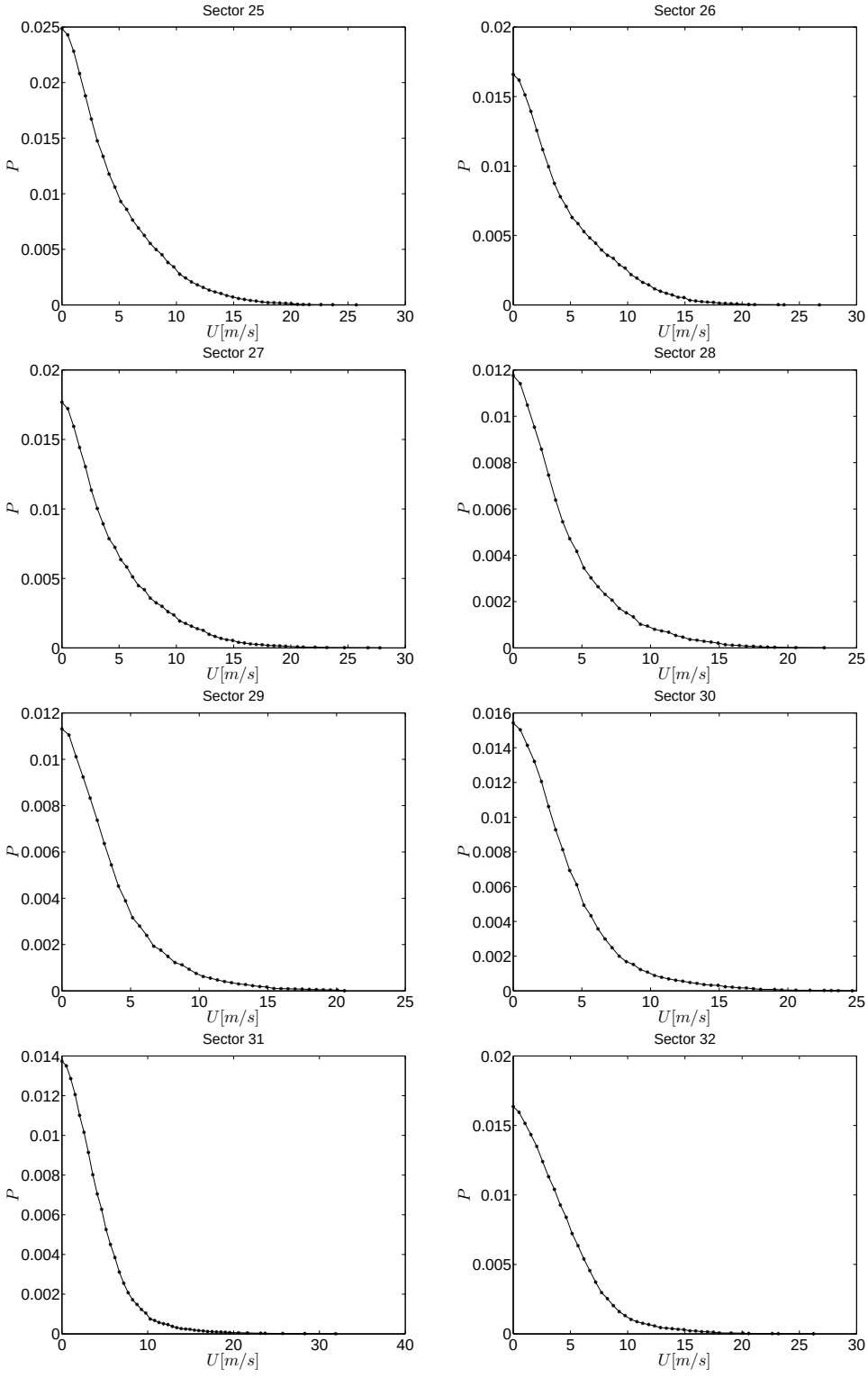

Fig. 3.4 (continued).

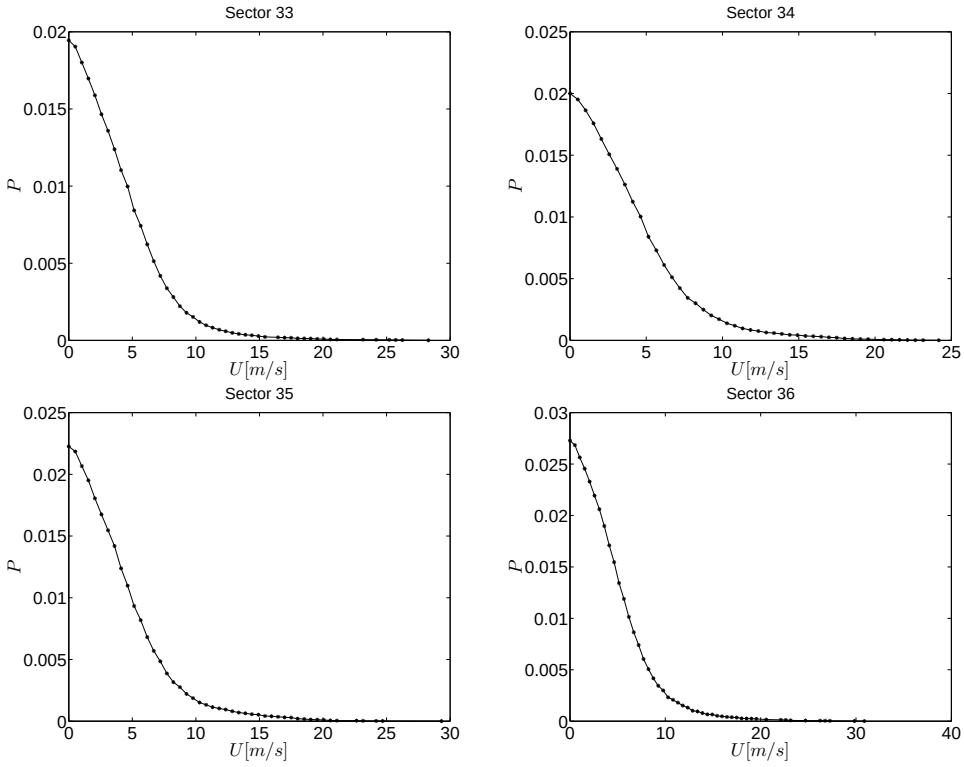

Fig. 3.4 (continued).

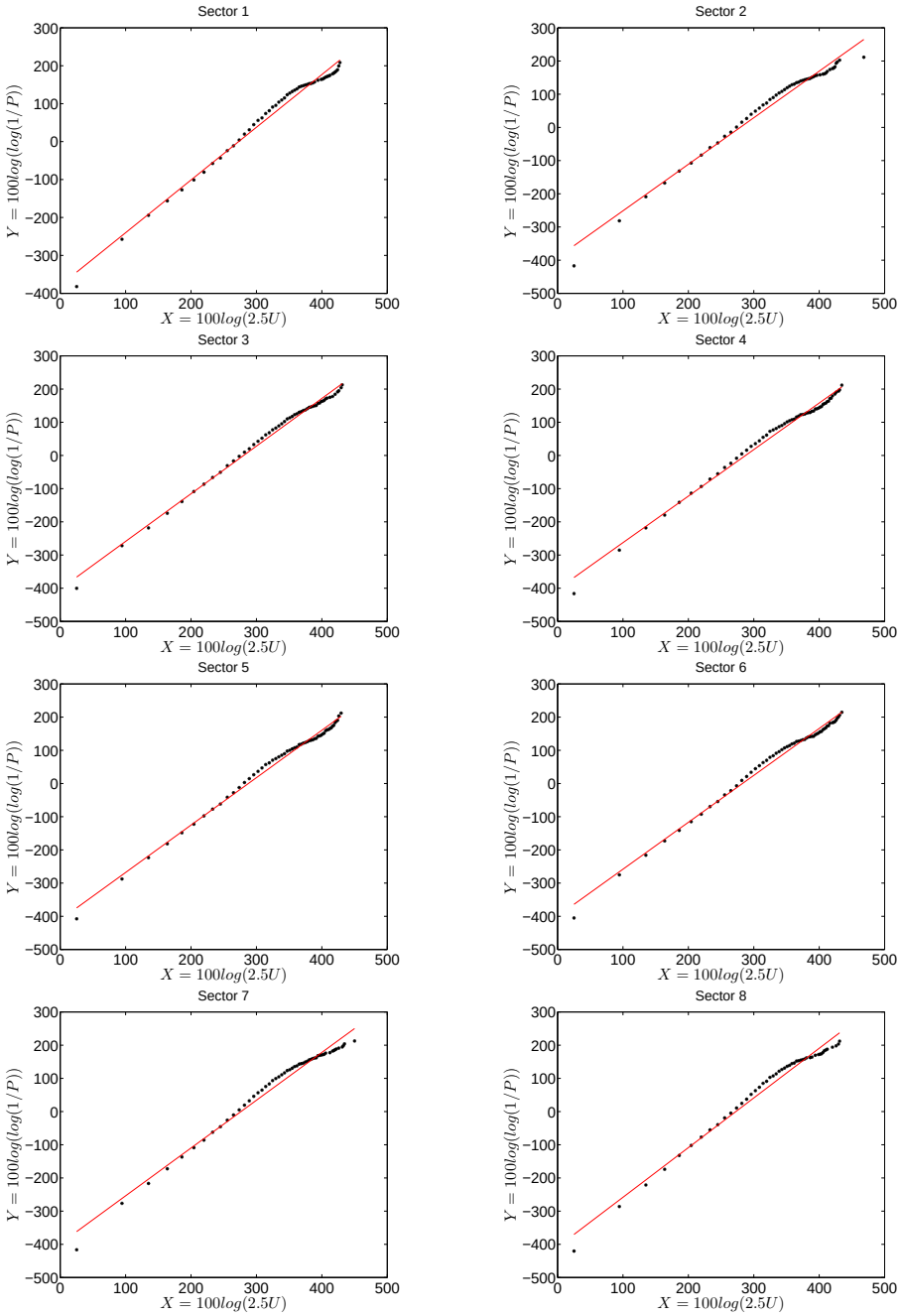

Fig. 3.5 Auxiliary variable plane for each sector [Eqs. (3.3)].

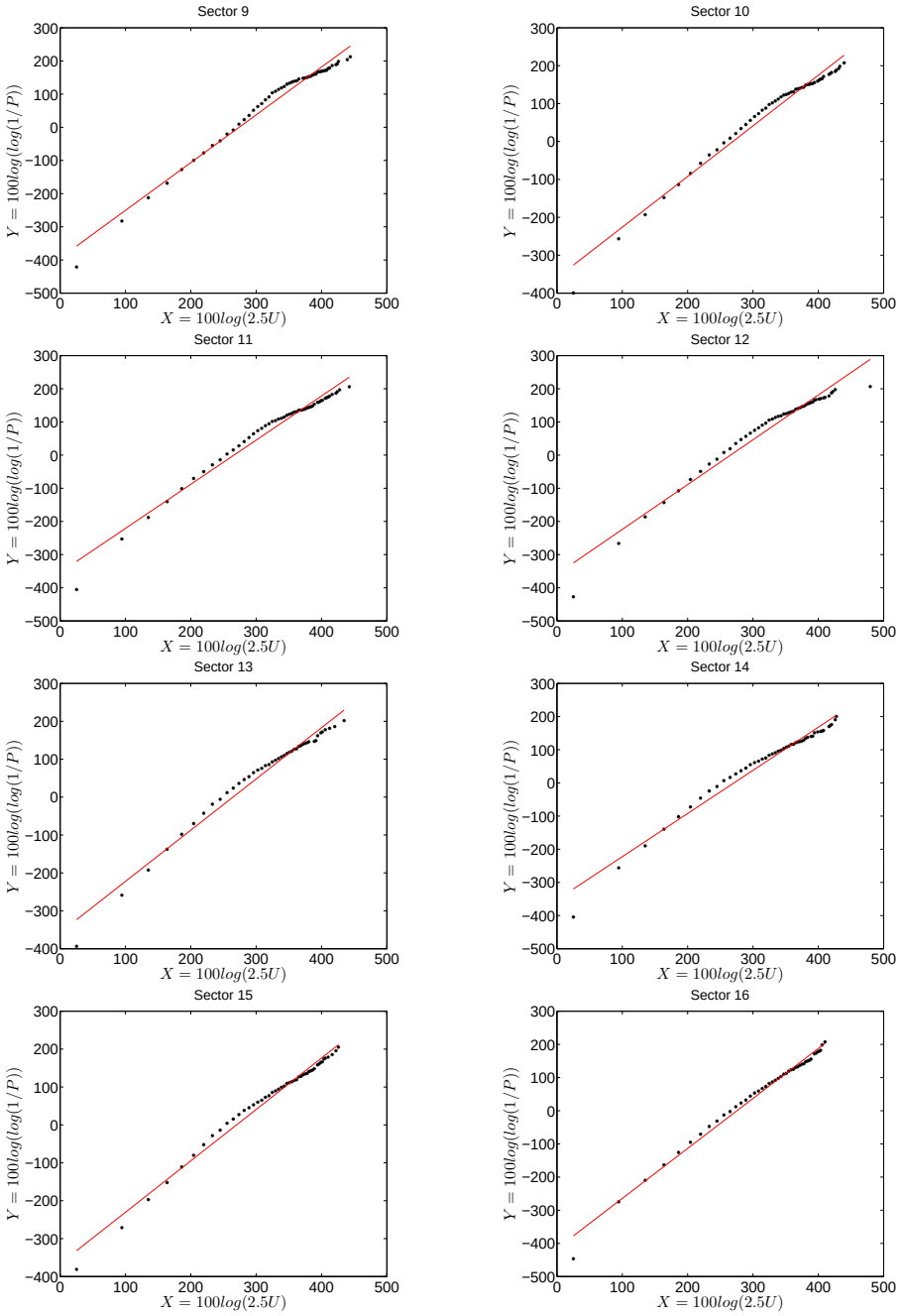

Fig. 3.5 (continued).

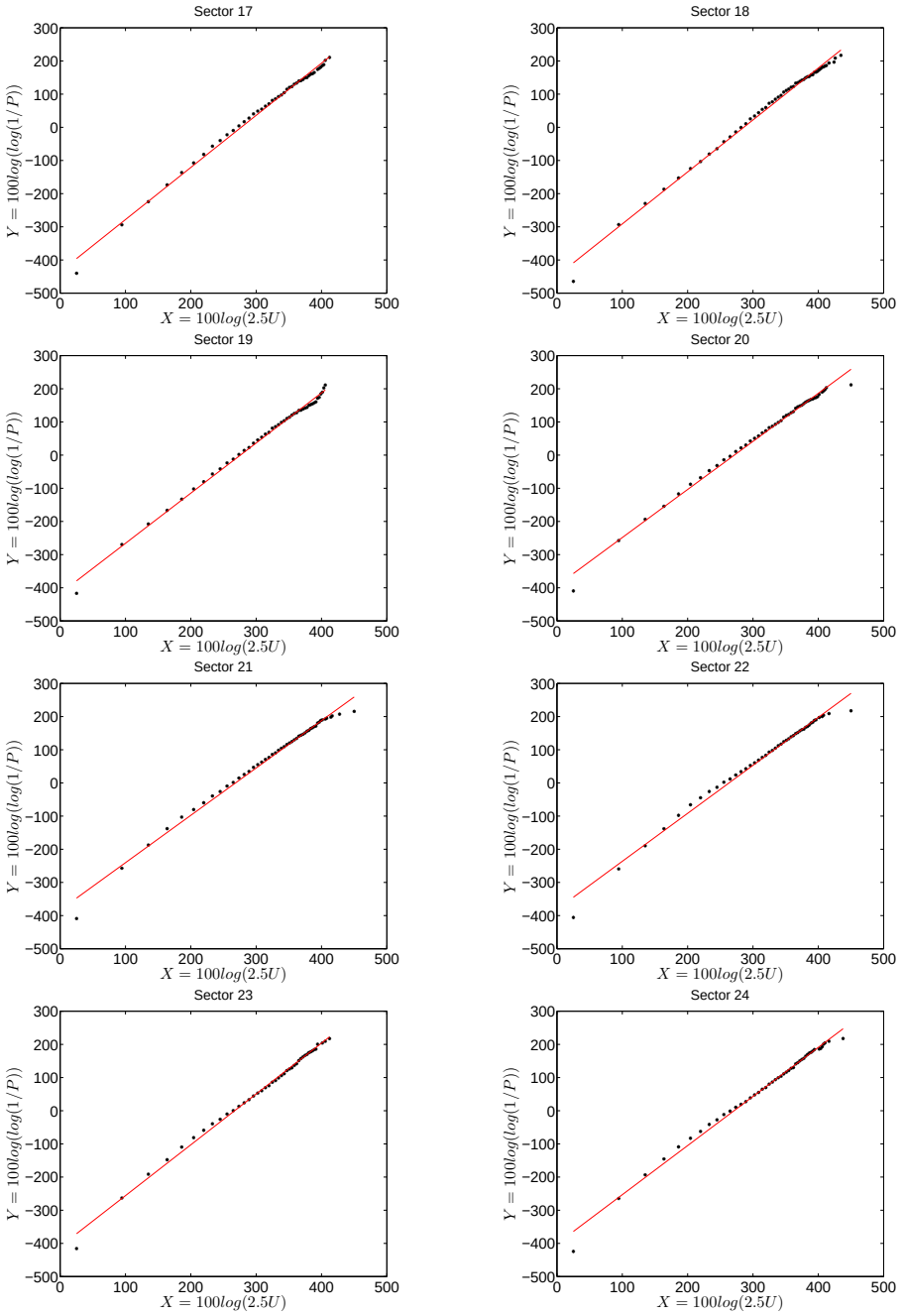

Fig. 3.5 (continued).

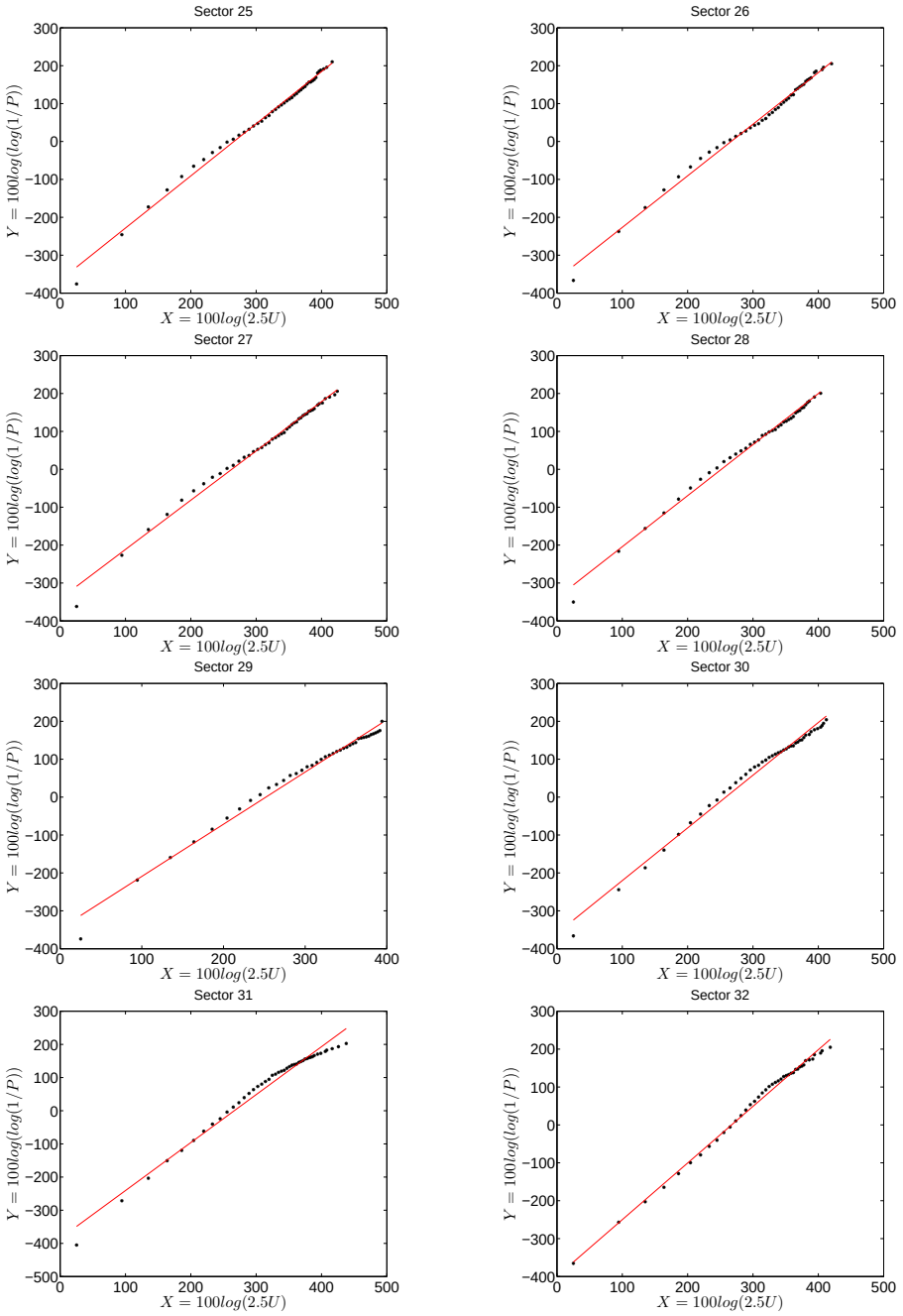

Fig. 3.5 (continued).

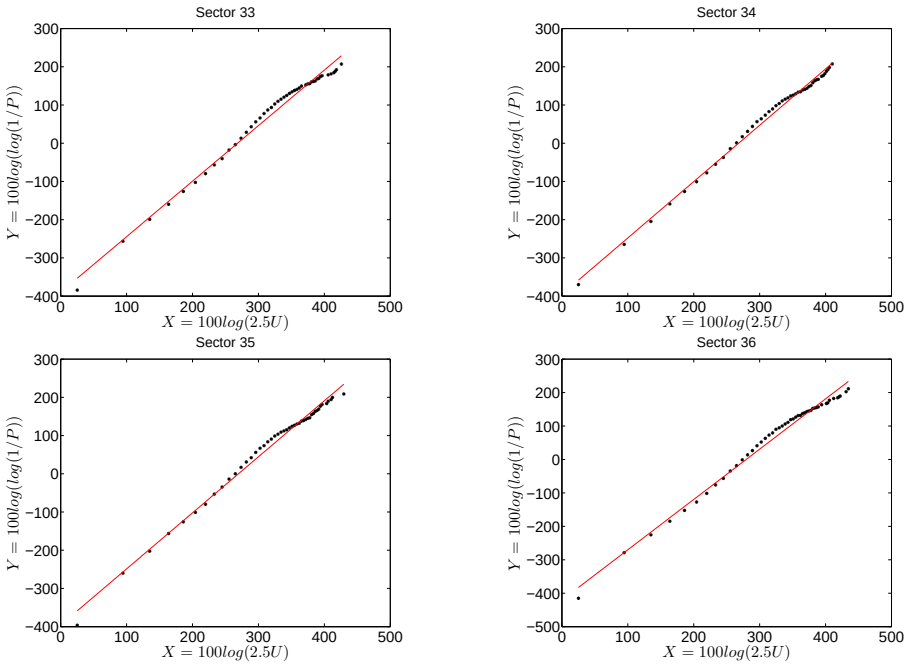

Fig. 3.5 (continued).

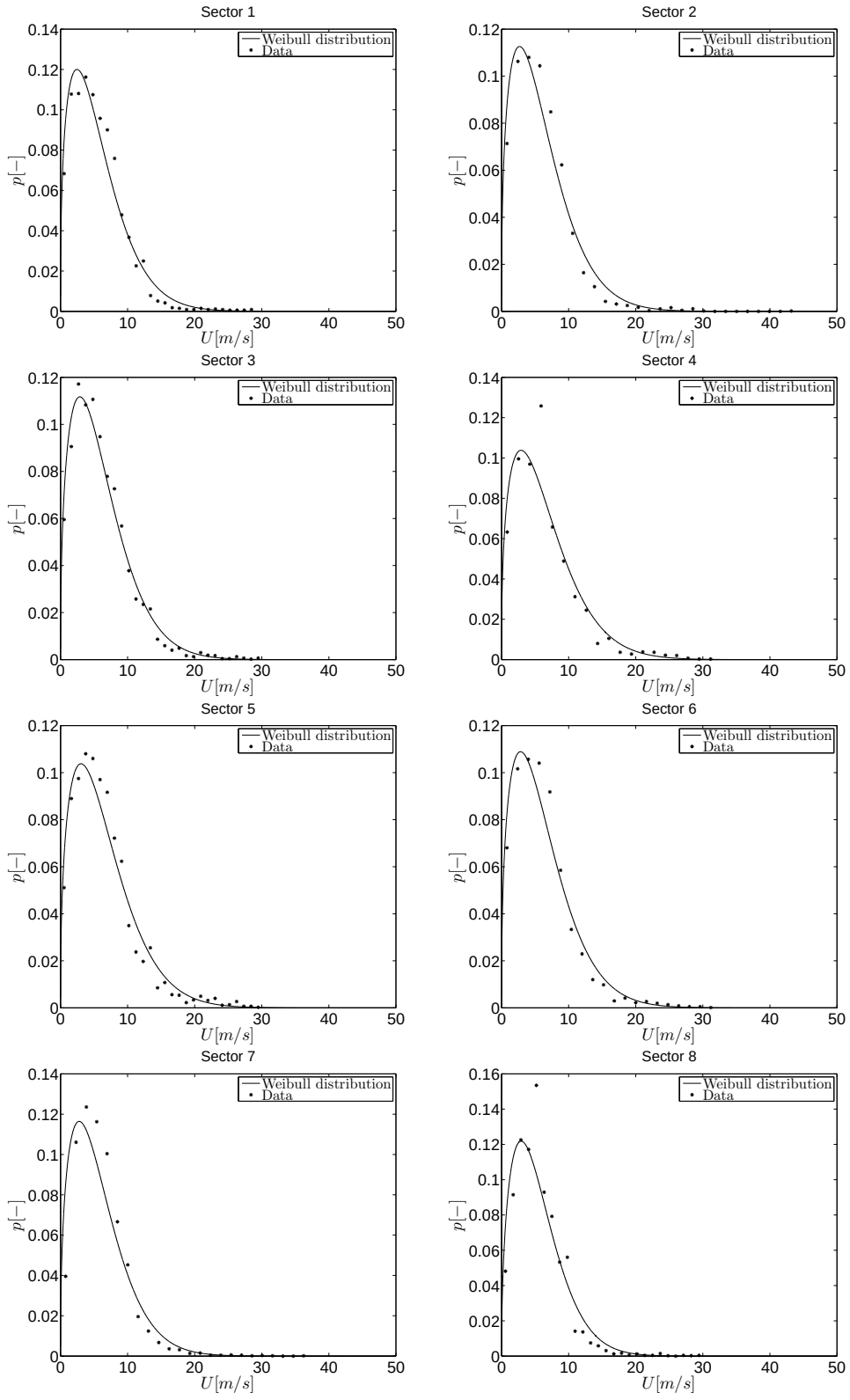

Fig. 3.6 Probability density function $p_i^*(u < U < u + du | \theta_{inf,i} < \theta < \theta_{sup,i})$ for each sector [Eq. (3.15)].

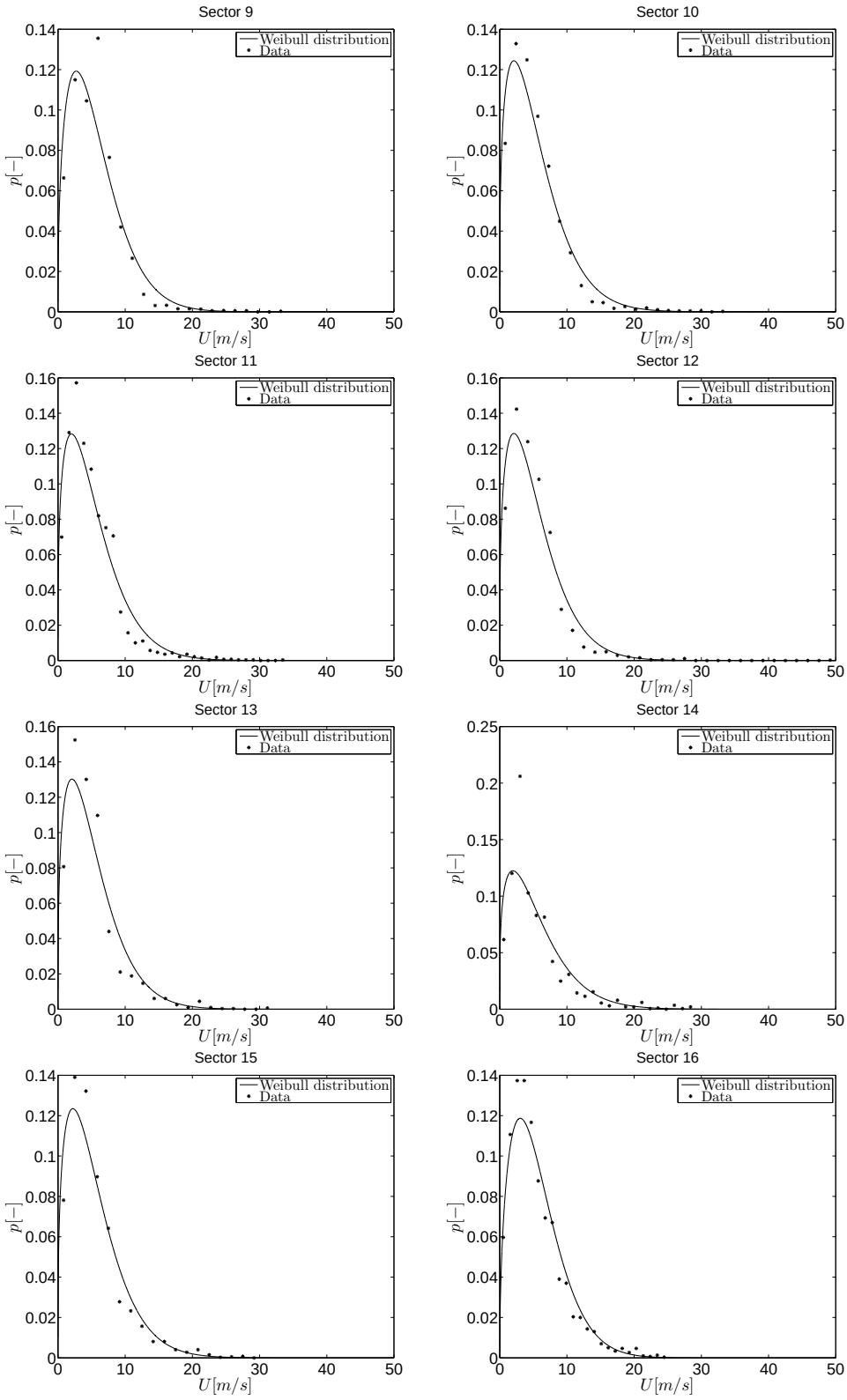

Fig. 3.6 (continued).

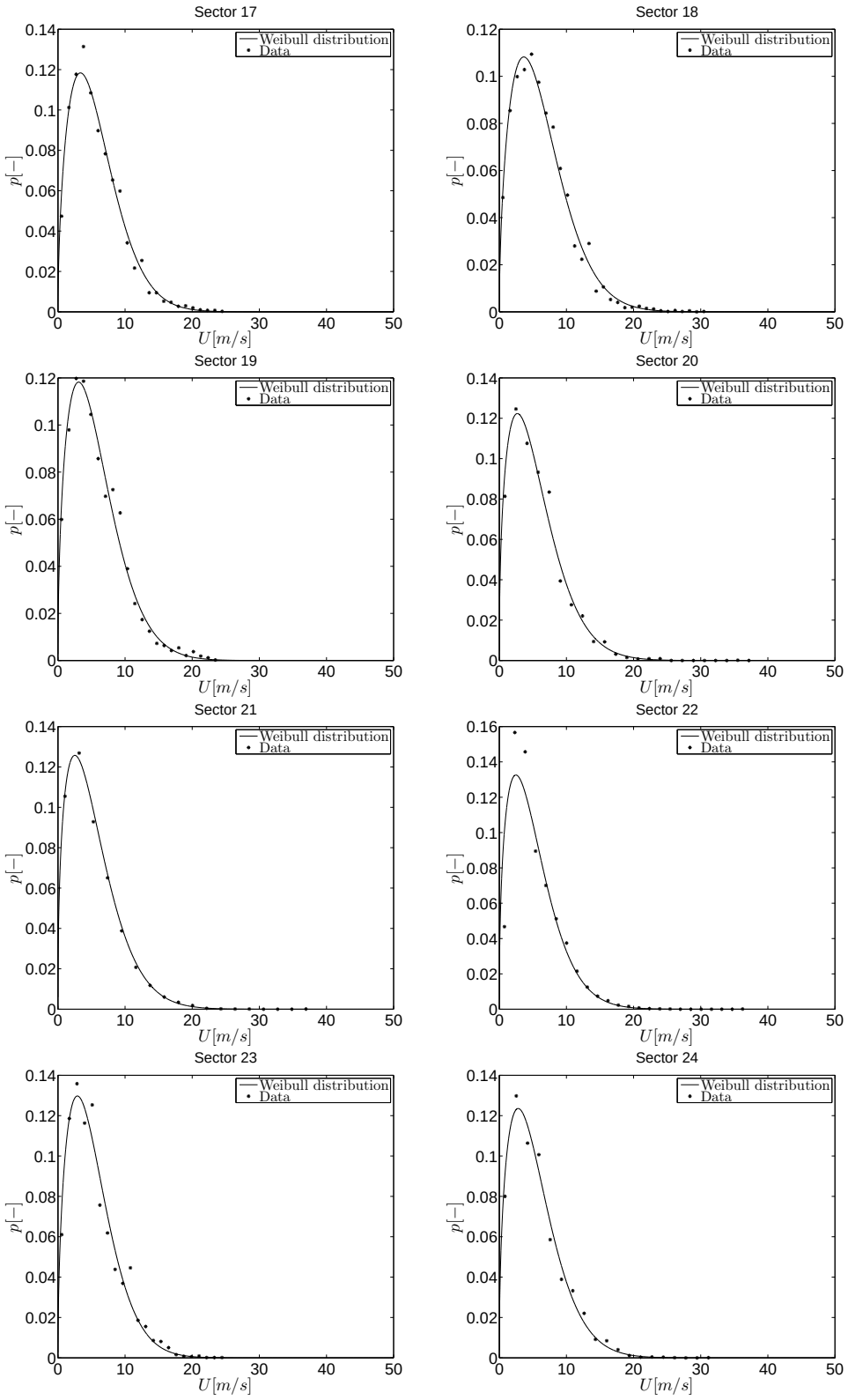

Fig. 3.6 (continued).

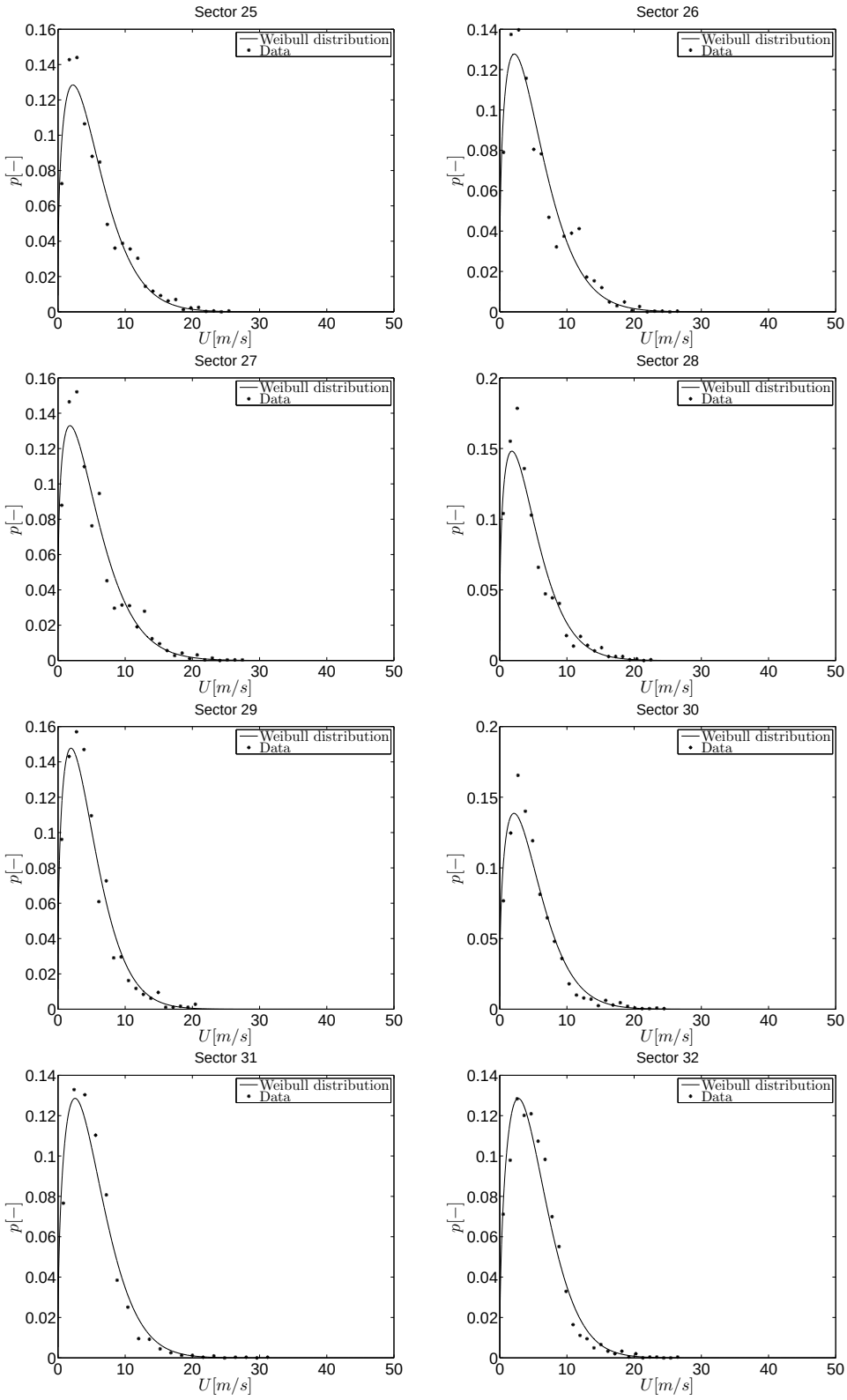

Fig. 3.6 (continued).

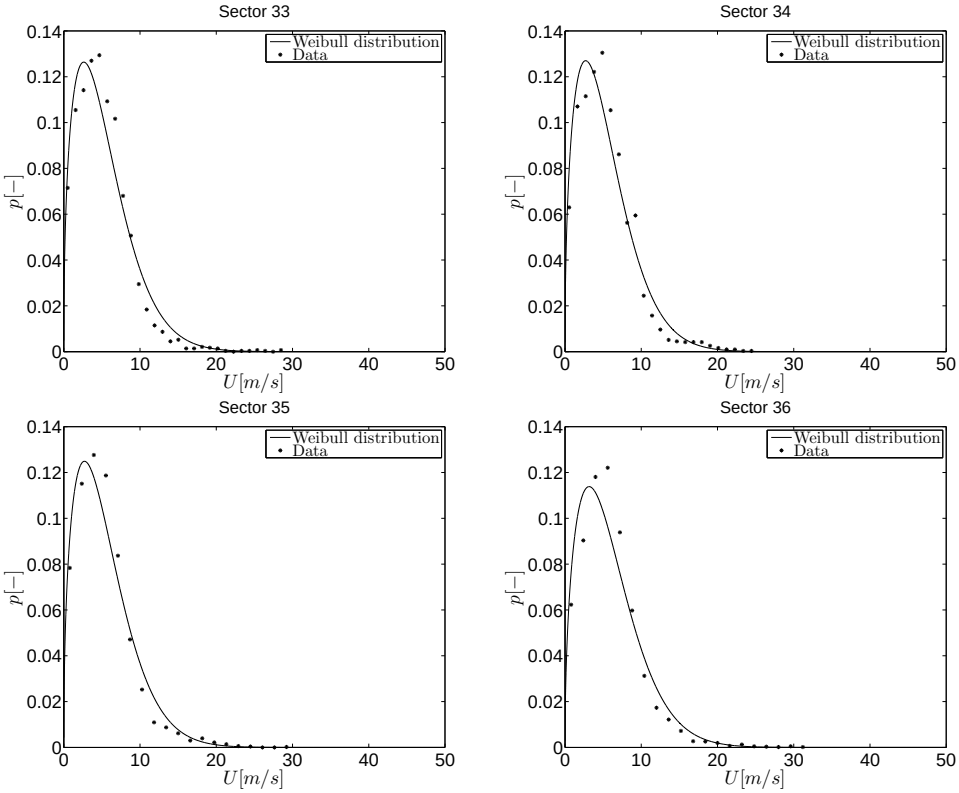

Fig. 3.6 (continued).

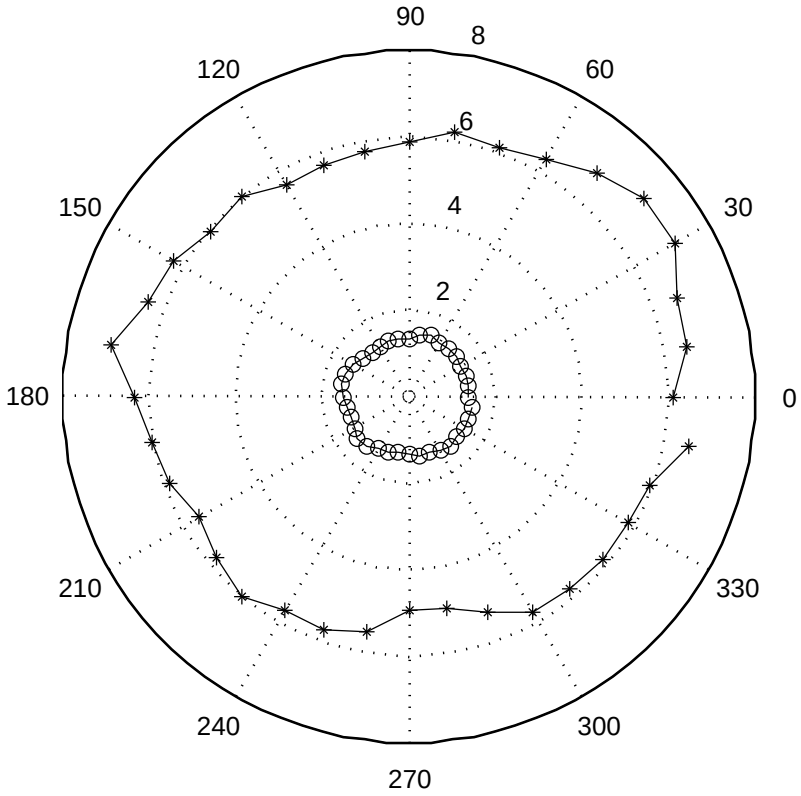

Fig. 3.7 Coefficients of the Weibull distribution for each sector: a (circle points); b (star points).

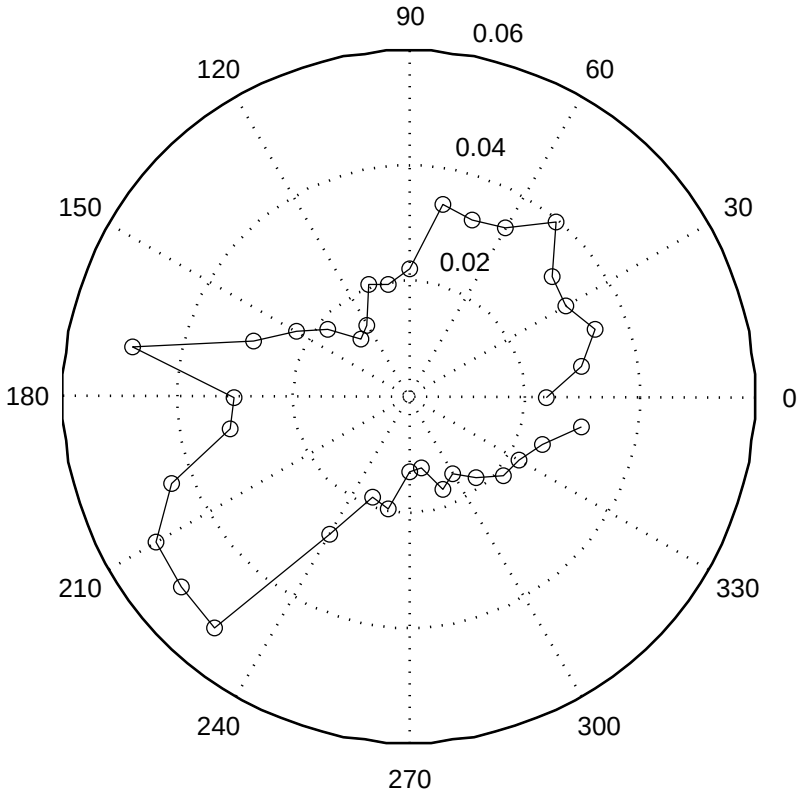

Fig. 3.8 Probability for each sector $P_i^*(\theta_{inf,i} < \theta < \theta_{sup,i})$ [Eqs. (3.18)].

Chapter 4

Vortex-Induced Vibration of Bridge Decks

4.1 Introduction

A bridge deck can be classified as a *bluff body*, i.e., a body in which its interaction with a fluid stream generates a separated flow over a substantial portion of its surface. For sharp-edged bluff bodies (e.g., rectangular cylinder), the separation points are fixed at its salient edges, whereas for bluff bodies with curved surface (e.g., circular cylinder) separation depends both on the shape and on the state of the boundary layer (Bearman, 1984). If separation of the boundary layer occurs, vorticity is introduced inside the wake and its behavior strongly influences the flow around the body as well as the corresponding actions (Buresti, 1998).

One of the main features of a bluff body is *vortex shedding*, which is a phenomenon observed since the antiquity, just thinking at the aeolian tones emitted by taut wires in a wind flow. In the 15th century, among the hydraulic studies of Leonardo da Vinci, experiments about the vortices in the wake of obstacles placed in a river (Fig. 4.1) were conducted (Da Vinci, 1828). Strouhal, in 1878, understood that taut wire vibrations were produced by the alternating shedding of vortices from both sides. Moreover, he found that the aeolian tones were proportional to the wind

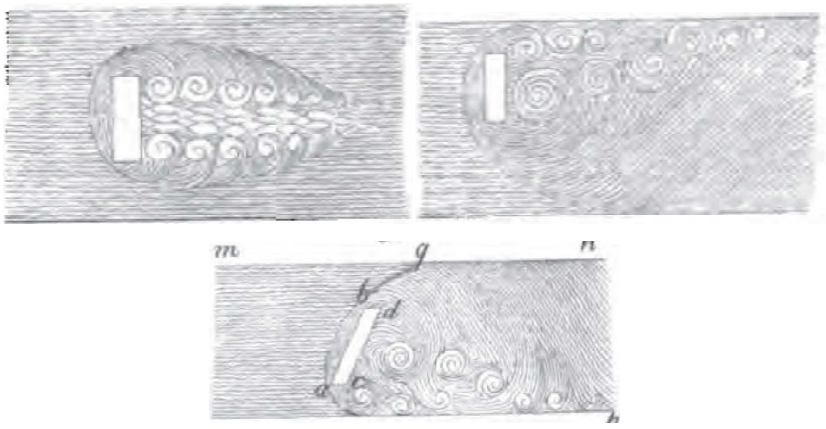

Fig. 4.1 Drawings on river flow around an obstacle (Da Vinci, 1828).

speed divided by the wire diameter and that the sound increased when the aeolian tones coincided with the wire natural frequency. In 1879, Lord Rayleigh observed that a violin string vibrated mainly in the cross flow direction than in the flow one. Benard, in 1908, stated that the periodicity of the wake of cylinder should be associated with the vortex shedding (Blevins, 2001). Von Karman in 1911, evaluating the stability of a vortex within two parallel rows of ideal inviscid vortices of opposite sign, found that the configuration was always unstable except for a particular antisymmetrical configuration having a particular ratio of l/h, where l is the distance between two consecutive vortices in the same row and h is the distance between the two rows (Buresti, 1998).

Vortex-Induced Vibration, called *lock-in* as well, is intended as a phenomenon in which the vibration of a body, immersed in a fluid flow, is governed by the shedding of vortices from its surface. Such a condition is realized for a bridge deck when the frequency of vortex shedding is very close to one of its natural frequencies, so large vibrations can be observed and both fatigue and discomfort problems can occur.

To shed light onto the complex behavior of bridge deck sections during vortex-induced vibrations, the understanding of the vortex shedding phenomenon on stationary elementary bluff bodies could be an useful guide (Section 4.2). Subsequently, the Section 4.3 deals with a brief literature review of oscillating bluff cylinders. Section 4.4 reports the limited numer of works present in the literature on yawed cylinders. Finally, the chapter ends with the conclusions.

4.2 Vortex shedding from fixed bluff bodies

On the phenomenon of vortex shedding from fixed bodies, hundreds of papers have been published. Therefore, considering the object of this work, an exhaustive explanation should take too much space, this is let to review papers (Marris, 1964; Mair and Maull, 1971; Berger and Wille, 1972; Bearman and Graham, 1980; Bearman, 1984; Williamson, 1996; Buresti, 1998; Matsumoto, 1999) and a famous book (Blevins, 2001).

Let us consider an infinitely long, rigid, and unconfined cylinder in a uniform oncoming cross-flow. In wind tunnel this ideal condition can be approximatively reproduced by a *sectional model*, which is a very rigid cylinder with a large enough *aspect ratio*[1] and with suitable end conditions, with very small solid blockage ratio (wall confinement) and free stream turbulence.

If the cylinder has a smooth surface as well, its roughness effects are negligible and a classical view of a vortex street can be observed (Fig. 4.2). Regions of concentrated vorticity with alternate senses of rotation are shed into the downstream flow from alternate sides of the body (Williamson, 1996).

An insight into the mechanism of vortex shedding was the *Gerrard's vortex-formation model* (Gerrard, 1966). The mutual interaction between the two separating shear layers is the key of the model. The circulation of a separated shear layer raises the corresponding vortex until it is strong enough to draw the opposing shear layer across the near weak. When the concentration of the opposite vorticity is sufficient, it cuts off further supply of circulation to the growing vortex, which is

[1]Defined as the ratio between the length of the model and its maximum cross-dimension; as experiences showed, it should be greater than 5 (Berger and Wille, 1972).

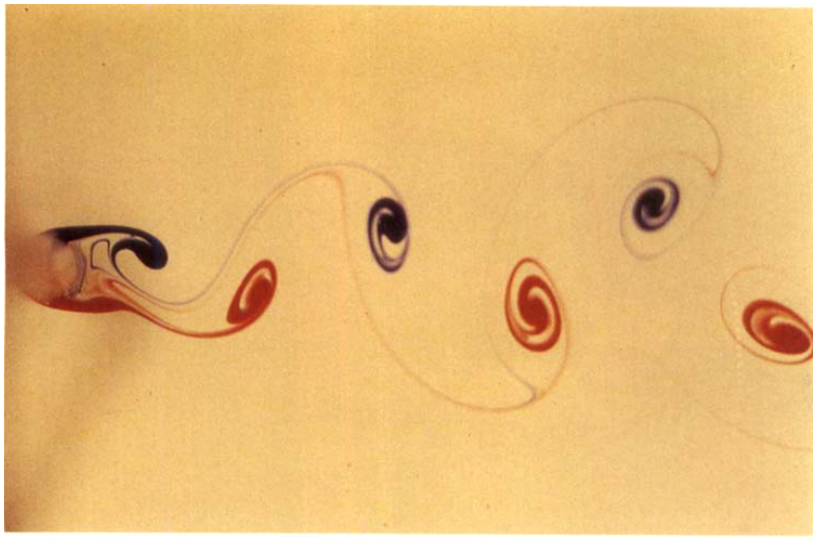

Fig. 4.2 Dye traces in a Karman vortex street behind a circular cylinder (Perry *et al.*, 1982).

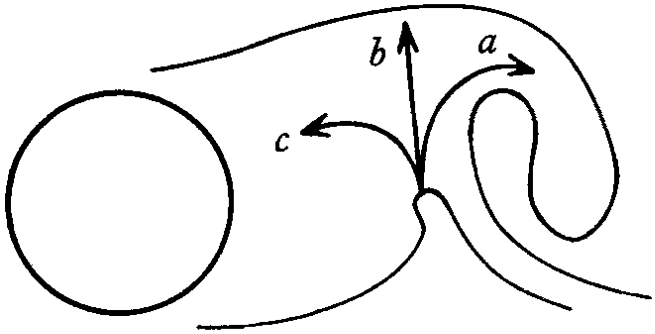

Fig. 4.3 Sketch of the formation region: arrows showing reverse flow (c) and entrainment (b) and (a) (Gerrard, 1966).

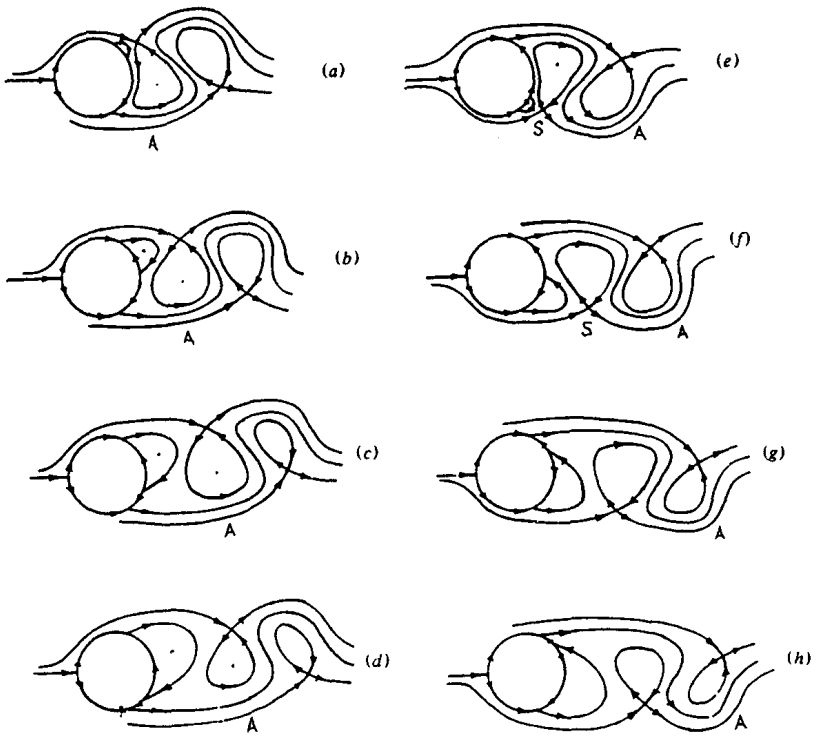

Fig. 4.4 Simplified model of vortex shedding (Williamson, 1996).

then shed. In Fig. 4.3 three entrainment processes are shown. Entrainment flow (a) is engulfed into the growing vortex while (b) goes into the developing shear layer, fluid (c) is temporarily entrained into the near-wake region (Bearman, 1984).

Another significant contribute can be found in Perry *et al.* (1982) analyzing instantaneous streamlines, obtained by flow visualizations, using *critical-point theory*. In a streamline pattern the points in which their slope is indeterminate are called *critical points*. The *saddle points* on the body contour can be considered either separation or reattachment points. In Fig. 4.4 only the streamlines that leave or terminate at a saddle point, called *separatrices*, are shown (Buresti, 1998). This model can be related to Gerrard's model, indeed, following Fig. 4.4, the anticlockwise vortex A is growing from (a) to (d) until a saddle point S (e), formed at the lower side of the body, cuts off any new supply of vorticity to the vortex and forms a new vortex at the body (Williamson, 1996).

The main parameter that describes vortex shedding for a generic section is the *Strouhal number St*, which is defined by:

$$St = \frac{f_s D}{U} \tag{4.1}$$

where f_s is the vortex shedding frequency, D is a significant cross dimension of the section and U is the mean wind velocity of the oncoming flow.

Finally, to characterize completely the aerodynamic of such a model, aerodynamic forces must be considered. In particular, for any two dimensional body immersed in a flow three forces can be individuated: drag, lift and torque. The first one has a frequency double than that of the lift force but its magnitude is almost

negligible. The torque force, theoretically zero due to the axial-symmetry of the section, is produced by the surface friction when each vortex is shed, but its magnitude is negligible as well. So, the only significant force is the cross-flow one, which can be characterized by the R.M.S. (root-mean-square) of the lift coefficient, defined as:

$$C'_L = \frac{L'}{1/2\rho U^2 D} \tag{4.2}$$

where L' is the R.M.S. of lift fluctuations, ρ is the density of the fluid, U is the undisturbed velocity of the oncoming flow and D is the cross-dimension of the section.

The flow field around the body immersed in a smooth stream, the Strouhal number and the R.M.S. of the lift coefficient, characterizing the aerodynamic features of the circular cylinder, depend on the Reynolds number (smooth surface and smooth flow are assumed). Indeed, Fig. 4.5 shows how the wake behind a circular cylinder is strongly influenced by the Reynolds number. In particular, plotting the base pressure coefficient [2] against the Reynolds number (Fig. 4.6), several regimes can be identified (see also Fig. 4.7 and Fig. 4.8). A detailed description of all the regimes for a circular cylinder can be found in Roshko (1993) and Williamson (1996).

Another important aerodynamic feature of an elongated model, e.g. circular cylinder, are the three dimensional effects. The mechanism that regulates three dimensional motions in a nominally two dimensional flow is not clear yet. In particular, there are both *extrinsic* effects (end effects and aspect ratio) and *instrinsic* three dimensional motion arising from natural instabilities. Intrinsic three dimensionality appears at $Re = 180$ and is present thereafter, due to the turbulent nature of the flow at high Reynolds numbers (Roshko, 1993). A detailed description of the instabilities that arise as Reynolds number increases can be found in Williamson (1996). The lack of two dimensionality can be assessed by measuring the spanwise variation of some unsteady quantities that characterize vortex shedding, e.g. fluctuating surface pressures, sectional lift forces or fluctuating velocities just outside the shear layers at separation (Bearman, 1984). Measuring their correlation by

$$R(e,z) = \frac{\overline{e_1 e_2}}{\overline{e^2}} \tag{4.3}$$

where e is the quantity under consideration, 1 and 2 are two points spaced at a spanwise distance z apart and $\overline{(\cdot)}$ is the mean value operator, it can be defined the *correlation length*

$$L = \int_0^\infty R(e,z)dz \tag{4.4}$$

For a circular cylinder, at a Reynolds number between 10^4 and 10^5, L varies between about three and six cylinder diameters (Bearman, 1984).

Finally, because of a body can be located inside both an atmospheric boundary layer or the wake of another body, the effects of the freestream turbulence must be taken into account. For rounded bodies with free separation points, such as circular cylinders, the turbulence effect mainly concerns the transition of the boundary layer over the body surface. This effect implies an anticipation of the *drag crisis*, which

[2] It is a pressure coefficient measured in the middle of the leeward face

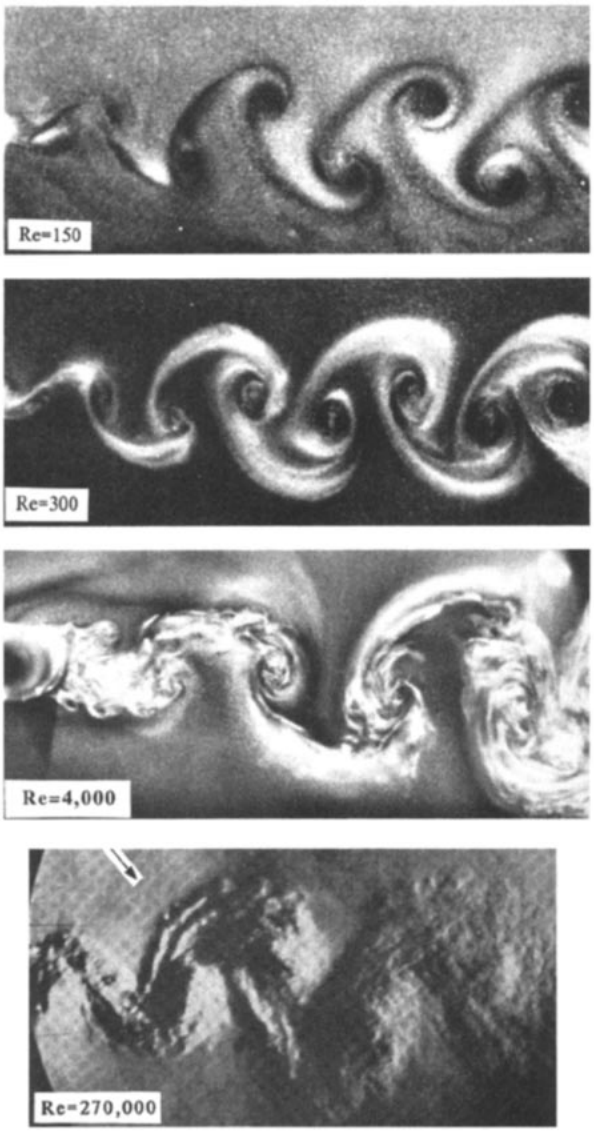

Fig. 4.5 Vortex-street from a circular section for different Reynolds numbers (Williamson, 1996).

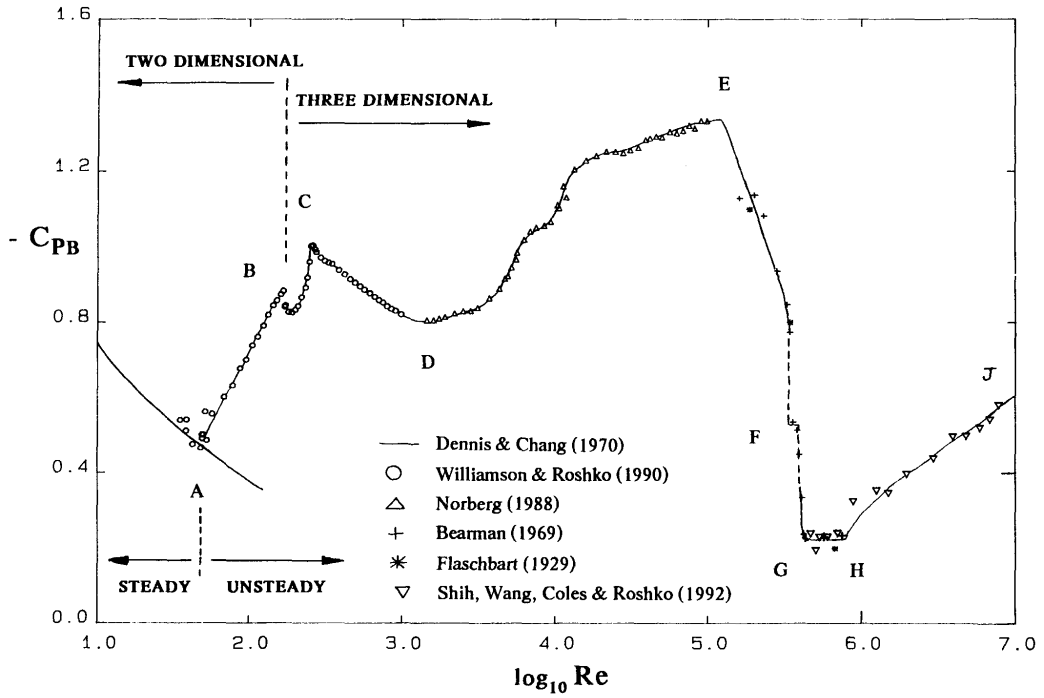

Fig. 4.6 Base pressure coefficient over a wide range of Reynolds numbers (Roshko, 1993).

consists in a reduction of the drag coefficient due to the delayed separation of the turbulent boundary layer over the body surface which produces a reduced width of the wake (Buresti, 1998).

The freestream turbulence field is mainly defined by two parameters: the *intensity* of turbulence I_u and the *longitudinal integral length scale* of turbulence L_u^x. Thus, a correct interpretation of the effects of turbulence must go towards the knowledge of the effects of each of these parameters. According to Basu's measurements, by increasing the intensity of turbulence with relatively small scale (of the order of one diameter), one obtains in the subcritical range a decrease of drag and then, after intensities of around 4%, an increase of it (Basu and Vickery, 1983). Moreover, small scale of turbulence ($L_u^x/D = 0.36$) can more easily affect the boundary layer, i.e., to anticipate the transition, than the large scales ($L_u^x/D = 4.3$).

4.3 Vortex shedding from oscillating bluff bodies

As experimental results have confirmed, the flow field generated by vortex shedding around an oscillating bluff body can show significant differences from that around a fixed one. In particular, if the body oscillates or the oncoming flow has an imposed oscillation or an acoustic noise is present, the flow field results completely modified and an increase of the span-wise correlation of the body is observed (Bearman, 1984). For the scope of the present work, only the vortex shedding from oscillating bluff bodies is treated.

Elastic or elastically supported cylinder with bluff section, characterized by a

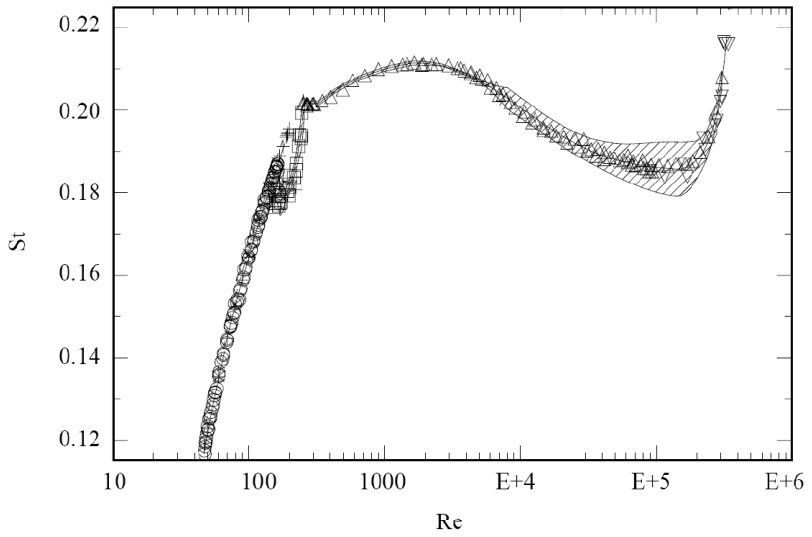

Fig. 4.7 Strouhal number versus Reynolds number (Norberg, 2003).

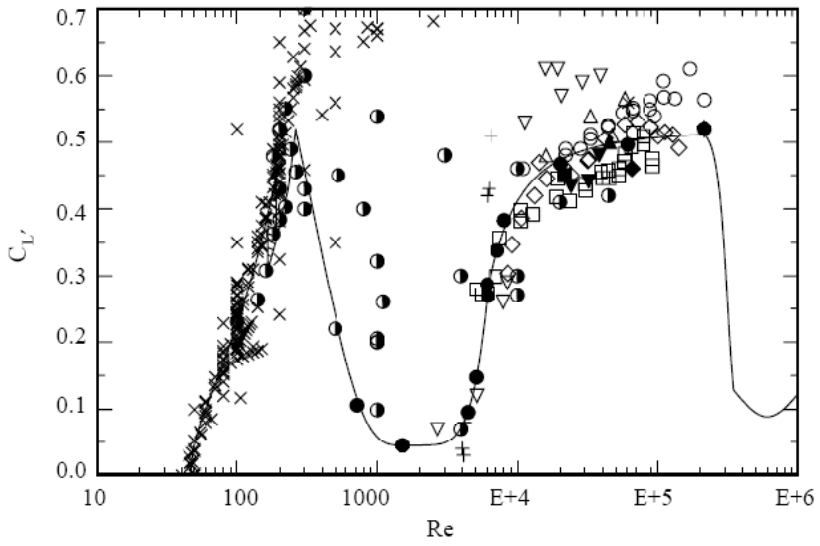

Fig. 4.8 R.m.s. lift coefficient versus Reynolds number (Norberg, 2003).

suitable *afterbody*[3], can show large across-wind oscillations when the vortex-shedding frequency is very close to the natural one. The Strouhal relation is violated for a range of ±25-30 % of the natural frequency and the vortex-shedding is controlled by the body motion. Such a phenomenon is called *lock-in, locking-on, synchronization, hydroelastic or fluid-elastic oscillations, wake capture, self-controlled or self-excited oscillation*, etc (Sarpkaya, 1979).

The parameters $U_{red} = U/f_n D$, called *reduced velocity*, and $Sc = 4\pi m\zeta/\rho D^2$, called *Scruton number*, are of major importance in determining the response and the range of synchronization for a given body (see Section 7.2 for more details on the importance of the Scruton number).

A famous example of the response obtained during lock-in oscillations of a lightly damped circular cylinder is reported in Feng (1968) (Fig. 4.9) [see Bearman (1984)]. As it can be observed, the higher response amplitude is observed when the reduced velocity is increased over a certain range than when it is decreased back over the same range. Such a phenomenon is called *hysteresis effect* and nowadays it is not fully understood yet. The jump in the response may be the consequence of a variable structural damping (e.g. structure support-wind interaction) or of a nonlinear spring behavior (Sarpkaya, 1979).

It is also known that the lock-in range is dependent on oscillation amplitude; in particular, the larger the amplitude the larger the range over which the vortex shedding frequency is locked to the body frequency. In Feng's results (Fig. 4.9) the lock-in range is extended from $U_{red} = 5$ to 7.4 but the cylinder freely vibrates and then also the amplitude changes. During forced-vibration tests, when the amplitude is fixed, the range of synchronization depends on the level of amplitude (Bearman, 1984).

The position of the resonant point, which is equal to the inverse of the Strouhal number, inside the lock-in range strongly depends on the cross-section of the body (Bearman, 1984). Experimental studies on different cross sections, such as D-section, circular section, triangular section and flat plate, can be found in Bearman and Currie (1979), Bearman and Obasaju (1982) and Bearman and Davies (1977).

Bishop and Hassan (1964), Honji and Taneda (1968), Tanida *et al.* (1973), Sarpkaya (1978) and Torum and Anand (1985) observed that during vortex-induced vibrations the drag coefficient C_D shows an increase (Bearman, 1984; Blevins, 2001). Three expressions for the prediction of the increase of the drag coefficient with the oscillation amplitude are reported in Blevins (2001):

$$\frac{C_{D|A_y>0}}{C_{D|A_y=0}} = \begin{cases} 1 + 2.1(A_y/D) & \text{Blevin's figure fit} \\ 1 + 1.043(2Y_{rms}/D)^{0.65} & \text{Vandiver (1983)} \\ 1 + 1.16\{[(1 + 2A_y/D)f_n/f_s] - 1\}^{0.65} & \text{Skop } \textit{et al.} \text{ (1973)} \end{cases} \tag{4.5}$$

where A_y is the amplitude of the transverse motion, $Y_{rms} = A_y/2^{0.5}$ for sinusoidal motion. Third expression is valid if $(1+2A_y/D)(f/f_s) > 1$, where f is the vibration frequency and f_s is the stationary cylinder shedding frequency.

An increase of the fluctuating lift coefficient $\tilde{C}_L$ is observed at lock-in oscillations, which is the result of the improved two dimensionality of the flow in such condition. A physical explanation of such a behavior consists in the increase of the strength of shed vortices over their fixed body values which provides higher values of the fluctuating lift.

[3]It is considered afterbody the part of the body behind the separation point.

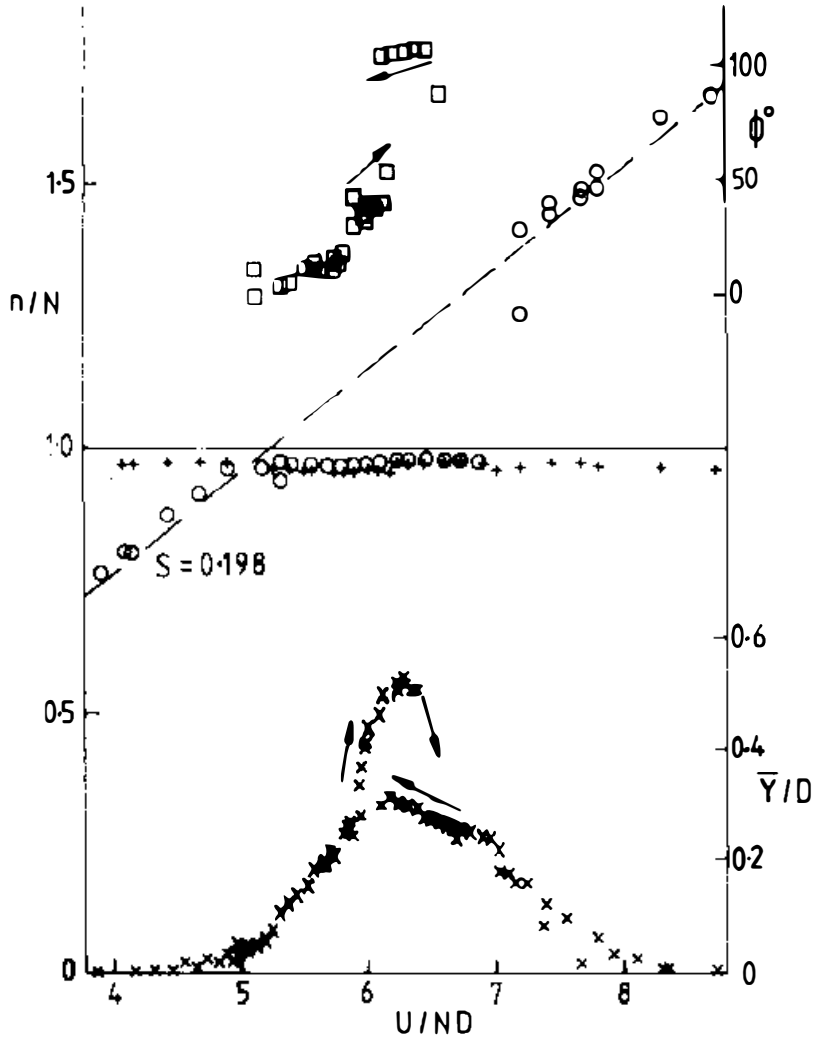

Fig. 4.9 Oscillation characteristics of an elastically-supported circular cylinder with $Sc = 2M\delta_s/\rho D^2 = 0.4$: ∘, vortex-shedding frequency; +, cylinder frequency; □, phase angle; ×, oscillation amplitude (Feng, 1968) [see Bearman (1984)].

The motion of the body gives rise to a synchronization of vortex shedding along the longitudinal length of the body itself. This provides an increase in the correlation length when vortex-induced vibrations occur. The threshold oscillation amplitude over which large increases of the correlation length are observed depends on the shape of the bluff body. In particular, for a circular cylinder the threshold is about 0.05 times the cross dimension, but for bodies with sharp-edges its value can be lower (Bearman, 1984). Fig. 4.10 shows the spanwise correlation of the flow along a square cylinder forced to oscillate at an amplitude of 0.1 times its cross dimension and at a reduced velocity where the vortex shedding and body frequencies coincide (Bearman and Obasaju, 1982). It can be observed that at the resonance reduced velocity the spanwise correlation is higher than those obtained at the same oscillation amplitude but at different reduced velocities.

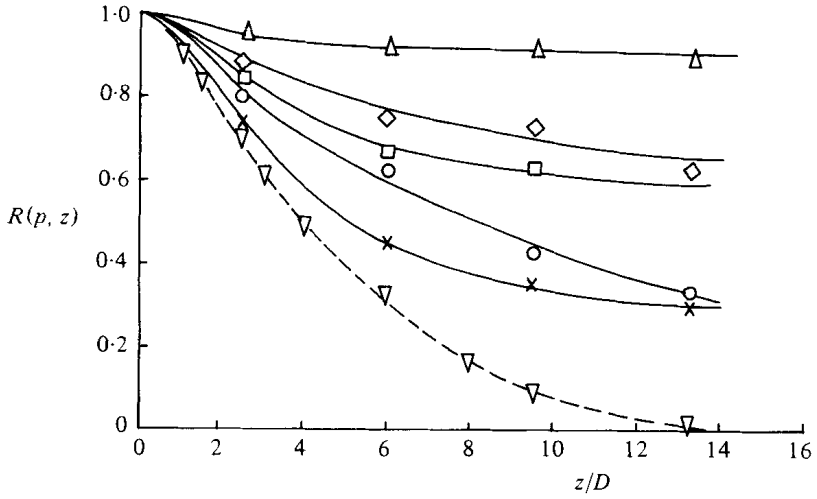

Fig. 4.10 Correlation of surface pressures vs. spanwise separation. $\bigtriangledown$, stationary body. Body oscillating with A/D = 0.1: $\bigtriangleup$ U/fD within the lock-in range 7.3-8.5; $\times$, U/fD = 6.2; $\bigcirc$, 7.0; $\Diamond$, 8.8; $\square$ 12 (Bearman, 1984).

4.4 Vortex shedding from yawed bluff bodies

The aerodynamic and aeroelastic behavior of a yawed bluff body is not fully understood and many conflicting results can be found in the literature. Moreover, to author knowledge, only circular cylinders have been investigated. As usual, the phenomenon has been studied both on fixed and vibrating cylinders.

Investigations on the boundary layer on yawed, infinitely long wings and bodies have shown that the characteristics of laminar boundary layers in planes normal to the axis of the body can be considered as independent of the axial flow (*Independence Principle*[4]). When turbulent flow exists, the flow in normal planes cannot be considered to be independent of the axial velocity (Bursnall and Loftin, 1951; Schlichting, 1979). In particular, the results of the experimental study of Bursnall and Loftin (1951) have shown that the flow and force characteristics of a yawed

[4]Also called *Crossflow Principle* or *Cosine Law.*

circular cylinder cannot be determined only by the component of the flow normal to the axis of the cylinder.

A very short review on vortex shedding from fixed and vibrating yawed circular cylinders may be found in Lucor and Karniadakis (2003).

For stationary cylinders, it seems that for large yaw angles the Independence Principle (IP) cannot be utilized but in the literature there is not agreement on the limit values of the yaw angle θ_{lim} at which the IP loss validity. For Surry and Surry (1967) θ_{lim} should be lower than 70^o. Atta (1968) showed that for $\theta < 35^o$ the vortex shedding frequency decreases nearly like the Cosine law, whereas for larger angles the decrease with increasing angle of yaw is lower than the proposed Cosine Law. Finally, Ramberg (1983) reported that the IP fails because the shedding frequency is always greater than that expected from the IP.

When the cylinder is vibrating, Koopman (1970) noticed a drastic decrease in the cylinder periodic response as well as a drop in the correlation of the lift force along the span for angles of yaw larger than 15^o. King (1977) observed an increase in the cross-flow response with the yaw angle to a corresponding decrease in the reduced damping. Moreover, he also observed sustained oscillations at yaw angles $\theta = 65^o$. Ramberg (1983) concluded that locked-in vortex wakes of vibrating yawed cylinders can be successfully described by the IP.

4.5 Conclusions

A short review on vortex shedding from fixed and oscillating bluff bodies was reported in this chapter to recall the main characteristics of the physical phenomenon necessary to create a mathematical model. The phenomenon under study is characterized by several physical characteristics whose incorporation into a mathematical model represents a very difficult task. However, for design applications to bridge decks the variations of the lock-in range width and the corresponding response with the Scruton number as well as the effects on the response of the angle of yaw should be taken into account. As it will be observed in the next chapter, no model is able to satisfy such requirements. In conclusion, from the experimental point of view, more studies should be carried out especially to understand the effects of the yaw angle.

Chapter 5

Modeling of Vortex-Induced Vibration of Bridge Decks

5.1 Introduction

The analytical prediction of the structural response of an elastically supported cylinder exposed to fluid flow, as a function of structural and flow parameters, would be a fundamental engineering goal. To achieve this objective analytically, the solution of the *Navier-Stokes equations* in the presence of an arbitrarily shaped moving boundary should be necessary. Although research works on CFD (*Computational Fluid Dynamics*) are proliferating, nowadays its application to engineering problems is limited by accuracy and the requirement of long computing time. Therefore, the attempt to construct a semi-empirical model for such a fluid-structure interaction problem seems to be the most convenient way.

In modeling the structural response to the wind is common practice to treat the response in the along-wind and across-wind direction separately. Although the theory of the along-wind response is relatively well developed (Davenport, 1961, 1962), an analogous result for across-wind response has not been obtained so far. Such a discrepancy is probably due to the different number of mechanisms which are involved into the two phenomena. In particular, for the along-wind response, only one mechanism, that of buffeting, is the dominant source of excitation; in contrast, for the across-wind response, three mechanisms play significant roles. The first source is produced by the pressure fluctuations associated with the shedding of vortices. The motion-dependent force, which is generated when the structure oscillate, is a further source. Finally, buffeting force arising from lateral component of turbulence in the oncoming flow completes the list (Vickery and Basu, 1983a).

Since the 1970's, several empirical models to estimate the across-wind response of bluff bodies have been proposed, which can be divided into two main classes:

- Single-Degree-of-Freedom models
- Two-Degree-of-Freedom models

In the next sections, with the objective to draw on them for constructing a new model, a complete state-of-the-art summary on the existing models will be attempted. In the next section, both for historical motivations and to know the main

parameters involved, the *harmonic model* will be treated alone, even though it belongs to the first class. Sections 5.3 and 5.4 treat the previously mentioned two classes of models. Some conclusions are drawn at the end of the chapter.

5.2 Harmonic model

Since the vortex shedding is a quasi-harmonic phenomenon it is reasonable to model its action as an equivalent harmonic function (Wyatt and Scruton, 1981)

$$F = \frac{1}{2}\rho U^2 D\tilde{C}_L sin(\omega_s t) \tag{5.1}$$

where ρ is the air density, U is the mean wind velocity, D is the cross-flow dimension of the body, $\tilde{C}_L = \tilde{L}/\frac{1}{2}\rho U^2 D$ is the amplitude coefficient of the alternating lift force; ω_s is the vortex shedding circular frequency and t is the time. During lock-in ($\omega_s = \omega_n$, where ω_n is the natural frequency of the body) the equation of motion can be written as follows:

$$m\left(\ddot{y} + 2\zeta_n\omega_n\dot{y} + \omega_n^2 y\right) = \frac{1}{2}\rho U_c^2 D\tilde{C}_L sin(\omega_n t) \tag{5.2}$$

and then the response amplitude is:

$$\tilde{y} = \frac{D}{8\pi}\frac{U_c^2\tilde{C}_L}{m\delta_n/\rho D^2} = \frac{D}{4\pi}\frac{\tilde{C}_L}{St^2 Sc} \tag{5.3}$$

where m is the mass per unit of length, y the across-flow degree-of-freedom of the body, ζ_n is the structural damping ratio, ω_n is the natural circular frequency, U_c is the critical velocity corresponding to the condition $\omega_s = \omega_n$, δ_n is the structural logarithmic decrement, St is the Strouhal number and Sc is the Scruton number as defined in the previous chapter. The harmonic model is linear and does not incorporate feedback effects between the structure and the flow. In fact, the coefficient $\tilde{C}_L$ does not depend on the amplitude of the response. As reported by Blevins (2001), by using $\tilde{C}_L = 1$, which is a conservative value for a circular section, the model provides a response of several diameters for most cylinders in water, whereas amplitude exceeding 1.5 diameters are never been estimated.

5.3 Single-Degree-of-Freedom models

Single-degree-of-freedom (SDoF) models are based on the assumption that an acceptable value of the structural response can be predicted if sufficient fluid dynamic effects can be taken into account in terms of a body response variable (Billah, 1989). Considering a bluff body mounted on linear springs and submerged in a fluid stream of uniform velocity U (Fig. 5.1), the following general form for the SDoF models can be used:

$$m\left(\ddot{y} + 2\zeta_n\omega_n\dot{y} + \omega_n^2 y\right) = F\left(y, \dot{y}, \ddot{y}, U, t\right) \tag{5.4}$$

where F is the fluid-induced force function per unit span. The effect of the wake dynamics into this equation can be incorporated by a correct choice of the aeroelastic function F. Following a common practice in the field of airfoil aeroelasticity, the

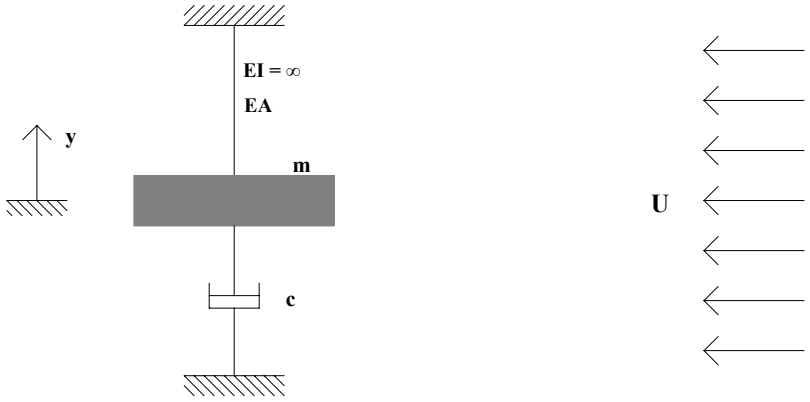

Fig. 5.1 Reference scheme for SDoF mathematical models.

coefficients in the SDoF models are postulated to be dependent on the reduced frequency $K = \omega_n D/U$.

According to Billah (1989), SDoF models can be subdivided into two classes:

- Models based on negative damping
- Models based on forced-coefficient data

The practical difference between the two types of models is that the aeroelastic coefficients in the former can be obtained by freely vibrating cylinders whereas the latter needs forced-vibration tests. In the following the two groups will be treated separately.

5.3.1 Negative damping models

In the negative damping models, the physical mechanism of energy transfer from the wake to the body during lock-in, is considered as an instability created by the downfall to zero of the total damping of the system (*Negative-damping-type instability*). Hence, the forcing F may be composed by an aeroelastic damping term whose coefficient is a function of the reduced frequency K. The other main characteristic, the self-limiting vibration, must be accompanied by a higher-order aeroelastic damping term that limits the divergent vibrations otherwise occurring. In the following, the models belong to this class will be chronologically explained.

Scruton linear model (1963)

As far as the writer knows, the first model of the unsteady forces acting on a bluff structure oscillating in a wind flow was proposed by Scruton (1963). Analogously to the methods used for airfoils, the aeroelastic forces could be represented by harmonic components in phase and in quadrature with the motion, in which the involved coefficients generally are frequency-dependent. Assuming a simple harmonic motion $y = y_0 e^{i\omega t}$, the following expression was proposed:

$$F = H_a y + K_a \dot{y} \tag{5.5}$$

Using the non dimensional forms $h_a = H_a/\rho D^2 f^2$ and $k_a = K_a/\rho D^2 f$, the force can be written as

$$F = \rho D^2 f(f h_a y + k_a \dot{y}) \tag{5.6}$$

where f is the frequency of the motion h_a and k_a are dependent only on the aerodynamic shape of the body, the reduced velocity, the amplitude of oscillation and the Reynolds number. In most cases it was found that at lock-in the in-phase force is negligible.

To individuate a condition at which instabilities like lock-in can occur, the following criterion was proposed:

$$[\delta_a + \delta_n]_{y_0} = 0 \tag{5.7}$$

where δ_a can be obtained by

$$\delta_a = \frac{\rho D^2 k_a}{2m} \tag{5.8}$$

simply obtained putting Eq. (5.6) into Eq. (5.4) and equating to zero the difference between the two damping terms. Although a method to evaluate the response during lock-in was not proposed, this form for modeling unsteady aerodynamic forces foreshadowed the famous flutter derivative formulation. Nevertheless, as it will be observed further on, for modeling vortex-induced vibration nonlinear effects cannot be neglected.

Scanlan linear model (1981)

Few years after the success of the flutter derivatives formulation for bridge decks (Scanlan and Tomko, 1971), Scanlan (1981) used it again for modeling the motion-induced part of the forcing assumed causing vortex-induced vibration

$$F = \frac{1}{2}\rho U^2 D \left[Y_1(K)\frac{\dot{y}}{U} + Y_2(K)\frac{y}{D} + \frac{1}{2}\tilde{C}_L(K) sin(\omega_s t + \phi) \right] \tag{5.9}$$

where $K = \omega_n D/U$; Y_1, Y_2 and ϕ are parameters to be fitted by wind tunnel test results.

The motion induced part of the force is a linear combination of both displacement and its derivative. Therefore, the first term can be considered as an aerodynamic damping and the second one as an aerodynamic stiffness.

Since the model is not able to take into account the nonlinearity of the phenomenon, it seems to be useless in predicting such a complicated behavior. At large amplitude of oscillation such a model may lead to an aerodynamic damping higher than the structural one, predicting an unbounded response without limit cycle. Moreover, as it will be cleared later by Scanlan (1998), the determination of flutter derivatives cannot follows the standard procedure. Conducting forced-vibration tests inside the lock-in region on a bridge deck model, Diana *et al.* (2006) have shown that changing the amplitude of vibration a strong nonlinear effect on flutter derivatives is obtained. Hence, a model that does not incorporate nonlinear effects cannot be considered able to model such a phenomenon.

Scanlan nonlinear model (1981)

With the aim of overcoming the limit of its previous model, Scanlan (1981) proposed a semi-empirical nonlinear model for the across-flow response based on the Van der Pol model (Van der Pol, 1920) that considers the following fluid-induced forcing fuction (Ehsan and Scanlan, 1990):

$$F = \frac{1}{2}\rho U^2(2D)\left[Y_1(K)\left(1-\epsilon\frac{y^2}{D^2}\right)\frac{\dot{y}}{U} + Y_2(K)\frac{y}{D} + \frac{1}{2}C_L(K)sin(\omega t+\theta)\right] \quad (5.10)$$

where $K = \omega D/U$ is the reduced frequency of vortex shedding, ω is the frequency during vortex-induced vibrations; ϵ, Y_1, Y_2 $C_L(K)$ and θ are parameters which must be determined during wind tunnel tests.

The parameters ϵ and Y_1 are related, respectively, to the nonlinear and linear component of the aerodynamic damping. In particular, the parameter ϵ allows to take into account that the oscillations are self-limiting. Finally, the parameter Y_2 represents the stiffness term. The vortex-shedding part is again modeled by a sinusoidal function.

According to Ehsan (1988), when large amplitude occurs, the vortex-shedding forces are negligible with respect to the motion-induced ones. Thus, during lock-in, the Eq. (5.10) can be reduced to the following form:

$$F = \frac{1}{2}\rho U^2(2D)\left[Y_1(K)\left(1-\epsilon\frac{y^2}{D^2}\right)\frac{\dot{y}}{U} + Y_2(K)\frac{y}{D}\right] \quad (5.11)$$

For estimating the unknown parameters, a method based on energy considerations was proposed by Scanlan (1981). In doing that, being interested in obtaining the parameters at lock-in, he neglects the contribution of the aerodynamic stiffness (no appreciable frequency shift exists). Then the Eq. (5.11) becomes

$$F = \frac{1}{2}\rho U^2(2D)\left[Y_1(K)\left(1-\epsilon\frac{y^2}{D^2}\right)\frac{\dot{y}}{U}\right] \quad (5.12)$$

The steady-state amplitude expression is then the following:

$$\frac{y_0}{D} = 2\sqrt{\frac{Y_1 - 4\pi ScSt}{\epsilon Y_1}} \quad (5.13)$$

where y_0 is the steady-state amplitude.

To identify the unknown parameters (Y_1, ϵ), oscillation amplitudes obtained for two experiments at closely spaced values of the mechanical damping are used. The parameters are associated with an average value obtained by two test damping ratios.

Subsequently, Ehsan and Scanlan (1990) proposed a new method based on a solution of the autonomous nonlinear differential equation obtained by the method of *slowly varying parameters*. The expression of the steady-state amplitude was expressed by:

$$\beta = \frac{y_0}{D} = \frac{2}{\sqrt{\epsilon}}\sqrt{1-\frac{2\zeta K_1}{m_r Y_1}} \quad (5.14)$$

where $m_r = \rho D^2/m$ is the *mass ratio* and K_1 is the reduced natural frequency. Manipulating the Eq. (5.14) it can be shown how it is exactly the same expression

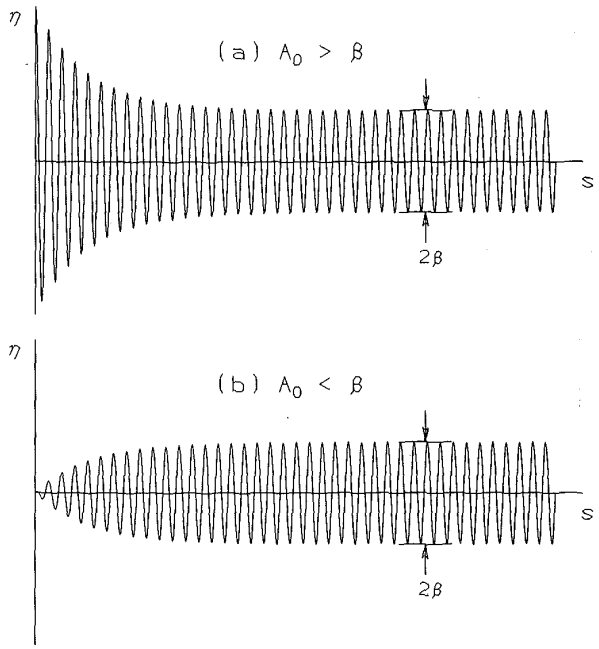

Fig. 5.2 Response at lock-in: a) Decay-to-Resonance test; b) Growth-to-Resonance test (Ehsan and Scanlan, 1990).

reported in Eq. (5.13). In this method, called *decay-to-resonance method*, a single test is necessary to estimate all the parameters in Eq. (5.11). An example of the displacements measurement during such a test is shown in Fig. 5.2. In the proposed procedure only the transient portion of the time history should be used, which is not easy to be extracted when slight beating phenomena are present in the steady-state oscillation.

It is very important to underline a strong limit in this model as well as in those which follow. As it can be seen in Fig. 5.3, both the parameters Y_1 and ϵ show a large variation with the damping ratio, therefore, if the Scruton number of the prototype is not very close to that of the model tested the value predicted will not be reliable.

As observed by Gupta *et al.* (1996), the parameters extracted from wind tunnel tests by the above methods (Scanlan, 1981; Ehsan and Scanlan, 1990) are less accurate under turbulent conditions and when the steady-state amplitude is so small that its estimation becomes difficult. Thus, they proposed a technique based on the concept of *invariant embedding*, originally developed by Bellman *et al.* (1966). The parameters can be identified by decay-to-resonance and growth-to-resonance tests as well as by the simple registration of the steady-state-amplitude. The same consideration done above can be repeated for this model, indeed variations of the parameters occur again (see Fig. 5.4, Fig. 5.5).

Vickery-Basu nonlinear model (1983)

Using random-vibration theory, Vickery and Basu (1983a) proposed a semi-empirical mathematical model for estimating the across-wind response of an elastically-supported

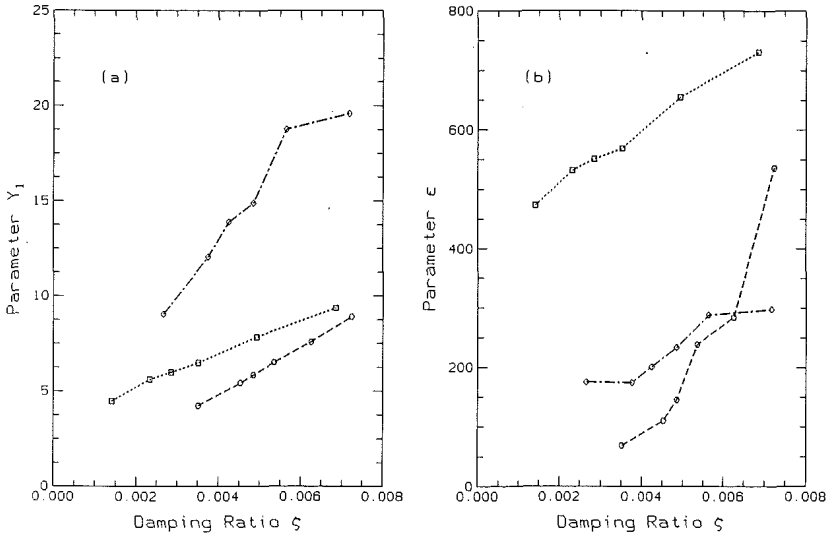

Fig. 5.3 Variation of the parameters with mechanical damping: Deer Isle Bridge section (K=0.798, circle symbol); Tacoma Narrows Bridge section (K=0.642, rhombus symbol); Rectangular section B/D= 4 (K=0.672, square symbol) (Ehsan and Scanlan, 1990).

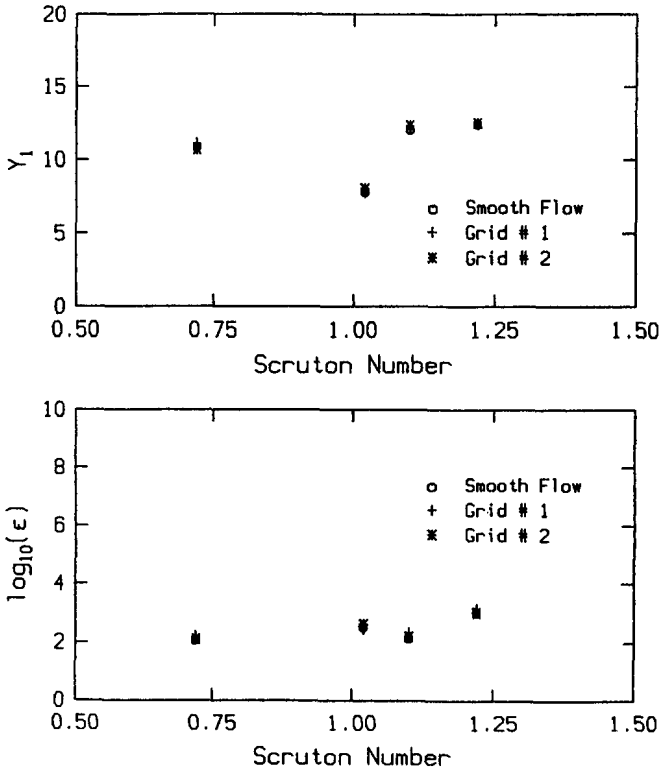

Fig. 5.4 Variation of the parameters with Scruton number for a smooth circular cylinder in smooth and turbulent flow. (Gupta *et al.*, 1996).

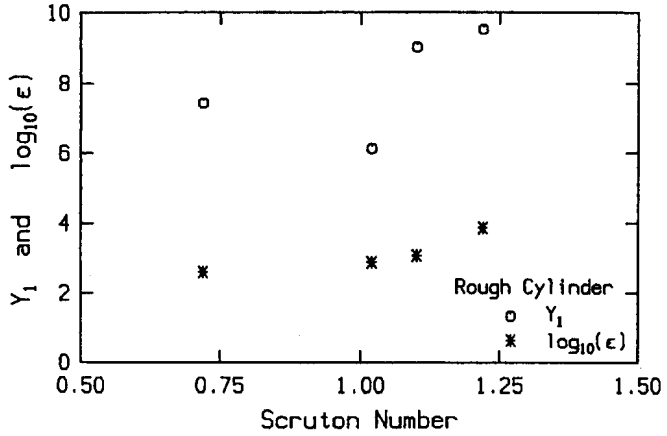

Fig. 5.5 Variation of the parameters with Scruton number for a rough circular cylinder in smooth and turbulent flow (Gupta *et al.*, 1996).

circular cylinder with constant diameter immersed in a smooth flow. The form of the forcing term for some aspects derives from that reported in Eq. (5.12):

$$F = \frac{1}{2}\rho U^2 D C_L(t) + 4\pi f_n \rho D^2 K_{a_0}\left[1 - \left(\frac{\tilde{y}}{\tilde{y_L}}\right)^2\right] \tag{5.15}$$

where $\tilde{y}_L$ is the R.M.S. value of the steady-state amplitude divided $\sqrt{2}$ and K_{a_0} is an aerodynamic damping coefficient for small amplitude.

The R.M.S. value of the response can be calculated through the following expression:

$$\frac{\tilde{y}}{D} = \left(\frac{\tilde{C_L'}}{8\pi^2}\right)\left(\frac{U}{f_0 D}\right)^2\left(\frac{\rho D^2}{m}\right)\sqrt{\frac{\frac{\sqrt{\pi}}{4B}\frac{f_o}{f_s}e^{-\left[\left(\frac{1-\frac{f_o}{f_s}}{B}\right)\right]^2}}{\eta_s + \eta_a}} \tag{5.16}$$

with

$$\tilde{C_L'}^2 = \int_0^h \tilde{C_L}^2 R_0(z_1, z_2) dz_1 dz_2 \tag{5.17}$$

where $\tilde{C_L}^2$ is the sectional R.M.S. lift coefficient and $R_0(z_1, z_2)$ is the spanwise correlation of lift force for a stationary cylinder. The aerodynamic damping can be evaluated by:

$$\eta_a = -\left(\frac{\rho D^2}{m}\right) K_{a_0}\left[1 - \left(\frac{\tilde{y}}{\tilde{y_L}}\right)^2\right] \tag{5.18}$$

The present model, with opportune modifications (Basu and Vickery, 1983; Vickery and Basu, 1983b), has been extensively applied to circular chimneys but, for the large amount of wind tunnel measurements needed, it is not useful for practical application in bridge engineering. It is important to underline the way the Scruton number effect on the oscillations is taken into account. Including the two limit

behavior, a Gaussian stochastic behavior at high Sc and a sinusoidal-deterministic behavior at low Sc, passing through a continuous transition zone it represents an attempt towards a unitary model. Moreover, such a model provides the possibility for the implementation of a probabilistic framework for risk-analysis calculation.

Goswami nonlinear model (1992)

For modeling the across-flow response of circular cylinders, a hybridization of the Scanlan nonlinear SDoF model (Scanlan, 1981) and a derived SDoF form of the Billah coupled model (Billah, 1989) was proposed by Goswami (1991) and Goswami *et al.* (1992, 1993b). The aeroelastic force is given by:

$$F = \frac{1}{2}\rho U^2 D \left[Y_1(K)\frac{\dot{y}}{U} + Y_2(K)\frac{y^2}{D^2}\frac{\dot{y}}{U} + J_1(K)\frac{y}{D} + J_2(K)\frac{y}{D}cos(2\omega_s t) \right] \quad (5.19)$$

The four terms composing F represent the mechanisms known for an elastically supported cylinder immersed in a fluid flow. Y_1 and Y_2 are related to the linear and nonlinear aerodynamic damping terms which are one the counterpart of the other when large amplitude occurs. In particular, the former gives rise to the self-excited oscillation introducing energy into the system. The latter, instead, provides a self-limited character to the model. J_1 term is the aerodynamic stiffness term, which, during wind vortex-induced vibrations, can be assumed as zero because the shift away from the still-air natural frequency is negligible. Finally, J_2 term (Billah's term) is a parametric stiffness coupling the wake and the cylinder, which excites the body at twice the Strouhal frequency. This term, suggested by Billah (1989), is representative of the contribution of the wake oscillator.

The procedure for identifying the parameters, as done in Ehsan and Scanlan (1990), was developed using the method of slowly varying parameters. Here, however, three parameters have to be determined (Y_1, Y_2 and J_2). So the decay-to-resonance test is not enough and the application of Fourier transform on overlapping windows of the signal is needed.

As it can be seen in Fig. 5.6, inside the lock-in region, the parameter Y_1 is positive, creating a negative-damping condition, and is approximatively constant when reduced velocity is changed. The parameter Y_2, regulating the limit-amplitude displacements, seems to be in agreement with the experimental observation. In fact, as mechanical damping increases, the depth of the curve decreases. The decreasing of the depth is produced by the inward displacement of the right edges. Such a behavior is consistent with that observed when, increasing the mechanical damping, the upper limit of lock-in region is reduced whereas the lower one is invariable. Finally, the parameter J_2 shows a very clear linear trend for each mechanical damping value. From the point of exact synchronization, at which J_2 vanishes, there is a linear increase which corresponds to the attainment of importance of the vortex-shedding force with respect to the aeroelastic one. Therefore, such a model seems to be able to capture the essential mechanisms of the process with the minimum number of physically motivated terms.

It is worth noting that Y_1 and Y_2 still depend on the Scruton number, therefore, the models results not useful for practical applications.

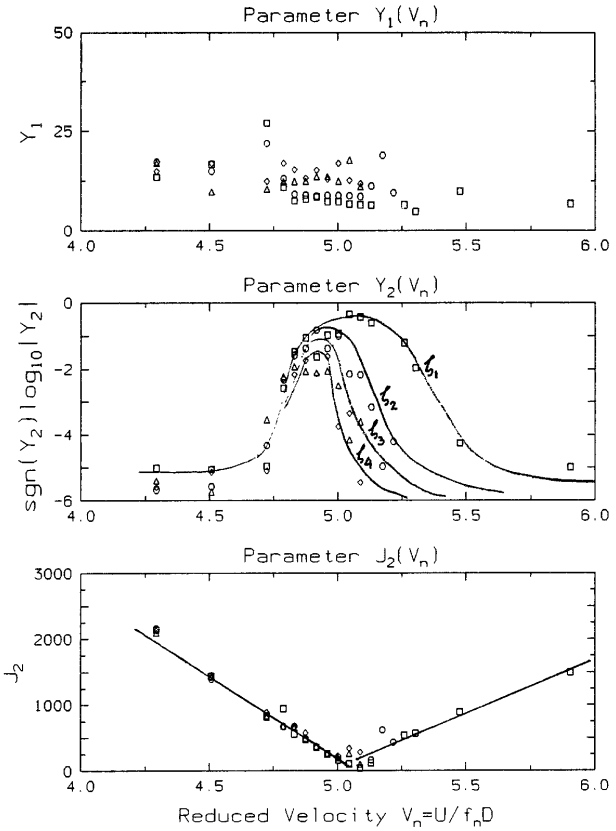

Fig. 5.6 Variation of the parameters with Scruton number and reduced velocity for a circular cylinder in smooth flow (Goswami *et al.*, 1993b).

Larsen nonlinear model (1993)

In modeling the vortex-induced vibration of bluff bodies, an attempt to improve the results obtained by Scanlan (1981) and Ehsan and Scanlan (1990) was made by Larsen (1993, 1995). Firstly, a generalization of the van der Pol model for the cross-wind force due to vortex shedding action was proposed:

$$F = m_r C_a \left(1 - \epsilon|\eta|^{2\nu}\right) \dot{\eta} \tag{5.20}$$

where C_a, ϵ and ν are dimensionless aerodynamic parameters to be determined during wind tunnel tests[1].

For an useful comparison with the Scanlan nonlinear model [see the Eq. (5.12)], defining y and $\dot{y}$ the displacement and the velocity of the structure and D its cross-wind dimension, the Eq. (5.20) can be written as:

$$F = \frac{1}{2}\rho U^2 (2D) C_a \left(1 - \epsilon \left|\frac{y}{D}\right|^{2\nu}\right) \frac{\dot{y}}{U} \tag{5.21}$$

Hence, by comparing the Scanlan nonlinear forcing term with that of this model, it can be seen that the parameter ν is the only difference.

As done by Scanlan (1981), the steady-state amplitude as a function of the Scruton number was obtained by equating the energy supplied by the vortex shedding process to the energy dissipated by the nonlinear restoring force and structural damping over one period of oscillation. Assuming that the vortex-induced oscillation is sinusoidal, the following expression was obtained:

$$\eta = \left[\frac{\pi}{I_c(\nu)\epsilon}\left(1 - \frac{Sc}{C_a}\right)\right]^{1/(2\nu)} \tag{5.22}$$

where $I_c(\nu) = \int_0^{2\pi} sin^2(p)|cos(p)|dp$ must be evaluated numerically. When $\nu = 1$, Eq. (5.22) corresponds exactly to Eq. (5.14) obtained by Scanlan (1981).

For identifying the aeroelastic parameters two identification procedures were proposed. The first one is constituted by the fitting of Eq. (5.22) to three measurements of the steady-state amplitude at three different values of the Scruton number, the same procedure was proposed in Scanlan (1981), where two parameters were identified through two tests.

According to the results shown in Larsen (1995), such a modification allows a better fitting of the experimental data (Fig. 5.7). In particular, the nonlinear model by Scanlan (1981) shows a response function with a curvature not consistent with the experimental trend. Furthermore, as the Scruton number at which no oscillations occur is lower than that of experimental tests, the model is not conservative. Instead, the harmonic model (Scruton, 1963) has the right curvature but it fails in the prediction of zero Scruton number. Finally, the nonlinear model by Larsen (1993) seems to give the best fitting of the data.

Actually, as observed in Goswami *et al.* (1993a), the refinement introduced by the model by Larsen (1993) to better fit the experimental results is a valuable exercise. Indeed, it is not particularly fruitful for engineering application to create an

[1]Looking at Larsen's papers (Larsen, 1993, 1995) one can see that the frequency f only appears in the second paper. This difference seems to be a mistake, so here the equation of the first paper is reported because is correct from a dimensional point of view.

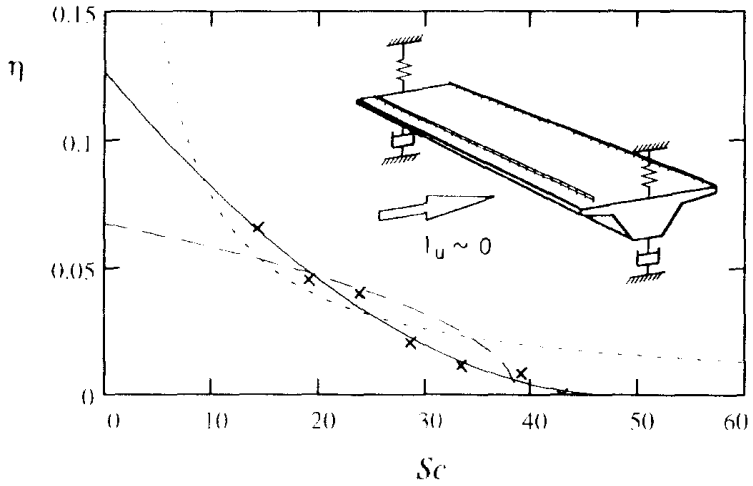

Fig. 5.7 Fitting of experimental data of a bridge deck by: Larsen (1995) (solid line), Scanlan (1981) (dashed line), Scruton (1963) (dotted line) [from Larsen (1995)].

accompanying empirical (and complex) differential equation to describe the motion. An appropriate graph, e.g. Fig. 5.6, should be enough in each particular instance.

As reported by Larsen (1995), although three different tests at three different Scruton numbers are needed to evaluate the parameters, more tests are desirable to enhance the confidence level, which leads to an expansion of the wind tunnel tests. Hence with the aim to reduce to one the tests needed, Larsen (1993), applying the *Krylov-Bogoliubov technique*, has obtained the following expression for the envelope of the resonant transient response:

$$a(t) = \frac{\beta}{\left[1 - [1 - (\beta/a_0)^{2\nu}]\, exp\left(-\nu f \frac{\rho D^2}{M}(C_a - Sc)t\right)\right]^{1/2\nu}} \tag{5.23}$$

where a_0 and β are the amplitude, respectively, at $t = 0$ and $t = \infty$. In Eq. (5.23) only two parameters are independent, because each one is related to the others through (5.22). No comparison is done with the analogous procedures already existing in the literature (Ehsan and Scanlan, 1990; Gupta *et al.*, 1996).

Scanlan linear model (1998)

With the aim of reconciling lock-in analysis with the flutter formulation (Scanlan and Tomko, 1971), taking into account the self-limited response of the phenomenon, an alternative model was suggested by Scanlan (1998). Here, the following equation of motion is suggested for the case of lock-in where vertical motion is predominant:

$$F = \frac{1}{2}\rho U^2 B \left[K H_1^* \frac{\dot{y}}{U} - C_L sin(\omega_n t)\right] \tag{5.24}$$

where H_1^* is the flutter derivative at lock-in; C_L is the forcing term at lock-in introduced to control the amplitude. The parameter H_1^* is determined by decay-to-resonance test, while, the steady-state amplitude allows to obtain C_L. In the paper no information is given about the variation of the parameters with the damping

coefficient. The model was applied to the data obtained in a previous study (Ehsan and Scanlan, 1990).

D'Asdia nonlinear model (2003)

Starting from a model developed for circular cylinders (D'Asdia and Noè, 1998; D'Asdia *et al.*, 1998; Noè *et al.*, 1998), D'Asdia *et al.* (2003) extended it to bridge decks. The numerical model, working in time domain, considers an alternating force with variable direction, frequency and phase, as a function of relative velocity. The total wind force per unit-length at time t is:

$$\vec{F}_w(t) = \vec{F}_{she}(t) + \vec{F}_{drag}(t) \tag{5.25}$$

The modulus of the force due to vortex shedding $\vec{F}_{she}(t)$, assumed always perpendicular to the relative velocity $V_{w,rel}(t)$ at the time $t - \Delta t$ (Fig. 5.8), is evaluated at the time t as a function of its value at the time $t - \Delta t$ by the following expression:

$$F_{she}(t) = \frac{1}{2}\rho D C_{L-she} V^2_{w,rel}(t) sin(\omega_{she}(t)t + \phi_{she}(t)) \tag{5.26}$$

where the relative velocity is:

$$V_{w,rel}(t) = \sqrt{V^2_w(t - \Delta t) + \dot{y}^2(t - \Delta t)} \tag{5.27}$$

in which V_w is the mean wind speed. The angle between the relative velocity and the horizontal axis is:

$$\alpha(t) = tan^{-1}\left(\frac{\dot{y}(t - \Delta t)}{V_w(t - \Delta t)}\right) \tag{5.28}$$

The mechanical circular frequency due to Strouhal law and the estimated instantaneous value of the across oscillation are, respectively:

$$\omega_{St}(t) = 2\pi St \frac{V_{w,rel}(t)}{D} \tag{5.29}$$

$$\tilde{\omega}(t) = \frac{\pi}{\tau_{(y=\bar{y})_n} - \tau_{(y=\bar{y})_{n-1}}} \tag{5.30}$$

where D is the height of the section and $\tau_{(y=\bar{y})_n}$ and $\tau_{(y=\bar{y})_{n-1}}$ represent the time instants corresponding to the last two zero-crossing of the function $y - \overline{y}$ where $\overline{y}$ is the mean vertical displacement of the deck. So the mechanical circular shedding frequency is given by:

$$\begin{cases} \omega_{she}(t) = \omega_{St}(t) & \text{if } \frac{\omega_{St}(t)}{\tilde{\omega}(t)} < \Omega_L \text{ or } \frac{\omega_{St}(t)}{\tilde{\omega}(t)} > \Omega_U \\ \omega_{she}(t) = \omega(t) & \text{if } \Omega_L \leq \frac{\omega_{St}(t)}{\tilde{\omega}(t)} \leq \Omega_U \end{cases} \tag{5.31}$$

where Ω_L and Ω_U define the lock-in interval frequency. The shedding phase angle is given by:

$$\phi_{she}(t) = [\omega_{she}(t - \Delta t) - \omega_{she}(t)]t + \phi_{she}(t - \Delta t) \tag{5.32}$$

The modulus of the drag force $\vec{F}_{drag}$ due to the drag and parallel to the relative wind velocity is:

$$F_{drag}(t) = \frac{1}{2}\rho D C_D V_{w,rel}^2(t) \tag{5.33}$$

The parameters which are needed to apply the model are the drag coefficient C_D, the lift coefficient C_{L-she}, the Strouhal number St and the two parameters Ω_L and Ω_U.

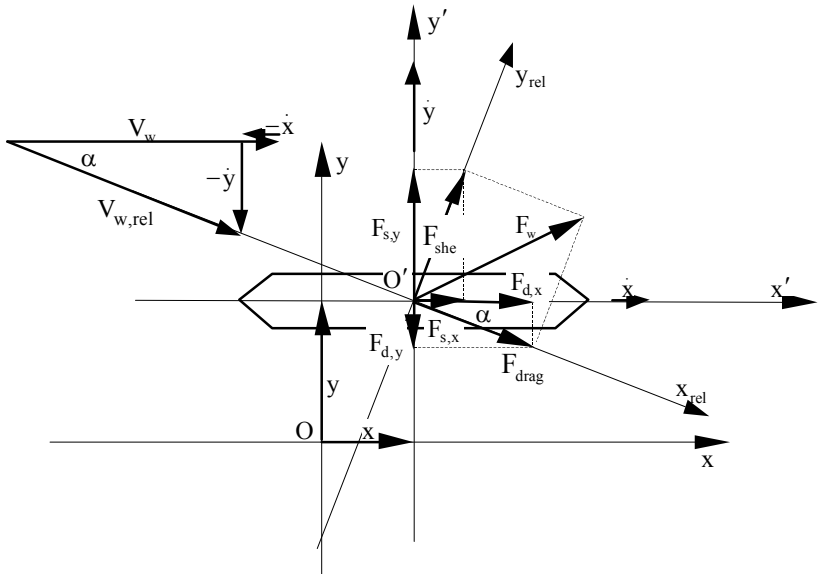

Fig. 5.8 Definition diagram for the D'Asdia nonlinear model (D'Asdia *et al.*, 2003).

5.3.2 Forced-coefficient data models

This type of models are based on force-coefficient data obtained by forced vibration tests. Their objective is to match as good as possible the body response. Since they belong to the class of the Single-Degree-of-Freedom models, all the complexity of the nonlinear wake-body interaction is taken into account by the forcing term alone.

Sarpkaya model (1978)

Sarpkaya (1978) [see Billah (1989)] expressed the cross-wind force acting on a rigid cylinder forced to vibrate harmonically transverse to a uniform flow by the following equation:

$$C_L = C_{mh} sin(\omega t) - C_{dh} cos(\omega t) \tag{5.34}$$

where the values of C_{mh} and C_{lh} were obtained for different oscillation amplitude from forced vibration tests. As it can be observed from Fig. 5.9, the values of the coefficients significantly increase in the vicinity of the condition f_f/f_s (f_f is the forcing frequency). The response was obtained by using the following equation:

$$m\left(\ddot{y} + 2\zeta_n \omega_n \dot{y} + \omega_n^2 y\right) = \frac{1}{2}\rho U^2 D C_L \tag{5.35}$$

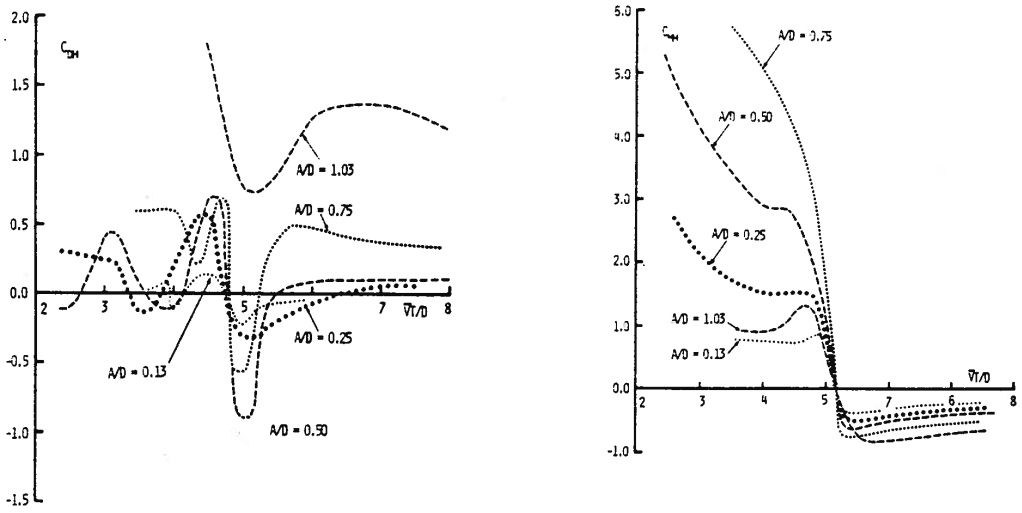

Fig. 5.9 Force coefficients C_{mh} and C_{lh} vs. reduced velocity around $f_f/f_s = 1$ (Sarpkaya, 1978).

According to Billah (1989), the response in the time domain predicted by the model is in contradiction with experimental results, primarily because motion ascribable to negative damping is not present.

Staubli model (1983)

The model proposed by Staubli (1983) provides the vibrations during lock-in of a freely vibrating cylinder by using force-coefficient data obtained by forced-vibration tests. The equation of the model is that of the classical linear oscillator forced by the flow:

$$m\left(\ddot{y} + 2\zeta_n\omega_n\dot{y} + \omega_n^2 y\right) = \frac{1}{2}\rho U^2 D C_L \tag{5.36}$$

where

$$C_L = \hat{C}_{Ln}cos(\omega_n t + \phi) + \hat{C}_{Ls}cos(\omega_s t) \tag{5.37}$$

in which $\hat{C}_{Ln}$ and $\hat{C}_{Ls}$ are the amplitudes of the lift coefficient components respectively at the oscillation and vortex shedding frequency. To evaluate the response during lock-in ($\omega_s \simeq \omega_n$), the vortex shedding part of the response was neglected. Therefore, the parameters which have to be estimated by forced vibration tests are $\hat{C}_{Ln}$ and ϕ. Assuming a sinusoidal response during lock-in, the previous equations provide others two equations which allow to implicitly obtain the oscillation amplitude and the circular frequency during lock-in.

Fig. 5.10 shows the results obtained with the situation of weak and strong damping compared to those obtained by free vibration tests. Even though a good agreement was obtained for the weak damping at the large amplitudes, that for the strong damping is not so good. Probably, such a discrepancy could be due to the assumption of neglecting the vortex shedding part of the force.

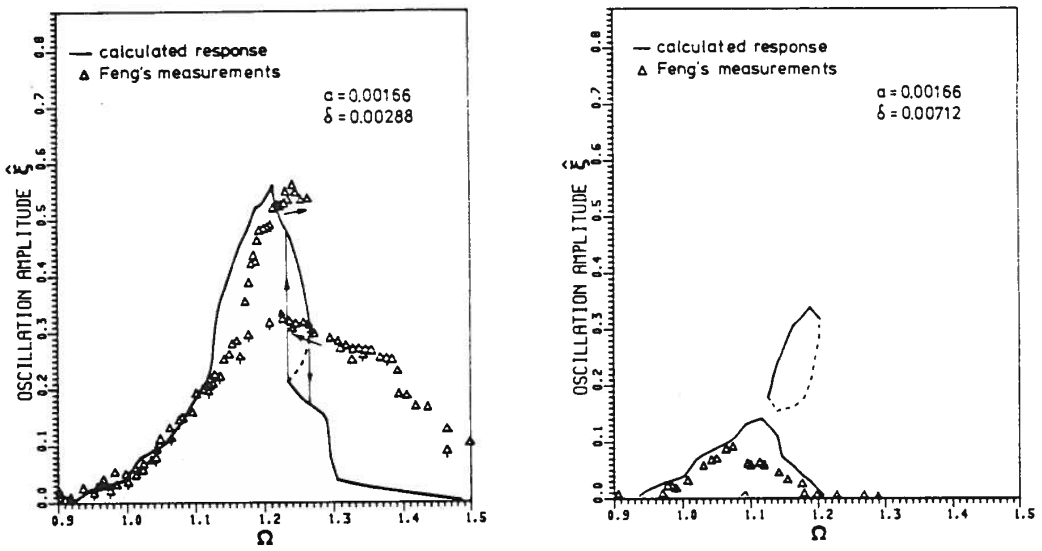

Fig. 5.10 Response of the elastically supported circular cylinder as a function of the ratio between the vortex-shedding frequency and the natural frequency: weak damping (left side) and strong damping (right side) (Staubli, 1983).

Iwan-Bothelo model (1985)

Iwan and Botelho (1985) proposed an analytical-empirical model for the vortex-induced oscillation of cylindrical structures. The model is calibrated on forced-coefficient data of Sarpkaya (1978) obtained in water and tries to predict the oscillation amplitude during lock-in of an elastically-supported cylinder. The following expression is used for modeling the system response:

$$m\left(\ddot{y} + 2\zeta_n \omega_n \dot{y} + \omega_n^2 y\right) = \frac{1}{2}\rho U^2 D C_L \tag{5.38}$$

where

$$C_L = C_{mh} sin(\omega t) - C_{dh} cos(\omega t) \tag{5.39}$$

in which C_{mh} and C_{dh} are referred to as inertia and drag coefficient, which are function of the oscillation amplitude as well as the reduced frequency.

In the model the locked-in response and the nonlocked-in response were treated separately. In particular, for the former was assumed the response $y = Asin\omega t$ whereas for the nonlocked-in case the response $y = Asin(\omega_s t - \phi)$ was considered. The former model is identical to that of Sarpkaya (1978). The peculiarity of the present model is the definition of detailed interpolation methods to obtain the curve for C_{mh} and C_{dh} from the experimental data.

In Fig. 5.11 is reported a comparison with experimental results. As it can be observed the maximum oscillation amplitude was well predicted. The synchronization curve is shifted to the left, centered about $f_s/f_n = 1$ and the extension of the lock-in band is considerably underestimated.

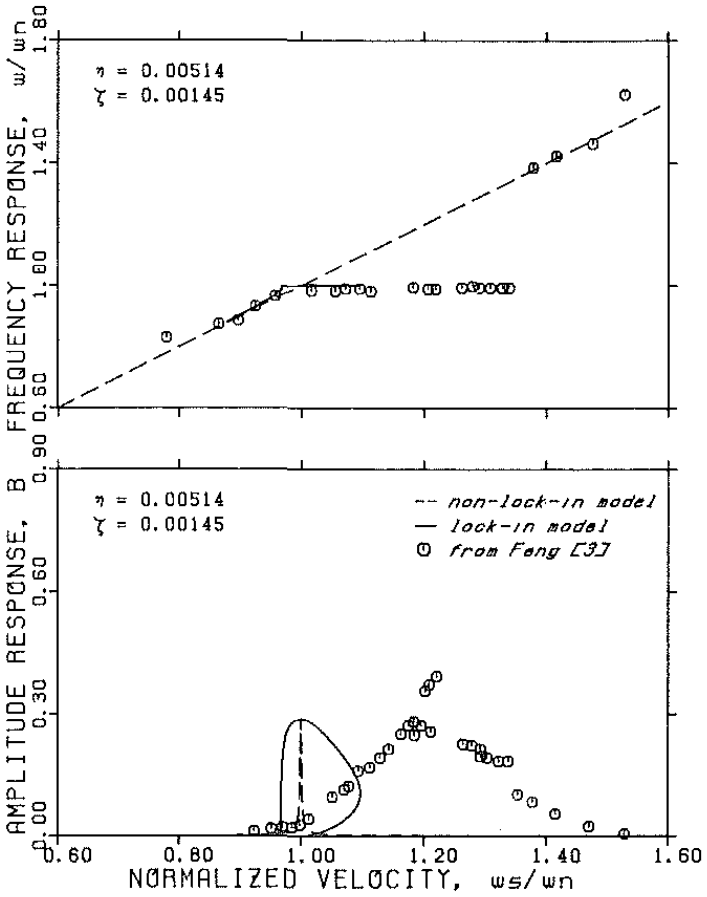

Fig. 5.11 Comparison of the model results with the experimental amplitude and frequency response for a circular cylinder in air (Iwan and Botelho, 1985).

5.4 Two-Degree-of-Freedom models

The main difference between 2 and 1-DoF models concerns the introduction in the former of a state or wake variable which is related to the fluid dynamics of the phenomenon. In particular, in the 2-DoF models the wake is treated as a separate oscillator coupled with that representing the body. This idea for modeling vortex-induced vibrations was first suggested by the work of Birkhoff (1953), who said that "the wake swings from side to side, somewhat like the tail of a swimming fish". He defined the wake oscillator for a stationary cylinder as a solid lamina identified by the region between the two shear layers behind the body in which low recirculation exists. Moreover, in the experiments of Bishop and Hassan (1964) was observed that, when an initial disturbance is imposed, the wake behaves like a mechanical oscillator in free vibrations with a frequency depending on the wind velocity. They concluded that in the wake there exists a nonlinear fluid oscillator.

5.4.1 Models based on Bishop-Hassan concept

Bishop and Hassan (1964) considered the wake as a nonlinear oscillator but did not assign to it any physical description. In contrast, Birkhoff (1953) identified the wake oscillator as a solid plate. Therefore, the 2-DoF models are now subdivided in those based on Bishop-Hassan concept and those on Birkhoff concept. In this subsection the former ones are treated.

Hartlen-Currie model (1970)

In the model proposed by Hartlen and Currie (1970) the instantaneous lift coefficient C_L was chosen as wake variable. The two equations are:

$$m\left(\ddot{y} + 2\zeta_n\omega_n\dot{y} + \omega_n^2 y\right) = \frac{1}{2}\rho U^2 D C_L \tag{5.40}$$

and

$$\ddot{C}_L - \alpha\omega_s\dot{C}_L + \frac{\gamma}{\omega_s}\dot{C}_L^3 + \omega_s^2 C_L = \frac{b\omega_n}{D}\dot{y} \tag{5.41}$$

where ω_s is the circular vortex-shedding frequency and α, γ and b are unknown constants. The nonlinear character of the wake was modeled by a van der Pol-type equation and the coupling term was assumed to be linear. When the cylinder is fixed ($y = 0$), the amplitude of the fluctuating lift coefficient is:

$$C_{L_0} = \sqrt{\frac{4\alpha}{3\gamma}} \tag{5.42}$$

which, if C_{L_0} is determined experimentally, defines the ratio α/γ. Instead, the parameters γ and b must be determined by fitting the experimental response.

In the following a synthesis of the careful study conducted by Billah (1989) on the Hartlen-Currie model is reported. When in Eq. (5.41) the right hand side is set equal to zero, it represents the lift force for the stationary cylinder. Under uniform flow, the equation represents a lift state which oscillates under infinitesimal disturbance and limit itself to a higher amplitude, independent of its initial conditions. Such non-periodic lift state is in agreement with experimental observations.

Moreover, even though the model predicts synchronization for a forced-vibration case, when only the wake-oscillator equation is considered with a known right hand side, the synchronization for a freely vibrating cylinder cannot be well predicted.

Fig. 5.12 shows that the model is able to predict body vibrations beyond the detuning limit of about 20-30% from $f_s/f_n = 1$, as reported in the literature. Fig. 5.13

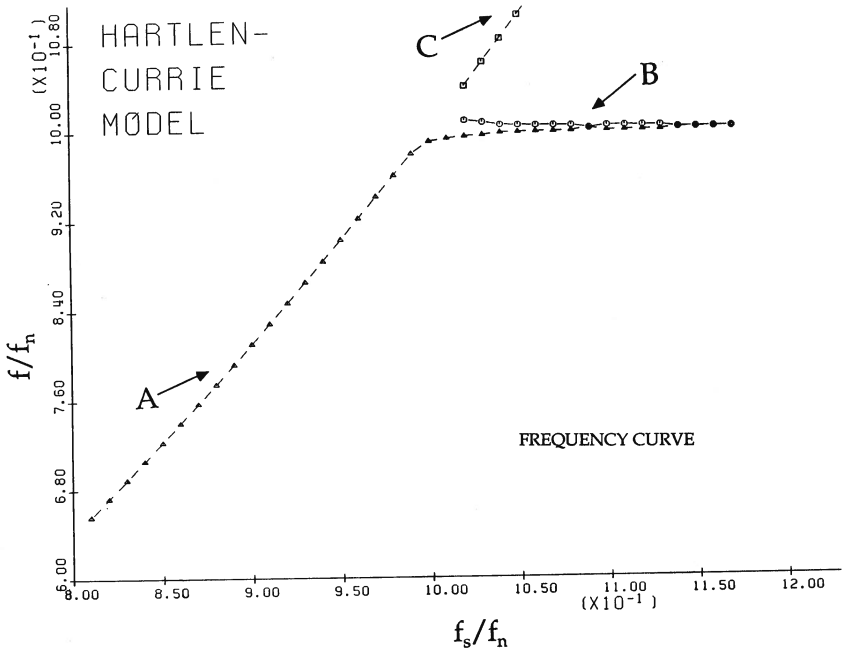

Fig. 5.12 Frequency curve for Hartlen-Currie model: f frequency of the cylinder oscillation, f_n natural frequency, f_s vortex shedding frequency (Billah, 1989).

reports the amplitude response curve provided by the model and the corresponding experimental results versus f_s/f_n. The theoretical curve is very narrow and abruptly ends when the maximum point is reached. As it can be observed, only a qualitative agreement is obtained with the experimental response. Fig. 5.14 reports the system response versus the wind speed. It is easy to observe that the model is not able to explain the phase jump observed experimentally, which does not depend on the structural damping and it has been observed also for higher damping values. In contrast with the experimental observation, the model considers the lift force coefficient in phase with the velocity of the body. In fact, as reported in Bishop and Hassan (1964) and Toebes and Eagleson (1961), the phase of the force depends on both frequency ratio f_s/f_n and the amplitude of vibration. These confirms a nonlinear interaction between body oscillation and wake dynamics.

Skop-Griffin model (1973)

To obtain a better fit of the experimental response, which is only qualitatively predicted by the Hartlen-Currie model, Skop and Griffin (1973) proposed the following coupled equations in which the instantaneous lift coefficient was modeled by a mod-

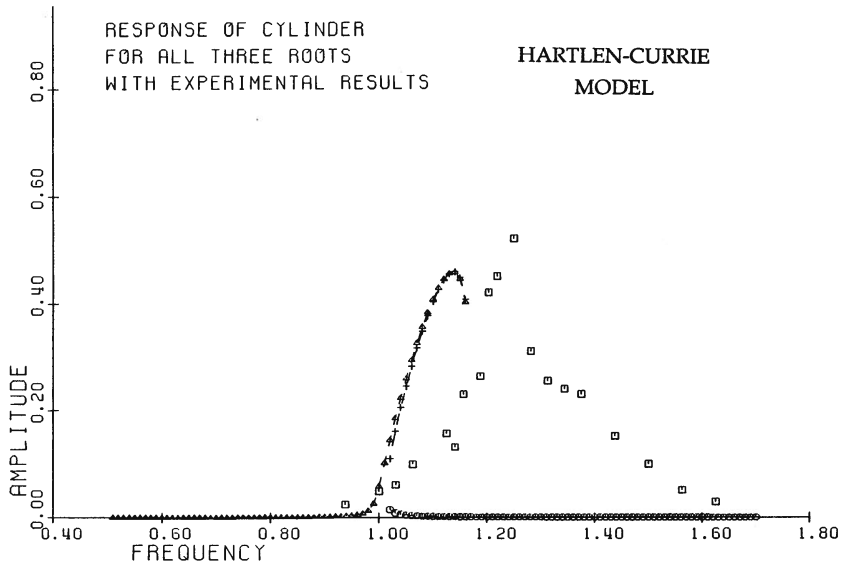

Fig. 5.13 Cylinder response for Hartlen-Currie model (Billah, 1989).

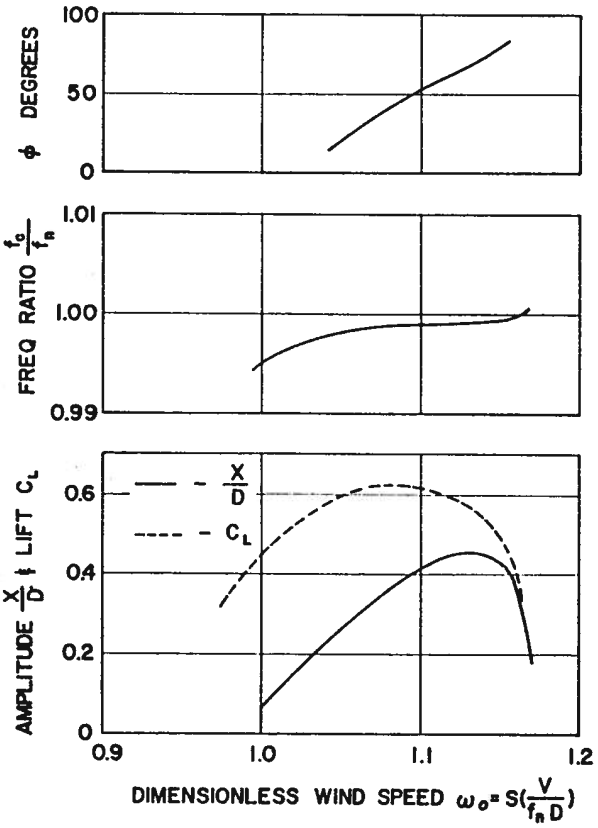

Fig. 5.14 System response versus wind speed: f_c frequency of the cylinder oscillation, f_n natural frequency, ϕ phase angle between the force and the response (Hartlen and Currie, 1970).

ified van der Pol equation:

$$m\left(\ddot{y} + 2\zeta_n \omega_n \dot{y} + \omega_n^2 y\right) = \frac{1}{2}\rho U^2 D C_L \tag{5.43}$$

and

$$\ddot{C}_L - \omega_s G C_{L_0}^2 \dot{C}_L + \frac{4G}{3\omega_s}\dot{C}_L^3 + \omega_s^2 C_L - \frac{4}{3}H\omega_s^2 C_L^3 = \frac{\omega_s F}{D}\dot{y} \tag{5.44}$$

in which five parameters must be identified by experimental results: ω_s, circular frequency of vortex shedding, C_{L_0}, lift force for a stationary cylinder and the parameters G, H and F.

Being the empirical parameters of the Hartlen-Currie model characterized by a large variation from experiment to experiment, the present model was also aimed to solve such problem, which makes the model useful for practical applications. Therefore, they postulated a set of relations between the empirical constants and the physical mass and damping parameters that govern the oscillatory response. In particular, they related the empirical constants to a combined mass-damping parameter, assuming that the response only depends on a single parameter[2]. Obviously, such relations are only valid for circular cylinders, therefore, the model is not applicable to sections with general shape such as bridge deck sections.

In Fig. 5.15 the good results obtained applying the model can be observed.

Successively, in Skop and Griffin (1975) to improve the prediction of the model, the equation for the lift coefficient was modified by adding additional terms. The effect was a small shift of the predicted response frequency. The new equation was the following:

$$\ddot{C}_L + \omega_s^2 C_L - \left[C_{L0}^2 - C_L^2 - \left(\frac{\dot{C}_L}{\omega_s}\right)^2\right](\omega_s G \dot{C}_L - \omega_s^2 H C_L) = \frac{\omega_s F}{D}\dot{y} \tag{5.45}$$

For the case of a fixed body the model shows an inconsistency with respect to the fluid dynamics of the phenomenon. In fact, for the lift coefficient of a stationary cylinder, there is an equation [Eqs. (5.44) or (5.45)] the coefficients of which are determined by the mechanical damping and the mass of the cylinder itself (Billah, 1989).

Iwan-Blevins model (1974)

A new way for modeling vortex-induced vibrations was followed by Iwan and Blevins (1974) which consists in formulating the model equations by using basic fluid dynamic concepts. They introduced a hidden flow variable w to take into account the effect of vortex shedding, which was a weighted average of the transverse displacement of the fluid near the body. This way allows to interpret the model constants in term of certain physical parameters. After the model parameters are estimated by back fitting experimental results of stationary and forced cylinders, the model is capable to predict the oscillation amplitude of elastically supported cylinder with a generic cross section.

[2]As it will be reported later on, in the literature this assumption is only valid for structures characterized by a large mass ratio such as the structures susceptible to wind action, but it seems not to be true for marine and off-shore structures, in which such ratio is much lower.

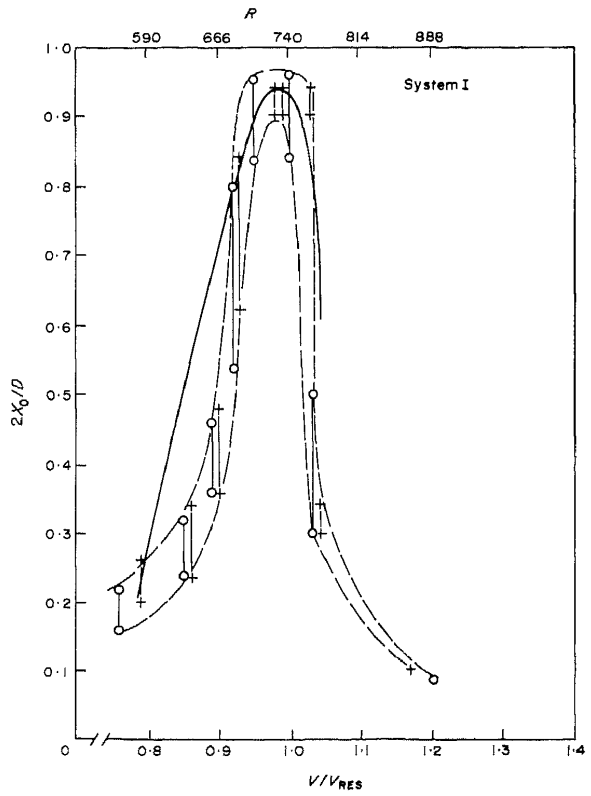

Fig. 5.15 Measured amplitude of vortex-excited oscillation as a function of free stream flow speed V for a circular cylinder. Dashed lines: envelope of the experimental measurements; Solid line: prediction of the resonant response obtained by the empirical model; V_{res}: wind velocity of the peak amplitude; Points (+) are taken with increasing wind velocity and (-) with decreasing wind velocity (Griffin *et al.*, 1973).

The basic fluid dynamic assumption are the following (Iwan and Blevins, 1974; Blevins, 2001):

- Inviscid flow outside the near wake;
- Periodical vortex street with a well-defined shedding frequency;
- Flow is two-dimensional;
- Force exerted on the cylinder by the flow depends on the velocity and acceleration of the flow relative to the cylinder.

Applying the momentum equation in the vertical direction y for a control volume which contains the cross-section of the cylinder, the following model equations were obtained:

$$\ddot{y} + 2\zeta_T \omega_n \dot{y} + \omega_n^2 y = a_3'' \ddot{w} + a_4'' \frac{U}{D} \dot{w} \tag{5.46}$$

$$\ddot{w} - (a_1' - a_4') \frac{U}{D} \dot{w} + a_2' \frac{1}{UD} \dot{w}^3 + K' \frac{u_t}{D} \omega_s w = a_3' \ddot{y} + a_4' \frac{U}{D} \dot{y} \tag{5.47}$$

where

$$\begin{array}{ll} K' = K/(a_0 + a_3) & \\ a_i' = a_i/((a_0 + a_3) & i = 1, 2, 3, 4 \\ a_i'' = \rho D^2 a_i/(m + a_3 \rho D^2); & i = 3, 4 \\ \omega_n = \sqrt{k/m}/(1 + a_3 \rho D^2/m) & \\ \zeta_t = (\zeta_s \sqrt{k/m}/\omega_n + \zeta_f)/(1 + a_3 \rho D^2/m) & \\ \zeta_s = c/2\sqrt{km} \qquad \zeta_f = a_4 \rho DU/(2m\omega_n) & \end{array}$$

u_t is the translational velocity of the vortex street, m is the mass per unit length of the cylinder, k is the support stiffness per unit length and c the support damping per unit length. ζ_T is the total effective damping coefficient, which is composed by the structural viscous damping ζ_s and the fluid viscous damping ζ_f.

From Eq.(5.47) it can be seen that the natural frequency of the fluid oscillator (vortex shedding frequency) is:

$$\omega_s = K' \frac{u_t}{U} \frac{U}{D} \tag{5.48}$$

As it is shown by experimental results (Iwan and Blevins, 1974), the ratio u_t/U is approximately constant for a wide range of Reynolds numbers, thus

$$\omega_s = 2\pi St \frac{U}{D} \tag{5.49}$$

Therefore after the value of the Strouhal number St and that of the ratio u_t/U are determined experimentally, the value of K' can be obtained.

It is important to observe that the coupling term, even though it is still linear, is constituted not only by the velocity of the body, as in the previous models, but by the acceleration as well.

A comparison of the response obtained applying the model with experimental data is reported in Fig. 5.16. It is clear that the response curve is not in agreement

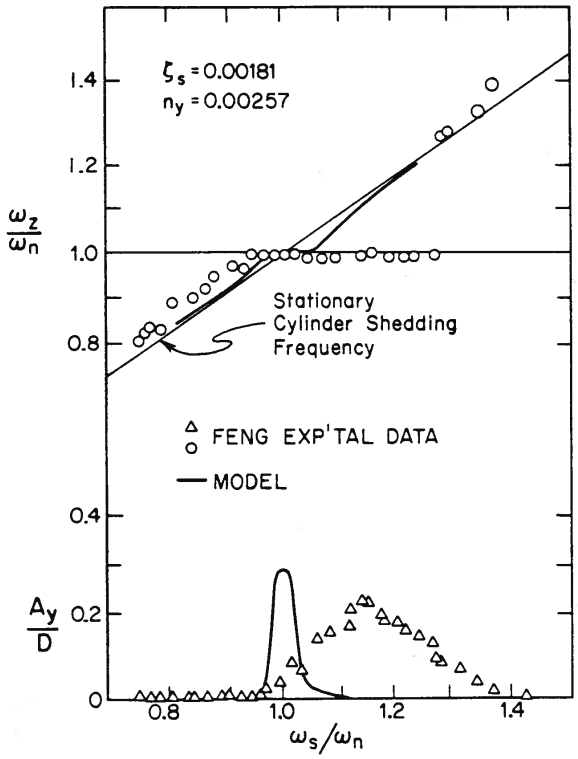

Fig. 5.16 System response for a circular cylinder (Iwan and Blevins, 1974).

with the experimental one. In particular, the shape is very narrow and then the lock-in range is smaller than the experimental one. The peak amplitude is overestimated and is located before the experimental value.

The peak amplitude of the model can be expressed in term of a single mass-damping parameter, as it is shown in the following formula:

$$\frac{y_{max}}{D} = \frac{0.07}{(1.9+\delta_r)St^2}\left[0.3+\frac{0.72}{(1.9+\delta_r)St}\right]^{1/2} \tag{5.50}$$

where $\delta_r = 4\pi m\zeta_s/(\rho D^2)$. Finally, the model predicts a maximum limiting amplitude of 1-2 diameters and its prevision gets worse when the vibration amplitude is less than one-tenth of the diameter (for high Scruton numbers). This is probably due to the two-dimensional assumption over which the model is based.

Landl model (1975)

An attempt to improve the Hartlen-Currie model was made by Landl (1975) with the introduction of a nonlinear aerodynamic damping term of the fifth order in the wake equation (Eq. 5.41). This term allows to reproduce qualitatively the hysteresis effect as well as the hard and soft excitations which characterize such a complex phenomenon. The model equations are the following:

$$m\left(\ddot{y}+2\zeta_n\omega_n\dot{y}+\omega_n^2 y\right) = \frac{1}{2}\rho U^2 D C_L \tag{5.51}$$

and

$$\ddot{C}_L + \alpha\omega_s\dot{C}_L - \frac{\gamma}{\omega_s}\dot{C}_L^3 + \frac{\beta}{\omega_n^5}\dot{C}_L^5 + \omega_s^2 C_L = \frac{b\omega_n}{D}\dot{y} \tag{5.52}$$

The parameters which have to be determined by fitting the experimental data are α, β, γ and b.

Whereas the Skop-Griffin model improves the response predictions with respect to the Hartlen-Currie model without introduce the modeling of different phenomena, the present model, even though only qualitative (Fig. 5.17), show the capacity to model different mechanisms such as the hysteresis effect and the soft and hard excitation.

In Fig. 5.18 is reported a comparison of the model previsions with experimental results. As it can be observed the model is not able to reproduce in this case all

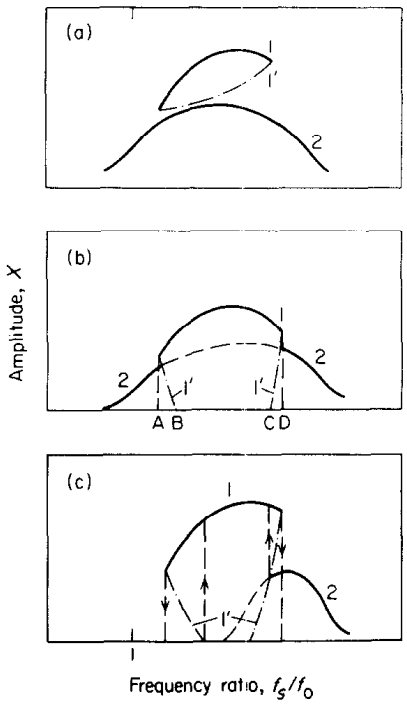

Fig. 5.17 Schematic plot of different vibration cases predicted by the model. Curve 2 was not obtained by the model (Landl, 1975).

the response amplitudes, but only the upper part of the response.

Dowell model (1981)

In Dowell (1981) a phenomenological approach to deduce the properties of the fluid oscillator was applied. In particular, only theoretical and experimental considerations for modeling the instantaneous lift coefficient were applied.

$$m\left(\ddot{y} + 2\zeta_n\omega_n\dot{y} + \omega_n^2 y\right) = \frac{1}{2}\rho U^2 D C_L \tag{5.53}$$

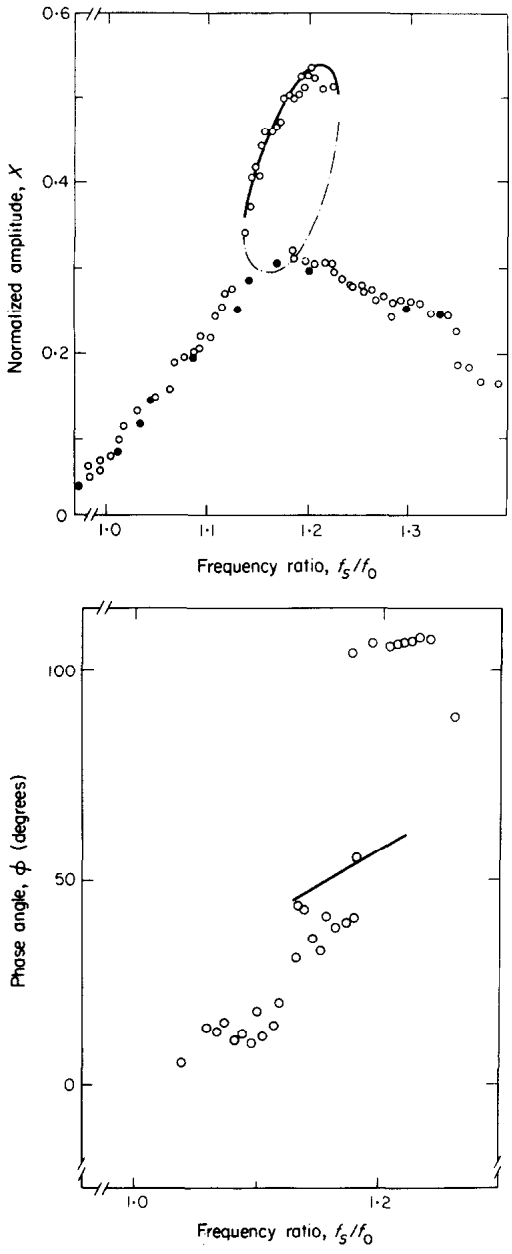

Fig. 5.18 Comparison of the system response predicted by the model with experimental data (Landl, 1975).

$$\ddot{C}_L - \epsilon\left[1 - 4\left(\frac{C_L}{C_{L_0}}\right)^2\right]\omega_s\dot{C}_L + \omega_s^2 C_L = \tag{5.54}$$

$$= -B_1\left(\frac{D}{U^2}\right)y + \omega_s^2\left[A_1\left(\frac{\dot{y}}{U}\right) - A_3\left(\frac{\dot{y}}{U}\right)^3 + A_5\left(\frac{\dot{y}}{U}\right)^5 - A_7\left(\frac{\dot{y}}{U}\right)^7\right]$$

where C_{L_0} is the limit cycle oscillation of the instantaneous lift coefficient when $y = 0$; ω_s is the vortex shedding circular frequency; $\epsilon, A_1, A_3, A_5, A_7, B_1$ are parameters which have to be estimated. To identify such empirical parameters wind tunnel tests on a stationary and forced cylinder have to be conducted.

The results obtained by the present model were compared with those given by the Skop-Griffin model and the results were broadly in agreement. In Fig. 5.19 are reported results obtained by applying the model. Even though the experimental

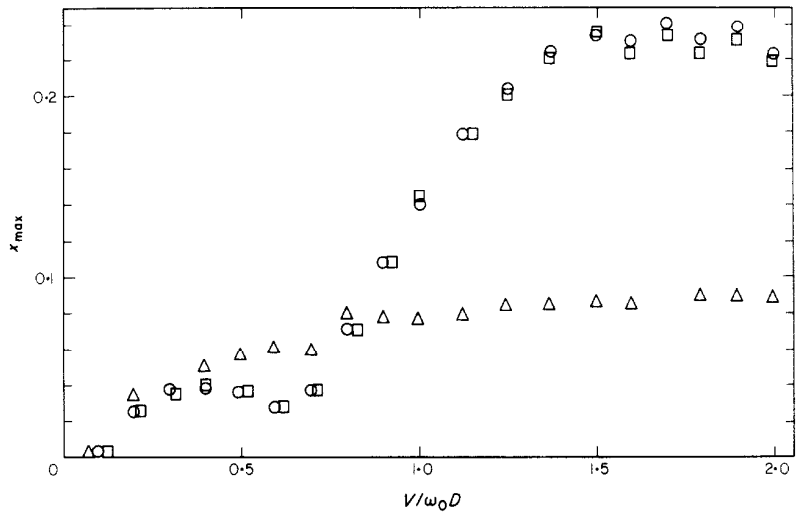

Fig. 5.19 Maximum structural deflection vs. flow velocity. Circle points: A_1 only; square points: A_1 and A_3; triangular points: $A_1 = A_3 = 0$. (Dowell, 1981).

data are not reported is clear the different trend obtained.

Benaroya-Lepore model (1983)

The phenomenon of vortex-induced vibration is characterized by many random factors which produce a significant scatter of the experimental data. Therefore, the work of Benaroya and Lepore (1983) provided a stochastic basis to model such a complex phenomenon by using wake-body oscillator models. Based on the model of Hartlen and Currie (1970) and Landl (1975), they proposed the following equations:

$$m\left(\ddot{y} + 2\zeta_n\omega_n\dot{y} + \omega_n^2 y\right) = \frac{1}{2}\rho U^2 D C_L \tag{5.55}$$

$$\ddot{C}_L + \alpha\dot{C}_L - \beta C_L^2\dot{C}_L + \gamma C_L^4\dot{C}_L + \omega_s^2 C_L = b\dot{y} \tag{5.56}$$

where the lift coefficient C_L is assumed to be a zero-mean narrow-band process and the velocity U is a broad-band process composed by a uniform, constant velocity plus oscillating waves.

An application of the model was done but no comparison with experimental data is shown. As reported by the authors, the contribution of the work is not a specific results but a methodology for modeling vortex-induced vibration.

Krenk-Nielsen model (1999)

A new approach to define the form of the coupling term for wake oscillator model was developed by Krenk and Nielsen (1999). The flow oscillator was thought as composed by a fluid mass around the body and then a generalized displacement variable was introduced to define its motion. The coupling term was obtained by assuming that the energy flows directly between the fluid and the structure, which means that the two forcing terms (that exerted by the flow on the structure and vice versa) must give rise to the same flow of energy at all time.

Moreover, it was assumed that the transverse force exerted by the fluid on the structure is proportional to the relative transverse velocity of the fluid mass. The equations of the model are:

$$m\left(\ddot{y} + 2\zeta_n\omega_n\dot{y} + \omega_n^2 y\right) = \frac{1}{2}\rho U^2 D\frac{\gamma}{U}\dot{w} \tag{5.57}$$

$$m_f\left[\ddot{w} - 2\zeta_f\omega_s\left(1 - \frac{w^2 + \dot{w}/\omega_s^2}{\omega_0^2}\right)\dot{w} + \omega_s^2 w\right] = -\frac{1}{2}\rho U^2 D\frac{\gamma}{U}\dot{y} \tag{5.58}$$

where $\gamma, m_f, \zeta_f, w_0, \omega_s$ are parameters which have to be determined fitting the experimental data.

The driving mechanism of the model is represented by a negative fluid damping coefficient in the form of a quadratic function of the amplitude, giving the negative damping for fluid amplitudes in the interval $(0, w_0)$.

The response curve is composed by two branches characterized by two frequency lock-in intervals around the natural structural frequency (Fig. 5.20). The two branches are also separated by a phase jump of nearly 180^o, as observed experimentally due to the transition between the modes obtained passing through the lock-in range.

Diana et al. model (2006)

Diana *et al.* (2006) proposed a model in which the flow oscillator was defined by an equivalent oscillator with proper aerodynamic mass, damping and stiffness and the last two aerodynamic characteristics were modeled with first and third order terms (Fig. 5.21). In the same way were defined the coupling terms with respect to the relative displacement between the body motion y and the state variable η. The equations adopted are the following:

$$\begin{aligned} &M\ddot{y} + R_{st}\dot{y} + K_{st}y = \\ &= \tfrac{1}{2}\rho U^2 B\left[-K_{1acc}\tfrac{(y-\eta)}{B} + K_{2acc}\tfrac{(y-\eta)^3}{B^3} - R_{1acc}\tfrac{(\dot{y}-\dot{\eta})}{\omega B} + R_{2acc}\tfrac{(\dot{y}-\dot{\eta})^3}{\omega^3 B^3}\right] \end{aligned} \tag{5.59}$$

$$\begin{aligned} &M_{aer}\ddot{\eta} = \\ &= \tfrac{1}{2}\rho U^2 B\left[K_{1acc}\tfrac{(y-\eta)}{B} - K_{2acc}\tfrac{(y-\eta)^3}{B^3} + R_{1acc}\tfrac{(\dot{y}-\dot{\eta})}{\omega B} - R_{2acc}\tfrac{(\dot{y}-\dot{\eta})^3}{\omega^3 B^3}\right] + \\ &+ \tfrac{1}{2}\rho U^2 B\left[-K_{1aer}\tfrac{\eta}{B} + K_{2aer}\tfrac{\eta^3}{B^3} + R_{1aer}\tfrac{\dot{\eta}}{\omega B} - R_{2aer}\tfrac{\dot{\eta}^3}{\omega^3 B^3}\right] \end{aligned} \tag{5.60}$$

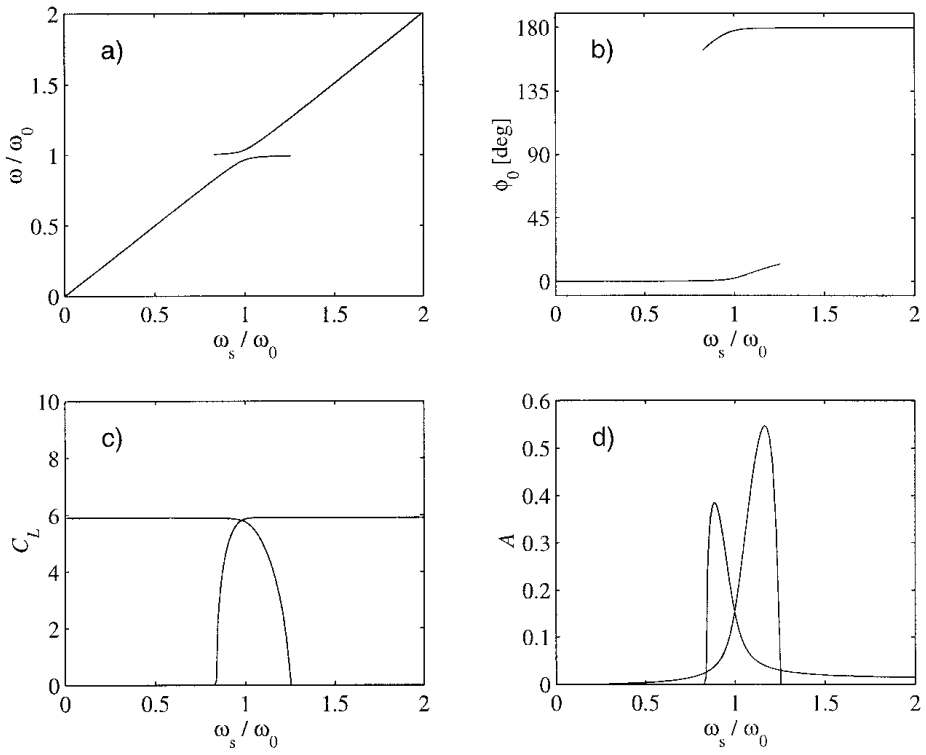

Fig. 5.20 Stationary response curve (Krenk and Nielsen, 1999).

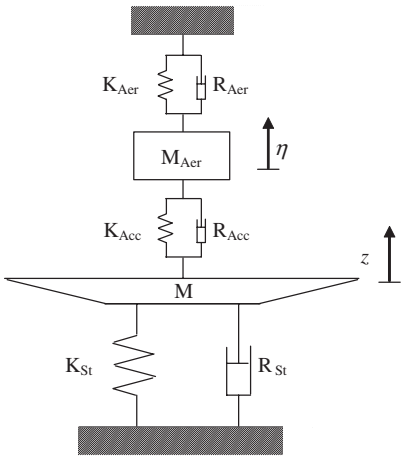

Fig. 5.21 Bridge deck section model with the equivalent oscillator (Diana *et al.*, 2006).

where M is the mass of the bridge deck; M_{aer} is the mass of the flow oscillator; η is an aerodynamic state variable representing the displacement of the nonlinear flow oscillator.

The model is characterized by eight parameters estimated by experimental tests. The equivalent oscillator only depends on the deck shape and to identify the aeroelastic parameters only free vibration tests are needed.

The results of the model are compared with experimental data obtained on the section of the Messina Strait Bridge (Fig. 5.22). As it can be observed, the results

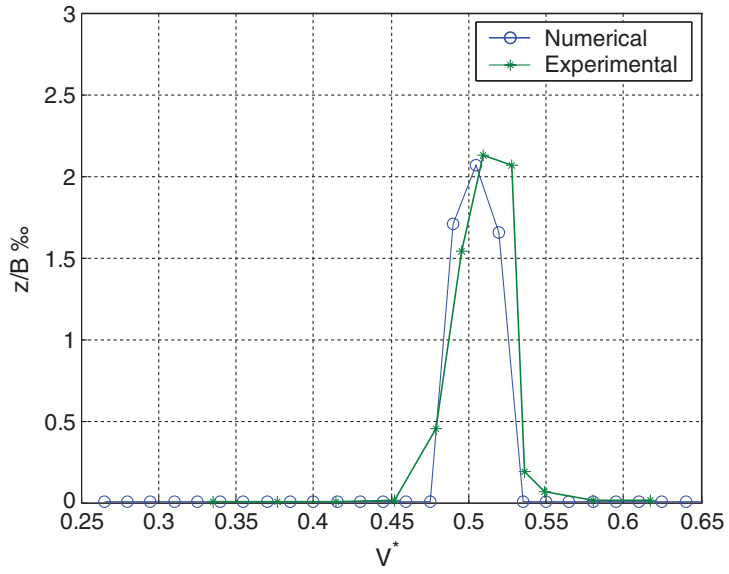

Fig. 5.22 Non-dimensional vibration amplitude vs. reduced velocity: numerical and experimental results (Diana *et al.*, 2006).

obtained are in good agreement with the experimental response.

It is worth noting that no study was conducted on the effect of the Scruton number on the aeroelastic parameters.

5.4.2 Models based on Birkhoff concept

With the aim to predict the order of magnitude of the Strouhal number for a stationary circular cylinder, Birkhoff (1953) used the idea that "the wake swings from side to side, somewhat like the tail of a swimming fish"to model the action of the fluid over the body by a solid lamina oscillating behind the cylinder. Such lamina, with its longitudinal axis parallel to that of the cylinder, was identified by the region between the two shear layers behind the body in which low recirculation exists (called also "dead-air"). Its rough estimation provided a good agreement with the observed value (St =0.2).

An extension of the Birkhoff's idea to the vibrating cylinder was done by Marris (1964), who considered the cross-wind acceleration $\ddot{y}$ of the vibrating cylinder as the cause of the oscillation of the separation points of the boundary layers attached to the body surface. Such oscillation suggests that the early wake is inclined of the time dependent angle $\theta(t)$ with respect to the direction of U. Moreover, the wake

shows large amplitude angular oscillation about the mean wind direction (Fig. 5.23). A general form for such kind of models is the following (Toebes and Eagleson, 1961):

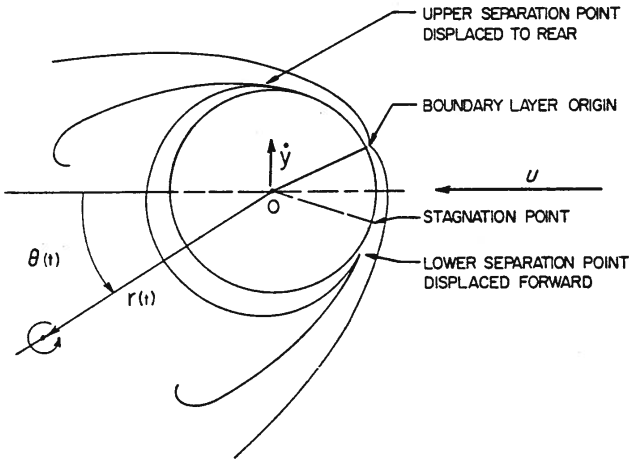

Fig. 5.23 Schematization of a wake model for a vibrating cylinder (Marris, 1964).

$$m\ddot{y} + c\dot{y} + ky = F \tag{5.61}$$

$$I\ddot{\theta} + c_w\dot{\theta} + k_w(\theta - \theta_0) = T \tag{5.62}$$

where θ is the instantaneous wake rotation angle, y is the body cross-wind displacement, T is the torque moment, F is the interaction force of the wake on the cylinder, I is the wake inertia, θ_0 is the relative angle between the flow velocity U and the relative velocity vector, m, c and k are the parameters of the body oscillator and c_w, k_w the wake parameters.

The models that will be reported in the next sections represent different ways to model the lock-in phenomenon starting from the previous two equations.

Funakawa model (1969)

Funakawa (1969) followed the Birkhoff's idea by using a wake oscillator represented by the mass of the dead-air region in the near wake of the cylinder. The wake oscillator was coupled to the body motion by an horizontal pendulum (Fig. 5.24). The equation of motion is[3]:

$$\ddot{y} - \frac{F_1 - C - F_3}{M}\dot{y} + \frac{F_4}{M}\dot{y}^3 + \frac{K + F_2}{M}y = 0 \tag{5.63}$$

in which the meaning of y, M, C and K is clear just looking at the Fig. 5.24. Instead,

[3]This model might be reported in the section relative to the Single-Degree-of-Freedom models, because it is based on a single equation of motion. It was chosen to report it in this section because it seems to be more important to underline the concept on which it is based.

F_1, F_2, F_3 and F_4 are given by:

$$\begin{aligned} F_1 &= f_m \left\{ \frac{A}{a\omega_0} sin(\delta_1 + \delta_2) - \frac{1}{U} \right\} \\ F_2 &= f_m \frac{A}{a} cos(\delta_1 + \delta_2) \\ F_3 &= \frac{1}{2} \rho C_D D U \\ F_4 &= \frac{1}{4} \rho C_D D \frac{1}{U} \end{aligned} \tag{5.64}$$

where a is the cylinder amplitude at resonance ($y = asin\omega_0 t$) and

$$\begin{aligned} A &= \frac{\sqrt{\left(0.625\omega_0 \frac{a}{d}\right)^2 + \left(\omega_v^2 \frac{a\omega_0}{U}\right)^2}}{\sqrt{\omega_v^2 - \omega_0^2)^2 + 4\epsilon^2\omega_0^2}} \\ \delta_1 &= tan^{-1} \frac{\omega_v \frac{a\omega_0}{U}}{\omega_0^2 0.625 \frac{a}{D}} \\ \delta_2 &= tan^{-1} \frac{2\epsilon\omega_0}{\omega_v^2 - \omega_0^2} \end{aligned} \tag{5.65}$$

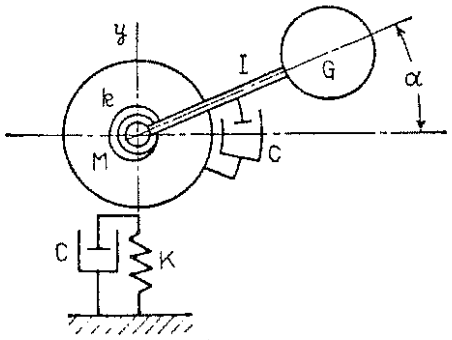

Fig. 5.24 Model of elastically supported cylinder (Funakawa, 1969).

Funakawa (1969) states that "the calculated result is able to explain these experimental phenomena substantially"but any result was shown.

Nakamura model (1969)

Nakamura (1969) proposed a model with two linear coupled equation [see Billah (1989)], i.e.,

$$m\ddot{y} + ky = -f\theta \tag{5.66}$$

$$I\ddot{\theta} + k_w\theta = -\frac{\ddot{y}}{b} \tag{5.67}$$

where f is the wake-coupling coefficient, b is a constant. Eqs. (5.66-5.67) are linear and are not capable of describing self-limiting amplitudes in the van der Pol solution.

Tamura-Matsui model (1979)

Tamura and Matsui (1979) proposed a Birkhoff-type wake-oscillator the length of which varies for a stationary cylinder (Fig. 5.25). The fluctuation of the length can

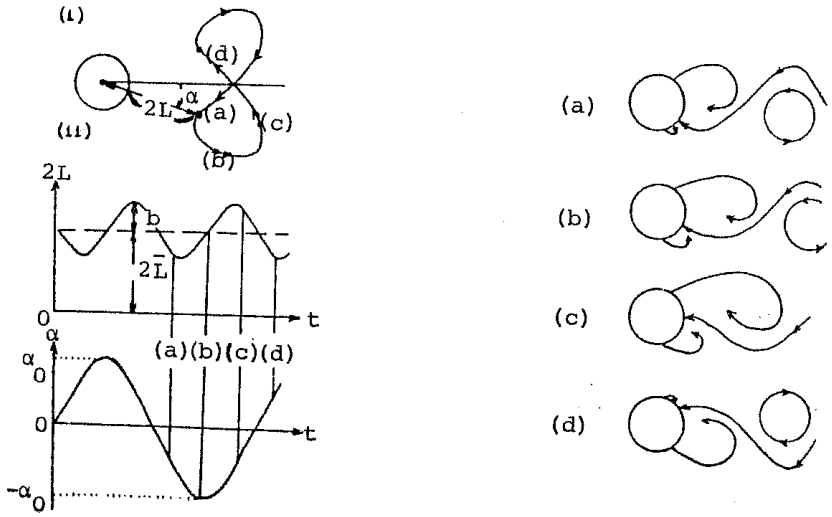

Fig. 5.25 Fluctuation of the length and the angular displacement of proposed wake-oscillator (left side) and velocity pattern behind a stationary circular cylinder during a half a period of vortex shedding (right side) (Tamura and Matsui, 1979).

be seen as the effect of a parametric damping on the wake oscillator system. The equations of the model are reported below:

$$\overline{I}\ddot{\alpha} - \overline{C}\left[1 - \left(\frac{4f^2}{C_{L0}^2}\right)\alpha^2\right]\dot{\alpha} + \overline{K}\left(\alpha + \frac{\dot{y}}{U}\right) = -\overline{I}\frac{\ddot{y}}{D/2 + \overline{L}} \tag{5.68}$$

$$M_C\ddot{y} + C_C\dot{y} + K_C y = -\frac{1}{2}\rho U^2 D s\left[f\left(\alpha + \frac{\dot{y}}{U}\right) + C_D\frac{\dot{y}}{U}\right] \tag{5.69}$$

where

$$\overline{I} = 2\rho\overline{L}H\left(\frac{D}{2} + \overline{L}\right)^2 \tag{5.70}$$

with $\overline{L} = 1.1D$ and $H = 1.25D$ semi-length and width of the dead air region obtained by experiments;

$$\overline{C} = \frac{2\sqrt{2}\rho U\Gamma_v(D/2 + \overline{L})}{\pi\alpha_0\omega_v} \tag{5.71}$$

in which Γ_v is the intensity of the vortex behind the wake oscillator, α_0 is the angular oscillation amplitude of the wake and ω_v is the angular natural frequency of the wake oscillator;

$$\overline{K} = 2\pi\rho U^2\overline{L}\left(\frac{D}{2} + \overline{L}\right) \tag{5.72}$$

M_C, C_C and K_C are the mass, damping coefficient and spring constant of the circular cylinder; s is the lenght of the cylinder; f is a constant factor estimated by experimental relationship between the magnus-effect lift and wake angular displacement for a rotating circular cylinder and, finally, C_D is the drag coefficient of the circular section.

The response predicted by the system is reported in Fig. 5.26. It can be ob-

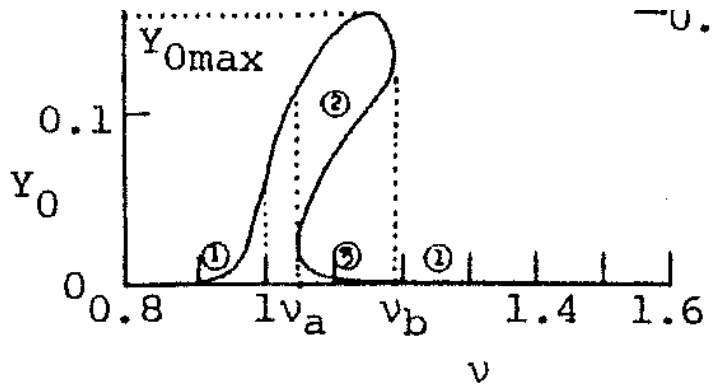

Fig. 5.26 System response predicted by the model (Tamura and Matsui, 1979).

served that the results are very similar to those predicted by the Hartlen-Currie model. Finally, comparisons with different experimental results have shown a good quantitative agreement (Tamura and Matsui, 1979).

5.5 Conclusions

The goal of a semi-empirical model for modeling vortex-induced vibration should be at least the prediction of the maximum body oscillation amplitude at values of the Scruton number different than that at which their parameters are estimated. The present study of the literature has shown that no model is able to carry out such a difficult task. Therefore, the improvement in this direction of one of this models would be a fundamental result.

The negative damping models try to carry out the previous task by using a single equation of the body oscillator forced by an aeroelastic forcing term. As it was previously shown (see for example Fig. 5.3), the significant variation of their aeroelastic parameters with respect to the Scruton number prevents such possibility.

The force-coefficient data models need only a particular type of device to impose forced vibrations, which is available in few laboratories. Moreover, they are not reliable in predicting response amplitude at different Scruton number.

The models based on Bishop-Hassan's concept or coupled model (Hartlen and Currie, 1970; Skop and Griffin, 1973; Iwan and Blevins, 1974; Landl, 1975; Dowell, 1981; Benaroya and Lepore, 1983; Krenk and Nielsen, 1999; Diana *et al.*, 2006) attempts to predict all the response amplitudes observed inside the synchronization region. The introduction of the wake oscillator coupled with that of the body is the way used to take into account the wake-body interaction. Despite the complexities involved, the models are not even able to predict all the main characteristics of the phenomenon at the Scruton number at which their parameters are estimated.

The only exception is the Skop-Griffin model which was realized with the scope of predicting quantitatively the cylinder oscillation amplitude without considering the other main characteristics of the lock-in phenomenon. It is also able to predict the maximum oscillation amplitude as a function of the Scruton number. Such a task was possible because it is only devoted to circular cylinders and then the determination of empirical relations to take into account the variation of their aeroelastic parameters with respect to the Scruton number was possible. Clearly, one such model cannot be applied to bridge decks because they are not characterized by standard cross-section shape.

Finally, the models based on the Birkhoff's concept (Funakawa, 1969; Nakamura, 1969; Tamura and Matsui, 1979) are clearly applicable to cross-sections with a short after-body, such as circular cylinders, in which the vortex-induced vibrations mainly depend on their interaction with the wake behind the body.

Chapter 6

Wind tunnel tests

6.1 Introduction

In this chapter the experimental work conducted in wind tunnel to analyse the Ehsan-Scanlan model is reported.

Static tests were carried out to verify the quality of the sectional model by comparing their aerodynamic characteristics with those reported in the literature for the same cross-section.

Ambient vibration tests on an elastically-supported rectangular cylinder were performed to obtain the peak-amplitude reduced velocity during lock-in at which the aeroelastic parameters have to be estimated. Such parameters were identified by conducting a particular type of test, called decay-to-resonance test.

A ratio between the vertical and torsional frequency of about 1.5 gave rise to an interaction between the two modes which would not allow to apply the present identification procedure, which requires that the frequencies are well separated. To solve the problem, much attention was payed in imposing the initial condition.

First of all, the experimental facilities and the instrumentation used are described. The design of the sectional model is reported and the experimental campaign is carefully treated with respect to its experimental set-up and results.

6.2 Experimental facilities

6.2.1 Wind tunnel

The wind tunnel tests were carried out in the CRIACIV[1] Boundary Layer Wind Tunnel in Prato, Italy (Fig. 6.1). The open circuit wind tunnel has a total length of about 22 m, and a test section of 2.40 m $\times$ 1.65 m with an upstream fetch of about 8 m (Fig. 6.2). The target wind speed, in the range of 0 to 30 m/s, is obtained by both the adjustment of the fan rotation speed and of the pitch of its 10 blades. A small longitudinal variability of the tunnel width accommodates for the formation of floor, ceiling and walls boundary layers, thus keeping the static pressure almost constant along the tunnel length.

[1] Inter-University Research Centre for Building Aerodynamics and Wind Engineering

Fig. 6.1 CRIACIV Boundary Layer Wind Tunnel.

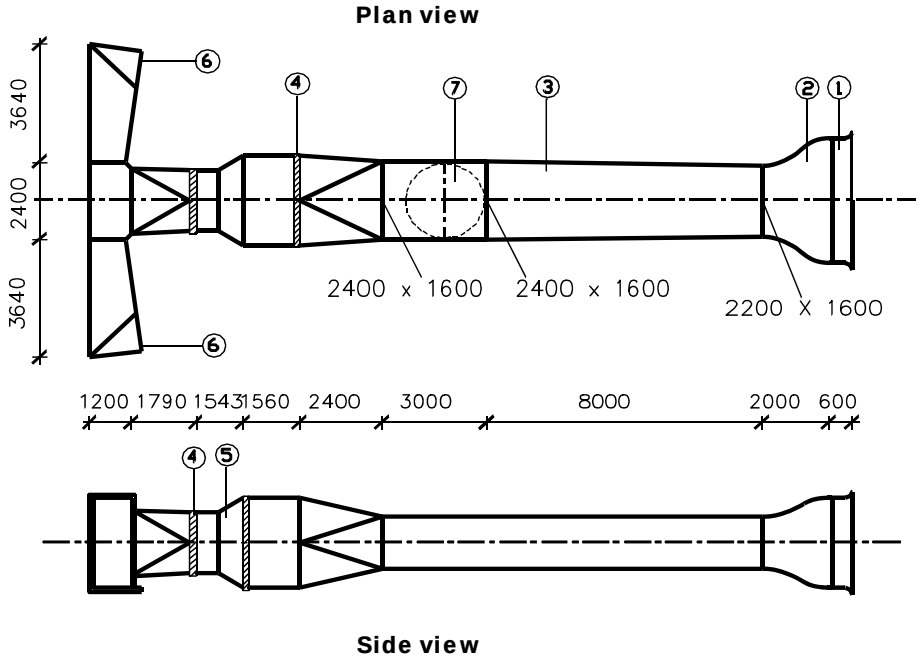

Fig. 6.2 Sketch of the CRIACIV Boundary Layer Wind Tunnel: 1. Inlet with honeycomb grid; 2. Contraction; 3. Boundary Layer development zone; 4. Elastic Joint; 5. Propeller (160kW); 6. Diffuser; 7. Test section with turntable.

Table 6.1 Main technical characteristics of the strain-gauges load cells.

Measure range	$0 \div 120$ N
Sensitivity	2 mV/V at end scale (FS)
Repeatability error	$\leq \pm 0.033\%$ FS
Error of non-linearity and hysteresis	$\leq \pm 0.023\%$ FS
Error of thermic variation of the zero-point	$\leq \pm 0.033\%$ FS
Creep error after 8 hours	$\leq \pm 0.033\%$ FS
Zero unbalancing	$\leq \pm 2\%$ FS
Maximal deflection at FS	≤ 0.6 mm
Safety limit load	50%
Coaxial fixing holes	IP65
Out of axis loads	insensitive until 10 cm

6.2.2 Instrumentation

For the aeroelastic tests reported herein the following instruments were adopted:

- A Pitot tube
- Six strain-gauges load cells
- Three laser transducers for displacements measurements

The Pitot tube measures the mean static and dynamic pressures of the oncoming flow and then, after the flow density is known, the mean wind speed can be obtained. It is located some meters upwind where an undisturbed flow can be found. The instrument is connected to a pressure transducer (Setra System, model 239) whose voltage signal is acquired by a PC by a data acquisition card (National Instruments AT-MIO 16XE50).

Six 535 QD strain-gauges load cells produced by DS EUROPE s.r.l., are used to measure the aerodynamic forces on the stationary section model (Fig. 6.3a). Their technical characteristics are reported in Table 6.1. The actual linearity of these instruments is checked as shown in Fig. 6.3b.

Three non-contact optical laser transducers (Micro-epsilon Model OptoNCDT 1605) were used to determine the model displacements during the tests (Fig. 6.4a). They uses a semiconductor with 675 nm wavelength and a maximum output power of 1mW, their functioning principle is based on triangulation. The output voltage range is ± 10 V which corresponds to a working displacement range of about $\pm$ 100 mm. The lasers are connected to a card (National Instruments AT-MIO 16XE50) and then logged through a PC. The characteristics of the lasers are reported in Tab. 6.2. The linearity of the three lasers was verified by a high precision mechanical distantiometry and the results are shown in Fig. 6.4b.

6.3 Set-up and model design

6.3.1 Sectional model design

A rectangular cross section was chosen because its simple shape allows a detailed study of several aerodynamic features of the flow field around it. In addition rect-

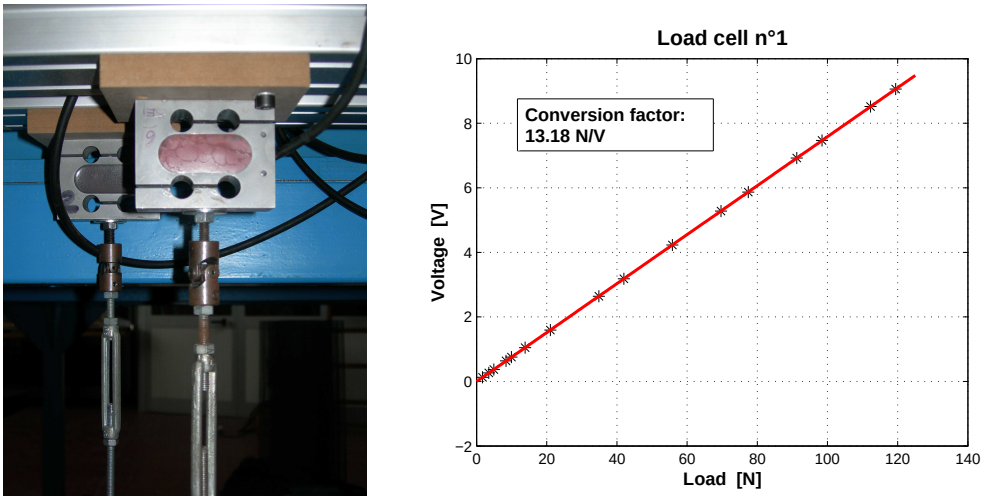

(a) (b)

Fig. 6.3 (a) View of a load cell; (b) relationship between load cell output voltage and actual force applied (Mannini, 2006).

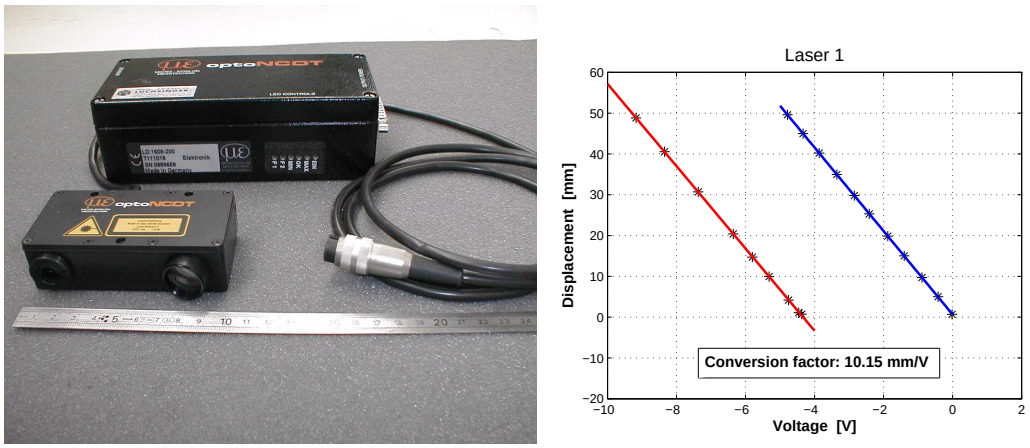

(a) (b)

Fig. 6.4 (a) View of a laser device for displacement measurements; (b) relationship between laser output voltage and actual object distance (Mannini, 2006).

Table 6.2 Micro-epsilon Model OptoNCDT 1605 laser characteristics.

Sensor type	Laser sensor
Model	LD 1605
Type	200
Measuring range	± 100 mm
Stand-off midrange	340 mm
Non-linearity $\leq \pm 0.3\%$ d.M.	600 μm
Resolution (noise) static	60 μm
Measuring spot dia. midrange	2 mm
Light source	Laser 1 mW, wavelength: red 675 nm
Sampling frequency	40 kHz
Laser class	2
Analogical Output	
Displacement	±10 V
Output impedance	appr. 0 Ohm (10 mA max.)
Angle dependance	appr. 0.5% when turning ±30 about long. axis
Rise time	0.1/0.2/2 or 20 msec selectable
Frequency response	10 kHz, 3 kHz, 250 Hz or 25 Hz
Temperature stability	0.03%/K
Intensity of reflecting light	1 V bis 10 V/max; 0 V bis +13 V
Permissible ambient light	2000 Lux
Life time	50000 h for laser-diode
Insulation	200 VDC, 0 V against housing
Max. vibration	10 g to 1 kHz
Operation temperature	0-50 C

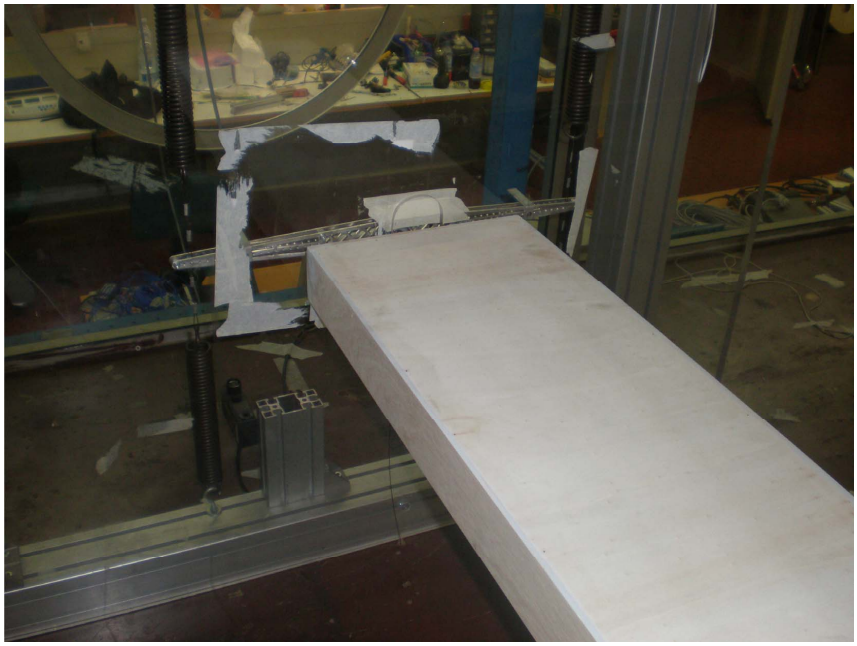

Fig. 6.5 View of the model in the test chamber.

angular cylinders are often assumed as an extreme schematization of bridge decks. Moreover, a width-to-depth ratio of 4 was used not only because it is a typical ratio of bluff bridge decks but also because it is supposed to give appreciable response amplitudes at lock-in.

As it was underlined in Chapter 4, the response during lock-in increases as Scruton number decreases[2]. For a circular section a value of 20 as threshold between large and small vibrations was pointed out[3]. Since the previous threshold depends on the shape of the section, to assess the Scruton number under which large vibrations occur for a rectangular section with $B/D = 4$, the results of Simiu and Miyata (2006) and Ehsan and Scanlan (1990) are considered. Moreover, Simiu and Miyata (2006) defined the Scruton number by $Sc = 2m\delta/\rho BD$, which provides values more in agreement with those of the circular cylinder obtained with the classical definition of the Scruton number. Obtaining significant vibrations is the design objective of the model, therefore, a Scruton number of the model as low as possible must be obtained. This means that a mass as low as possible and a depth of the cross section as high as possible have to be provided. The reduction of the mass is limited by the stiffness of the model, the increase of the depth of the cross section instead is fixed by the blockage ratio. To reduce the weight (2.9 kg) the model was composed by two lateral faces of plywood and two vertical faces made of a hard wood (toulipier) to obtain edges as sharp as possible (Fig. 6.5). The width and the depth of the cross section are respectively $B = 0.3$ m and $D = 0.075$ m and a longitudinal length L =0.986 m gives rise to an aspect ratio $L/B = 3.28$. The longitudinal tube was made of alluminium (2700 kg/m^3). A solid blockage of 2 %[4] was obtained fixing the

[2]As it will reported in Chapter 7, this statement is rigorously valid only for structures susceptible to wind.

[3]That is true when the Scruton number is defined as $2m\delta/\rho D^2$.

[4]As the blockage ratio given by the columns of the support frame located about 25 cm windward

Fig. 6.6 View of the test chamber during the experiments.

depth of the cross section at 7.5 cm. Before designing the elastic support, to check the stiffness of the model, a frequency of 72.90 Hz of its first mode on fixed supports was calculated.

6.3.2 Elastic support design

The model was supported elastically by a set of 8 springs, each of them with a stiffness of 5340 N/m. This value, which must be as high as possible to avoid a low lock-in wind speed, was limited by the force necessary to impose the initial displacement and by the resistance of the elements constituting the set-up. In particular, for an initial displacement of 7.5 mm (0.1 D) a force of 320.4 N had to be applied. The vertical and torsional frequencies estimated were 14.3 Hz and 21.5 Hz, respectively, assuming an eccentricity of the springs of 30 cm. Finally, vertical and torsional lock-in wind speeds of 7.6 and 11.5 m/s were expected.

6.3.3 Experimental set-up

A schematization and a photo of the experimental set-up are shown in Fig. 6.6 and Fig. 6.7. The mass of the model-elastic support system was 6.0 kg (mass of the section model, mass of the moving support parts and participating mass of the springs), that is $m = 6.085$ kg/m. The vertical frequency measured in still air f_n was high enough (13.43 Hz) to observe the phenomenon of synchronization at a sufficiently high wind speed ($U \cong 8.5$ m/s, observed during the test). The damping

was 7.5 %, to maintain the total blockage ratio under 10 % that of the model alone was fixed to 2 %. It is worth noting that in this case the quantification of the real blockage ratio is not easy because the two columns are located upwind with respect to the sectional model.

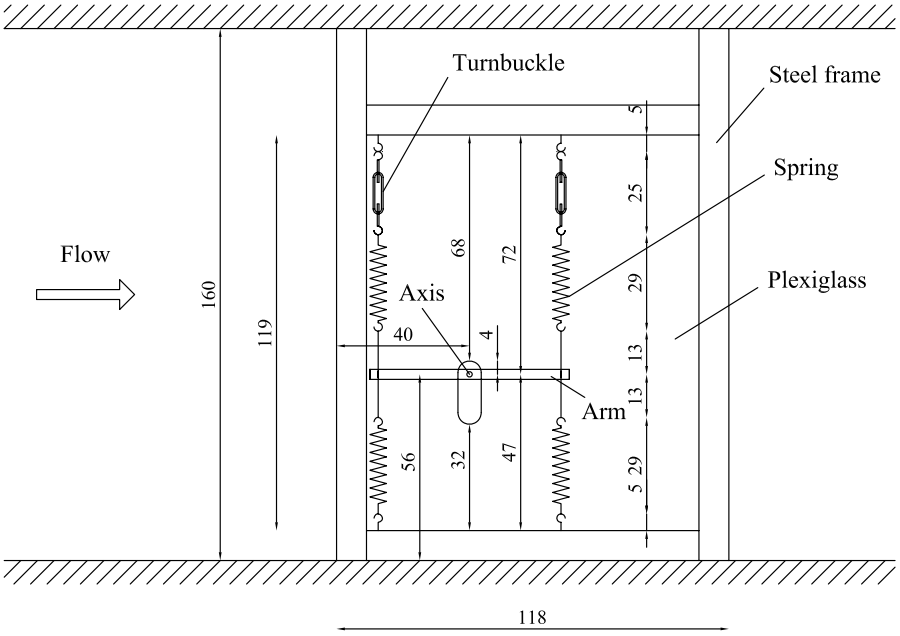

Fig. 6.7 Sketch of the experimental set-up.

Table 6.3 Main characteristics of the experimental set-up.

D (mm)	B (mm)	L (mm)	St (-)	m (kg/m)	m_r (-)	f_n (Hz)	ζ (%)	Sc (-)
75	300	986	0.136	6.085	0.0011	13.43	0.21	6.0

ratio measured in still air was 0.0021 and the corresponding Scruton number was 6.0 (defined as $4\pi m\zeta/\rho BD$). In Fig. 6.8 the free vibration response of the model is reported. Two vertical plates in plexiglass were used to foster a bidimensional flow. The main characteristics of the set-up are summarized in Tab. 6.3.

6.4 Experimental program

To measure the two frequencies and the damping coefficient of the sectional model, free vibration tests in still air were carried out.

All the wind tunnel tests were conducted in smooth flow[5].

Static tests were carried out for different wind velocity to check the stability of the results with respect to the Reynolds number and for different angles of attack. They were needed to verify the quality of the model by comparing their aerodynamic characteristics with those reported in the literature for the same cross-section.

Ambient vibration tests were performed on an elastically-supported cylinder with its longitudinal axis orthogonal to the flow. The scope of the tests was that of individuating the reduced velocity of the peak amplitude response at which the aeroelastic

[5]As it can be observed from other tests carried out during the same period on a rectangular cylinder in smooth flow in the same wind tunnel (Bartoli *et al.*, 2011), the intensity and the longitudinal integral scale length of the turbulence in the test chamber ($I_u \cong 3\%$, $L_u \cong 10$ cm, at $U \cong 10$m/s) resulted higher than the classical thresholds ($I_u = 1\%$, $L_u \cong 0$) used to define if a flow can be considered as smooth.

Fig. 6.8 Aeroelastic set-up.

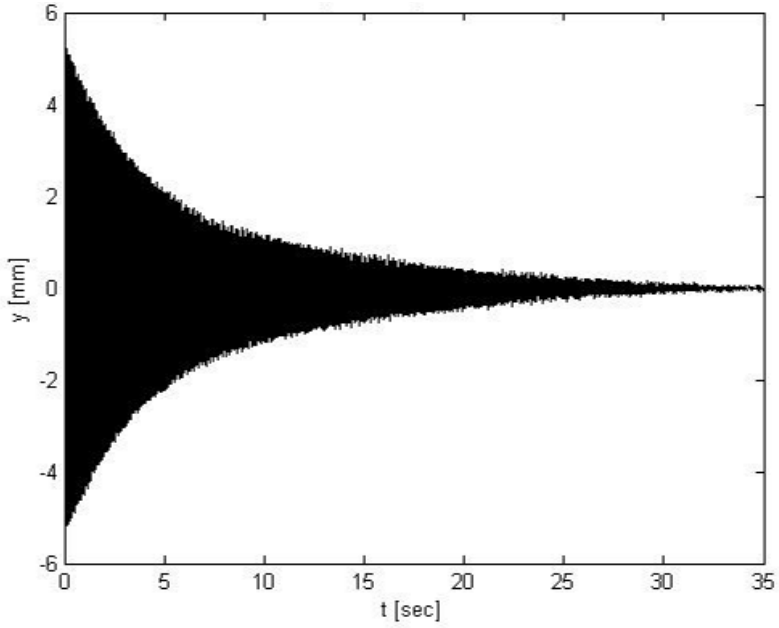

Fig. 6.9 Experimental response in the heaving mode recorded during a free vibration test in still air.

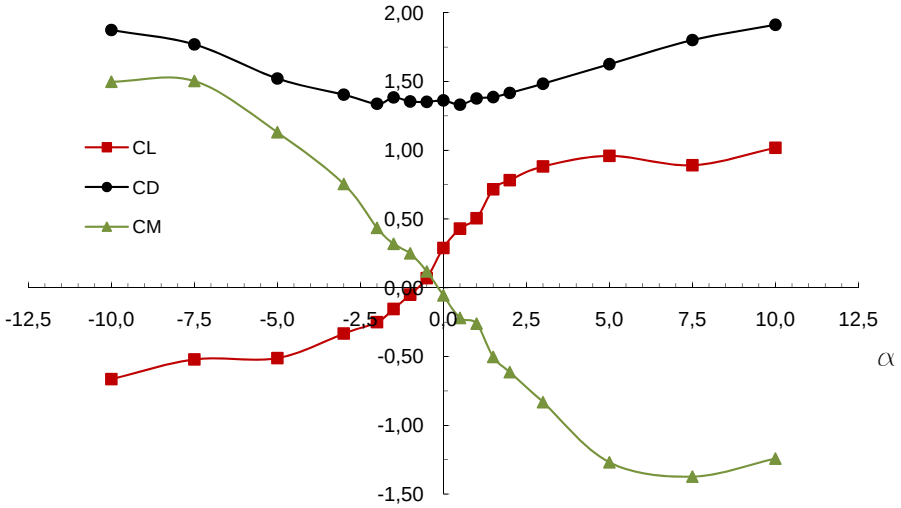

Fig. 6.10 Aerodynamic coefficients for different angles of attacks.

parameters have to be estimated. Moreover, the ambient vibration response of the model was registered by both increasing and decreasing the wind speed to observe the possible existence of the hysteresis effect. The Reynolds number during the tests was about 40000 (normalized with respect to D).

Finally, decay-to-resonance tests were carried out at the peak-amplitude reduced velocity to estimate the aeroelastic parameters. Such tests were also repeated inside the lock-in region at different reduced velocity to understand the variation of the aeroelastic parameters.

6.5 Experimental response

6.5.1 Static tests

Fig. 6.10 reports the three aerodynamic coefficients C_D, C_L and C_M for a range of the angle of attack from -10^o to 10^o. The minimum drag and lift coefficients were respectively 1.352 and 0.07, both at a value of the angle of attack of -0.5^o. In particular, the value of the drag coefficient is a little higher than the superior extreme of the range reported in the literature [$C_D = 1.1 - 1.2$, Shimada and Ishihara (2002)] by using CFD. The lift coefficient at 0^o should be equal to zero for a rectangular section, but the value of 0.07 can be considered acceptable. Finally, the minimum values of the two coefficients are obtained at an angle of attack near zero because the flow in the test chamber was observed to be inclined of the same angle (Bartoli *et al.*, 2011).

The Strouhal number ($S_t = f_s D/U$, where f_s is the frequency of vortex shedding) measured during static tests was 0.136, which is in agreement with the values 0.13-0.14 given by Shimada and Ishihara (2002). The wind velocity during the test was about 16 m/s.

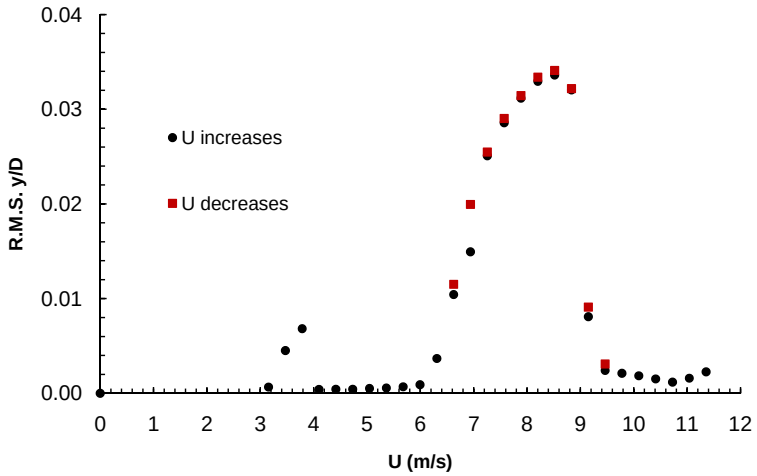

Fig. 6.11 R.M.S. values of the non-dimensional response amplitude vs. wind velocity: black circular/red squares refer to results obtained after wind velocity is increased/decreased.

6.5.2 Ambient vibration tests

The root-mean-square (R.M.S.) values of the response amplitude during the synchronization are reported in Fig. 6.11. It is interesting to observe that no hysteretic effects were observed. Moreover, due to the large stiffness of the springs used and the consequent high vertical frequency, it was also possible to detect the synchronization with the first subharmonic of the natural vertical frequency.

To demonstrate the reproducibility of the results, tests were repeated three times with results in good agreement among them (Fig. 6.12).

The R.M.S. of the non-dimensional amplitude obtained in the present wind tunnel tests were compared with the ambient vibration responses of the literature (Fig. 6.13). The comparison is not easy due to the different test conditions. Moreover, it is not clear if the vibration amplitudes of the literature results are R.M.S. values or the amplitude of the response.

The tests were carried out with a vertical to torsional frequency ratio of about 1.55. As it can be observed in Fig. 6.14, such value of the frequency ratio give rise to an appreciable interaction between the two modes. In particular, an interaction between the first subharmonic of the torsional degree of freedom and the harmonic of the vertical one is shown. A low interaction with the harmonic of the rolling mode is also present.

6.5.3 Decay-to-Resonance tests

To identify the aeroelastic parameters Y_1 and ϵ of the model proposed in Scanlan (1981), a particular type of wind tunnel test, called decay-to-resonance test, has to be conducted. It consists in measuring the response amplitude at the wind velocity corresponding to the maximum response, after imposing to the model an initial displacement larger than the limit-cycle amplitude measured at lock-in. The experimental signal during such a test and a close-up of its transient part is reported in Fig. 6.15. It is clear the strong effect of the torsional mode on the decaying response of the vertical mode. Such a signal does not allow to identify the aeroelastic pa-

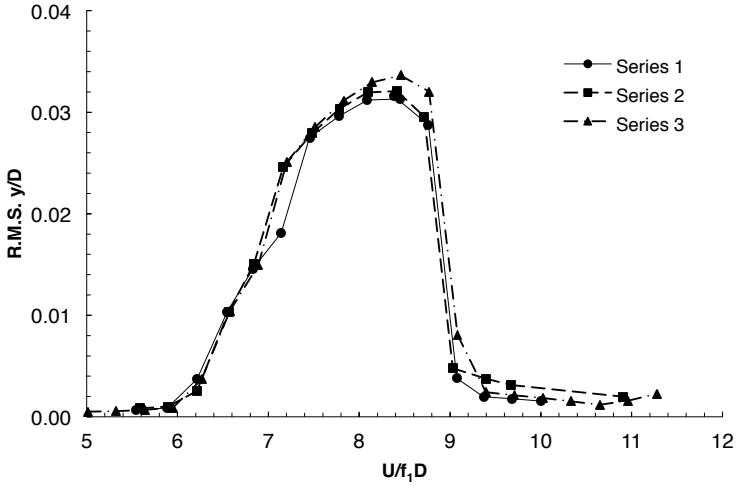

Fig. 6.12 R.M.S. values of the non-dimensional response amplitude vs. reduced velocity (f_1 = vertical natural frequency).

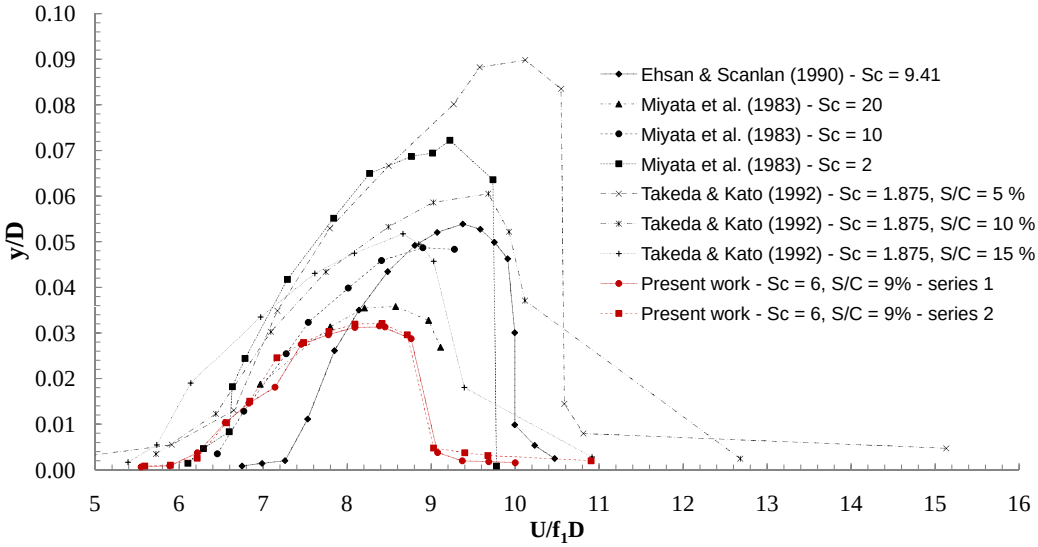

Fig. 6.13 Comparison between the R.M.S. values of the non-dimensional response amplitude vs. reduced wind velocity obtained in the present work and those of the literature.

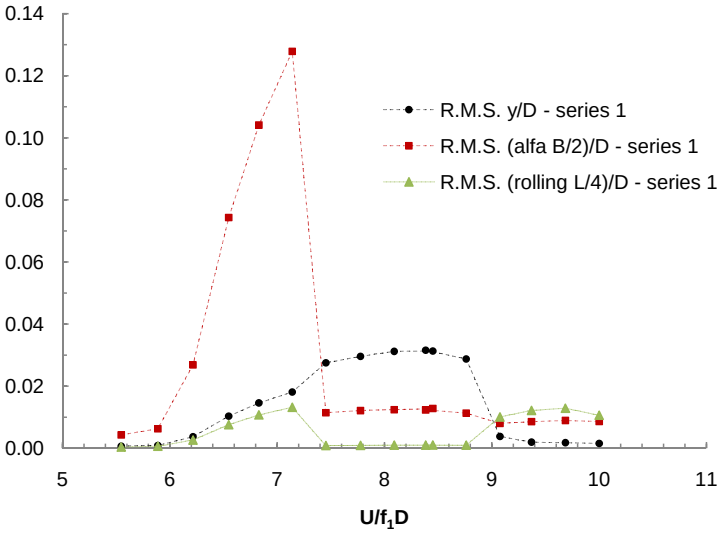

Fig. 6.14 R.M.S. values of the non-dimensional response amplitude vs. reduced wind velocity. Black circles: vertical degree of freedom; red squares: pitching degree of freedom; green triangles: rolling degree of freedom.

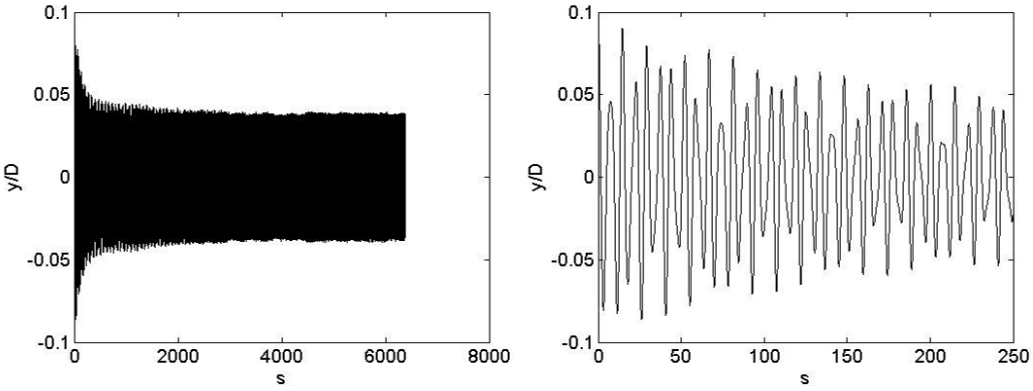

Fig. 6.15 Non-dimensional displacement signal recorded during a decay-to-resonance test versus dimensionless time $s = Ut/D$: a) complete signal; b) close-up of the transient part.

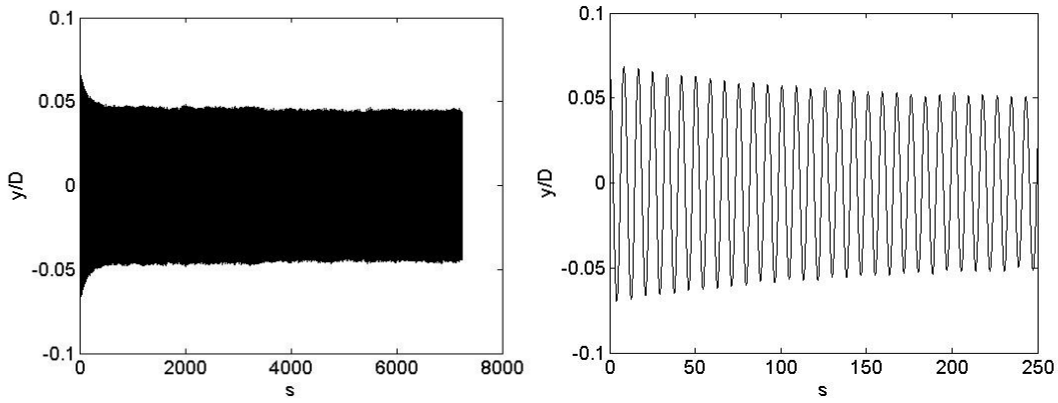

Fig. 6.16 Non-dimensional displacement signal recorded during a decay-to-resonance test versus dimensionless time $s = Ut/D$ with the torsional mode restricted: a) complete signal; b) close-up of the transient part.

rameters with the procedure proposed in Ehsan and Scanlan (1990), which can be applied to system with well separated frequencies. Therefore, to apply the procedure to the model it was necessary to pay attention in imposing the initial condition to avoid the interaction between the two modes. In particular, when the vertical initial condition is imposed to the model the vertical degree of freedom is restrained. In this condition, being the torsional degree of freedom the only one of the system, lock-in oscillations in the torsional mode can occur. Therefore, to avoid of obtaining a coupled signal as the one reported in Fig. 6.15, the model was realized from the initial condition before the torsional lock-in oscillations due to the synchronization with the first subharmonic of the torsional degree of freedom taking place. Fig. 6.16 shows the response obtained after such strategy was applied.

6.6 Conclusions

Wind tunnel tests were carried out in order to analyse the Ehsan-Scanlan model in the next chapter.

A 4:1 rectangular cross-section was chosen for the section model used to estimate the aeroelastic parameters of the empirical model, because it allows to compare the results with those reported in the literature. The sectional cylinder was designed to have a weight as low as possible which implies a low Scruton number and then large oscillations at lock-in. Being the aerodynamic/aeroelastic behavior of a bluff body with sharp edges strongly dependent on the actual sharpness of its edges, two vertical faces of the model were made of an hard wood (toulipier).

Wind tunnel tests on the fixed rectangular cylinder were carried out to verify the quality of the section model by comparing its aerodynamic characteristics (C_D, C_L, C_M, and St) with those presented in the literature obtained from section models with the same cross section. The results showed that the model is suitable to conduct aeroelastic tests.

Ambient vibrations increasing and decreasing the wind speed were carried out and their results were compared with those reported in the literature. It was observed how the comparison is not easy because of the different values of Scruton number, blockage ratio, set-up, oncoming flow, frequency ratios and so on. The high lock-

in wind speed obtained due to the high vertical frequency obtained by using stiff springs allowed to observe also the synchronization with the first subharmonic of the vertical mode. No hysteretic effect was observed probably due to the relatively high value of the Scruton number.

The vibrating system was characterized by a ratio between the torsional and vertical mode of 1.5 which gave rise to a coupling between the modes. Such a behavior would prevent the application of the model under study, therefore, much attention was spent in imposing the initial condition.

Chapter 7

Van der Pol-type modeling for wind vortex-induced vibrations

7.1 Introduction

As reported in section 5.5, the goal of an empirical model for vortex-induced vibrations should be the prediction for any section shape of the maximum body oscillation amplitude at values of mass and damping different from those at which the model parameters were estimated. Unfortunately in the literature no model is able to accomplish this task. Therefore, any improvement in this direction would be a fundamental result.

Moreover, an empirical model for vortex-induced vibrations of line-like structures of complex sections such as bridge decks may be useful for practical applications if it requires few and relatively simple wind tunnel tests. Such characteristics can be found in the single-degree-of-freedom (SDoF) models, although they only provide the maximum oscillation amplitude without giving any information about the velocity range of lock-in and the pattern of the oscillation amplitudes inside it.

Among the SDoF models, that proposed by Ehsan and Scanlan (1990) satisfies the previous requirement: a single wind tunnel test with a relatively simple experimental setup, called decay-to-resonance test, is needed to estimate its parameters. It represents an improvement of the model proposed by Scanlan (1981), which takes into account the self-limiting behavior of the lock-in phenomenon by a van der Pol-type equation with two aeroelastic parameters that were estimated by two wind tunnel tests for two very close values of the damping coefficient. Approximating the regime solution of the van der Pol-type equation with a sinusoid, Scanlan (1981) obtained an expression for the limit cycle amplitude depending on the Scruton number only. The improvement given in Ehsan and Scanlan (1990) to the original model regards a more efficient identification procedure based on the approximate solution of the nonlinear equation provided by the method of slowly varying parameters (Van der Pol, 1920), which allows to estimate the two aeroelastic parameters by a single wind tunnel test.

Despite its practical feasibility, the model had not great applicability due to its unreliability in predicting the experimental responses at structural conditions different from those at which the aeroelastic parameters were estimated (Scanlan, 2004). This limit is apparent just observing the strong dependence of the aeroelastic parameters on the structural damping ratio (Ehsan and Scanlan, 1990). Although the

model does not allow reliable predictions varying the Scruton number, the parameters identified on the section model can be used to calculate the response of the full bridge considering the actual modal properties of the structure. In particular, an attempt to take into account the imperfect spanwise correlation of the aeroelastic force was done by employing the wind tunnel data obtained through forced vibration tests on section models (Ehsan and Scanlan, 1990).

In the present work the Ehsan-Scanlan model was deeply studied and the results of the wind tunnel tests reported in the previous chapter are used to conduct numerical calculations.

First of all, the physical coherence of the van der Pol-type equation used to model vortex-induced vibrations of structures prone to wind excitation (bridges, towers, chimneys, cables, etc.) was highlighted. In fact, it is known that for such structures, characterized by large mass ratios, the maximum limit cycle oscillation amplitude at lock-in depends on a single mass-damping parameter only, called Scruton number. In agreement with the approximate solution used in the Ehsan-Scanlan model, the numerical integrations of the equation of motion conducted in this study confirmed such behavior in the regime solution of the van der Pol-type equation.

Moreover, the validity of the assumption (quasi-liner system) standing behind the identification procedure employed by Ehsan and Scanlan (1990) to determine the aeroelastic parameters of the model is demonstrated.

In addition, the bridge response expression proposed in the literature was lightly modified to take into account not only the modal contribute of the deck but also that of the other structure elements.

Finaly, it is also highlighted the strong dependence of the aeroelastic parameters on the choice of the limit-cycle oscillation amplitude of the experimental signal, which is not always simple to define.

In the next section the key role played by the Scruton number in wind engineering applications is discussed, then in section 7.3 the Ehsan-Scanlan model is outlined and a modified version for the bridge response is proposed. Section 7.4 demonstrates by means of numerical integrations the physical coherence of the model, the validity of the approximate solution and identification procedure used in the Ehsan-Scanlan model. Section 7.5 shows the effect of the definition of the experimental limit-cycle oscillation amplitude on the results. Finally, in section 7.6, some conclusions are reported.

7.2 Mass-damping parameter

In this section the results available in the literature are discussed to clarify the role of the Scruton number. In fact, one of the fundamental questions in the study of vortex-induced vibrations concerns the understanding of the conditions under which the classically employed mass-damping parameters can be utilized to predict the peak-amplitude response (Khalak and Williamson, 1999; Williamson and Govardhan, 2004). In the literature different definitions for the mass-damping parameter can be found (Khalak and Williamson, 1999). Vickery and Watkins (1964) plotted the peak amplitude at lock-in of flexible cantilevers versus a stability parameter $K_s = \pi^2 m^* \zeta$, where $m^* = 4m/(\pi \rho D^2)$ is the mass ratio, m the mass of the structure per unit length, ρ the air density, D the height of the cross section and ζ the structural damping). Scruton (1963) used a similar parameter ($Sc = \pi m^* \zeta/2$), later

called Scruton number (Zdravkovich, 1982); Skop and Griffin (1973) proposed the Skop-Griffin parameter ($S_g = 2\pi^3 St^2 m^* \zeta$, where St is the Strouhal number).

Under the assumption of a sinusoidal aeroelastic force and structural response with the same frequency, Bearman (1984) showed qualitatively how the maximum amplitude depends on the mass and damping coefficient separately only if the mass ratio is low enough to allow a significant shift of the frequency during vortex-induced vibrations with respect to the still-air value.

Sarpkaya (1979), analyzing the equation of the wake oscillator model proposed by Hartlen and Currie (1970), underlined that the response of the system is independently governed by the damping and the mass and that, in general, the equation cannot be formulated in terms of a single mass-damping parameter. According to Sarpkaya (1978) the mass ratio and the damping affect separately the maximum oscillation amplitude when $S_g < 1$. In contrast, for Khalak and Williamson (1999) the previous limit should be reduced of two orders of magnitude.

It is evident that in the literature there is not a definitive agreement on the actual role played by the mass-damping parameter in the case of structures characterized by a low mass ratio ($m^* = 1-20$, i.e., marine and off-shore structures). Nevertheless, Zdravkovich (1990) states: "Scruton combined the mass ratio and damping into a single parameter which proved to be useful in wind engineering ($m^* > 100$)". For example, the mass ratio of a steel cable of circular cross section is 6280, that of a 60 m high steel chimney (Dyrbye and Hansen, 1997) is about 113 ($m = 1000$ kg/m, $D = 3$ m and thickness $t = 10$ mm). Nevertheless, it is important to remark that the threshold indicated by Zdravkovich (1990) is mainly referred to sections similar to a circle and it can be taken only as a rough reference for very different geometries, such as those of bridge sections. In this case it would be more reasonable to redefine the mass ratio by normalizing the mass per unit length with the area of a rectangle with the same width B and height D of the deck section instead of the area of a circle, thus obtaining $m^{**} = m/(\rho BD)$. Consequently, for instance it results that the mass ratio of the approaching span of the Great Belt East Bridge (Larsen and Walther, 1997), which showed significant oscillations due to vortex-induced vibrations, is about 71 ($m = 16 \cdot 10^3$ kg/m, $D = 7$ m, $B = 25.8$ m), that of the Tacoma Narrows Bridge (Bartoli and Mannini, 2008) is about 116 ($m = 4250$ kg/m, $D = 2.44$ m, $B = 12.0$ m), while the mass ratio of the Normandy Bridge (Bartoli and Mannini, 2008) is about 150 ($m = 13700$ kg/m, $D = 3.08$ m, $B = 23.8$ m). Significantly higher values of the mass ratio for these bridge decks would have been obtained by employing the definition of m^*.

The statement by Zdravkovich (1990) is confirmed by the results presented in Griffin *et al.* (1982) [reported in Bearman (1984) and Khalak and Williamson (1999)] for a circular cylinder with values of the mass ratio significantly lower than 100 (Fig. 7.1). It can be seen that similar values of the mass-damping parameter (in this case $2m\delta/(\rho D^2)$, where δ is the logarithmic decrement) provide maximum oscillation amplitudes which are practically identical, though the shape of the resonance curve is not the same.

In conclusion, according to the literature, for structures prone to the wind action (characterized by a mass ratio higher, say, than 100), the maximum oscillation amplitude during lock-in seems to depend on the Scruton number alone.

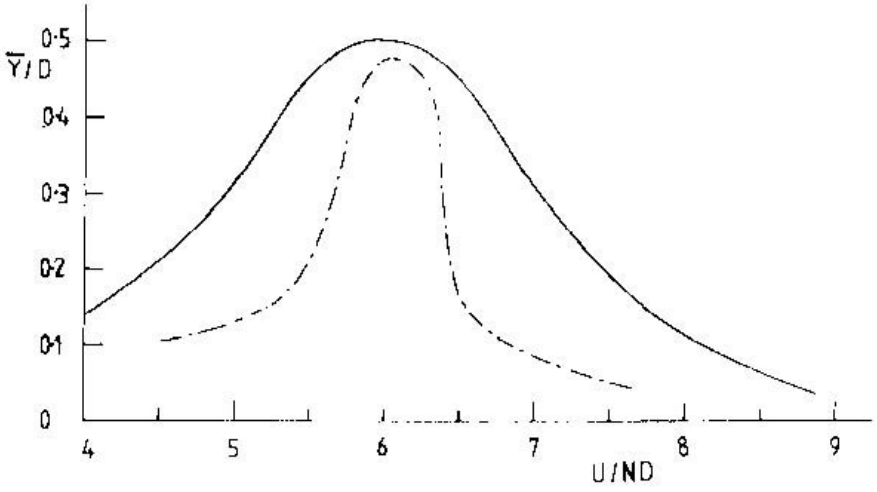

Fig. 7.1 Non-dimensional cross-flow amplitude versus reduced velocity for a circular cylinder. Solid line: water, $4m/(\pi\rho D^2) = 4.8$, $\delta = 5.1 \times 10^{-2}$, $2m\delta/(\rho D^2) = 0.39$; dotted line: air, $4m/(\pi\rho D^2) = 43.3$, $\delta = 4.3 \times 10^{-3}$, $2m\delta/(\rho D^2) = 0.29$ ($\overline{Y}$ is the cross-flow amplitude and N the vertical frequency in still air) (after Griffin et al., 1982).

7.3 Van der Pol-type modeling of vortex-induced vibrations

As reported by Sarpkaya (1979), a question frequently raised in the literature is "why an equation of the van der Pol kind should at all describe fluid-body interaction?". Actually, as experimental validations demonstrated, such a model does not seem to describe the previously mentioned interaction (Sarpkaya, 1979).

An attempt to formulate a mathematical model starting from basic concepts of fluid dynamics was made by Iwan and Blevins (1974). In their model they applied the conservation of momentum in a control volume around the oscillating body and, assuming the weighted average of the transversal flow velocity as fluid dynamic variable, under several assumptions they obtained a van der Pol equation for the wake oscillator. This van der Pol-type equation is very similar to that reported in Hartlen and Currie (1970), where a phenomenological approach was used. Nevertheless, Iwan and Blevins's derivation of the van der Pol equation does not seem fully convincing, as discussed by Sarpkaya (1979), Bearman (1984) and Billah (1989).

However, what has encouraged many researchers to use a van der Pol-type equation for modeling vortex-induced oscillations is its high versatility in predicting many relaxation oscillations, such as the beating of the heart. In particular, for small values of the parameters that multiplies the nonlinear term, the model allows a limit cycle with nearly harmonic features, as it is for vortex-induced vibrations.

As it was previously stated, different van der Pol-type equations were proposed as models of vortex-induced vibrations. In particular, Scanlan (1981) proposed a semi-empirical nonlinear model for the across-flow response, that considers the following equation:

$$m(\ddot{y} + 2\zeta\omega_1\dot{y} + \omega_1^2 y) = F(y, \dot{y}, t) \tag{7.1}$$

$$F(y,\dot{y},t)=\frac{1}{2}\rho U^2(2D)\left[Y_1(K)\left(1-\epsilon\frac{y^2}{D^2}\right)\frac{\dot{y}}{U}+Y_2(K)\frac{y}{D}+\frac{1}{2}C_L(K)sin(\omega t+\theta)\right] \tag{7.2}$$

where ω_1 is the circular natural frequency in still air, U the mean wind speed, $K=\omega D/U$ is the reduced frequency during vortex-induced vibrations (being ω the corresponding circular frequency of vibration under wind), θ the phase angle of the harmonic force due to vortex shedding, $Y_1(K)$, ϵ, $Y_2(K)$, $C_L(K)$ are parameters which have to be determined through wind tunnel tests. The parameters Y_1 and ϵ are related, respectively, to the linear and nonlinear component of the aerodynamic damping. In particular, ϵ allows to take into account that the oscillations are self-limiting. The parameter Y_2 represents the aerodynamic stiffness term. Finally, the vortex-shedding part of the force is modeled by a sinusoidal function through the C_L coefficient. According to Ehsan (1988) [see Ehsan and Scanlan (1990)], when large amplitudes occur, the vortex-shedding force is negligible with respect to the motion-induced one. Thus, at lock-in Eq. (7.2) can be reduced to the following form:

$$F(y,\dot{y},t)=\frac{1}{2}\rho U^2(2D)\left[Y_1(K)\left(1-\epsilon\frac{y^2}{D^2}\right)\frac{\dot{y}}{U}+Y_2(K)\frac{y}{D}\right] \tag{7.3}$$

In addition, since there is not an appreciable shift between the frequency of the system at lock-in and its natural frequency in still air, the parameter Y_2 can be neglected (Ehsan and Scanlan, 1990; Marra *et al.*, 2011b). Therefore the previous equation becomes:

$$F(y,\dot{y},t)=\frac{1}{2}\rho U^2(2D)\left[Y_1(K)\left(1-\epsilon\frac{y^2}{D^2}\right)\frac{\dot{y}}{U}\right] \tag{7.4}$$

To obtain the aeroelastic parameters (ϵ and Y_1) by a single wind tunnel test, one needs to have a solution of Eq. (7.1). Nevertheless, due to its nonlinear character, a closed-form solution is not available. Introducing the quasi-linear system approximation, the method of slowly varying parameters can be applied (Van der Pol, 1920) and an approximate harmonic solution with variable amplitude can be obtained:

$$\frac{y(s)}{D}=A(s)cos(K_1 s-\psi_0) \tag{7.5}$$

where its envelope is described by the following expression:

$$A(s)=\frac{\beta}{\sqrt{1-\left(\frac{A_0^2-\beta^2}{A_0^2}\right)e^{-(\alpha\beta^2/4)s}}} \tag{7.6}$$

being $s=Ut/D$ the non-dimensional time, ψ_o the phase at time $s=0$, A_0 the initial-condition dimensionless displacement,

$$\alpha=m_r Y_1\epsilon \tag{7.7}$$

$$\beta=\frac{2}{\sqrt{\epsilon}}\sqrt{1-\frac{2\zeta K_1}{m_r Y_1}}=\frac{2}{\sqrt{\epsilon}}\sqrt{1-\frac{B}{D}\frac{ScSt}{Y_1}} \tag{7.8}$$

where $m_r=\rho D^2/m=4/(\pi m^*)$ is the mass ratio, as defined in Ehsan and Scanlan (1990), $K_1=\omega_1 D/U$ is the reduced natural frequency, $Sc=4\pi m\zeta/(\rho BD)$ is the Scruton number as defined hereafter and $St=f_s D/U$ the Strouhal number, being f_s

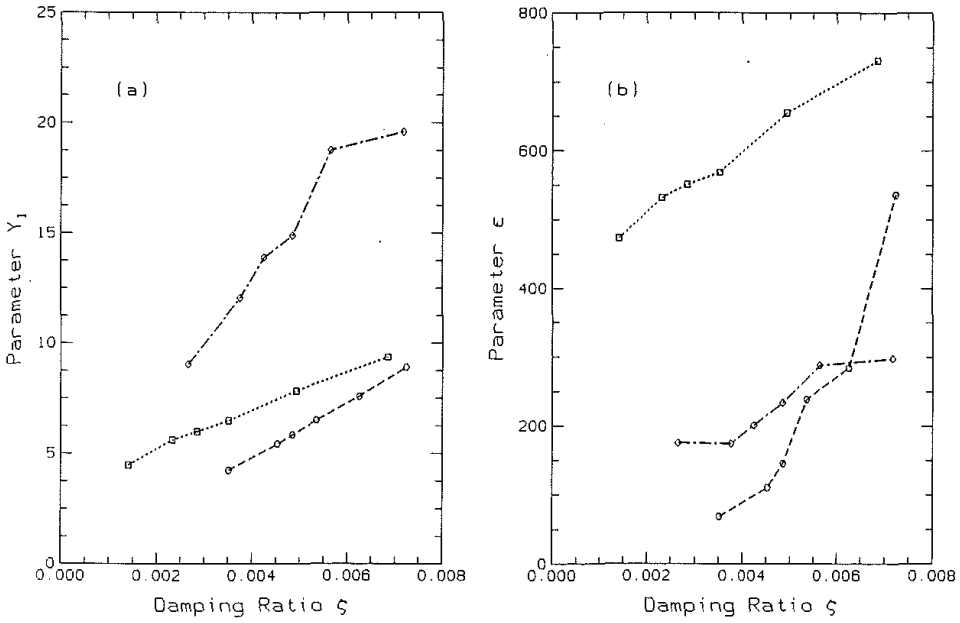

Fig. 7.2 Variability of the aeroelastic parameters Y_1 and ϵ with respect to the damping coefficient (after Ehsan and Scanlan, 1990).

the frequency of vortex shedding. Once the structural (m, ζ, ω_1) and the aeroelastic parameters (Y_1, ϵ) have been identified, the model provides the value of the limit cycle response amplitude through Eq. (7.8). It is easy to observe that the response is supposed to depend on the Scruton number alone rather than on the mass and damping coefficient separately. Eq. (7.8) for the limit cycle amplitude β has been determined in Ehsan and Scanlan (1990) by applying the method of slowly varying parameters. Nevertheless it was first obtained by Scanlan (1981) by assuming a purely sinusoidal motion and equating to zero the balance of energy over one cycle of oscillation, considering the energy dissipated by the viscous forces and that introduced into the system by the interaction with the flow field (Scanlan, 1981; Simiu and Scanlan, 1996).

As previously reported, this model seems to be unreliable to predict the response away from the structural conditions at which the parameters were estimated (Ehsan and Scanlan, 1990), due to the large variability of Y_1 and ϵ observed by changing the damping ratio and therefore the Scruton number, as shown in Fig. 7.2 (already reported in Chapter 5). Therefore, a reliable prevision needs wind tunnel tests at a Scruton number as close as possible to that of the prototype. In order to evaluate the practical effect of these changes of the aeroelastic parameters with the Scruton number, solution of Eq. (7.8) is plotted for different values of ϵ and Y_1. In particular, Fig. 7.3 was obtained by fixing to 1000 the value of the self-limiting parameter ϵ and letting Y_1 assume the values 5, 10 and 15. It is evident that the amplitudes predicted in the three cases are very different. It is also worth noting that when the Scruton number approaches to zero the three curves converge to the same limit cycle amplitudes. Therefore, ϵ regulates the maximum oscillation amplitude at the limit $Sc \to 0$. From Fig. 7.3 it can also be remarked the key role played by the parameter Y_1 in the energy feeding into the system. In fact, if Y_1 is increased, the Scruton

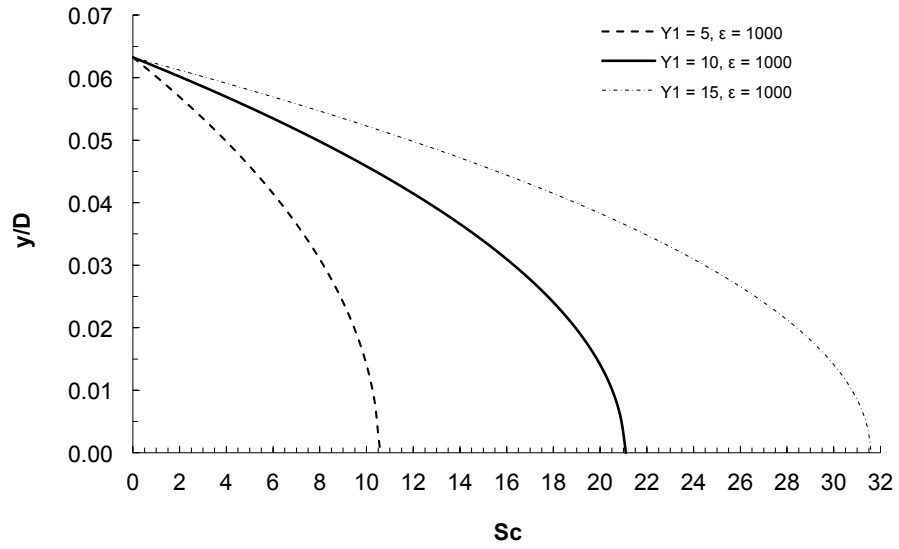

Fig. 7.3 Non-dimensional amplitude of the van der Pol limit cycle oscillations versus Scruton number ($Sc = 4\pi m\zeta/(\rho BD)$) for different values of the parameter Y_1 with $\epsilon = 1000$.

number at which the limit cycle oscillations vanish increases as well. Therefore, the parameter Y_1 is crucial for istance for the design of damping devices. In Fig. 7.4 Y_1 is fixed to 10, while the parameter ϵ assumes the values 500, 1000 and 1500. Once again significant differences in the limit cycle amplitudes predicted by the van der Pol model are apparent. It can also be observed that all the curves converge to the same value of the Scruton number for which the limit cycle oscillations disappear, which in turn depends on the value of the parameter Y_1. Conversely, the difference in the limit cycle amplitudes is maximum at very low Scruton numbers (up to 73 % in this case). In conclusion, the variations of the aeroelastic parameters identified for different values of the Scruton number, as reported in Fig. 7.2, are definitely non-negligible but imply significant differences in the predicted response amplitudes.

7.3.1 Identification of the aeroelastic parameters

In order to identify the previously mentioned aeroelastic parameters ϵ and Y_1 of the model proposed by Scanlan (1981), the procedure reported in Ehsan and Scanlan (1990) was followed. By the transient part of the response, using the approximate solution of the nonlinear differential equation obtained by the method of slowly varying parameters (Eq. (7.5)), the parameters ϵ and Y_1 can be identified. Considering the transient part of the signal in Fig. 6.16 a set of data $[s, A(s)]$ can be extracted and then transformed into $[s, Z(s)]$ by defining

$$Z(s) = ln\left\{\frac{A_0^2[A^2(s) - \beta^2]}{A^2(s)(A_0^2 - \beta^2)}\right\} \tag{7.9}$$

where β is the limit-cycle response amplitude. A regression line passing through the origin can be fitted to the data set $[s, Z(s)]$ with the least-squares method (Fig. 7.5),

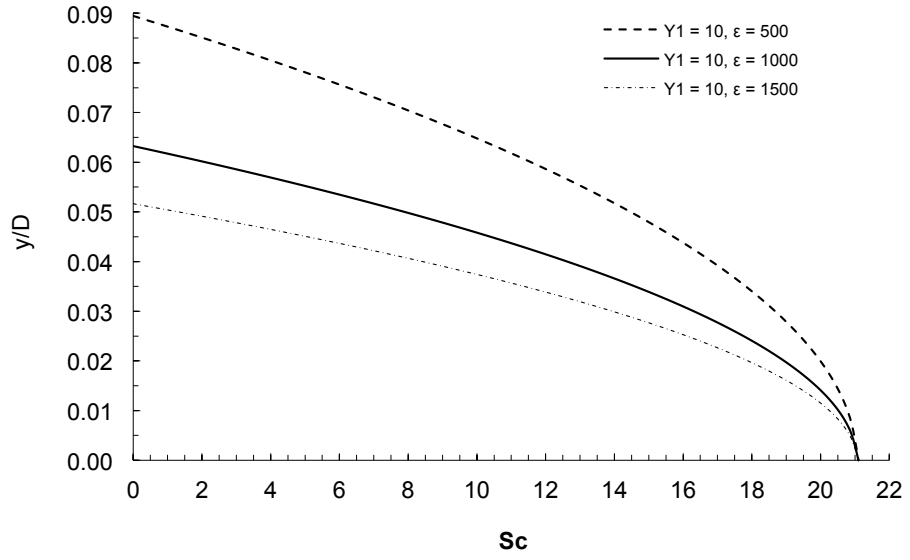

Fig. 7.4 Non-dimensional amplitude of the van der Pol limit cycle oscillations versus Scruton number ($Sc = 4\pi m\zeta/(\rho BD)$) for different values of the parameter ϵ with $Y_1 = 10$.

from which the slope a is obtained through the relation:

$$Z = as \tag{7.10}$$

where

$$a = \frac{\alpha\beta^2}{4} \tag{7.11}$$

The values of the parameters estimated through Eqs. (7.6) - (7.8) are $Y_1 = 6.27$ and $\epsilon = 1082.2$, which are in agreement with those reported in Ehsan and Scanlan (1990), taking into account the non-identical test conditions (differences in the model, set-up, Scruton number, reduced velocity, blockage ratio, residual turbulence, etc.).

It is also worth noting that the frequency under wind undergoes a shift from 13.43 Hz to 13.506 Hz, that is in non-dimensional form from $K_1 = 0.7464$ to $K = 0.7506$. This small difference of 0.56 % implies a value of $Y_2 = (K_1^2 - K^2)/m_r = -5.70$. As the corresponding structural stiffness term is higher than Y_2 by two orders of magnitude, the latter is practically negligible.

After the identification of the aeroelastic parameters, the approximate solution, whose envelope is given by Eq. (7.6), was compared with the measured time history of vertical displacement and good agreement is observed (Fig. 7.6).

Using the MULS method (Modified Unifying Least Squares method), proposed in Bartoli *et al.* (2009), it was possible to remark that the reconstructed response is not able to exactly reflect the frequency of the experimental signal, which slightly varies with time. In fact, in the transient part the frequency is about 13.494 Hz ($K = 0.750$), showing a non-negligible dependence on the amplitude of vibration, whereas in the regime part it increases to 13.506 Hz ($K = 0.7506$). The estimation of the aeroelastic parameters with the method proposed by Ehsan and Scanlan (1990)

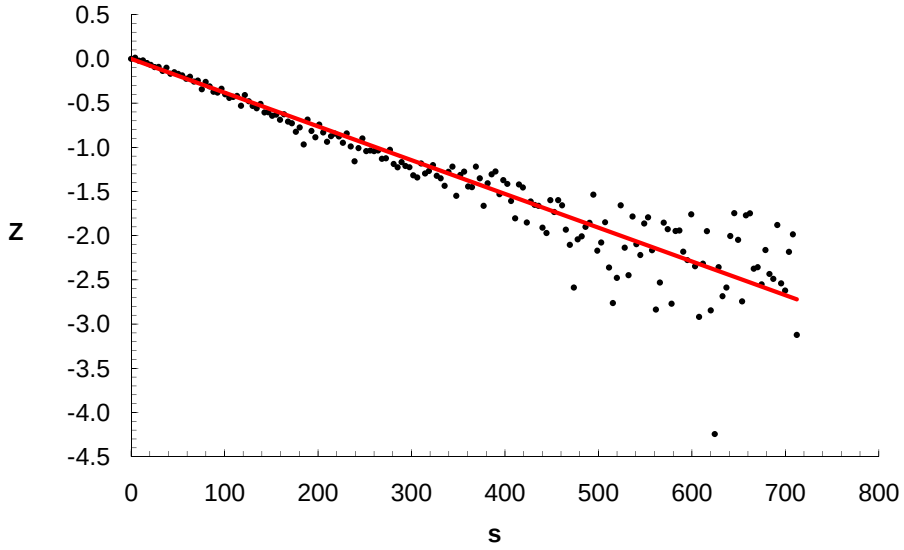

Fig. 7.5 Linear regression of the experimental data used to estimate the aeroelastic parameters.

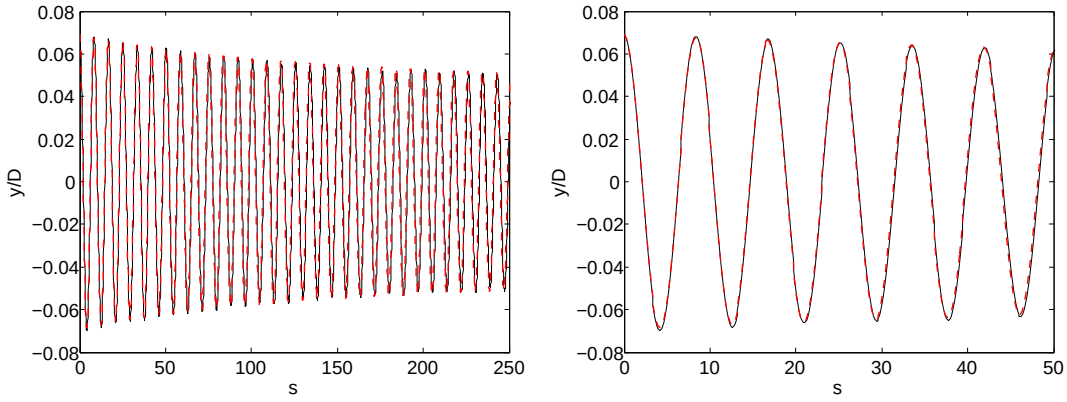

Fig. 7.6 Comparison between the experimental signal (solid line) and the solution of Eq. (7.5) (dotted line).

was also repeated by using the actual frequency during lock-in, but the differences in the results were negligible.

7.3.2 Bridge response

The prototype bridge response of each mode $y_{peak,i}$, assuming the flow orthogonal to the bridge longitudinal axis, may be estimated by using the model proposed by Ehsan and Scanlan (1990). To do that, it is necessary to take into account that the aeroelastic forces are not perfectly correlated along the bridge spans. Starting from the equation of the linear oscillator forced with a van der Pol-type aeroelastic force [Eqs. (7.1) and (7.4)]:

$$m(\ddot{y} + 2\zeta_i\omega_1\dot{y} + \omega_1^2 y) = \frac{1}{2}\rho U^2(2D)Y_1\left(1 - \epsilon\frac{y^2}{D^2}\right)\frac{\dot{y}}{U} \tag{7.12}$$

if the natural frequencies of the bridge are well separated it may be assumed that the lock-in oscillation occurs on a single mode. Therefore, the vertical motion y_i in the i-th mode may be expressed as

$$y_i(x,t) = \phi_i(x)\xi_i(t)D \tag{7.13}$$

Substituting Eq. (7.13) into Eq. (7.12):

$$\begin{aligned} &m\left[\phi_i(x)D\ddot{\xi}_i + 2\zeta_i\omega_1\phi_i(x)D\dot{\xi}_i + \omega_1^2\phi_i(x)D\xi_i\right] = \\ &= \frac{1}{2}\rho U^2(2D)Y_1\left(1 - \epsilon\phi_i^2(x)D^2\frac{\xi_i^2}{D^2}\right)\phi_i(x)D\frac{\dot{\xi}_i}{U} \end{aligned} \tag{7.14}$$

Multiplying both sides of the previous equation by $\phi_i(x)$ and integrating on the entire structure:

$$\begin{aligned} &\int_{structure} m(x)\phi_i^2(x)dx\left[\ddot{\xi}_i + 2\zeta_i\omega_1\dot{\xi}_i + \omega_1^2\xi_i\right] = \\ &= \rho UD\left\{\int_{structure} Y_1\left[1 - \epsilon\phi_i^2(x)\xi_i^2\right]\phi_i^2(x)dx\right\}\dot{\xi}_i \end{aligned} \tag{7.15}$$

Since the forcing term acts only on the deck, the integral on the left side is just extended on the deck:

$$\begin{aligned} &\int_{structure} m(x)\phi_i^2(x)dx\left[\ddot{\xi}_i + 2\zeta_i\omega_1\dot{\xi}_i + \omega_1^2\xi_i\right] = \\ &= \rho UD\left\{\int_0^L Y_1\left[1 - \epsilon\phi_i^2(x)\xi_i^2\right]\phi_i^2(x)dx\right\}\dot{\xi}_i \end{aligned} \tag{7.16}$$

By assuming a full spanwise correlation of the aeroleastic forces then the aeroelastic parameters may assume constant value (their two-dimensional values) along the span and hence the integrals in the previous equation can be taken out leading to the following expression:

$$\begin{aligned} &\int_{structure} m(x)\phi_i^2(x)dx\left[\ddot{\xi}_i + 2\zeta_i\omega_1\dot{\xi}_i + \omega_1^2\xi_i\right] = \\ &= \rho UD\left[Y_1\int_0^L \phi_i^2(x)dx - Y_1\epsilon\xi_i^2\int_0^L \phi_i^4(x)dx\right]\dot{\xi}_i \end{aligned} \tag{7.17}$$

Dividing both sides by $\int_0^L \phi_i^2(x)dx$:

$$\frac{\int_{structure} m(x)\phi_i^2(x)dx}{\int_0^L \phi_i^2(x)dx}\left[\ddot{\xi}_i + 2\zeta_i\omega_1\dot{\xi}_i + \omega_1^2\xi_i\right] = \tag{7.18}$$
$$= \rho U D\left[Y_1 - Y_1\epsilon\frac{\int_0^L \phi_i^4(x)dx}{\int_0^L \phi_i^2(x)dx}\xi_i^2\right]\dot{\xi}_i$$

the expression of the equivalent mass can be extracted:

$$m_e = \frac{\int_{structure} m(x)\phi_i^2(x)dx}{\int_0^L \phi_i^2(x)dx} \tag{7.19}$$

Defining

$$R = \frac{\int_0^L \phi_i^4(x)dx}{\int_0^L \phi_i^2(x)dx} \tag{7.20}$$

Eq. (7.18) becomes:

$$m_e\left[\ddot{\xi}_i + 2\zeta_i\omega_1\dot{\xi}_i + \omega_1^2\xi_i\right] = \rho U D Y_1(1 - \epsilon R\xi_i^2)\dot{\xi}_i \tag{7.21}$$

The vertical displacement $y(x,t)$ at lock-in is calculated considering that the net energy loss or gain per cycle of oscillation is zero at lock-in (Ehsan and Scanlan, 1990):

$$\int_0^T \left[2\zeta_i\omega_i m_e\dot{\xi}_i - \rho U D Y_1(1 - \epsilon R\xi_i^2)\dot{\xi}_i\right]\dot{\xi}_i dt = 0 \tag{7.22}$$

Assuming a sinusoidal form for the generalized coordinate $\xi_i(t) = \xi_{0,i}cos(\omega_i t)$, where $\omega_i \cong \omega_1$, the following expression for the amplitude of the generalized coordinate $\xi_{0,i}$ can be obtained:

$$2\zeta_i\omega_1 m_e\omega_1\pi\xi_{0,i}^2 - \rho U D Y_1\omega_1\pi\xi_{0,i}^2 + \rho U D Y_1\epsilon R\omega_1\frac{\pi}{4}\xi_{0,i}^4 = 0 \tag{7.23}$$

and then

$$\xi_{0,i}^2 = 4\frac{\rho U D Y_1 - 2\zeta_i\omega_1 m_{eq}}{\rho U D Y_1\epsilon R} = \frac{4}{\epsilon R} - \frac{2\zeta_i\omega_1 m_e}{\rho U D Y_1} \tag{7.24}$$

$$\xi_{0,i} = 2\sqrt{\frac{1 - \frac{2\zeta_i\omega_1 m_e}{\rho U D Y_1}}{\epsilon R}} = \frac{1}{\sqrt{R}}\frac{2}{\sqrt{\epsilon}}\sqrt{1 - \frac{2\zeta_i\omega_1 m_e}{\rho U D Y_1}} = \frac{1}{\sqrt{R}}\frac{2}{\sqrt{\epsilon}}\sqrt{1 - \frac{2\zeta_i K_1}{m_r^* Y_1}} \tag{7.25}$$

Finally, by defining the expression of the limit-cycle amplitude reported in Eq. (7.8) with β_i^*, one obtains:

$$\xi_{0,i} = \frac{1}{\sqrt{R}}\beta_i^* \tag{7.26}$$

It is worth noting that Eq. (7.26) is the same reported in the work of Ehsan and Scanlan (1990) except for the presence of the parameter m_r^*. Here, it is seemed

more realistic to consider not only the mass of the deck but also the contribute of the other parts of the structure (cables, suspenders, towers, etc.) to determine the response of each mode.

The parameters Y_1 and ϵ define the aeroelastic forces on the deck and may vary along the bridge span. In the literature, the *modified modal integral method* (Ehsan and Scanlan, 1990; Ehsan *et al.*, 1990) and the *variable parameter method* (Ehsan *et al.*, 1990) can be found to take into account the imperfect spanwise correlation. Here, only the first one is considered.

The method is based on the assumption that the aerodynamic forces are highly correlated at spanwise locations where the oscillations amplitude are high and viceversa. Therefore, to take into account the imperfect spanwise correlation of the aeroelastic forces the following modified forms of the modal integrals were formulated:

$$\Phi_p^m = \sum_{j=1}^{N} \left[\int_{-bL_j}^{0} g_{1j}(x_j)\phi^p(x_j)\frac{dx_j}{L} + \int_{0}^{aL_j} g_{2j}(x_j)\phi^p(x_j)\frac{dx_j}{L} \right] \tag{7.27}$$

where $p = 2$ or 4, $N = n+1$ where n is the number of nodes of $\phi(x)$, L is the length of the suspended span, x_j is the coordinate corresponding to the j-th segment of length L_j between successive nodes, centered at the antinode of the mode, a and b are fractions of L_j on either side of the origin of x_j. Shape functions $g_{1j}(x_j)$ and $g_{2j}(x_j)$ are assumed to define the loss of spanwise correlation for the i-th segment of the bridge in the left and right with respect to the origin of x_j (Fig. 7.7).

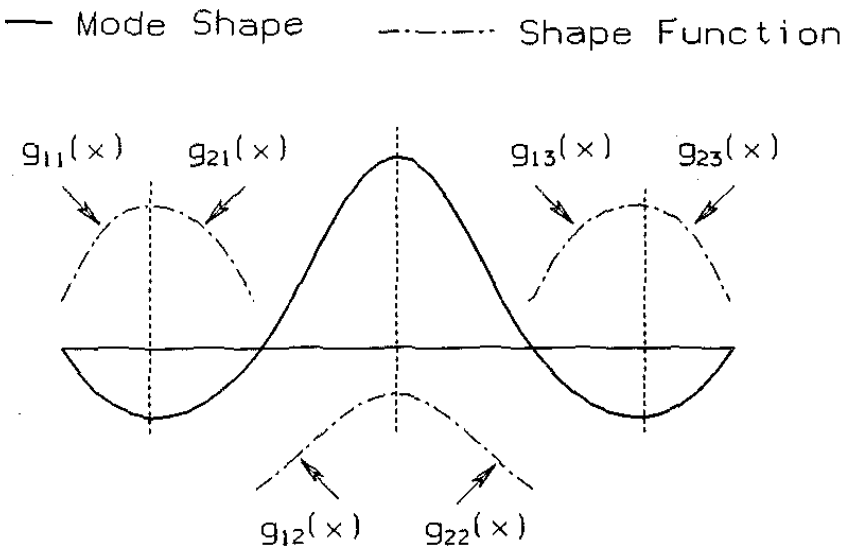

Fig. 7.7 Definition diagram for shape function (Ehsan and Scanlan, 1990).

The shape functions should be obtained by measuring force correlations on flexible models (full aeroelastic model, taut-strip model) in wind tunnel. Due to the difficulties to conduct such complex and expensive tests, Ehsan and Scanlan (1990) developed a method to determine the shape fuctions from tests on a rigid model (elastically-supported sectional model) under forced-vibration tests. It consists in defining an exponential form for taking into account the loss of spanwise correlation

whose coefficients depend on the oscillation amplitude through the curves obtained during forced-vibration tests at different oscillation amplitudes. They suggests the following expression:

$$g(x,\eta) = exp[-f_1(\eta)x^{f_2(\eta)}] \tag{7.28}$$

where $\eta = y/D$ and the two functions $f_1(\eta)$ and $f_2(\eta)$ depend on the cross section shape of the deck.

A more simplistic approach was proposed by Ehsan *et al.* (1989) and Ehsan *et al.* (1990) [see Ehsan and Scanlan (1990)], the shape function $g(x)$ follows the bridge mode shape, particularly of those positions of the span where the modal displacements are large. Therefore, $g(x)$ may be approximated by the mode shape $\bar{\phi}(x)$, i.e.

$$g(x) = \bar{\phi}(x) = |\phi(x)| \tag{7.29}$$

so that the modified modal integral (Eq. 7.27) may be written as

$$\Phi_p^m = \int_0^L \bar{\phi}(x)\phi^p(x)\frac{dx}{L} \tag{7.30}$$

Starting from Eq. (7.16), the effect of the loss of correlation may be taken into account by using the modified modal integral reported in Eq. (7.27) or Eq. (7.30):

$$\begin{aligned}\int_{structure} m(x)\phi_i^2(x)dx\left[\ddot{\xi}_i + 2\zeta_i\omega_1\dot{\xi}_i + \omega_1^2\xi_i\right] = \\ = \rho U D\left[Y_1\Phi_2^m - Y_1\epsilon\xi_i^2\Phi_4^m\right]\dot{\xi}_i\end{aligned} \tag{7.31}$$

where

$$\Phi_2^m = \int_0^L g(x)\phi^2(x)\frac{dx}{L} \tag{7.32}$$

$$\Phi_4^m = \int_0^L g(x)\phi^4(x)\frac{dx}{L} \tag{7.33}$$

Finally, after manipulations as those used to obtain Eq. (7.26), the following expression for the non-dimensional limit-cycle oscillation amplitude may be written:

$$\xi_{0,i} = \frac{1}{\sqrt{R_{mod}}}\frac{2}{\sqrt{\epsilon}}\sqrt{1 - \frac{2\zeta_i K_1\Phi_2}{m_r^* Y_1\Phi_2^m}} \tag{7.34}$$

where

$$R_{mod} = \frac{\Phi_4^m}{\Phi_2^m} \tag{7.35}$$

$$\Phi_2 = \int_0^L \phi^2(x)\frac{dx}{L} \tag{7.36}$$

The considerations on m_r^* done for Eq. (7.26) may be repeated for Eq. (7.34). From Eq. (7.13) the peak of the vertical limit cycle oscillation amplitude of the deck in the i-th mode is given by:

$$y_{peak,i} = \xi_{0,i}D \tag{7.37}$$

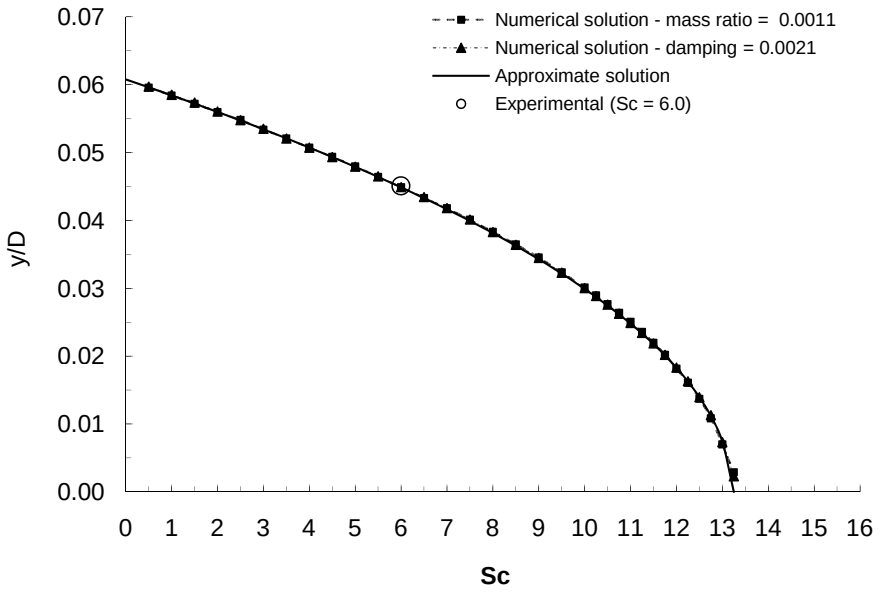

Fig. 7.8 Non-dimensional amplitude of the van der Pol limit cycle oscillations versus Scruton number ($Sc = 4\pi m\zeta/(\rho BD)$): approximate solution proposed by Ehsan & Scanlan (1990) (solid line); numerical solution varying only the damping coefficient (square points); numerical solution varying only the mass ratio (triangular points).

7.4 Coherence of the model for wind-sensitive structures and validation of the quasi-linear assumption

The physical coherence of the van der Pol-type equation in modeling the lock-in oscillations for a fluid-body system with a relatively large mass ratio can be perceived by solving numerically the equations of motion (7.1) and (7.4) through an implicit Runge-Kutta method (TR-BDF2 integration scheme). Fig. 7.8 reports the curves of the oscillation amplitudes versus the Scruton number obtained by the approximate solution proposed in Ehsan and Scanlan (1990) [Eqs. (7.5)-(7.8)], as well as the numerical integration results of Eqs. (7.1) and (7.4) for various Scruton numbers, obtained by keeping constant in the first case the mass ratio and in the second case the damping coefficient. All these results are based on the aeroelastic parameters obtained in section 7.3.1 using the identification procedure proposed in Ehsan and Scanlan (1990) ($Y_1 = 6.27$, $\epsilon = 1082.2$). Obviously, the regime amplitude predicted by the approximate solution is in agreement with the experimental result. Moreover, for any Scruton number the actual solution of the equation of motion practically coincides with the approximate solution. The correspondence of the results clearly confirms the reliability of the identification procedure of the parameters as well as the validity of the assumption standing behind it (quasi-linear system). Fig. 7.9 reports in the phase space representation the numerical solution of the equation of motion for a low, medium and high value of the Scruton number. It is apparent that in all the range of interest of the mass-damping parameter the assumption of harmonic motion for the limit-cycle oscillations (Scanlan, 1981) is definitely acceptable.

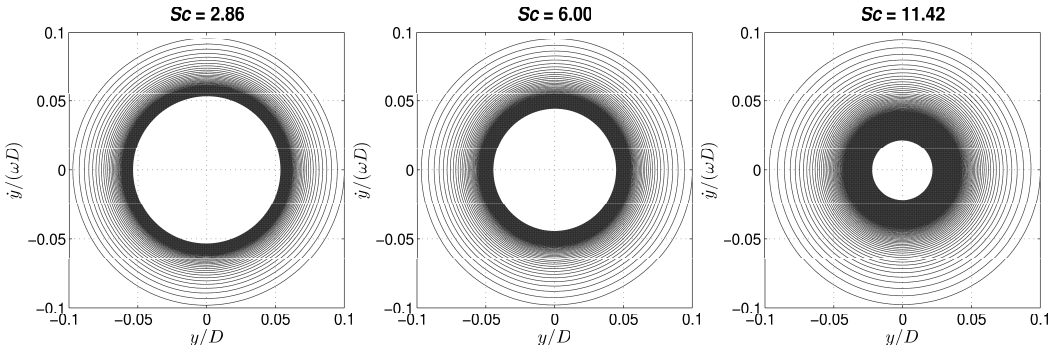

Fig. 7.9 Phase space diagrams of the numerical solution of Eqs. (7.1) and (7.4) for a low, medium and high value of the Scruton number.

Table 7.1 Aeroelastic parameters for various length of the decay-to-resonance signal used in the identification procedure (β =0.0451).

Δs	Y_1	ϵ
$0-100$	6.18	1069.0
$0-200$	6.57	1121.8
$0-300$	6.53	1116.7
$0-400$	6.39	1098.4
$0-500$	6.41	1100.8
$0-600$	6.38	1097.0
$0-700$	6.29	1084.9
$0-716$	6.27	1082.2

7.5 Robustness of the identification procedure

To investigate the robustness of the identification procedure, once the limit cycle amplitude was estimated ($\beta = 0.0451$), the aeroelastic parameters were identified changing the length of the transient part of the time history considered from $s = 100$ to $s = 716$. As reported in Tab. 7.1, the small differences in the values of the parameters obtained seem to confirm the robustness of the identification procedure.

Nevertheless, the values of the aeroelastic parameters strongly depend on the value of β, which in turn is not univocally determined for the experimental signal as the limit cycle amplitude slightly varies according to the time history portion considered (Fig. 7.10). In particular, Fig. 7.11 reports a comparison between the limit cycle amplitude given by Eq. (7.5) at different Scruton numbers by using the parameters estimated through the method proposed by Ehsan and Scanlan (1990). It is apparent that the results of the identification with the Ehsan-Scanlan's procedure is influenced by the value of the limit cycle amplitude β for the time history analyzed. The determination of this parameter for an experimental signal is slightly uncertain and such a figure demonstrates how very small differences in the choice of β can imply non-negligible variations in the value of Y_1 and therefore in the limit cycle amplitudes predicted by the model for high values of the Scruton number (see also Fig. 7.3). This is mainly due to the fact that Y_1 is linearly dependent to the slope a of the line of Eq. (7.10) and the latter is sensitive to the value chosen for the

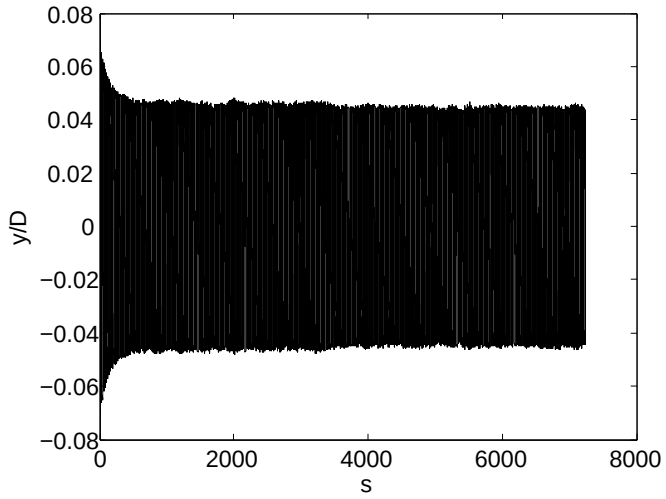

Fig. 7.10 Non-dimensional displacement signal recorded during a decay-to-resonance test versus dimensionless time $s = Ut/D$.

limit cycle amplitude β, due to the definition of $Z(s)$ in Eq. (7.9). In addition, the same equation requires a shortening of the portion of the signal considered for the identification with the Ehsan-Scanlan procedure when for instance β is fixed to 0.0465, a value which is only 3 % larger than the reference value considered so far and which could be reasonable for the first part of the experimental regime response. In fact, in this case one has to limit to process the signal up to s = 474 (instead of s = 716) for the estimation of α [Eqs. (7.9)-(7.11)].

7.6 Conclusions

The literature review (see section 5.5) has shown that so far no model seems to be able to properly predict vortex-induced vibrations. In particular, once the model parameters have been estimated for a certain value of the Scruton number, response predictions for different values of the mass-damping parameter seem to be unreliable.

This study focused on the Ehsan-Scanlan model because its simplicity make it useful for practical applications to bridge decks if no variability of its parameters with the Scruton number would have been observed. For such a scope a particular type of wind tunnel tests (see Chapter 6), called decay-to-resonance tests, were carried out to estimate the aeroelastic parameters of the model.

In the present Chapter, it was first suggested to consider the mass of all the structural members (deck, cables, towers, etc.) in the calculation of the lock-in response of the entire bridge not only that of the deck as reported in Ehsan and Scanlan (1990).

Moreover, it was observed that the equation over which the model is based, a van der Pol-type equation, is coherent with the physical characteristics of the phenomenon. In fact, according to the literature (Zdravkovich, 1990), the maximum oscillation amplitude at lock-in for structures prone to the wind action (i.e., characterized by a high mass ratio) depends on the Scruton number alone. Even though

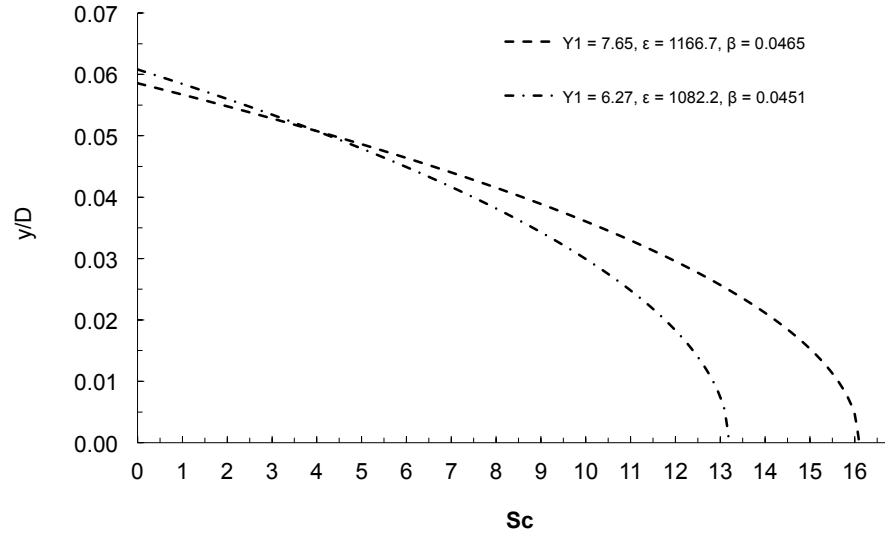

Fig. 7.11 Two limit curves in term of non-dimensional limit-cycle oscillation amplitude versus Scruton number given by applying the Ehsan-Scanlan's model.

the general solution of the van der Pol-type equation depends on the mass ratio and the damping coefficient separately, the regime response is only a function of the Scruton number, as confirmed by numerical integrations.

In addition, the numerical solutions of the equation of motion showed that the approximate result based on the method of slowly varying parameters is accurate for all the values of the Scruton number in the range of interest. Nevertheless, the analyses performed in this work demonstrated that attention must be paid to the determination of the limit cycle amplitude of the experimental response time history, as the results of the Ehsan-Scanlan's identification method may be sensitive to this parameter.

Chapter 8

Direct numerical identification of aeroelastic parameters at lock-in

8.1 Introduction

In the last chapter it was shown that the estimation of the aeroelastic parameters by using the approximate solution of the nonlinear differential equation used in the Ehsan-Scanlan model is accurate for all the values of the Scruton number in the range of interest. Nevertheless, the analyses performed demonstrated that attention must be paid to the determination of the limit cycle amplitude of the experimental response time history, as the results of the Ehsan-Scanlan identification method are sensitive to this parameter (see Section 7.5). Thus, it would be useful to setup an identification procedure in which no definition of the limit-cycle oscillation amplitude of the experimental signal is needed.

Moreover, as previously highlighted, since no model is able to accurately predict the vortex-induced vibration, an improvement of the Ehsan-Scanlan model would be an important goal considering its practical feasibility. Nevertheless, for a modified version of the previous model no approximate solution could be available. Therefore, a numerical identification of the aeroelastic parameters directly based on the nonlinear differential equation could be the unique tool available.

In this chapter, to achieve the two previously mentioned objectives, the aeroelastic parameters are directly estimated on the nonlinear differential equation by a numerical procedure.

Next section describes the method used in the direct numerical identification. Sections 8.3 and 8.4 report the results obtained and the tests conducted to evaluate its robustness. Finally, conclusions follow at the end.

8.2 Procedure and algorithm

Starting from a guess set of parameters, ϵ and Y_1 are progressively modified and the differential equation is numerically integrated until a minimum of an error function is attained. The error function is defined as the sum of the absolute value of the differences at each time step between the envelope of the experimental signal $\hat{\eta}_{exp}$

and that of the solution of the differential equation $\hat{\eta}_{num}$:

$$Error = \sum_{i=1}^{N} |\hat{\eta}_{i,exp} - \hat{\eta}_{i,num}| \tag{8.1}$$

where N is the number of experimental points which obviously coincides with that of the numerical ones. Such a definition of the error function allows to avoid the strong effect of the frequency parameter K on the results. In fact, since the frequency of the experimental signal slightly varies with the oscillation amplitude (see Section 7.3.1), a definition of the error function as the difference at each point between the two signals would imply a strong dependence of the results on the parameter K and on the length of the signal considered for the identification (Marra *et al.*, 2011a). In particular, since the frequency of the experimental signal changes with the time and all the points of the signal (not only the points of its envelope) are considered by the error function, the reduced frequency K would become the key parameter to minimize the error. Thus, its evaluation would assume more importance than that of the aeroelastic parameters Y_1 and ϵ which instead should be the object of the identification.

The famous Nelder-Mead simplex algorithm, implemented in the MatLab's *fminsearch* function, is applied as direct search method of minimization. Details on the algorithm can be found in Lagarias *et al.* (1998).

The integration of the non-linear differential equation is carried out with the MatLab's *ode45* function.

The identification procedure is applied to the equation of motion with the aeroelastic term used in the Ehsan-Scanlan's model (Eqs. 7.1 and 7.4), which is reported below:

$$m\left(\ddot{y} + 2\zeta\omega_1\dot{y} + \omega_1^2 y\right) = \frac{1}{2}\rho U^2(2D)Y_1\left(1 - \epsilon\frac{y^2}{D^2}\right)\frac{\dot{y}}{U} \tag{8.2}$$

8.3 Direct numerical identification of artificially generated signals

The procedure is initially tested on artificially generated signals given by the numerical integration of Eq. (8.2) with Y_1 and ϵ arbitrarily fixed (10 and 1000, respectively). In this case, the values identified are exactly those fixed to generate the signal.

To evaluate the robustness of the identification procedure the parameters were identified at first on a signal obtained by integrating the van der Pol-type equation with known parameters ($Y_1 = 10$, $\epsilon = 1000$) with superimposed different levels of Gaussian white noise [noise-to-signal ratios in terms of root-mean-square (RMS) equal to 2.5, 5 and 10%] . Since the artificially generated signals are random processes, the identification was repeated many times by generating 100 signals. The main statistical characteristics of the aeroelastic parameters (mean values and coefficients of variation) are reported in Tab. 8.1. The results show the good performance of the identification procedure for low levels of noise ($\leq 5\%$), whereas if the noise is increased the procedure loses its reliability. It is worth noting that the usual level of noise of an experimental signal is closer to the low values (Fig. 8.1) and therefore such noise allows to obtain a reliable estimation of the aeroelastic parameters by using the present procedure. In addition, Fig. 8.2 reports the probability density

Table 8.1 Parameters estimated on the artificially generated van der Pol signal for different levels of noise.

$RMS(noise)/RMS(signal)$ [%]	Y_1		ϵ	
	$Mean$	$CoV[\%]$	$Mean$	$CoV[\%]$
2.5	9.6423	2.45	960.5254	0.8
5	9.1811	4.86	904.2052	1.74
10	7.9213	9.63	771.0475	4.21

Table 8.2 Effect of the signal length on the identification procedure.

s_{max}	Y_1	ϵ	$Error/s_{max}$
100	0.10	5269.7	0.000187
200	3.41	1079.0	0.000152
300	5.16	1083.9	0.000143
400	6.42	1097.0	0.000129
500	6.57	1108.0	0.000120
600	6.69	1110.2	0.000117
700	6.70	1111.2	0.000115
800	6.81	1115.5	0.000118
900	7.03	1126.1	0.000129
1000	7.16	1128.0	0.000133
1100	7.15	1127.0	0.000130
1200	7.28	1131.1	0.000132
1300	7.35	1133.0	0.000132
1400	7.31	1131.1	0.000129
1500	7.29	1131.1	0.000127

function obtained from the sample of 100 generated signals and the corresponding Gaussian distribution. Despite limited size of the sample, it can be observed that for all the levels of noise considered the probability density functions of the two random variables Y_1 and ϵ could be well approximated by a Gaussian distribution with the same mean and R.M.S. value.

8.4 Direct numerical identification of the experimental signal

The direct numerical identification was also applied to the experimental signal obtained by decay-to-resonance tests. In Fig. 8.3 both the envelope of the experimental data and the one of the numerical solution at the last iteration are shown. The parameters were identified for different lengths of the experimental signal and the results are reported in Tab. 8.2. Except for very short lengths of the signal ($s_{max} = 100 - 300$), which give unacceptable results, the remaining values confirm the robustness of the procedure. In Fig. 8.4 the variation of the aeroelastic parameters and that of the error function are shown. It can be observed that such a variation is contained inside the band of variation given by the Ehsan-Scanlan identification

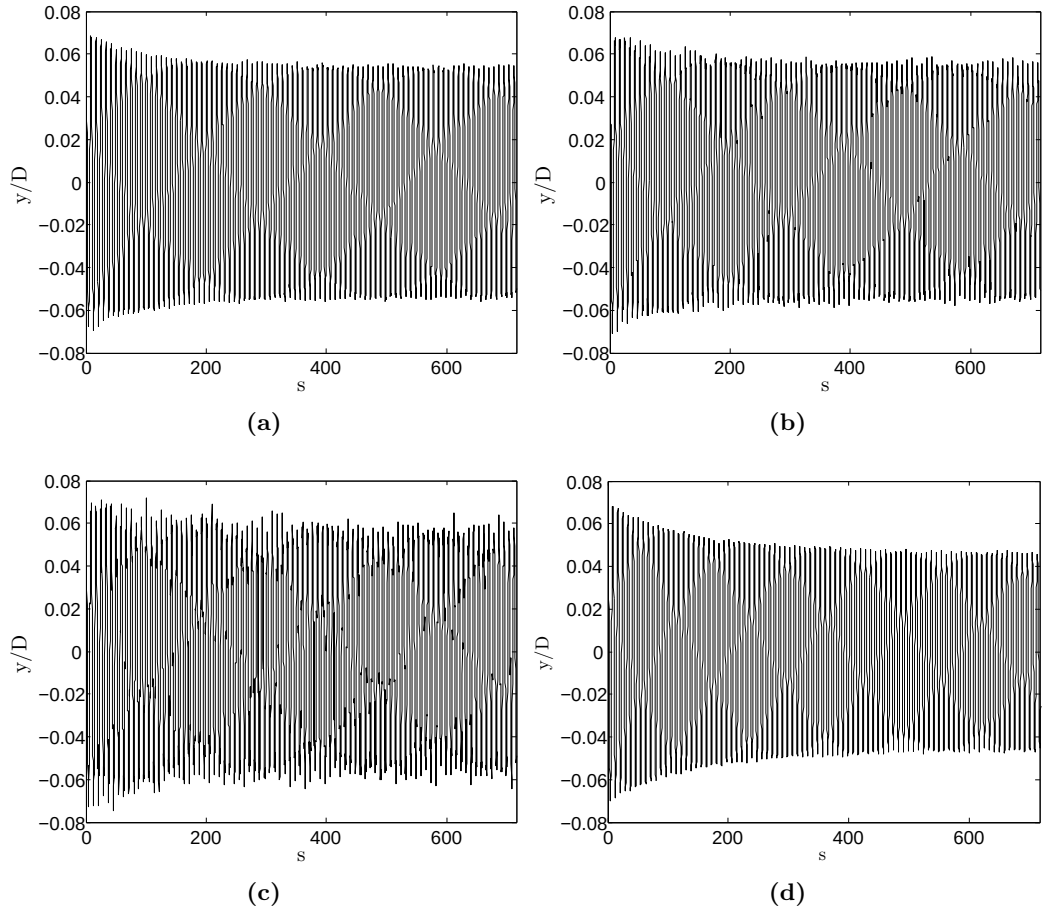

Fig. 8.1 Articifially generated signals with RMS(noise)/RMS(signal) = (a) 2.5 %, (b) 5%, (c) 10% and experimental signal (d) ($s_{max} = 716$).

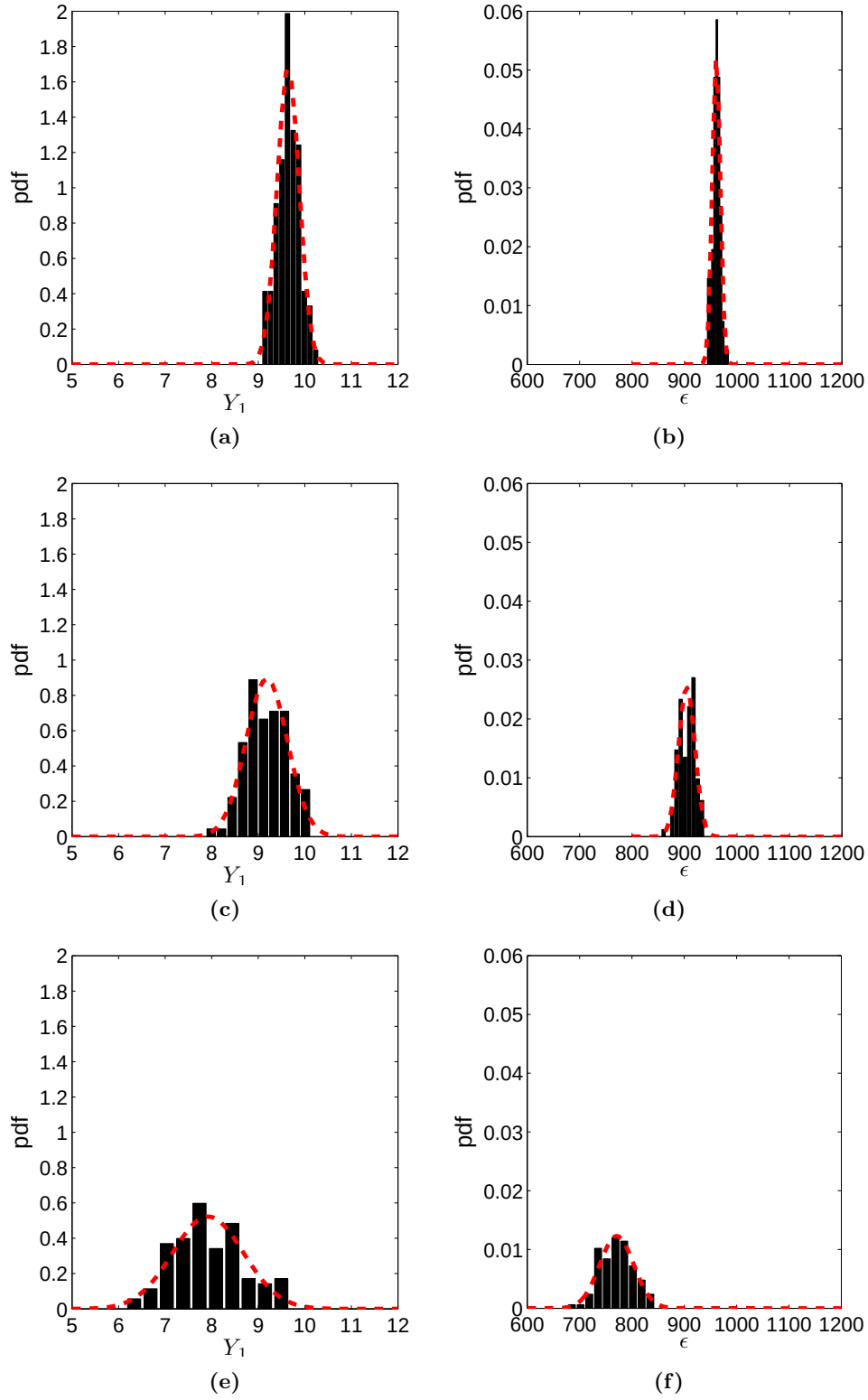

Fig. 8.2 Probability density functions and Gaussian probability density functions of Y_1 and ϵ obtained by direct numerical identification of a van der Pol signal (guess values: $Y1 = 8$, $\epsilon = 1200$) with a noise-to-signal ratio of 2.5% (frames a and b), 5% (frames c and d) and 10% (frames e and f).

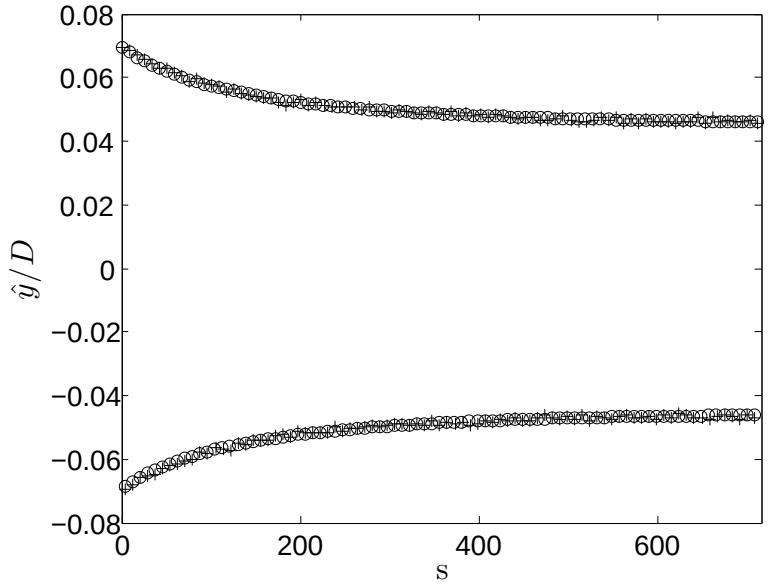

Fig. 8.3 Envelope of the experimental signal (cross points) against that of the numerical solution at the last iteration (rounded points).

procedure ($Y_1 = 6.27 - 7.65$ and $\epsilon = 1082.2 - 1166.7$, corresponding to $\beta = 0.0451$ and 0.0465; see Section 7.5 for more details). This results clearly confirms that the procedure is as robust as that proposed by Ehsan and Scanlan (1990). Fig. 8.5 reports a comparison between the limit cycle amplitude given by Eq. (7.8) at different Scruton numbers by using the parameters estimated through the direct numerical identification and those obtained with the method proposed by Ehsan and Scanlan (1990). It is apparent that the results of the numerical identification fall inside the two limit curves obtained with the procedure of the literature. Fig. 8.6 shows, for the length of the signal $s_{max} = 1000$, the values of the aeroelastic parameters and the error function (divided for s_{max}) at each iteration step during the research of the minimum of the objective function. As it can be observed, the iterations end when no variation of the results is observed.

8.5 Conclusions

In Chapter 7, the Ehsan-Scanlan identification procedure was applied to an experimental signal obtained during wind tunnel tests, in order to estimate the aeroelastic parameters of the van der Pol-type model for vortex-induced vibrations. The major limit of this procedure seems to be its strong sensitivity to the choice of the limit cycle amplitude. With the aim to ride out such limit, an alternative method consisting in the estimation of the parameters directly from the nonlinear equation is adopted. That may be also useful for possible future improvements of the van der Pol-type equation, in case no approximate solution is available. The procedure is validated through artificially generated signals with known parameters and different noise-to-signal ratios. As expected, the dispersion of the results increases with the level of noise but the procedure remains stable except for very high values of

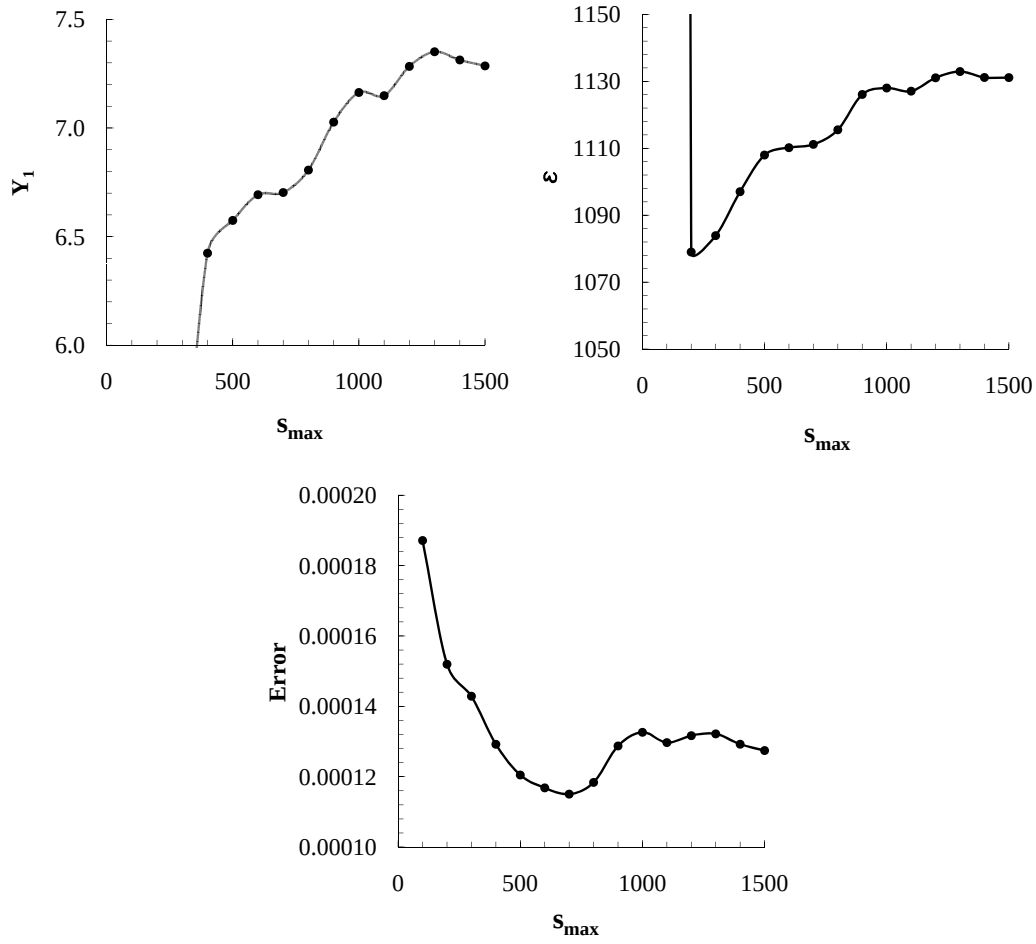

Fig. 8.4 Estimation of the parameters Y_1, ϵ and error function versus the length of the experimental signal.

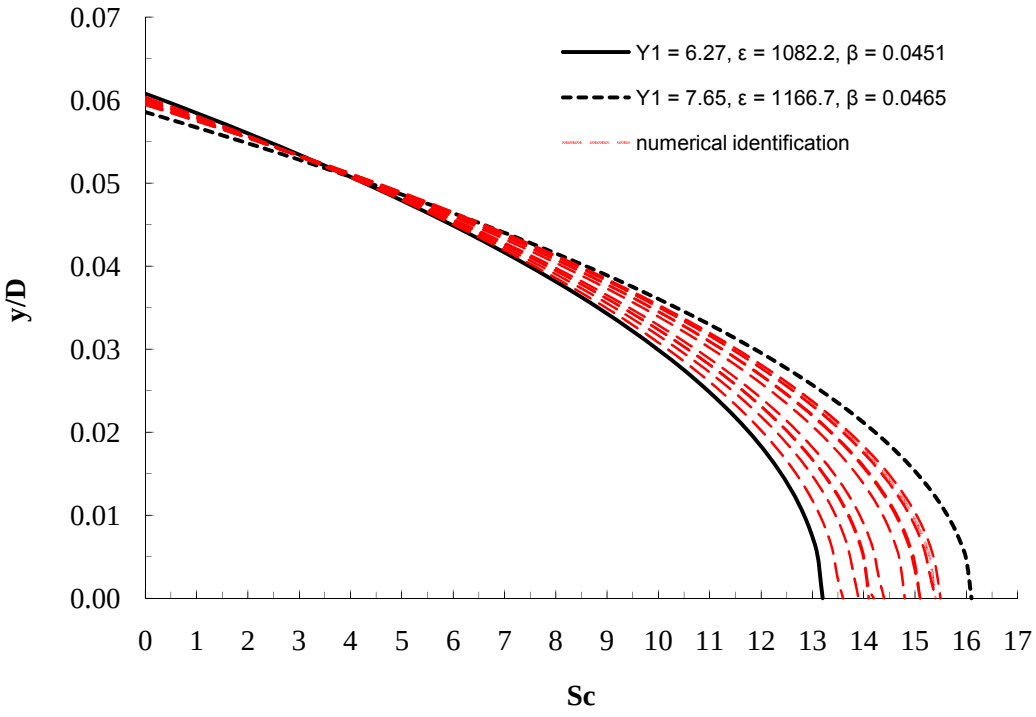

Fig. 8.5 Limit cycle oscillation amplitudes versus Scruton number obtained by Eq. (7.8) with the aeroelastic parameters given by the Ehsan-Scanlan procedure (black solid and dashed lines) and the direct numerical identification for different lengths of the signal considered (red dashed lines).

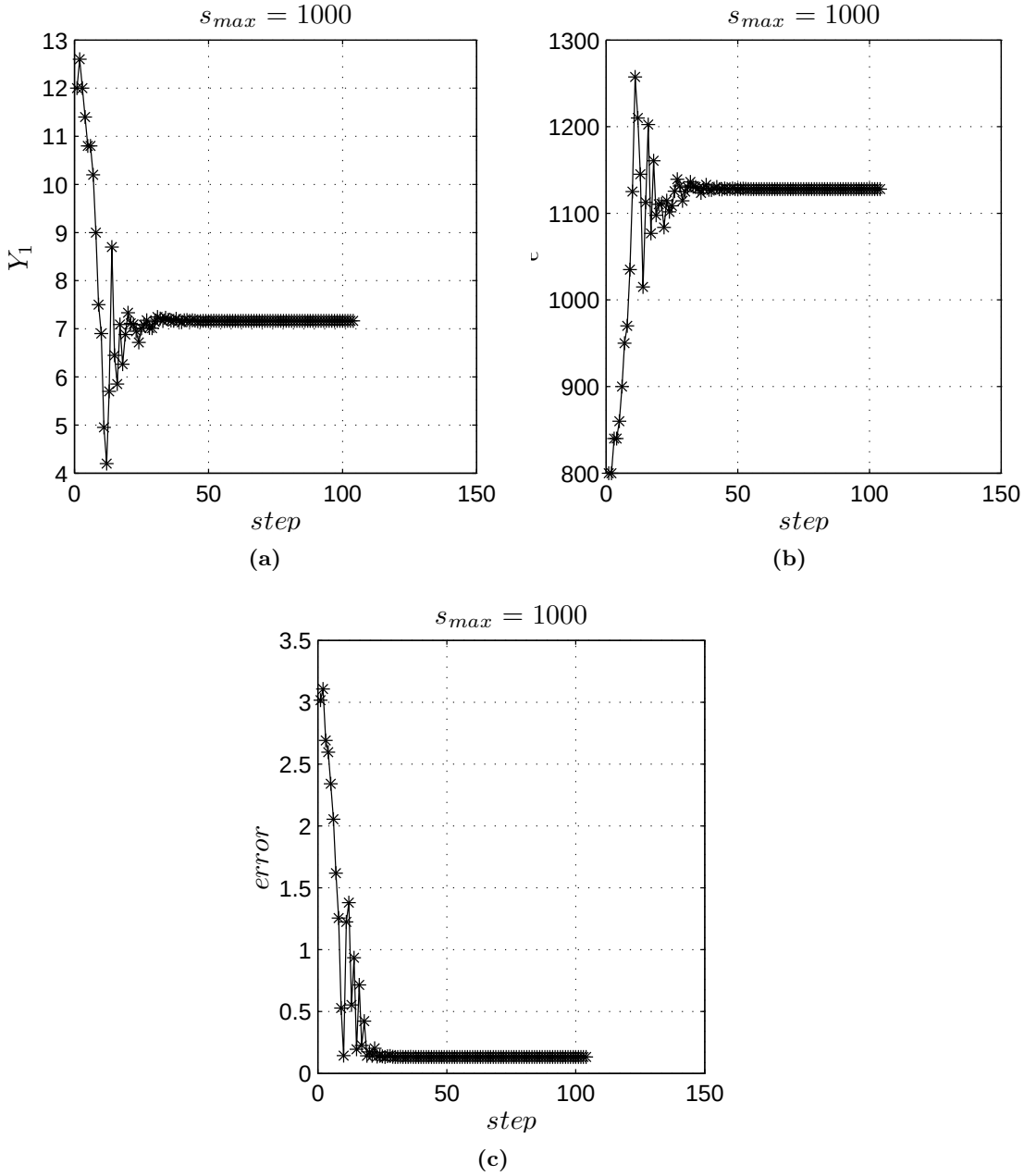

Fig. 8.6 Values of the aeroelastic parameters and of the error function at each step during the error minimization procedure ($s_{max} = 1000$).

noise, which are much higher than that usually encountered in wind tunnel tests and therefore of no practical interest. Finally, this identification method is applied to the experimental signal. The direct numerical identification method results as robust as the identification procedure proposed by Ehsan and Scanlan (1990). In fact, the results obtained by the direct numerical identification fall inside the band of values provided by the method from the literature as a consequence of a small variation in the choice of the limit cycle amplitude.

Chapter 9

Procedure for VIV-risk analysis of bridge decks

9.1 Introduction

In this chapter a procedure to conduct the Vortex-Induced Vibration (VIV) risk analysis of bridge decks is proposed. By assembling the contributions of the Chapters 3, 6, 7 and 8 and following both the risk management framework and the Performance-Based Design approach reported in Chapter 2, a procedure for a quantitative evaluation of the risk due to vortex shedding of bridge decks is developed.

In the present work only the risk identification and assessment parts of the general risk management framework proposed by Pliefke *et al.* (2007) are developed. The risk identification phase is composed by the definition of the system as well as the individuation of the hazard. The system is represented by a *bridge deck* and the hazard by the *vortex-shedding action* on the deck. The risk assessment phase is constituted by the risk analysis part, where the risk is quantified, and the risk evaluation part in which the different sources of risk due to each hazard are compared. Here, only the vortex-shedding action is considered as hazard and then the risk evaluation part is omitted. Therefore, the risk assessment process is only composed by the risk analysis, in which the probability of failure, associated with the overcome of a certain comfort threshold, will be estimated by a PEER-type equation.

The procedure proposed will be applied to an idealized case study and the effects of the assumptions standing behind the risk procedure will be shown. Finally, knowing the probability of failure due to the vortex-shedding action of the bridge analyzed, which is the probability to have a lock-in response higher than a discomfort threshold, an estimation of the risk in terms of the average number of days per year in which the bridge has to be closed to traffic is given.

9.2 Risk analysis procedure

As already said, the result of the risk analysis is the quantification of the risk associated with a certain hazard. In the present procedure is treated the quantification of risk due to vortex shedding related to the comfort of the occupants of the bridge. The first step consists in the definition of a high performance level (limit acceleration) as serviceability limit state. Such a limit state can be defined by using the deck vertical acceleration during lock-in.

The calculation of risk is conducted by using a PEER-type equation. In particulat, if y_{lim} is the serviceability limit state of the structural response, the probability of failure can be obtained in the following way:

$$P_{failure} = 1 - P(0 \leq y \leq y_{lim}) \tag{9.1}$$

with

$$P(0 \leq y \leq y_{lim}) = \int_0^{y_{lim}} \int_0^{\infty} \int_0^{2\pi} p(y \mid U, \theta) q(U, \theta) dU d\theta dy \tag{9.2}$$

where y is the vertical displacement of the deck, U is the mean wind speed at the deck level. The function $q(U, \theta)$ corresponds to the hazard term $p(IM)$ of Eq. (2.1) and it is the joint probability density function of both the mean wind speed U and yaw angle θ. In particular, $dp(IM)$ can be seen as $dq(U, \theta) = q(U, \theta) dU d\theta$. The function $p(y|U, \theta)$ corresponds to the vulnerability term $p(EDP|IM)$ of Eq. (2.1) and represents the probability density function of the vertical displacement y, given U and θ. Knowing the two functions, the probability of exceedence of a certain limit threshold of the vertical displacement y_{lim} can be calculated.

The risk analysis procedure proposed in this study is reported in Fig. 9.1.

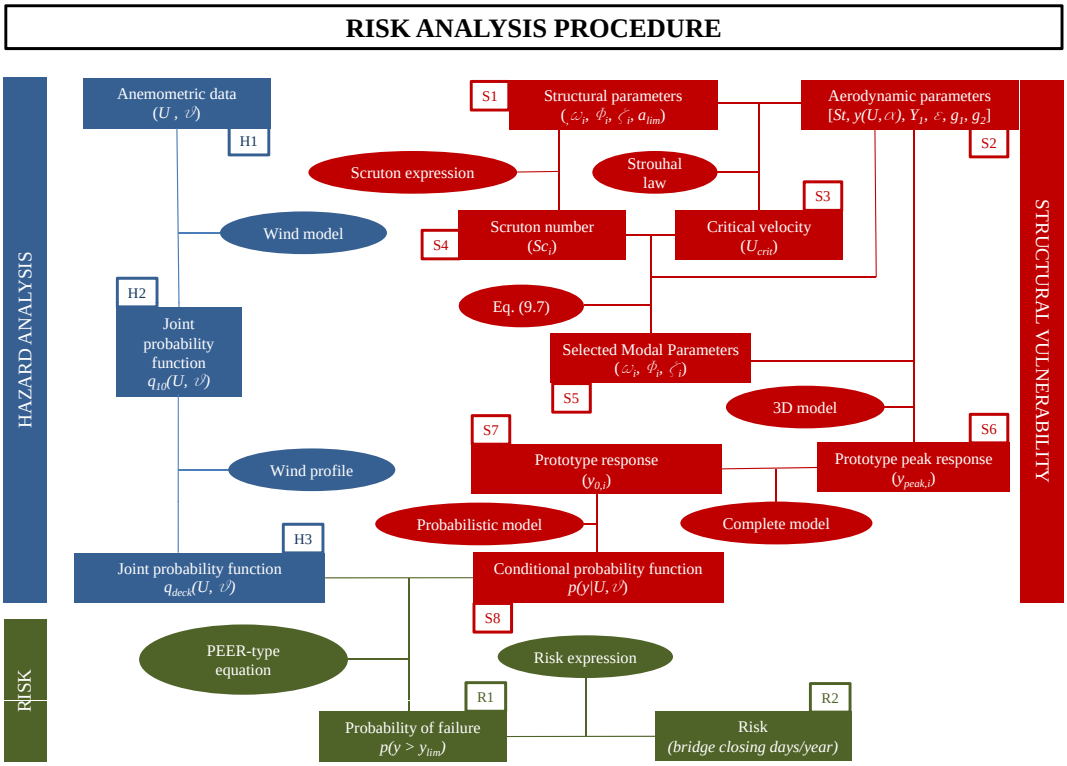

Fig. 9.1 Diagram of the risk analysis procedure proposed.

9.2.1 Hazard analysis

The function $q(U, \theta)$ is called hazard term because it is the joint probability density function of both the mean wind speed U and yaw angle θ. To evaluate such a

function the steps reported in Fig. 9.1 (blue boxes) may be followed.

Wind data have to be taken from anemometric stations close to the bridge (**box H1**). Here, it is assumed that the anemometer from which data are available is located at the bridge position (**hyp H1**).

A joint probability density function of U and θ is obtained by using a model able to characterize the main features of the wind in the site of the bridge (**box H2**). According to the Weibull model reported in Eq. (3.2), the joint probability function used in this procedure is:

$$q_i(U,\theta) = p(u < U < u + dU, \theta_{inf,i} < \theta < \theta_{sup,i}) = \frac{a_i}{b_i}\left(\frac{u}{b_i}\right)^{(a_i-1)} exp\left[-\left(\frac{u}{b_i}\right)^{a_i}\right] \tag{9.3}$$

where a_i and b_i represent the coefficients of the i-th sector defined by $\theta_{inf,i}$ and $\theta_{sup,i}$. The function reported in Eq. (9.3) is referred to the height of the anemometer located 10 m over the ground, which is generally different from the deck level (Fig. 9.2). In general, the probability of a certain wind velocity at the anemometer level [given by Eq. (9.3)] corresponds with a different wind velocity at the deck level. Therefore, a wind profile has to be defined to obtain the wind probability at the deck level. Given the difficulties in defining a mean wind profile at moderate wind speed (see Section 3.2 for more details) a constant profile is generally used (**hyp H2**). Therefore, Eq. (9.3) is also valid at the deck level (**box H3**).

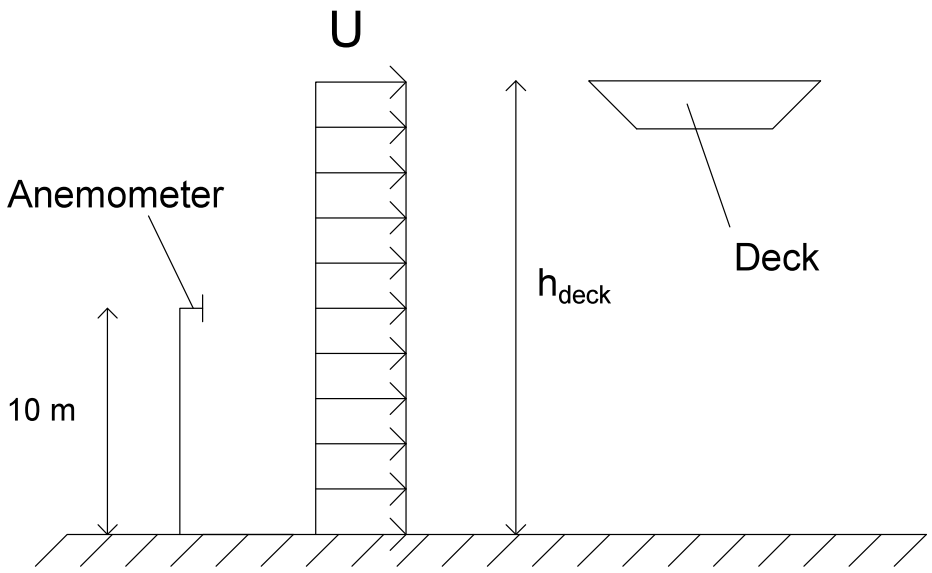

Fig. 9.2 Wind speed profile assumed in the procedure.

9.2.2 Structural vulnerability

Structural vulnerability is the part of the procedure proposed (Fig. 9.1: red boxes) in which the term $p(y|U,\theta)$ of Eq. (9.2) is obtained.

The risk analysis procedure needs both structural and aerodynamic parameters. Modal parameters (modal shapes, frequencies and damping ratios for each mode)

and the vertical limit acceleration represent the structural input parameters (**box S1**). In particular, by using a Finite Element Model (FEM) the modal parameters are determined. The definition of the modal damping ratios, which can be accurately determined only after the structure is built by carrying out dynamic tests (Muscolino, 2002), is crucial. Nevertheless, there are some studies which help to define the modal damping ratios during the design phase [see Blevins (2001)]. In particular, Davenport (1981) suggests that, independently from the specific mode, in long-span suspension bridges damping decreases with increasing frequency. Ito *et al.* (1973) indicate that short-span bridges (high fundamental frequency) present higher damping than long-span bridges. Moreover, no relationship between the material employed (concrete or steel) and damping was found by Ito *et al.* (1973). Fig. 9.3 reports the damping factors for various modes of long-span suspension bridges compiled by Davenport (1981) and Littler and Ellis (1987) and demonstrates the previous statements. More cautionarily, Frandsen (2001) suggests to use modal logarithmic

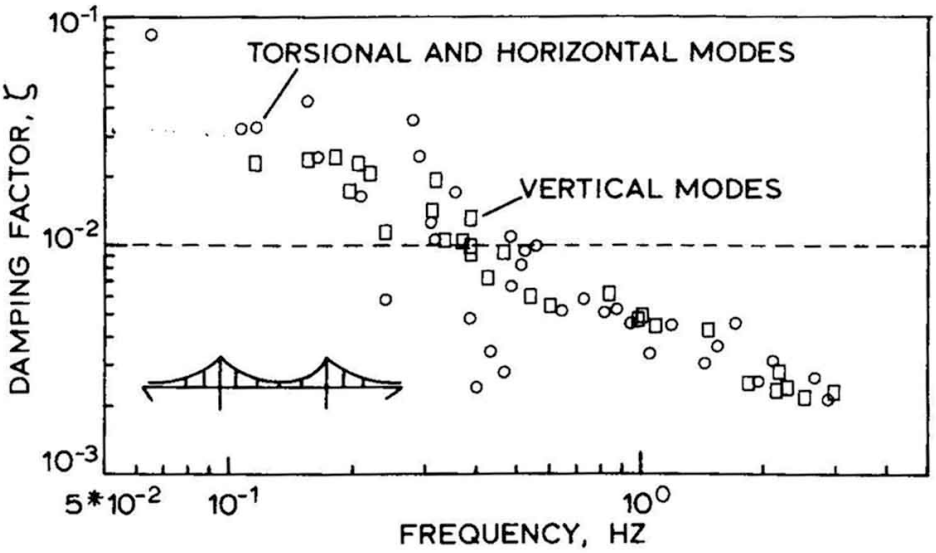

Fig. 9.3 Damping ratios for long-span suspension bridges (Davenport, 1981; Littler and Ellis, 1987).

decrements between 0.005 and 0.01 [$\zeta \cong \delta/(2\pi) = 0.0008 - 0.0016$]. In the present procedure the effect of damping ratio on the results is investigated. First of all, a value of 0.0008 for the damping ratio is assumed for each mode (**hyp S1a**). After, assuming that the damping decreases by increasing the frequency (Davenport, 1981) and using as extreme values those reported in Frandsen (2001), the following linear relation is considered (**hyp S1b**):

$$\zeta_i = 0.0016 - \frac{0.0016 - 0.0008}{f_{max} - f_{min}}(f_i - f_{min}) \tag{9.4}$$

where f_{min} and f_{max} are respectively the frequency of the lower and higher mode considered in the lock-in analysis.

The vertical limit acceleration a_{lim} used is the one proposed by Frandsen (2001), which suggests a tolerance limit of $a_{lim} = 0.05g$ (g is the gravity acceleration) as a visible amplitude limit, three times lower than that used to avoid physical discomfort.

Aerodynamic input parameters have to be determined by wind tunnel tests (**box S2**): static tests to estimate the Strouhal number (St); ambient vibration tests (see Section 6.5.2) to measure the response during lock-in [$y(U, \theta)$]; decay-to-resonance tests (see Section 6.5.3) for estimating the aeroelastic parameters (Y_1, ϵ); finally, forced vibration test to obtain the correlation functions (which will be defined later).

An important parameter in VIV of bluff bodies is the critical velocity (**box S3**). It represents the wind speed at which synchronization is supposed to occur. Critical velocity may be obtained by the following equation which derives from the Strouhal law [Eq. (4.1)]:

$$U_{crit,i} = \frac{f_i D}{St} \tag{9.5}$$

Among the vertical modes of the structure, a selection of those which could be susceptible to lock-in oscillations must be done. As reported in Section 4.3, the Scruton number represents a key parameter for a quantitative description of the vulnerability of each mode (**box S4**). Its expression for the i-th mode is reported below:

$$Sc_i = \frac{4\pi m_{e,i}\zeta_i}{\rho B D} \tag{9.6}$$

The selection of the modes prone to lock-in oscillations is considered by considering all the modes for which (**box S5**):

$$Sc_i < Sc_0 \tag{9.7}$$

where Sc_0 represents, according to the VIV model considered, the Scruton number at which no oscillations occur.

The peak of the vertical limit cycle oscillation amplitude of the deck in the i-th mode (**box S6**) is given by Eq. (7.37) in which $\xi_{0,i}$ can be obtained by using Eq. (7.26) (**hyp S2a**) or alternatively Eq. (7.34) when the loss of spanwise correlation is taken into account (**hyp S2b**). The corresponding vertical accelerations can be calculated by the following equation:

$$a_i = y_{peak,i}\omega_i^2 \tag{9.8}$$

As shown in Fig. 6.11, the response during lock-in is a function of the mean wind velocity and wind tunnel test provides its behaviour at a particular value of the Scruton at which the tests are carried out. Since the Scruton number of the structure will be different from that of the tests, the use of the curve reported in Fig. 6.11 would be useless because it is very sensitive to its value. Moreover, no model is able to predict its variations. Therefore, in this study, it is assumed a schematic response during lock-in. In particular, the two functions $f(U)$ reported in Fig. 9.4 a,b are considered (**hyp S3a,b**).

The lock-in response is also influenced by the yaw angle (see section 4.4). In particular, the lock-in oscillations of real bridges seem to occur for wind directions almost perpendicular to the bridge deck (Larsen *et al.*, 2000), even though experimental results on circular cylinders have shown that such oscillations can occur also for yawed wind directions (Koopman, 1970; King, 1977). Therefore, the simple form reported in Fig. 9.4c for the function $h(\theta)$ is assumed (**hyp S4**). The estimation of

the parameters $U_{1,i}$, $U_{2,i}$, θ_1, θ_2, θ_3 and θ_4 should be conducted by using experimetal curves $f(U)$ and $h(\theta)$ obtained at a Scruton number lower than that of the prototype.

The model proposed here to take into account all the previous features is explained by the following equation (**box S7**):

$$y_{0,i} = y_{peak,i} f_i(U) h(\theta) \tag{9.9}$$

where $y_{peak,i}$ is the maximum oscillation amplitude obtained for the i-th mode by applying the Ehsan-Scanlan model (box S6) where the flow is considered orthogonal to the bridge axis. The real response will be obtained by multiplying the previous term by two functions which take into account the effects on the response amplitude due to the mean wind speed and the yaw angle (**hyp S5**). The function $f_i(U)$ and

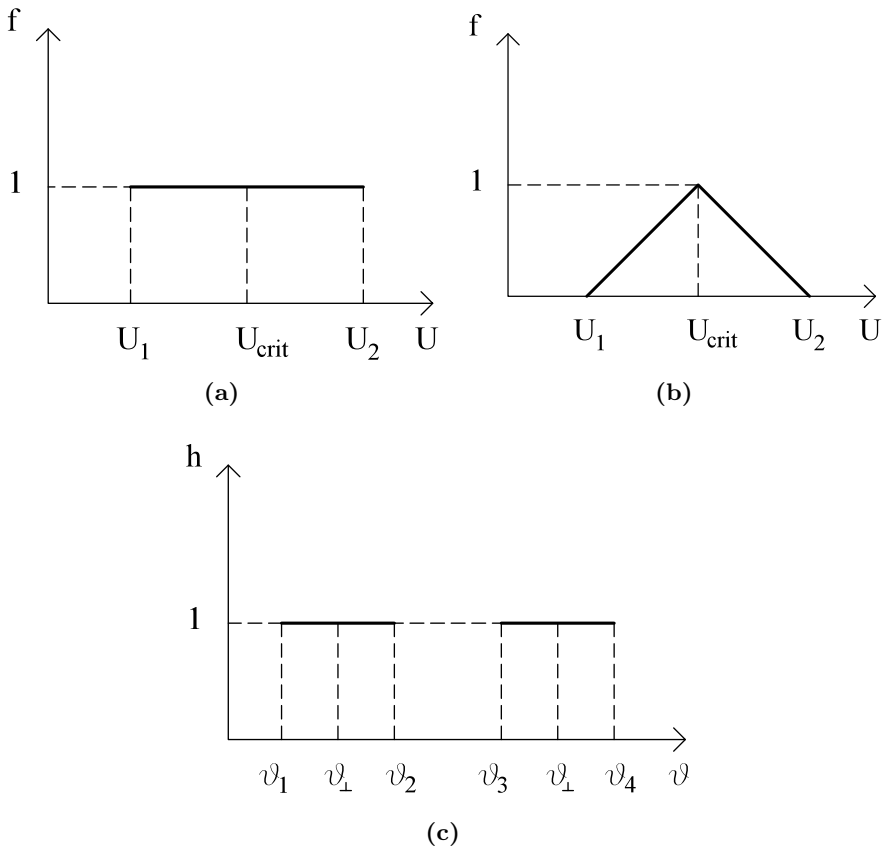

Fig. 9.4 Definition of the model functions $f_i(U)$ and $h(\theta)$.

$h(\theta)$ are merely defined as

$$f_i(U) = \begin{cases} 1 & \forall U \in [U_{1,i}, U_{2,i}] \\ 0 & \text{elsewhere} \end{cases} \tag{9.10}$$

$$h(\theta) = \begin{cases} 1 & \forall \theta \in [\theta_1, \theta_2] \text{ and } [\theta_3, \theta_4] \\ 0 & \text{elsewhere} \end{cases} \tag{9.11}$$

for the case represented in Fig. 9.4a, c, whereas for that reported in Fig. 9.4b, c the function $f_i(U)$ is given by the following expressions:

$$f_i(U) = \begin{cases} \frac{1}{U_{crit,i}-U_{1,i}}(U - U_{1,i}) & \forall U \in [U_{1,i}, U_{crit,i}] \\ 1 - \frac{1}{U_{2,i}-U_{crit,i}}(U - U_{crit,i}) & \forall U \in [U_{crit,i}, U_{2,i}] \\ 0 & \text{elsewhere} \end{cases} \tag{9.12}$$

Since the model proposed in Eq. (9.9) is deterministic, the conditional probability function (**box S8**) is simply represented by a Dirac delta function (Fig. 9.5):

$$p_i(y \mid U, \theta) = \delta(y - y_{0,i}) \tag{9.13}$$

where

$$\delta(y - y_{0,i}) = \begin{cases} 1 & \text{if } y = y_{0,i} \\ 0 & \text{elsewhere} \end{cases} \tag{9.14}$$

in which $y_{0,i}$ depends on U and θ by the function $f(U)$ and $h(\theta)$. Eq. (9.13) represents the probability to have a certain oscillation amplitude y in the i-th mode given a certain value of U and θ.

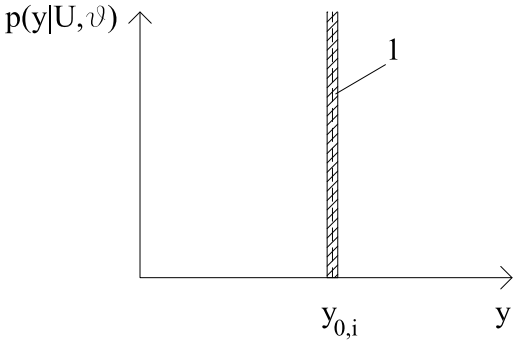

Fig. 9.5 Conditional probability function $p(y \mid U, \theta)$.

9.2.3 Probability of failure

The probability of failure (**box R1**) is the sum of the probability to have a deck vertical displacement in each mode higher than the corresponding limit threshold $y_{lim,i}$. It can be obtained by the following expression:

$$P_F = 1 - \sum_{i=1}^{N} \left[\int_0^{y_{lim,i}} \int_0^{2\pi} \int_0^{\infty} p_i(y|U,\theta) q(U,\theta) dU d\theta dy \right] \tag{9.15}$$

where N is the number of modes.

$y_{lim,i}$ is the limit amplitude threshold for the i-th mode and may be obtained by using the following equation:

$$y_{lim,i} = \frac{a_{lim}}{\omega_i^2} \tag{9.16}$$

According to Eq. (9.13), the previous equation becomes

$$P_F = 1 - \sum_{i=1}^{N} \left[\int_0^{y_{lim,i}} \int_0^{2\pi} \int_0^{\infty} \delta(y - y_{0,i}) q(U,\theta) dU d\theta dy \right] \tag{9.17}$$

If $f(U) = h(\theta) = 1$ (hyp 3a, see Fig. 9.4a, 9.4b) the response in the lock-in range ($[U_{1,i}, U_{2,i}]$, $[\theta_1, \theta_2]$ and $[\theta_3, \theta_4]$) is $y = y_{0,i}$, which is given by Eq. (9.9). In the case

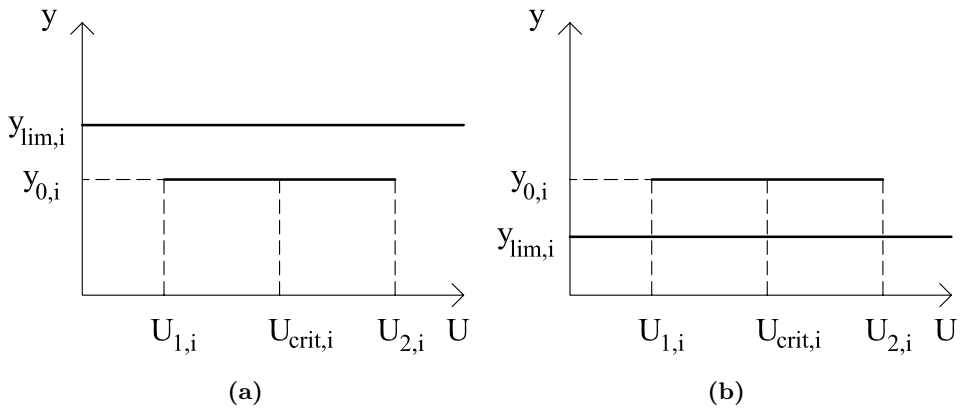

Fig. 9.6 Case: a) limit amplitude higher than lock-in response and b) viceversa.

shown in Fig. 9.6a, where $y_{0,i} \leq y_{lim,i}$, the probability of failure associated to such a mode is zero. In fact, due to the definition of $\delta(y - y_{0,i})$ [Eq. (9.14)], in Eq. (9.17) the integration of y gives values different than zero [$\delta(y - y_{0,i}) = 1$] only when:

- $y = 0$ and U and θ assume values **outside** the lock-in range ($[U_{1,i}, U_{2,i}]$, $[\theta_1, \theta_2]$ and $[\theta_3, \theta_4]$);
- $y = y_{0,i}$ and U and θ assume values **inside** the lock-in range ($[U_{1,i}, U_{2,i}]$, $[\theta_1, \theta_2]$ and $[\theta_3, \theta_4]$).

This means that the integration over y in Eq. (9.17) can be eliminated and the term inside square brackets becomes:

$$\int_0^{2\pi} \int_0^{\infty} q(U,\theta) dU d\theta = 1 \tag{9.18}$$

and then the probability of failure P_F expressed by Eq. (9.17) results equal to 0.

Instead, in the case shown in Fig. 9.6b, where $y_{0,i} > y_{lim,i}$, the function $\delta(y - y_{0,i})$ is different from zero only when $y = 0$ and U and θ assume values **outside** the lock-in range ($[U_{1,i}, U_{2,i}]$, $[\theta_1, \theta_2]$ and $[\theta_3, \theta_4]$). Therefore, Eq. (9.17) can be simplified in:

$$P_F = \sum_{i=1}^{N} \left[\int_{\theta_1}^{\theta_2} \int_{U_{1,i}}^{U_{2,i}} q(U,\theta) dU d\theta + \int_{\theta_3}^{\theta_4} \int_{U_{1,i}}^{U_{2,i}} q(U,\theta) dU d\theta \right] \tag{9.19}$$

where $U_{1,i}$ and $U_{2,i}$ are respectively the lower and upper wind velocity of the lock-in range for the i-th mode. Analogous considerations can be done for the case in which $f_i(U)$ is of triangular shape.

It is worth noting that the extremes of integration $U_{1,i}$ and $U_{2,i}$ in Eq. (9.19) have to be recalculated to take into account that the wind direction is also inclined with respect to the bridge axis. In particular, being the vortex-shedding frequency defined by the wind speed component orthogonal to the deck axis, the integration has to be done over a range of wind velocities given by the sum of the orthogonal and axial wind speed components which depend on the value of the yaw angle (Fig. 9.7). Assuming the validity of the Independence Principle (see Section 4.4), the following formula may be used to evaluate the total wind speed component:

$$U^*_{1,i}(\theta) = \frac{U_{1,i}}{-sin(\alpha - \theta_i)} \tag{9.20}$$

where $U_{1,i}$ is substituted by $U_{2,i}$ to obtain $U^*_{2,i}(\theta)$ and α is the angle between the deck axis and the reference direction of the wind speed (beginning of the sector I: $0 - 10^o$). Therefore, in Eq. (9.19) the extremes of integration of the second integrals

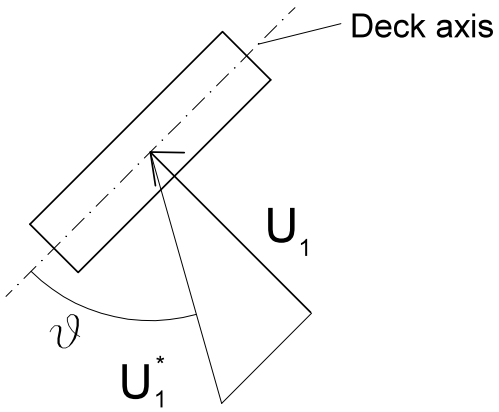

Fig. 9.7 Wind vector yawed respect to bridge axis.

depend on θ and then

$$P_F = \sum_{i=1}^{N} \left[\int_{\theta_1}^{\theta_2} \int_{U^*_{1,i}(\theta)}^{U^*_{2,i}(\theta)} q(U,\theta) dU d\theta + \int_{\theta_3}^{\theta_4} \int_{U^*_{1,i}(\theta)}^{U^*_{2,i}(\theta)} q(U,\theta) dU d\theta \right] \tag{9.21}$$

When the lock-in response is given by $y_{0,i} = y_{peak,i} f(U)$ [Eqs. (9.9, 9.10)] (hyp S3b), Eq. (9.21) becomes:

$$P_F = \sum_{i=1}^{N} \left[\int_{\theta_1}^{\theta_2} \int_{\overline{U}^*_{1,i}(\theta)}^{\overline{U}^*_{2,i}(\theta)} q(U,\theta) dU d\theta + \int_{\theta_3}^{\theta_4} \int_{\overline{U}^*_{1,i}(\theta)}^{\overline{U}^*_{2,i}(\theta)} q(U,\theta) dU d\theta \right] \tag{9.22}$$

where the integration is conducted over a restricted range of lock-in $[\overline{U}^*_{1,i}, \overline{U}^*_{2,i}]$ because of the response $y_{0,i} = y_{peak,i} f_i(U)$ is not constant as in the previous case where $y_{0,i} = y_{peak,i}$.

Eq. (9.21) are implemented by using the following expressions:

$$P_F = \sum_{i=1}^{N} \sum_{j=1}^{M} \left[\int_{U^*_{1,i,j}}^{U^*_{2,i,j}} q_j(U) dU + \int_{U^*_{1,i,j}}^{U^*_{2,i,j}} q_j(U) dU \right] \tag{9.23}$$

where:

$$q_j(U) = \frac{a_j}{b_j}\left(\frac{u}{b_j}\right)^{(a_j-1)} exp\left[-\left(\frac{u}{b_j}\right)^{a_j}\right] \tag{9.24}$$

N is the number of modes prone to lock-in oscillations and M is the number of sectors of the wind direction in which the lock-in oscillations can occur. Analogously for Eq. (9.22):

$$P_F = \sum_{i=1}^{N}\sum_{j=1}^{M}\left[\int_{\overline{U}^*_{1,i,j}}^{\overline{U}^*_{2,i,j}} q_j(U)dU + \int_{\overline{U}^*_{1,i,j}}^{\overline{U}^*_{2,i,j}} q_j(U)dU\right] \tag{9.25}$$

where $\overline{U}^*_{1,i}$ and $\overline{U}^*_{2,i}$ are determined by applying Eq. (9.20) to $\overline{U}_{1,i}$ and $\overline{U}_{2,i}$ given by:

$$\begin{aligned}\overline{U}_{1,i} &= U_{1,i} + (U_{crit,i} - U_{1,i})\frac{y_{lim,i}}{y_{peak,i}} \\ \overline{U}_{2,i} &= U_{crit,i} + (U_{2,i} - U_{crit,i})\left(1 - \frac{y_{lim,i}}{y_{peak,i}}\right)\end{aligned} \tag{9.26}$$

The risk in terms of average value of days per year in which the bridge has to be closed to traffic (**box R2**) can be estimated by the following product:

$$Risk = P_F \cdot d_{year} \tag{9.27}$$

where $d_{year} = 365$ is the number of days per year.

9.3 Application of the procedure

As previously said, the risk analysis procedure proposed will be applied to an idealized case study with the following characteristics:

- the bridge is located on the site of the Monte Argentario station (Tuscany, Italy);
- the dynamic characteristics of the bridge are those of the Bosphorus Bridge I;
- the cross section of the deck is a rectangular section with width to depth ratio of 4.

9.3.1 Hazard analysis

Box H1 – Anemometric data

The data analyzed in Chapter 3 are used in the hazard analysis of the present case study. Therefore, according to hyp H1, the bridge is located in the site of the anemometric station from which the data have been obtained (Monte Argentario station, located in Tuscany, Italy).

Box H2 – Joint probability density function

The joint probability density function used is the Weibull distribution for which the two parameters have been obtained for each sector and reported in Table 3.1.

$$q_{10,i}(U,\theta) = p(u < U < u + du, \theta_i < \theta < \theta_i + \Delta\theta) = \frac{a_i}{b_i}\left(\frac{u}{b_i}\right)^{(a_i-1)} exp\left[-\left(\frac{u}{b_i}\right)^{a_i}\right] \tag{9.28}$$

where $q_{10,i}(U,\theta)$ is the joint probability density function relative to the anemometer position (10 m over the ground).

Box H3 – Deck joint probability function

According to hyb H2 (a constant wind profile is assumed) the joint probability density function at the deck level is equal to that at the quote of the anemometer.

9.3.2 Structural vulnerability analysis

Box S1 – Structural parameters

The Bosphorus Bridge I connects the European and Asian parts of Istanbul. It was designed in 1969 and its construction started in 1970. It was completed and went into use in 1973. It has a 1074 m main span and 243 m side spans (Fig. 9.8a, 9.8c, 9.8d). The deck of the Bosphorus Bridge is a hollow box girder (3 m high and 28 m wide) and hangers ensure the suspension of the deck. Bosphorus Bridge hangers are of the inclined type. Bridge towers are a steel box construction and are 165 m high. Bosphorus Bridge was designed to carry six lanes of highway traffic (Erdogan *et al.*, 2007). Modal analysis is once gain performed with the software SAP with the finite-element model displayed in Fig. 9.8b. The frequency and the damping coefficient of each mode, according to the hyphoteses hyp S1a and hyp S1b, are reported in Table 9.1. Finally, the modal shapes and the corresponding sinusoidal approximation functions are shown in Fig. 9.9.

Box S2 – Aerodynamic parameters

No aerodynamic parameters are available for the deck section reported in Fig. 9.8d and then the aerodynamic parameters of the 4:1 rectangular section estimated in Chapter 6 are used (Table 9.2).

As previous said (see Section 9.2.2), the values of the parameters which describe the functions $f_i(U)$ and $h(\theta)$ (U_1, U_2, θ_1, θ_2, θ_3, θ_4) reported in Fig. 9.4 cannot be obtained by using the lock-in response shown in Fig. 6.11 because it would be nonconservative since the Scruton number during the tests ($Sc = 6$) was higher than that of the prototype (see box S4). Therefore, literature results will be used.

Finally, the correlation functions g_1 and g_2 are given by Eq. (7.28) in which the functions $f_1(\eta)$ and $f_2(\eta)$ depend on the deck shape. For the rectangular section considered in this study no tests have been carried out to estimate the previous functions and then those found in the literature for three sections and reported below are considered and the corresponding results are compared (Ehsan and Scanlan,

(a)

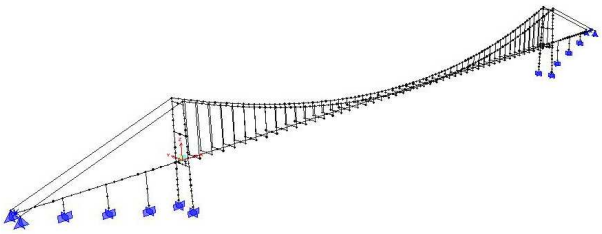

(b)

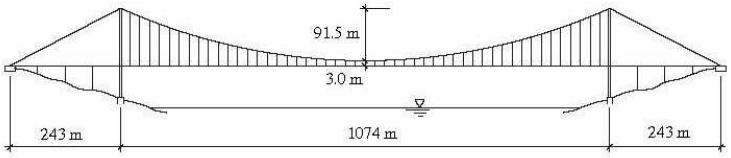

(c)

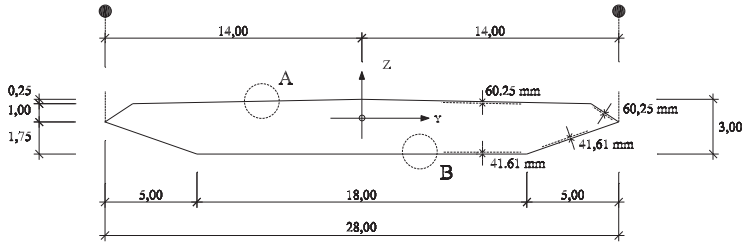

(d)

Fig. 9.8 Bosphorus Bridge I: (a) night view; (b) finite element model for the modal analysis; (c) main features of the geometry of the structure; (d) cross-section of the deck.

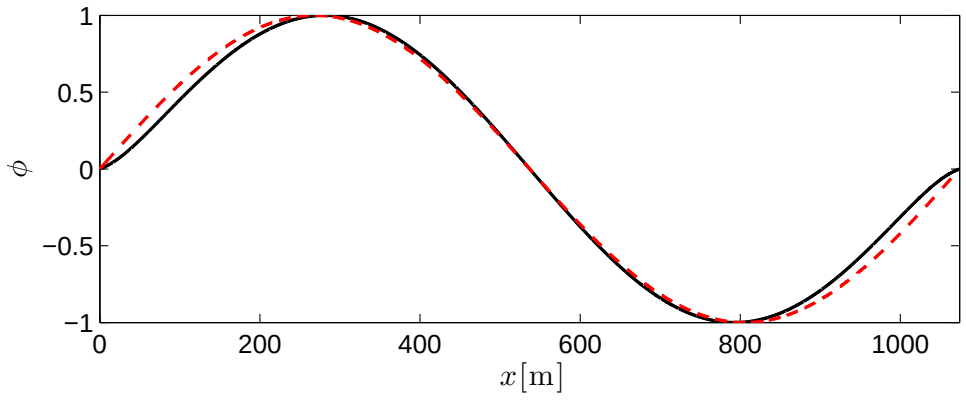

(a)

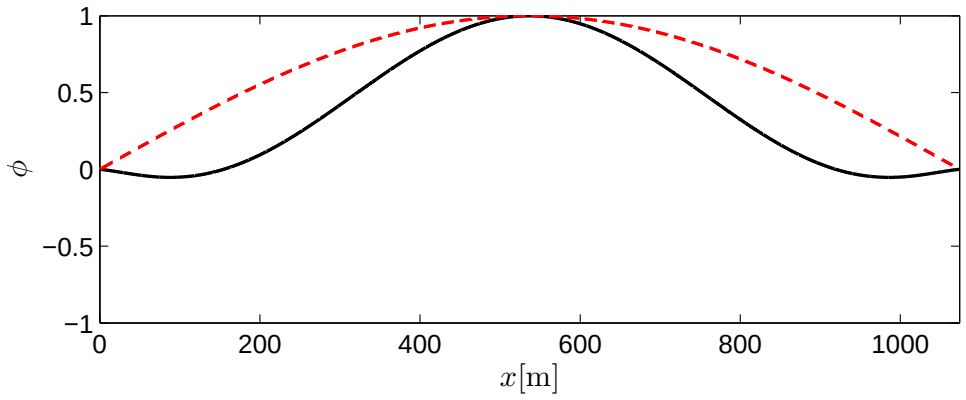

(b)

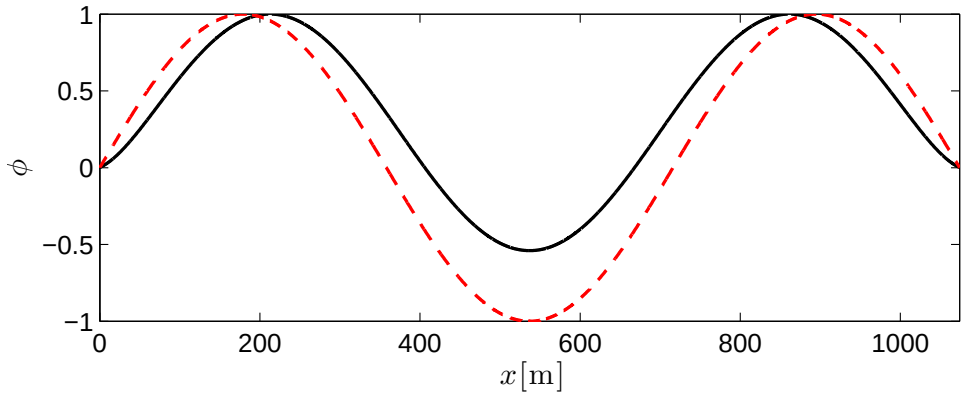

(c)

Fig. 9.9 Vertical modal shapes (black solid curve) and the corresponding sinusoidal approximations (red dashed curve).

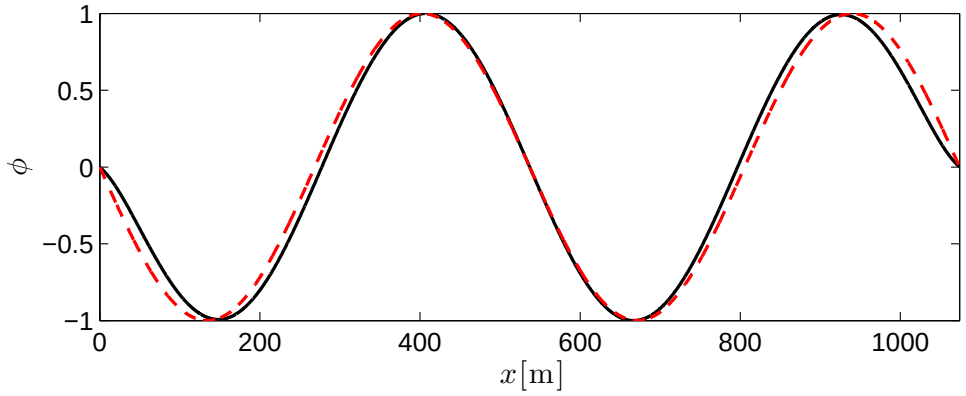

(d)

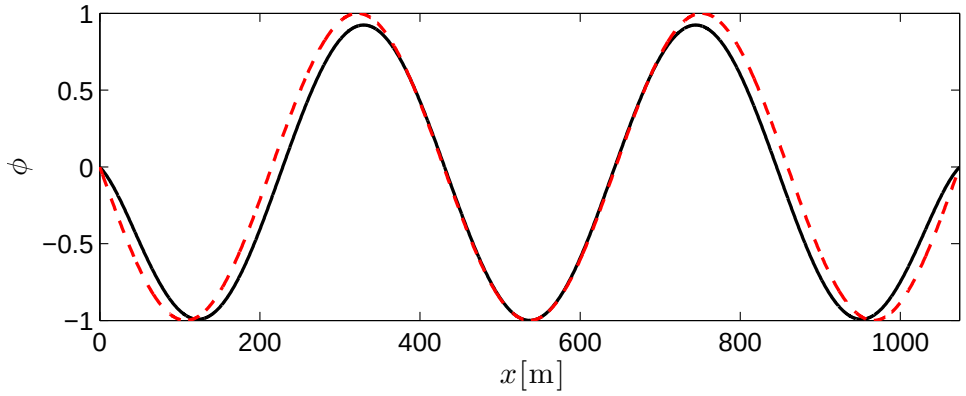

(e)

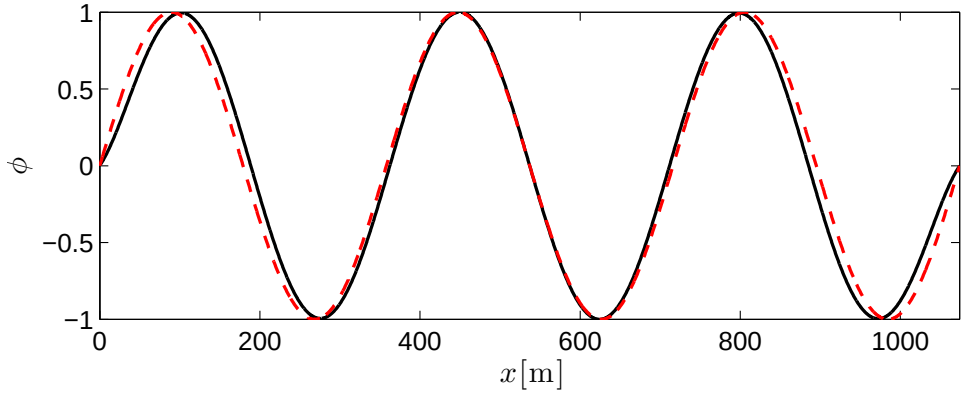

(f)

Fig. 9.9 (continued).

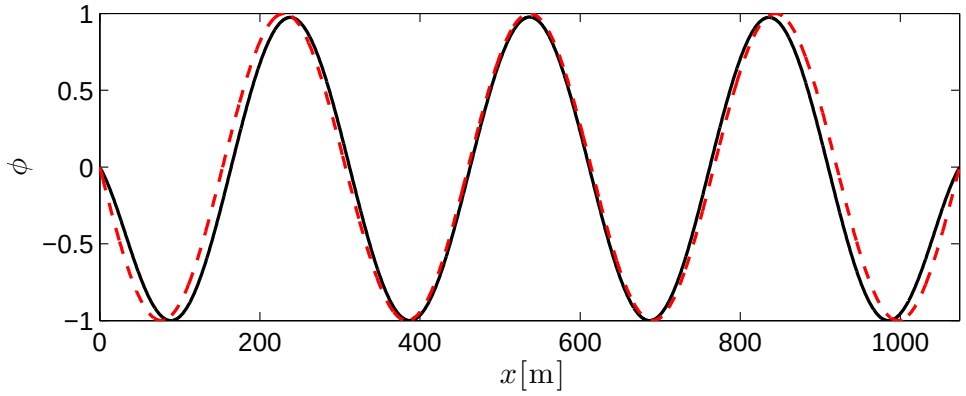

(g)

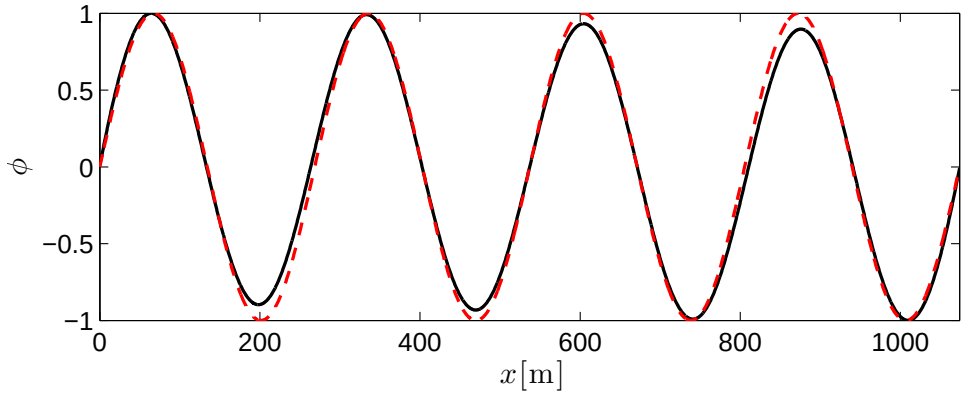

(h)

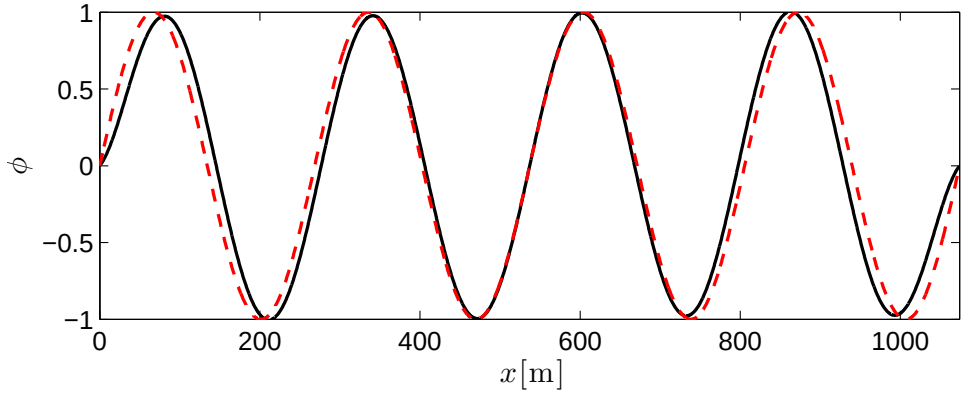

(i)

Fig. 9.9 (continued).

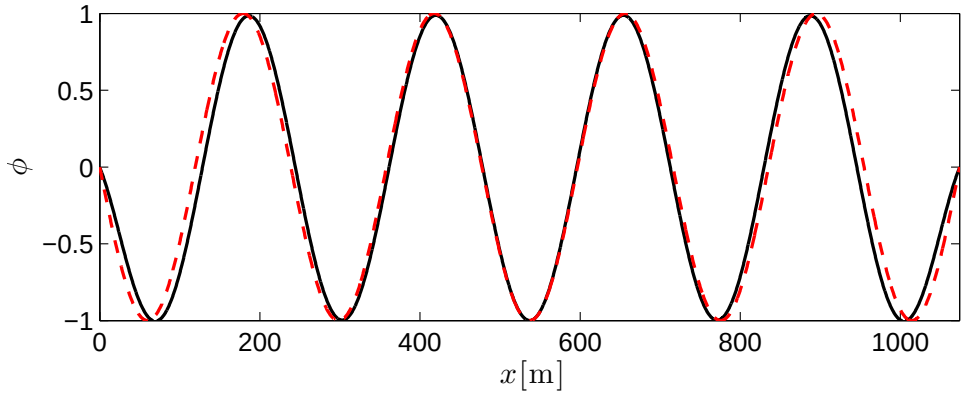

(j)

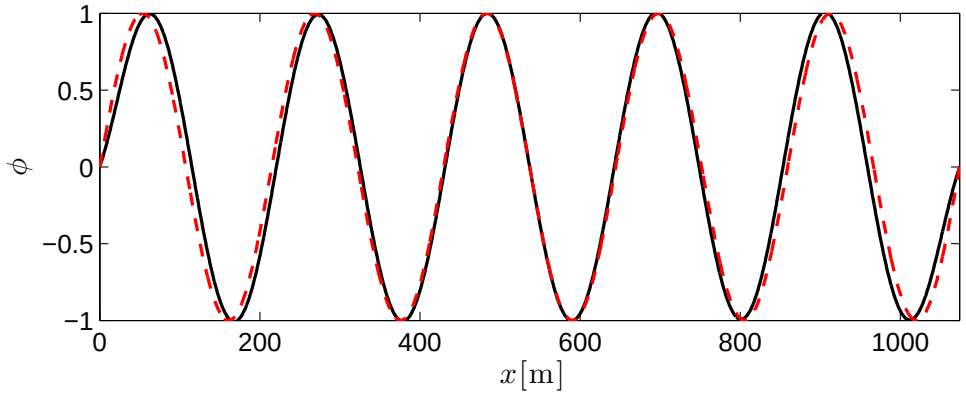

(k)

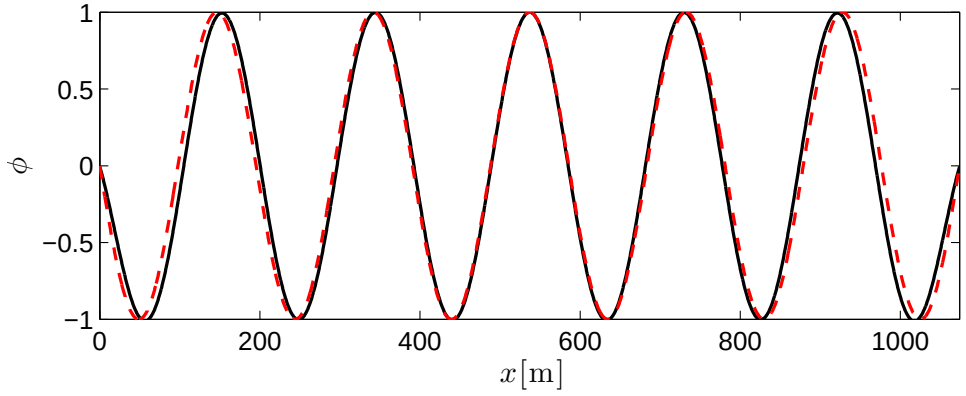

(l)

Fig. 9.9 (continued).

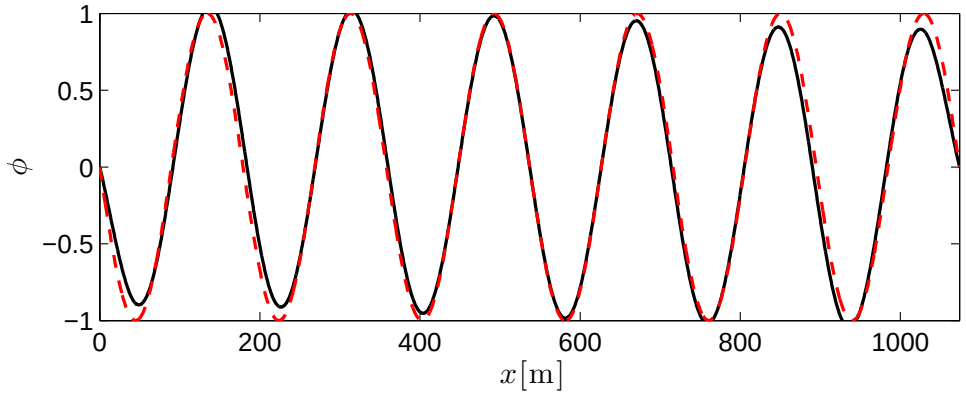

(m)

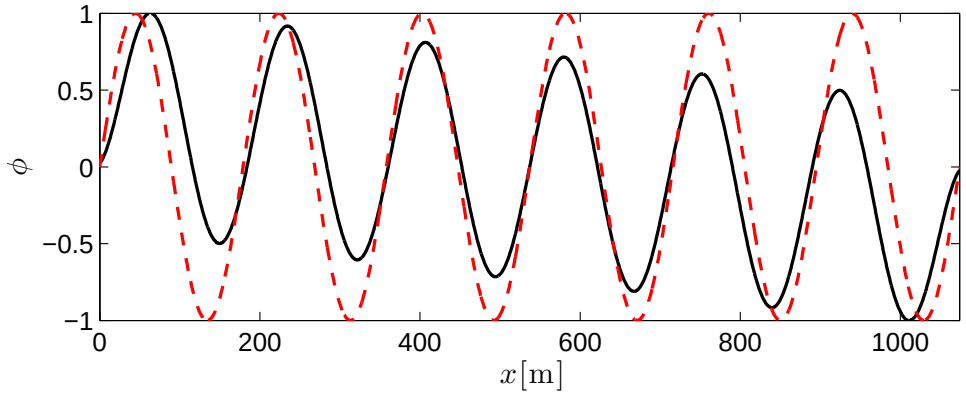

(n)

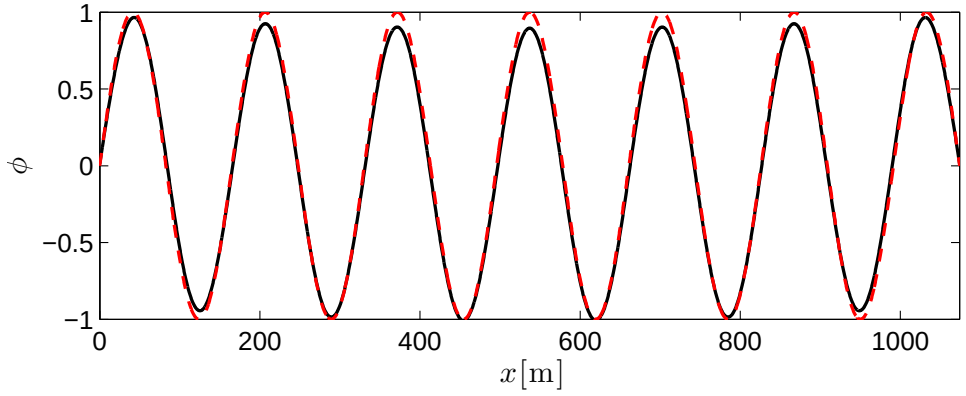

(o)

Fig. 9.9 (continued).

Table 9.1 Modal analysis results for Bosphorus Bridge I

Vertical mode	Number	Type	Frequency [Hz]	ζ_i [a] [-]	ζ_i [b] [-]
I	2	antisymmetric	0.146	0.0008	0.0016
II	3	symmetric	0.162	0.0008	0.00159
III	4	symmetric	0.226	0.0008	0.00155
IV	6	antisymmetric	0.291	0.0008	0.00151
V	11	symmetric	0.381	0.0008	0.00146
VI	13	antisymmetric	0.474	0.0008	0.00140
VII	18	symmetric	0.582	0.0008	0.00133
VIII	23	antisym. + long.	0.666	0.0008	0.00128
IX	25	antisym. + long.	0.706	0.0008	0.00125
X	28	symmetric	0.828	0.0008	0.00118
XI	34	antisymmetric	0.969	0.0008	0.00109
XII	40	symmetric	1.123	0.0008	0.00100
XIII	43	antisymmetric	1.279	0.0008	0.00090
XIV	46	antisymmetric	1.342	0.0008	0.00086
XV	50	symmetric + long.	1.445	0.0008	0.00080

[a] hyp S1a
[b] hyp S1b

Table 9.2 Aerodynamic and aeroelastic characteristics of a 4:1 rectangular section.

St	Y_1	ϵ
0.136	$6.27 - 7.65^a$	$1082.2 - 1122.6^a$

[a] It is considered a range of values for the aeroelastic parameters (see Section 7.5 for details)

Table 9.3 Critical velocity, equivalent mass and Scruton number for each vertical mode of the Bosphorus Bridge

Vertical mode	U_{crit} [m/s]	m_e [kg/m]	Sc^a [-]	Sc^b [-]
I	3.22	13967	3.12	6.24
II	3.57	13600	3.04	6.04
III	4.99	13817	3.09	5.99
IV	6.42	13800	3.08	5.81
V	8.40	13699	3.06	5.58
VI	10.46	13698	3.06	5.36
VII	12.84	13579	3.03	5.04
VIII	14.69	67358	15.05	24.08
IX	15.57	16767	3.75	5.86
X	18.27	13507	3.02	4.45
XI	21.38	13632	3.04	4.14
XII	24.77	13548	3.03	3.79
XIII	28.21	16950	3.79	4.26
XIV	29.60	56462	12.61	13.56
XV	31.88	108390	24.21	24.21

[a] hyp S1a
[b] hyp S1b

1990; Ehsan *et al.*, 1990; Ricciardelli, 2010):

$$\text{Square section} = \begin{cases} f_1(\eta) = \frac{0.052}{(0.298+\eta^{0.25})} \\ f_2(\eta) = \frac{0.065}{(0.042+\eta)} \end{cases} \tag{9.29}$$

$$\text{Circular section} = \begin{cases} f_1(\eta) = \frac{0.05-\eta}{(2.5+95\eta)} \\ f_2(\eta) = 1 \end{cases} \tag{9.30}$$

$$\text{H section} = \begin{cases} f_1(\eta) = \frac{0.01578}{(0.02694+\eta)} \\ f_2(\eta) = 0.5 \end{cases} \tag{9.31}$$

Box S3 – Critical velocities

The critical velocity for each mode is reported in Table 9.3 and may be evaluated by using Eq. (9.5) with $D = 3$m, $St = 0.136$ (Table 9.2) and the frequencies given in Table 9.1.

Box S4 – Scruton number

The Scruton number of each mode can be obtained by using Eq. (9.6) in which the equivalent mass is obtained by Eq. (7.19), the damping ratios are reported in Table 9.1, the air density is 1.25 kg/m^3 and the depth of the cross section is 3 m. The results are reported in Table 9.3. The high values of the equivalent mass for the modes VIII, XIV and XV can be justified as the effect of the participation to the motion of the tower as well as the longitudinal motion of the deck.

Box S5 – Vortex-Induced Vibration modes

The Scruton number after which no oscillations occur Sc_0 is given by the empirical model used into the analysis. In particular, in the present procedure the Ehsan-Scanlan's model[1] is considered and then the corresponding Sc_0 can be obtained by looking at Fig. 8.5 ($Sc_0 = 13$).

The modal shapes prone to vortex-induced vibrations may be obtained by considering the results reported in Table 9.3. According to the Ehsan-Scanlan model, all the modes with a Scruton number higher than 13 should be excluded because no vortex-induced vibrations are supposed to occur. Therefore, only modes VIII, XIV and XV are not considered during the analysis.

Box S6 – Prototype peak response

When a full spanwise correlation is assumed (hyp S2a), the response of the prototype for each mode may be obtained by using Eq. (7.26), in which the parameter R [Eq.(7.20)] depends on the modal shapes. According to Fig. 9.9, the modes I, IV, V, VI, VII, IX, X, XI, XII, XIII may be approximated by the corresponding sinusoidal forms. In the first two columns of Table 9.4, by using the aeroelastic parameters $Y_1 = 6.27$ and $\epsilon = 1082.2$, the fully correlated peak response $\hat{y}_i^{fc}$ for two different values of the damping ratio (hyp S1a and hyp S1b) is reported for each mode. Instead, the last two columns are obtained by using $Y_1 = 7.65$ and $\epsilon = 1122.6$. The accelerations obtained by using Eq. (9.8) are reported in Table 9.5.

The imperfect spanwise correlation may be taken into account by using Eq. (7.34). The results are reported in Table 9.6 and 9.7. Ehsan and Scanlan (1990) suggest to approximate the correlation functions g_1 and g_2 by the sinusoidal forms used to represent the modes. It can be observed that, both for the fully correlated case and imperfect spanwise correlated one, the variation of the two aeroelastic parameters given by the application of the Ehsan-Scanlan identification procedure provides small variations in terms of the limit-cycle oscillation amplitude of the entire bridge. Instead the effect of the damping coefficient is more visible especially for the first modes where it is higher than that of the mode characterized by higher frequencies.

The results obtained by using sinusoidal functions as correlation functions are compared for the mode I with those given by three different correlation functions evaluated by wind tunnel tests on square, circular and H cross sections (Fig. 9.10). In Table 9.8 the results obtained for the first vertical mode are reported in the fully correlated case and in the cases in which the loss of correlation is taken into account by using both the sinusoidal and experimental curves as correlation functions. As it can be observed the use of the sinusoidal assumption for the correlation functions overestimates the response especially for the circular cross section.

Box S7 – Prototype response

At this step Eq. (9.9) has to be used. The term $y_{peak,i}$ was defined in the previous step (Box S6), here the parameters of the two functions $f_i(U)$ and $h(\theta)$ have to

[1]Even though the Ehsan-Scanlan's model does not give reliable predictions as the other existing models it is used in the present procedure because it is considered useful for practical applications to bridge decks (more details can be found in Section 7.1).

Table 9.4 Prototype peak response $\hat{y}_i^{fc}$ in the case of full spanwise correlation of the aeroelastic forces

Vertical mode	$\hat{y}_i^{fc\,a,d}$ [m]	$\hat{y}_i^{fc\,b,d}$ [m]	$\hat{y}_i^{fc\,a,e}$ [m]	$\hat{y}_i^{fc\,b,e}$ [m]
I	0.1799	0.1426	0.1789	0.1513
II[c]	0.1831	0.1472	0.1819	0.1552
III[c]	0.1873	0.1518	0.1863	0.1598
IV	0.1802	0.1482	0.1792	0.1553
V	0.1805	0.1512	0.1794	0.1575
VI	0.1805	0.1541	0.1794	0.1596
VII	0.1808	0.1579	0.1796	0.1624
IX	0.1730	0.1478	0.1737	0.1550
X	0.1809	0.1650	0.1798	0.1677
XI	0.1807	0.1685	0.1795	0.1703
XII	0.1809	0.1726	0.1797	0.1734
XIII	0.1726	0.1672	0.1734	0.1693

[a] hyp S1a
[b] hyp S1b
[c] The real shape of the mode is considered
[d] $Y_1 = 6.27$, $\epsilon = 1082.2$
[e] $Y_1 = 7.65$, $\epsilon = 1122.6$

Table 9.5 Prototype vertical acceleration a_i^{fc}/g in the case of full spanwise correlation of the aeroelastic forces

Vertical mode	$a_i^{fc}/g^{a,d}$ [-]	$a_i^{fc}/g^{b,d}$ [-]	$a_i^{fc}/g^{a,e}$ [-]	$a_i^{fc}/g^{b,e}$ [-]
I	0.0154	0.0122	0.0153	0.0130
II[c]	0.0193	0.0155	0.0192	0.0164
III[c]	0.0385	0.0312	0.0383	0.0329
IV	0.0614	0.0505	0.0611	0.0529
V	0.1054	0.0883	0.1048	0.0920
VI	0.1632	0.1393	0.1622	0.1443
VII	0.2464	0.2153	0.2449	0.2214
IX	0.3471	0.2964	0.3485	0.3109
X	0.4993	0.4553	0.4960	0.4627
XI	0.6826	0.6366	0.6784	0.6435
XII	0.9178	0.8760	0.9119	0.8801
XIII	1.1360	1.1007	1.1413	1.1147

[a] hyp S1a
[b] hyp S1b
[c] The real shape of the mode is considered
[d] $Y_1 = 6.27$, $\epsilon = 1082.2$
[e] $Y_1 = 7.65$, $\epsilon = 1122.6$

Table 9.6 Prototype peak response $\hat{y}_i^{ic}$ in the case of imperfect spanwise correlation of the aeroelastic forces

Vertical mode	$\hat{y}_i^{ica,d}$ [m]	$\hat{y}_i^{icb,d}$ [m]	$\hat{y}_i^{ica,e}$ [m]	$\hat{y}_i^{icb,e}$ [m]
I	0.1683	0.1227	0.1688	0.1357
II[c]	0.1699	0.1253	0.1703	0.1378
III[c]	0.1704	0.1246	0.1713	0.1381
IV	0.1688	0.1298	0.1691	0.1406
V	0.1690	0.1336	0.1694	0.1433
VI	0.1690	0.1372	0.1694	0.1458
VII	0.1694	0.1419	0.1696	0.1492
IX	0.1602	0.1292	0.1627	0.1402
X	0.1696	0.1506	0.1698	0.1555
XI	0.1692	0.1547	0.1695	0.1586
XII	0.1695	0.1597	0.1697	0.1623
XIII	0.1596	0.1532	0.1623	0.1575

[a] hyp S1a
[b] hyp S1b
[c] The real shape of the mode is considered
[d] $Y_1 = 6.27$, $\epsilon = 1082.2$
[e] $Y_1 = 7.65$, $\epsilon = 1122.6$

Table 9.7 Prototype vertical acceleration a_i^{ic}/g in the case of imperfect spanwise correlation of the aeroelastic forces

Vertical mode	$a_i^{ica,d}$ [m/s^2]	$a_i^{icb,d}$ [m/s^2]	$a_i^{ica,e}$ [m/s^2]	$a_i^{icb,e}$ [m/s^2]
I	0.0144	0.0105	0.0145	0.0116
II[c]	0.0179	0.0132	0.0180	0.0146
III[c]	0.0350	0.0256	0.0352	0.0284
IV	0.0575	0.0442	0.0576	0.0479
V	0.0987	0.0780	0.0989	0.0837
VI	0.1528	0.1240	0.1531	0.1319
VII	0.2309	0.1935	0.2312	0.2034
IX	0.3213	0.2593	0.3263	0.2812
X	0.4679	0.4154	0.4684	0.4291
XI	0.6394	0.5847	0.6405	0.5994
XII	0.8600	0.8104	0.8611	0.8237
XIII	1.0509	1.0085	1.0682	1.0367

[a] hyp S1a
[b] hyp S1b
[c] The real shape of the mode is considered
[d] $Y_1 = 6.27$, $\epsilon = 1082.2$
[e] $Y_1 = 7.65$, $\epsilon = 1122.6$

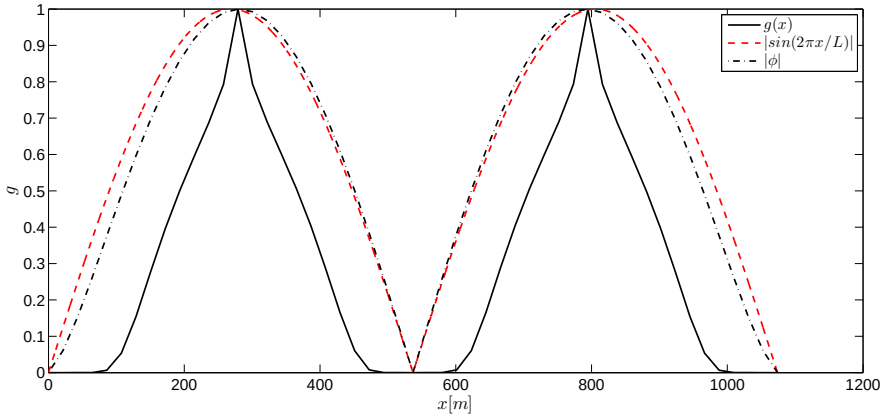

(a)

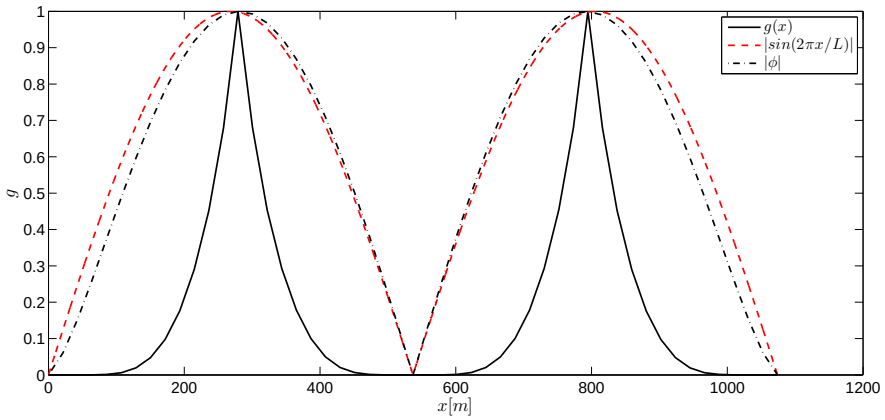

(b)

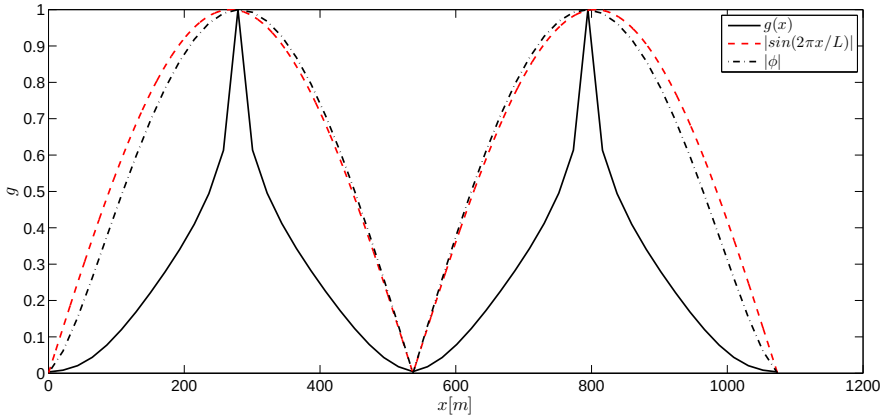

(c)

Fig. 9.10 Comparison between real modal shape (dash-dot line), sinusoidal modal shape function (red dashed line) and experimental correlation function (solid line) of (a) square section, (b) circular section and (c) H section for the first vertical mode.

Table 9.8 Prototype peak response $\hat{y}_i^{ic,g}$ in the case the spanwise correlation of the aeroelastic forces is taken into account by the experimental correlation functions $g(x)$ compared with the previous assumtions

Vertical mode	$\hat{y}_i^{fc}$ [m]	$\hat{y}_i^{ic}$ [m]	$\hat{y}_i^{ic,g}$ [m]
I	0.1799	0.1683	0.1361[a]
I	-	-	0.0805[b]
I	-	-	0.1144[c]

[a] Square section
[b] Circular section
[c] H section
[d] Results obtained with $Y_1 = 6.27$, $\epsilon = 1082.2$ and hyp S1a

be chosen [Eqs. (9.10, 9.11, 9.12)]. In particular, according to Sarpkaya (1979) (see Section 4.3), the Strouhal relation is violated for a range of the ±25-30 % of the natural frequency and the vortex-shedding is controlled by the body motion. Therefore, each mode is associated with a different extension of the lock-in range (Table 9.9). To define the function $h(\theta)$ one needs to know what is the range of yaw angles for which lock-in occurs for the deck section considered. To do that wind tunnel tests should be carried out to measure the cross flow response for different values of the angle of yaw. In this study, such wind tunnel tests were not performed and then it is conservatively assumed (see Section 4.4) that the lock-in response occurs in the range of $\pm 70^o$ around the normal direction $\theta = 90^o$, which means that $\theta_1 = 30$, $\theta_2 = 170$, $\theta_3 = 210$ and $\theta_4 = 350$.

Box S8 – Probabilistic response

The structural vulnerability part ends at this step. It is represented by the term $p(y|U, \theta)$ reported in Eq. (9.13), which is known for each mode by using the results of the previous steps.

9.3.3 Risk

Box R1 – Probability of failure

Assuming the validity of the Independence Principle the critical velocities reported in Table 9.9 can be recalculated to obtain the new extremes of integration to evaluate the integral in Eq. (9.21−9.22). By considering Eq. (9.20), where $U_{1,i}$ is the component of the wind speed orthogonal to the deck axis (U_1 and U_2 in Table 9.9) and $\alpha = 10^o$ is the angle between the deck axis and the reference direction of the wind speed, the extremes of integration have to be recalculated for each mode and for each sector.

The probability of failure is calculated neglecting the first three modes because $y_{0,i} < y_{lim}$ for $i = 1 - 3$ [Table 9.10 obtained by using Eq. (9.16)] and then the corresponding probability of failure is zero. When hyp 3a [Eq. (9.21)] is assumed,

Table 9.9 Parameters of $f(U)^a$

Vertical mode	U_1 [m/s]	U_{crit} [m/s]	U_2 [m/s]
I	2.25	3.21	4.19
II	2.50	3.56	4.64
III	3.49	4.99	6.49
IV	4.49	6.42	8.35
V	5.88	8.40	10.92
VI	7.32	10.46	13.60
VII	8.99	12.84	16.69
IX	10.90	15.57	20.24
X	12.79	18.27	23.75
XI	14.97	21.38	27.79
XII	17.34	24.77	32.30
XIII	19.75	28.21	36.67

[a] It is conservatively assumend that the Strouhal relation is violated for a range of the ± 30 % of the natural frequency

one obtains:

$$P_F = 0.0848 \tag{9.32}$$

whereas

$$P_F = 0.0385 \tag{9.33}$$

when hyp 3b [Eq. (9.22)] is considered[2].

Box R2 – Risk

The risk in term of average value of days per year in which the bridge has to be closed to traffic (box R2) is given by Eq. (9.27):

$$Risk = 30.94 \text{ days/year} \tag{9.34}$$

considering hyp 3a and

$$Risk = 14.05 \text{ days/year} \tag{9.35}$$

for hyp 3b.

9.4 Conclusions

In this chapter a procedure to perform the VIV-risk assessment of bridge decks was developed. The general risk management framework developed into the IGC 802 was adapted to frame the problem under study. The risk in terms of days per

[2]Both probabilities are evaluated by considering the first column of Table 9.4, where the maximum response amplitude was obtained.

Table 9.10 Values of y_{lim} for each mode

Vertical mode	$y_{lim,i}$ [m]
I	0.5829
II	0.4734
III	0.2433
IV	0.1467
V	0.0856
VI	0.0553
VII	0.0367
IX	0.0249
X	0.0181
XI	0.0132
XII	0.0099
XIII	0.0076

year in which the bridge has to be closed were evaluated by using a PEER-type equation based on the Performance-Based Design approach. Finally, the procedure was applied to an idealized case study to show the effects of the assumptions standing behind the procedure.

To develop the risk analysis and then to quantify the risk associated to the vortex-shedding action on bridge decks, some important assumptions were done.

In the hazard analysis, the lack of knowledge on the mean wind speed profile at moderate wind velocities was highlighted and the strong assumption of constant wind profile (hyp H2) was considered.

As the difficulties in bridge engineering to predict the damping ratio during the design phase, in the structural vulnerability part, the effects of two assumptions (hyp S1a, b) on the values of the modal damping ratios were analyzed. In particular, modest differences in terms of limit-cycle oscillation amplitudes were observed. The effects of the imperfect spanwise correlation of the aeroelastic forces during lock-in (hyp S2a, b) was analyzed too. In this case, the differences are significant especially if the correlation functions used in the analysis are obtained by wind tunnel tests. The effects in terms of days per year in which the bridge has to be closed were analyzed by assuming two different shapes (constant and triangular shapes) of the lock-in response (hyp S3a, b). The results have shown that significant differences are obtained in the two cases. The lack of knowledge on the effects of the angle of yaw on the lock-in response have led to consider a constant response (hyp S4) inside the range of yaw angle in which according to the literature the lock-in response can occur. Finally, it is worth noting that to conduct a careful risk analysis a stochastic model of the response should be available. Unfortunately, to date not even a deterministic model for predicting vortex-induced vibrations of bridge decks is available. Therefore, in the present procedure, the Ehsan-Scanlan's model was used because it needs only a wind tunnel test to estimate its aeroelastic tests. However, it is underlined that it is unreliable to predict the lock-in response for values of the Scruton number different than that at which its aeroelastic parameters are estimated.

Chapter 10

General conclusions and outlooks

The present dissertation deals with the risk assessment of bridge decks due to vortex-shedding, which is nowadays recognized as a key issue in the design of flexible bridges.

The research activity developed represents a contribute in the risk management research as well as in the wind engineering one. In the risk management field, a procedure to quantify the risk associated to vortex-shedding of bridge decks was proposed. In the wind engineering field, the main effort was employed for improving the present capacity of modeling vortex-induced vibrations of bridge decks. In particular, the contributions of the present dissertation are the following:

- Development of a procedure to conduct the vortex-shedding risk assessment of bridge decks;
- Application of the procedure to an idealized case study;
- Experimental tests in wind tunnel have shown a certain interaction between the two degree of freedom (heaving and pitching) of the sectional model during lock-in both in ambient vibrations and decay-to-resonance tests;
- The coherence of the van der Pol-type equation in modeling vortex-induced vibrations of wind-sensitive structures was demonstrated;
- The validity of the assumptions of an identification procedure present in the literature was demonstrated;
- A limit in the identification procedure proposed in the literature is constituted by the difficulties in the choice of the limit-cycle oscillation amplitude from the experimental signal, whose value gives rise to significant difference in the aeroelastic parameters estimated;
- A direct numerical identification method was proposed to estimate the aeroelastic parameters of a possible modified version of the van der Pol-type equation of the model present in the literature.

In developing the risk analysis procedure proposed in the present dissertation several lacks of knowledge were individuated which can encourage researches in several directions and which are listed in the following:

- Improvements should be done in modeling the mean wind speed profile in the atmospheric boundary layer at moderate wind velocities;
- The importance of the structural damping ratio on vortex-induced vibrations ask for a more accurate definition of its value in the initial phase of the design. This objective could be obtained by increasing the number of tests on real bridges;
- Measurements of the spanwise correlation of the aeroelastic forces during lock-in should be done for different cross-sections in order to lead to more accurate predictions of the full bridge response;
- A reliable model for vortex-induced vibrations of bluff bodies should be necessary for reducing the wind tunnel tests during lock-in and to improve the present unreliable predictions;
- Wind tunnel tests on yawed cylinders should be carried out by considering cross-sections different than the circular one. In particular, response measurements on freely vibrating cylinders with different angle of yaw are necessary;
- Wind tunnel tests on a freely vibrating cylinder should be performed with different frequency ratios between the two degree of freedom in order to show the effect of the interaction between the modes on the lock-in response.

Bibliography

AS/NZS-Standard (1999). Risk management.

Atta, C. W. V. (1968). Experiments on vortex shedding from yawed circular cylinders. *AIAA J.*, **6**, 931–933.

Augusti, G. and Ciampoli, M. (2008). Performance-based design in risk assessment and reduction. *Probabilistic Engineering Mechanics*, **23**(4), 496 – 508. Dedicated to Professor Ove Ditlevsen.

Augusti, G., Borri, C., and Niemann, H.-J. (2001). Is aeolian risk as significant as other environmental risks? *Reliability Engineering & System Safety*, **74**(3), 227 – 237.

Bartoli, G. and Mannini, C. (2008). A simplified approach to bridge deck flutter. *Journal of Wind Engineering and Industrial Aerodynamics*, **96**(2), 229 – 256.

Bartoli, G., Contri, S., Mannini, C., and Righi, M. (2009). Toward an improvement in the identification of bridge deck flutter derivatives. *J. of Eng. Mech.*, **135**(8), 771–785.

Bartoli, G., Borsani, A., Mannini, C., Marra, A. M., Procino, L., and Ricciardelli, F. (2011). Wind tunnel study on the aerodynamics of a 5:1 rectangular cylinder in smooth flow. In *Proceedings of the 13th International Conference for Wind Engineering*, Amsterdam, The Netherands.

Basu, R. and Vickery, B. (1983). Across-wind vibrations of structure of circular cross-section. part ii. development of a mathematical model for full-scale application. *Journal of Wind Engineering and Industrial Aerodynamics*, **12**(1), 75 – 97.

Battista, R. C. and Pfeil, M. S. (2000). Reduction of vortex-induced oscillations of rio-niteroi bridge by dynamic control devices,. *J. Wind Eng. and Ind. Aerodyn.*, **84**, 273–288.

Bearman, P. W. (1984). Vortex shedding from oscillating bluff bodies. *Annual Review of Fluid Mechanics*, **16**(1), 195–222.

Bearman, P. W. and Currie, I. G. (1979). Pressure fluctuation measurements on an oscillating circular cylinder. *Journal of Fluid Mechanics*, **91**, 661–677.

Bearman, P. W. and Davies, M. E. (1977). The flow about oscillating bluff structures. In K. J. Eaton, editor, *Proc. Int. Conf. Wind Eff. Build. Structures, 4th*, pages 285–295. Cambridge Univ. Press.

Bearman, P. W. and Graham, J. M. R. (1980). Vortex shedding from bluff bodies in oscillatory flow: A report on euromech 119. *Journal of Fluid Mechanics Digital Archive*, **99**(02), 225–245.

Bearman, P. W. and Obasaju, E. D. (1982). An experimental study of pressure fluctuations on fixed and oscillating square section cylinders. *Journal of Fluid Mechanics*, **119**, 297–321.

Bellman, R., Kagiwada, H. H., Kalaba, R. E., and Sridhar, R. (1966). Invariant imbedding and nonlinear filtering theory. *J. Astronautical Sci.*, **13**(3), 110–115.

Benaroya, H. and Lepore, J. (1983). Statistical flow-oscillator modeling of vortex-shedding. *Journal of Sound and Vibration*, **86**(2), 159 – 179.

Berger, E. and Wille, R. (1972). Periodic flow phenomena. *Annual Review of Fluid Mechanics*, **4**(1), 313–340.

Billah, K. (1989). *A study of Vortex Induced Vibration*. Ph.D. thesis, Princeton University, New Jersey.

Birkhoff, G. (1953). Formation of vortex streets. *J. App. Physics*, **24**, 209–231.

Bishop, R. and Hassan, A. (1964). The lift and drag forces on a circular cylinder oscillating in a flowing fluid. *Proceedings of the Royal Society of London. Series A, Mathematical and Physical Sciences*, **277**, 51–75.

Blevins, R. D. (2001). *Flow-Induced Vibration*. Krieger Publishing Company, Malabar, Florida.

Boccotti, P. (2000). *Wave mechanics for ocean engineering*. Elsevier Oceanography Series.

Boccotti, P. (2004). *Idraulica Marittima*. UTET Libreria, 2nd edition.

Buonopane, S. G. and Billington, D. P. (1993). Theory and history of suspension bridge design from 1823 to 1940. *Journal of Structural Engineering*, **119**(3), 954–977.

Buresti, G. (1998). Vortex shedding from bluff bodies. In R. . Davenport, editor, *Wind Effects on Buildings and Structures*. Balkema, Rotterdam.

Bursnall, W. J. and Loftin, L. K. (1951). Experimental investigation of the pressure distribution about yawed circular cylinder in the critical reynolds number range. Technical report, Langley Aeronautical Laboratory, Langley Field, Va.

Carta, J., Ramírez, P., and Bueno, C. (2008a). A joint probability density function of wind speed and direction for wind energy analysis. *Energy Conversion and Management*, **49**(6), 1309–1320.

Carta, J., Bueno, C., and Ramírez, P. (2008b). Statistical modeling of directional wind speeds using mixture of von Mises distributions: Case study. *Energy Conversion and Management*, **49**(5), 897–907.

Carta, J., Ramirez, P., and Velazquez, S. (2009). A review of wind speed probability distributions used in wind energy analysis. *Renewable and Sustainable Energy Reviews*, **13**(5), 933–955.

Clobes, M., Willecke, A., and Peil, U. (2011). Shape-dependent characteristics of full-scale wind profiles. *Journal of Wind Engineering and Industrial Aerodynamics*, **99**(9), 919 – 930.

Cook, N. J. (1985). *The designer's guide to wind loading of building structures — Part 1: Background, damage survey, wind data and structural classification.* Building Research Establishment.

Cornell, C. and Krawinkler, H. (2000). Progress and challenges in seismic performance assessment. PEER Center News. http://peer.berkeley.edu/news/2000spring/index.html.

Da Vinci, L. (1828). *Moto e misura dell'acqua.* Bologna a spese di Francesco Cardinali.

D'Asdia, P. and Noè, S. (1998). Vortex induced vibration of reinforced concrete chimneys: in situ experimentation and numerical previsions. *Journal of Wind Engineering and Industrial Aerodynamics*, **74-76**, 765 – 776.

D'Asdia, P., Noè, S., and Viskovic, A. (1998). Distacco di vortici da corpo elastico cilindrico a sezione circulare: un nuovo modello numerico autolimitante ed autoregolato. In *Atti del V Convegno Nazionale di Ingegneria del Vento IN-VENTO 1998*, Perugia. (in italian).

D'Asdia, P., Sepe, V., Caracoglia, L., and No, S. (2003). A model for vortex-shedding induced oscillations of long-span bridges. In B. Publishers, editor, *Proceedings of the 2nd International Structural Engineering and Construction Conference (ISEC-02)*, volume 3, pages 2331–2336. University of Rome, Italy.

Davenport, A. G. (1961). The application of statistical concepts to the wind loading of structures. *Proc. Inst. Civ. Eng. (London)*, **19**, 449–472.

Davenport, A. G. (1962). The response of slender line-like structures to gusty winds. *Proc. Inst. Civ. Eng. (London)*, **23**, 389–408.

Davenport, A. G. (1981). Reliability of long span bridges under wind loading. In *Proceedings of the ICOSSAR '81 3rd International Conference on Structural Safety and Reliability*, volume 4, Trondheim, Norway. Elsevier Scientific Publishing ompany, Amsterdam.

Deaves, D. and Lines, I. (1997). On the fitting of low mean windspeed data to the Weibull distribution. *Journal of Wind Engineering and Industrial Aerodynamics*, **66**(3), 169–178.

Diana, G., Resta, F., Belloli, M., and Rocchi, D. (2006). On the vortex shedding forcing on suspension bridge deck. *Journal of Wind Engineering and Industrial Aerodynamics*, **94**(5), 341 – 363. The eighth Italian National Conference on Wind Engineering IN-VENTO-2004.

Dowell, E. (1981). Non-linear oscillator models in bluff body aero-elasticity. *Journal of Sound and Vibration*, **75**(2), 251 – 264.

Dyrbye, C. and Hansen, S. (1997). *Wind loads on structures.* John Wiley & Sons.

Ehsan, F. (1988). *The vortex-induced response of long, suspended-span bridges.* Ph.D. thesis, Princeton University.

Ehsan, F. and Scanlan, R. H. (1990). Vortex-induced vibrations of flexible bridges. *Journal of Engineering Mechanics*, **116**(6), 1392–1411.

Ehsan, F., Scanlan, R. H., and Bosch, H. R. (1989). Modeling spanwise correlation effects in the vortex-induced response of flexible bridges. In *Proceedings of the Sixth U.S. Nat. Conf. on Wind Engineering*, Houston, Tex.

Ehsan, F., Scanlan, R. H., and Bosch, H. R. (1990). Modeling spanwise correlation effects in the vortex-induced response of flexible bridges. *Journal of Wind Engineering and Industrial Aerodynamics*, **36**(Part 2), 1105 – 1114.

Erdogan, H., Akp?nar, B., Gulal, E., and Ata, E. (2007). Monitoring the dynamic behaviors of the bosporus bridge by gps during eurasia marathon. *Nonlin. Processes Geophys.*, **14**, 513–523.

Feng, C. C. (1968). *The measurements of vortex-induced effects in flow past stationary and oscillating circular and D-section cylinders.* Master's thesis, Univ. Br. Columbia, Vancouver.

Frandsen, J. B. (2001). Simultaneous pressures and accelerations measured full-scale on the great belt east suspension bridge. *Journal of Wind Engineering and Industrial Aerodynamics*, **89**(1), 95 – 129.

Fujino, Y.and Yoshida, Y. (2002). Wind-induced vibration and control of trans-tokyo bay crossing bridge. *Journal of Structural Engineering*, **128**, 1012–1025.

Funakawa, M. (1969). The vibration of a cylinder caused by wake force in a flow. *Bull. JSME*, **12**, 1003–1010.

Gerrard, J. H. (1966). The mechanics of the formation region of vortices behind bluff bodies. *Journal of Fluid Mechanics Digital Archive*, **25**(02), 401–413.

Goswami, I. (1991). *Vortex-Induced vibration of circular cylinders.* Ph.D. thesis, Johns Hopkins University, Baltimore, Maryland.

Goswami, I., Scanlan, R. H., and Jones, N. P. (1992). Vortex shedding from circular cylinders: Experimental data and a new model. *Journal of Wind Engineering and Industrial Aerodynamics*, **41**(1-3), 763 – 774.

Goswami, I., Scanlan, R., and Jones, N. (1993a). Closure of the discussion on "vortex-induced vibration of circular cylinder. II: New model". *Journal of Engineering Mechanics.*

Goswami, I., Scanlan, R. H., and Jones, N. P. (1993b). Vortex-induced vibration of circular cylinders. II: New model. *Journal of Engineering Mechanics*, **119**(11), 2288–2302.

Griffin, O., Skop, R., and Koopmann, G. (1973). The vortex-excited resonant vibrations of circular cylinders. *Journal of Sound and Vibration*, **31**(2), 235 – 249, IN1–IN3.

Griffin, O., Ramberg, S., and Jones, N. (1982). Some recent studies of vortex-shedding with application to marine tubulars and risers. *J. Energy Resour. Technol.*, **104**, 2–13.

Gupta, H., Sarkar, P. P., and Mehta, K. C. (1996). Identification of vortex-induced-response parameters in time domain. *Journal of Engineering Mechanics*, **122**(11), 1031–1037.

Hartlen, R. T. and Currie, I. G. (1970). Lift-oscillator model of vortex-induced vibration. *Journal of Engineering Mechanics Division (ASCE)*, **96**(5), 577–591.

Honji, H. and Taneda, S. (1968). Vortex wakes of oscillating circular cylinders. Technical report, Res. Inst. Appl. Mech.

Ito, M., Katayama, T., and Nakazono, T. (1973). Some empirical facts on damping of bridges. In *Proceedings of the Symposium on Resistance and Ultimate Deformability of Structures Acted on by Well Defined Loads*, Lisbon.

Iwan, W. and Blevins, R. D. (1974). A model for vortex induced oscillation of structures. *Journal of Applied Mechanics*, **41**(3), 581–586.

Iwan, W. and Botelho, D. (1985). Vortex-induced oscillation of structures in water. *J. Wtrwy., Port, Coastal & Ocean Engrg. ASCE*, **111**, 289–303.

Kasperski, M. (2009). Specification of the design wind load — a critical review of code concepts. *J. Wind Eng. and Ind. Aerodyn.*, **97**.

Khalak, A. and Williamson, H. (1999). Motions, forces and mode transitions in vortex-induced vibrations at low mass-damping. *Journal of Fluids and Structures*, **13**, 813–851.

King, S. (1977). Vortex excited oscillations of yawed circular cylinders. *J. Fluids Engrg.*, **99**, 495–502.

Koopman, G. H. (1970). Wind-induced vibrations of skewed circular cylinders. Technical report, The Catholic University of America.

Krenk, S. and Nielsen, S. (1999). Energy balanced double oscillatior model for vortex-induced vibrations. *Journal of Engineering Mechanics*, **125**, 263–271.

Kumarasena, T.and Scanlan, R. and Ehsan, F. (1991). Wind-induced motions of deer isle bridge. *Journal of Structural Engineering*, **117**, 3356–3374.

Lagarias, J. C., Reeds, J. A., Wright, M. H., and Wright, P. E. (1998). Convergence properties of the nelder-mead simplex method in low dimensions. *SIAM Journal of Optimization*, **9**(1), 112–147.

Landl, R. (1975). A mathematical model for vortex-excited vibrations of bluff bodies. *Journal of Sound and Vibration*, **42**(2), 219 – 234.

Larose, G., Larsen, S., Larsen, A., Hui, M., and Jensen, A. (2003). Sectional model experiments at high reynolds number for the deck of a 1018 m span cable-stayed bridge. In *Proceedings of 11th International Conference on Wind Engineering Lubbock*, page 373380, TX, USA.

Larsen, A. (1993). A generalized model for assessment of vortex-induced vibration of flexible structures. In *Proceedings of the First IAWE European and African Regional Conference*.

Larsen, A. (1995). A generalized model for assessment of vortex-induced vibrations of flexible structures. *Journal of Wind Engineering and Industrial Aerodynamics*, **57**(2-3), 281 – 294.

Larsen, A. and Walther, J. (1997). Aeroelastic analysis of bridge girder sections based on discrete vortex simulations. *J. Wind Eng. Ind. Aero.*, **67/68**, 253–265.

Larsen, A., Esdahl, S., Andersen, J., and Vejrum, T. (2000). Strorebaelt suspension bridge: vortex shedding excitation and mitigation by guide vanes. *J. Wind Eng. and Ind. Aerodyn.*, **88**, 283–296.

Littler, J. D. and Ellis, B. R. (1987). Ambient vibration measurements of the humber bridge. In *Proceedings of the International Conference on Flow-Induced Vibrations*, pages 259–266, Cranfield, England.

Lucor, D. and Karniadakis, G. E. (2003). Effects of oblique inflow in vortex-induced vibrations. *Flow, Turbulence and Combustion*, **71**, 375–389.

Mair, W. A. and Maull, D. J. (1971). Bluff bodies and vortex shedding - a report on euromech 17. *Journal of Fluid Mechanics Digital Archive*, **45**(02), 209–224.

Mannini, C. (2006). *Flutter vulnerability assessment of flexible bridges*. Ph.D. thesis, University of Florence (Italy)/TU Braunschweig (Germany).

Marra, A. M., Mannini, C., Bartoli, G., and Fanelli, D. (2011a). Direct numerical identification of aeroelastic parameters at lock-in. In *Proceedings of the 13th International Conference for Wind Engineering*, Amsterdam, The Netherands.

Marra, A. M., Mannini, C., and Bartoli, G. (2011b). Van der pol-type equation for modeling vortex-induced oscillations of bridge decks. *Journal of Wind Engineering and Industrial Aerodynamics*, **99**(6-7), 776 – 785. The Eleventh Italian National Conference on Wind Engineering, IN-VENTO-2010, Spoleto, Italy, June 30th - July 3rd 2010.

Marris, A. (1964). A review on vortex streets, periodic wakes, and induced vibration phenomena. *Journal of Basic Engineering*, pages 185–196.

Matsumoto, M. (1999). Vortex shedding of bluff bodies: A review. *Journal of Fluids and Structures*, **13**(7-8), 791 – 811.

Muscolino, G. (2002). *Dinamica delle strutture*. McGrow-Hill, Milano.

Nakamura, Y. (1969). Vortex excitation of a circular cylinder treated as binary flutter. *Rep. Res. Inst. App. Mech., Kyushu Univ.*, **13**, 217–234.

Noè, S., D'Asdia, P., and Fathi, S. (1998). Simulazione della risposta dinamica di strutture cilindriche elastiche soggette a distacco dei vortici. studi su un modello numerico. In *Atti del V Convegno Nazionale di Ingegneria del Vento IN-VENTO 1998*, Perugia. (in italian).

Norberg, C. (2003). Fluctuating lift on a circular cylinder: review and new measurements. *Journal of Fluids and Structures*, **17**, 57–96.

Owen, J., Vann, A.M.and Davies, J., and Blakeborough, A. (1996). The prototype testing of kessock bridge: response to vortex shedding. *J. Wind Eng. Ind. Aero.*, **60**, 91–108.

Paulotto, C., Ciampoli, M., and Augusti, G. (2004). Some proposals for a first step towards a performance based wind engineering. In *Proceedings of the first international forum on in engineering decision making.*

Peil, U. (1998). Life cycle prediction of guyed masts. In *The First International Congress dedicated to the art, science and practice of structural engineering*, San Francisco, California, USA.

Peil, U. and Nolle, H. (1994). On fatigue of guyed masts due to wind load. In G. Schueller and J. Shinozuka M., Yao, editors, *Proceedings of ICOSSAR - The 6th International Conference on Structural Safety and Reliability*, Austria. A.A. Balkema / Rotterdam / Brookfield.

Peil, U. and Telljohann, G. (1999). A wind turbulence model based on long-term measurements. In L. . L. Larsen, editor, *Wind Engineering into the 21st Century - Proceedings of the Tenth International Conference on Wind Engineering*, pages 147–153, Copenhagen, Denmark. A.A. Balkema / Rotterdam / Brookfield.

Perry, A. E., Chong, M. S., and Lim, T. T. (1982). The vortex-shedding process behind two-dimensional bluff bodies. *Journal of Fluid Mechanics Digital Archive*, **116**(-1), 77–90.

Pliefke, T., Sperbeck, S., and Urban, M. (2006). The probabilistic risk management chain - general concepts and definitions. Internal discussion paper, International Graduate College 802.

Pliefke, T., Sperbeck, S., Urban, M., Peil, U., and Budelmann, H. (2007). A standardized methodology for managing disaster risk - an attempt to remove ambiguity. In *V International Pobabilistic Workshop*, Ghent.

Ramberg, S. E. (1983). The effects of yaw and finite length upon the vortex wakes of stationary and vibrating circular cylinders. *Journal of Fluid Mechanics*, **128**, 81–107.

Repetto, M. and Solari, G. (2004). Directional wind-induced fatigue of slender vertical structures. *Journal of Structural Engineering*, **130**(7).

Ricciardelli, F. (2010). Effects of the vibration regime on the spanwise correlation of the aerodynamic forces on a 5:1 rectangular cylinder. *Journal of Wind Engineering and Industrial Aerodynamics*, **98**(4-5), 215 – 225.

Roshko, A. (1993). Perspective on bluff body aerodynamics. *Journal of Wind Engineering and Industrial Aerodynamics*, **49**, 79–100.

Sarpkaya, T. (1978). Fluid forces on oscillating cylinders. *J. Wtrwy. Port. Coast. And Oc. Div. ASCE*, **104**, 275–290.

Sarpkaya, T. (1979). Vortex-induced oscillations a selective review. *Journal of Applied Mechanics*, **46**, 241–258.

Scanlan, R. H. (1981). On the state-of-the-art methods for calculations of flutter, vortex-induced and buffeting response of bridge structures. Technical report, FHWA/RD-80/050, Nat. Tech. Information Service, Springfield, Va.

Scanlan, R. H. (1998). Bridge flutter derivatives at vortex lock-in. *Journal of Structural Engineering*, **124**(4), 450–458.

Scanlan, R. H. (2004). *Aeroelasticity in Civil Engineering*, chapter in *A modern course in aeroelasticity*, pages 299–376. Kluwer Academic Publishers.

Scanlan, R. H. and Tomko, J. (1971). Airfoil and bridge deck flutter derivatives. *J. Engrg. Mech. Div., ASCE*, **97**(6), 1717–1737.

Schlichting, H. (1979). *Boundary layer theory.* McGrow-Hill, New York.

Scruton, C. (1963). On the wind-excited oscillations of stacks, towers and masts. In *Proceedings of the International Conference on the Wind Effects on Buildings and structures*, pages 798–837. Teddington, Middlesex, 1963.

Shimada, K. and Ishihara, T. (2002). Application of a modified model to the prediction of aerodynamic characteristics of rectangular cross-section cylinders. *J. Fluids Struct.*, **16**, 465–485.

Simiu, E. and Miyata, T. (2006). *Design of Buildings and Bridges for Wind: A Practical Guide for ASCE-7 Standard Users and Designers of Special Structures.* John Wiley and Sons.

Simiu, E. and Scanlan, R. (1996). *Wind effects on structures.* John Wiley & Sons, third edition.

Skop, R. and Griffin, O. (1973). A model for the vortex-excited resonant response of bluff cylinders. *Journal of Sound and Vibration*, **27**(2), 225 – 233.

Skop, R. and Griffin, O. (1975). On a theory for the vortex-excited oscillations of flexible cylindrical structures. *Journal of Sound and Vibration*, **41**(3), 263 – 274.

Skop, R. A., Griffin, O. M., and Ramberg, S. E. (1973). Strumming predictions for the seacon ii experimental mooring. In *Offshore Technology Conference.*

Smith, I. (1980). Wind induced dynamic response of the wye bridge. *Eng. Struct.*, **2**(4), 202–208.

Staubli, T. (1983). Calculation of vibration of an elastically mounted cylinder using experimental data from a forced oscillation. *J. Fluid Engrg.*, **105**, 225–229.

Surry, J. and Surry, D. (1967). The effect of inclination on the strouhal number and other wake properties of circular cylinders at subcritical reynolds numbers. Technical report, Institute for Aerospace Studies, University of Toronto.

Takle, E. S. and Brown, J. M. (1978). Note on the use of weibull statistics to characterize wind-speed data. *Journal of Applied Meteorology*, **17**, 556–559.

Tamura, Y. and Matsui, G. (1979). Wake-oscillator model of vortex-induced oscillation of circular cylinder. In *Proceedings of the Fifth International Conference on Wind Engineering*, pages 1085–1094, Fort Collins, Colorado, USA.

Tanida, Y., Okajima, A., and Watanabe, Y. (1973). Stability of a circular cylinder oscillating in uniform flow or in a wake. *Journal of Fluid Mechanics*, **61**, 769–784.

Toebes, G. and Eagleson, P. (1961). Hydroelastic vibrations of flat plates related to trailing edge geometry. *J. Basic Eng., Trans. of ASME*.

Torum, A. and Anand, N. M. (1985). Free span vibrations of submarine pipelines in steady flows-effect of free-stream turbulence on mean drag coefficients. *Journal of Energy Resources Technology*, **107**, 415–420.

Van der Pol, B. (1920). A theory of the amplitude of free and forced triode oscillation. *Radio Review*, **I**, 701.

Vandiver, J. K. (1983). Drag coefficients of long-flexible cylinders. In *Offshore Technology Conference*.

Vickery, B. and Basu, R. (1983a). Across-wind vibrations of structures of circular cross-section. part i. development of a mathematical model for two-dimensional conditions. *Journal of Wind Engineering and Industrial Aerodynamics*, **12**(1), 49 – 73.

Vickery, B. and Basu, R. (1983b). Simplified approaches to the evaluation of the across-wind response of chimneys. *Journal of Wind Engineering and Industrial Aerodynamics*, **14**(1-3), 153 – 166.

Vickery, B. and Watkins, B. (1964). Flow-induced vibrations of cylindrical structures. In R. Silvester, editor, *Proceedings of the First Australian Conference on Hydraulics and Fluid Mechanics*. New York, Pergamon Press.

Weibull, W. (1951). A statistical distribution function of wide applicability. *J. Appl. Mech.*, **18**, 293–297.

Williamson, C. and Govardhan, R. (2004). Vortex-induced vibrations. *Annual Review of Fluid Mechanics*, **36**(1), 413–455.

Williamson, C. H. K. (1996). Vortex dynamics in the cylinder wake. *Annual Review of Fluid Mechanics*, **28**(1), 477–539.

Wyatt, T. A. and Scruton, C. (1981). A brief survey of the aerodynamic stability problems of bridges. *Bridge Aerodynamics, TTL, London*, pages 21–31.

Zdravkovich, M. (1982). Scruton number: a proposal. *J. of Wind Eng. And Ind. Aero.*, **10**, 263–265.

Zdravkovich, M. (1990). On origins of hysteretic responses of a circular cylinder induced by vortex shedding. *Flugwiss Weltraumforsch.*, **14**, 47–58.